Stazione Zoologica Anton Dohrn Napoli

UNIVERSITÀ POLITECNICA DELLE MARCHE

Research Doctorate in "Life and Environmental Sciences"

Curriculum Marine Biology and Ecology
Cycle XXXV

An integrative approach to study the seasonality and biodiversity of benthic diatoms in the Adriatic and Tyrrhenian Seas

Presented by
Apurva Subhash Mule

Supervisors
Prof. Cecilia Totti
Dr. Diana Sarno

Italy, 2023

This project was co-financed by UnivPM, Ancona &
Stazione Zoologica Anton Dohrn, Naples

Summary

Microphytobenthos (MPB) is a poorly explored component of marine ecosystem despite their high contribution to primary productivity and main role in the trophic chain and in biogeochemical cycles. Benthic diatoms, which are the main component of the MPB community, are less studied compared to planktonic diatoms.

This study aims to increase the knowledge on the biodiversity and community structure of the subtidal benthic diatoms of the Mediterranean Sea. In the first part of the thesis, seasonal abundance and composition of benthic diatoms were studied at two stations of Marche coast (N Adriatic) using light microscopy. A total of 118 taxa were observed. Among these, 83 taxa were described in detail by SEM analysis. At both stations, benthic diatoms showed a marked seasonality, with maximum abundance, biomass and biodiversity in spring and minimum in summer. At both stations the motile forms were the most important component of the diatom communities followed by the adnate forms. The plocon forms were less abundant than the others but in autumn they contributed significantly to the biomass. This study highlighted that no marked spatial variability occurred in the study area as the community diversity and seasonal pattern were similar at the two stations.

In the second part of this study, 59 diatom strains were isolated from sediments collected at two stations located in the Northern Adriatic and 11 stations in the Tyrrhenian Sea (Campania region) for morphological and molecular characterization. All strains were observed and imaged in light microscopy. Their 18S RNA gene sequences were determined and placed in a phylogenetic tree cointaining 541 partial sequences of the 18S rRNA gene. Then 13 strains selected among those having a questionable position were analyzed at SEM and TEM for detailed ultrastructural analysis and species identification. This study highlighted the lack of data for many taxa and the need to use an integrative approach, based on both morphological and molecular analysis, to improve the taxonomy and classification system of benthic diatoms for a better understanding of the species ecology.

Keywords: benthic diatoms, ecology, phylogenesis, ultrastructure

Acknowledgments

First, I wish to thank my two supervisors, Prof. Cecilia Totti and Dr. Diana Sarno for their continuous support and advice. I am genuinely grateful to them for introducing me to the world of 'Diatom' ecology. Our knowledge sharing sessions developed my interest in diatom taxonomy. To Prof. Cecilia Totti, many thanks for kindly receiving me in this new country and promptly responding to all my queries besides work. To Dr. Diana Sarno, heartful thanks for dealing with me over the long distance and providing new perspectives to look at things. To both of them, I acknowledge their trust, patience, and graciousness in dealing with a sometimes stubborn and single-minded student.

I am utterly grateful to Dr. Tiziana Romagnoli for showering knowledge, love, and care upon me. Her excellent skills from sampling to electronic microscopic observations and patience while explaining the work made me enjoy this difficult taxonomic world of benthic diatoms.

My sincere and deepest gratitude to Dr. Weibe Kooistra for introducing me with molecular world. I am always grateful for all the lab techniques you guided me with and lasting discussions on the phylogeny of diatoms and more. Thank you for welcoming me into your home and sharing delicious recipes. Also, I am thankful to Dr. Marina Montresor for her invaluable inputs and direction during the study.

I am very grateful to my colleagues and staff in the Polytechnic University of Marche, Ancona and the Stazione Zoologica Anton Dohrn, Naples. It is hard to mention everyone who works or worked there but thank you everyone for your steady and generous support and companionship. In spite of all the difficulties and complaints, you kept showing up every morning with an undying passion for the science you do! Special thanks to Francesca Neri, Marika Ubaldi, and Dr. Stefano Accoroni for being patient with me and giving memories for lifetime. Their enormous contribution to this work was absolutely essential.

I take this opportunity to thank my friends who became family in this wonderful country, Sarah, Jana, Marta, and Claudia. You created ‘home’, away from home.

Finally, from beyond the Seas, special thanks to my parents, sister, and brother for being my supporters and much more. I cannot imagine getting through this thesis without your constant love and understanding.

List of Figures

List of Tables

List of Acronyms

AA	Apical Axis - valve length (in μm)
EM	Electron microscopy
F	Fibulae
LM	Light microscopy
MPB	Microphytobenthos
N Adriatic Sea	Northern Adriatic Sea
PA	Pervalvar Axis- (in μm)
PN	Portonovo (sampling station in N Adriatic Sea)
rbcL	Plastid gene encoding RUBISCO
SEM	Scanning Electron Microscopy
SG	Senigallia (sampling station in N Adriatic Sea)
SSU rDNA	Nuclear gene encoding small ribosomal subunit
TA	Transapical Axis- valve width (in μm)
TS	Transapical striae.
V4 SSU rDNA	Region of SSU rDNA

Chapter 1. General introduction

1.1 Importance of benthic diatoms

Diatoms, or Bacillariophyta (Karsten, 1928), constitute one of the most diverse phyla of microalgae, with currently over 18,000 described species (Guiry & Guiry, 2023). They are ubiquitous in nature where they live in a variety of different environments, and can be either planktonic (free-floating) or benthic (lying on or attached to substrata) (Figure. 1). Diatoms contribute globally almost 40% of marine primary production of carbon (Nelson et al., 1995) and the species diversity of benthic diatoms is extremely high, showing a bewildering variety of forms and shapes, and many different lifestyles. Benthic diatoms form a biofilm on the sediment, which plays an important role in nutrient cycling and sediment stabilization, particularly in the intertidal and shallow subtidal zones. Also, they provide a food resource to meio- and microfaunal grazers (Evrard et al., 2012; Miller et al., 1996). The abundance and composition of diatom communities are influenced by biotic and abiotic factors like grazing, nutrients and environmental parameters (Soininen et al., 2007). Since diatom species often have specific ecological requirements, their community composition can provide information about ecological conditions, in fact, diatoms are used widely as indicators of the good environmental status of marine and freshwater communities alike. Therefore, it is not surprising that benthic diatoms have attracted considerable research interest (Round et al., 1990).

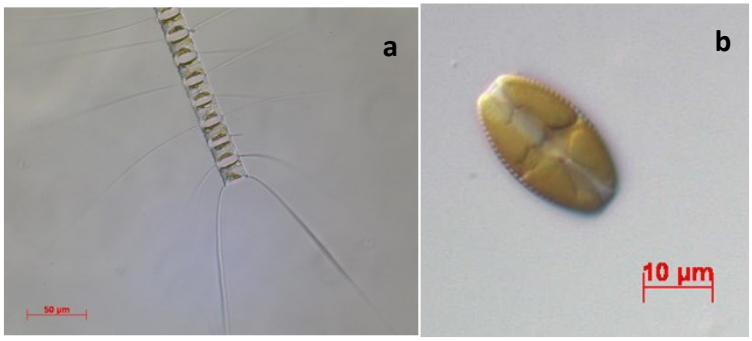

Figure 1: a) Centric planktonic (*Chaetoceros constrictus*) b) Benthic pennate (*Amphora pediculus*)

1.2 The silica cell wall

The diatom's defining feature is the composite silica cell wall, called a frustule, which is composed of two valves (one valve – the epivalve, and a slightly smaller one – the hypovalve) and two series of girdle bands, which hold these valves together, and which are also known as cingular bands (Figure. 2). The epivalve and its accompanying girdle bands fit over the hypovalve and its girdle bands like a lid on a box. Each valve and its set of girdle bands are, together, called a theca, i.e., epitheca or hypotheca (Figure. 2). Together, the frustule elements enclose the cell entirely, and in the meantime, their composite nature allows growth and cell division. The valves form the morphologically most elaborate parts, and the classification of the diatoms is based mainly on their morphological and ultrastructural characteristics.

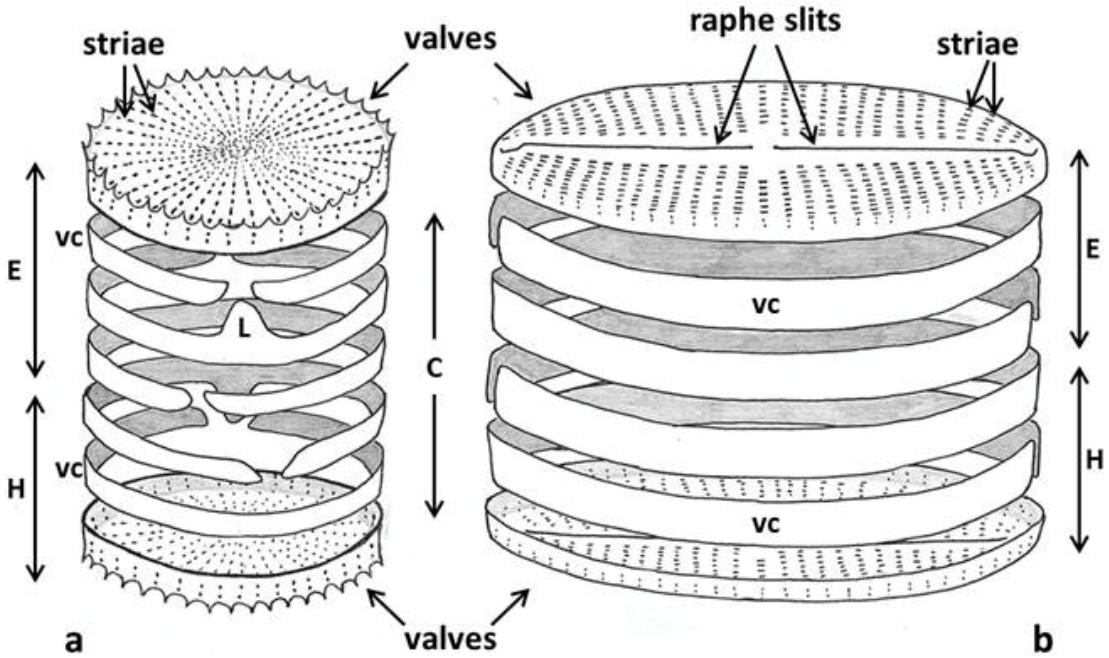

Figure 2: Illustration of the structure of a diatom frustule (from Cox, 2014); a) a radial centric diatom; b) a raphid pennate diatom. C indicates the cingular bands, all together called a cingulum. E indicates the epitheca, which includes the epivalve and its set of cingular bands or epicingulum. H indicates the hypotheca, which includes the hypovalve and its hypocingulum. The cingular band nearest to the valve is called a valvocopula (VC). L indicates ligula, a lip-like structure on the cingular band.

1.3 Life cycle

Valves and cingular bands are formed by means of silica deposition onto an organic matrix within specialised vacuoles, called silica deposition vesicles. When a diatom cell divides mitotically (Figure. 3), the dividing nuclei migrate to their halves of the mother cell. The daughter cells separate and silica deposition vesicles for the valves and cingular bands are formed against the new plasmalemma. Each one grows from a pattern centre and silica is deposited in an amorphous form against the organic matrix that functions as a scaffold. When the new frustule element is fully formed, the membrane of the silica deposition vesicle fuses with the plasmalemma, resulting in the deposition of the frustule element to the cell exterior. This way each daughter cell inherits one theca from the mother cell and forms a new theca that fits tightly inside the one inherited from the mother cell. This mode of cell division and theca formation has consequences for the life cycle of the diatoms. With each division the epitheca of the mother cell remains epitheca of the daughter cell and the newly formed theca is called hypotheca. Yet, the hypotheca of the mother cell now becomes the epitheca of the other daughter cell and a new hypotheca is formed inside it. Thus, with ongoing mitotic divisions the cells in a cell line become, on average, smaller and smaller whereas the variance of their size increases. This phenomenon is known as the MacDonald-Pfitzer rule of diatom growth (MacDonald, 1869; Pfitzer, 1871). To escape from this miniaturisation trap, diatoms need to go through sexual reproduction and formation of an auxospore. This auxospore forms a type of specialized silica bands called properizonial and perizonial bands, that are formed in sequence, and which allows the cell to re-establish its original, initial cell size (Figure. 3).

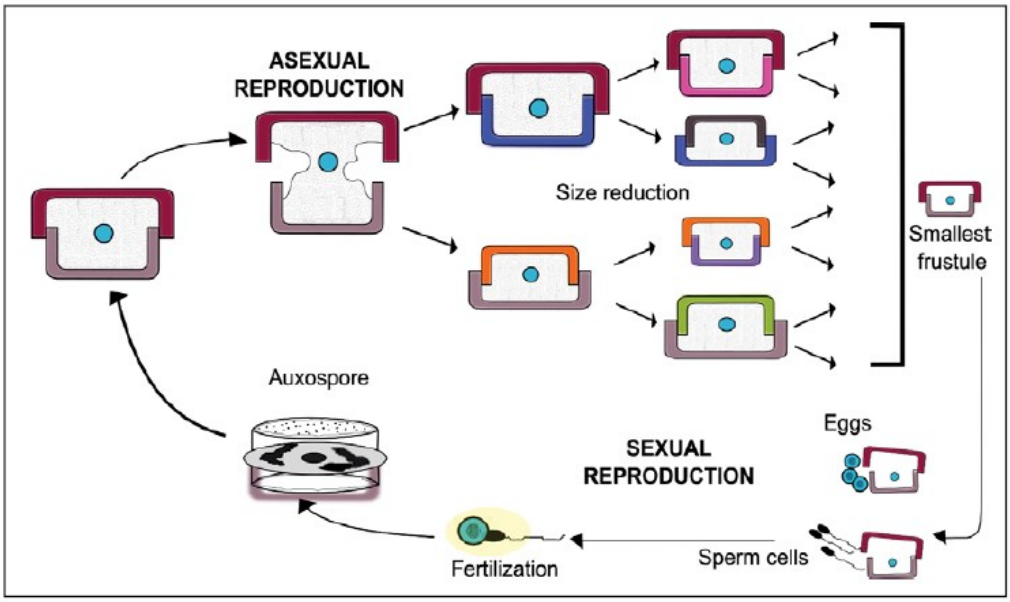

Figure. 3: Schematic representation of the lifecycle of diatoms with agamic and sexual reproduction.

1.4 Valve structure

Diatom valves exhibit a radial or pennate-shaped pattern centre, called an annulus or a midrib or a sternum, respectively, depending on the group of diatoms (Round et al., 1990). Perpendicular on this pattern centre, striae are organised, composed of rows of poroids or areolae, which allow exchange with the environment. The striae are interspersed by interstriae, also known as virgae (singular virga), i.e., solid silica bands between the striae. The fine connection bars linking the virgae are called vimines (singular vimen). The virgae and the vimines (Figure. 4) create an elaborate network of areolae (Cox, 2011, 2012, 2014; Cox & Ross, 1981). In addition to all these fine areolae, diatom frustules show a variety of specialized structures and processes (tubes) through the cell wall. Since their presence depends on the lineage to which the species belong, I will present them when describing these lineages.

1.5 Diatom lineages, their morphological and ultrastructural characteristics

The diatoms are classified commonly into centrics and pennates. Centric valves show a central annulus from which striae radiate outwards. Within the centric diatoms, there are the radial centrics or Coscinodiscophyceae, which possess a more or less circular outline, and the polar centrics or Mediophyceae, which show polarity in their valve outline (i.e., deviating from a circle). Pennate valves are usually elongated and are characterized by a keel-like structure, called a midrib or a sternum, which stretches along the apical axis of the valve (i.e., the axis between the two apices of the valve). Perpendicular upon the apical axis, striae are organized parallel alongside one another (i.e., parallel along the transapical axis). The pennates, or Bacillariophyceae, can be classified into raphid pennates, which possess a raphe slit in the sternum, enabling them to move actively (Figure. 3) and araphid pennates, those without such a raphe slit (Round et al., 1990), and, therefore, are non-motile. With ca. 14,300 described species, Bacillariophyceae is by far the most diverse among the diatoms whereas Mediophyceae and Coscinodiscophyceae include a mere 1,841 and 1,531 described species, respectively (Guiry & Guiry, 2023).

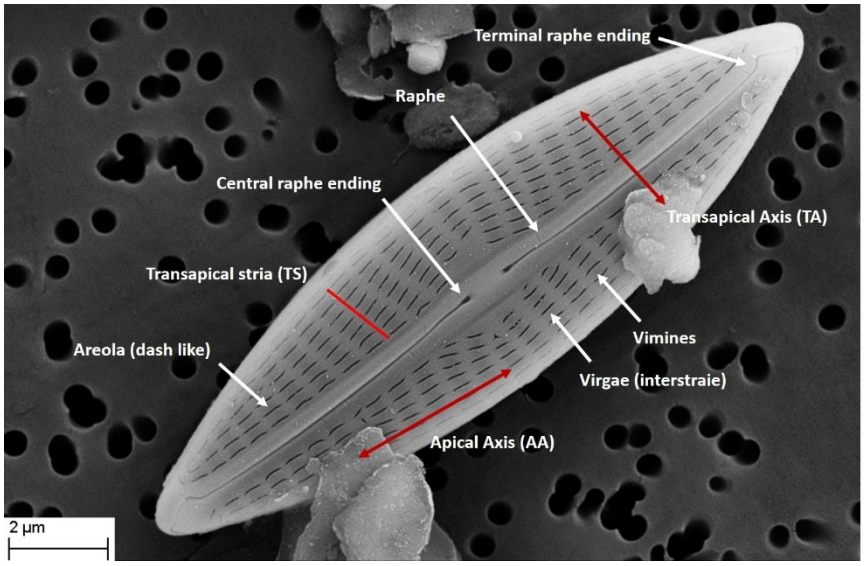

Figure. 4: Ultrastructure of pennate diatoms showing morphological characters.

Apart from the overall valve ultrastructural details of pattern centres, virgae and vimines (Figure. 4), diatom valves exhibit additional structures in the form of tubes and appendices. The most common

of these is the labiate process or rimoportula (plural rimoportulae), a tube through the valve that is compressed lip-like on the valve's interior side. In Coscinodiscophyceae they are found along the valve perimeter, in Mediophyceae inside the central annulus or near the valve apices, and in the araphid Bacillariophyceae near the valve apices. The functions of the rimoportulae are not exactly clarified. One peculiarity is that their lip-like shape essentially closes these tubes off from the valve exterior. In the raphid Bacillariophyceae, the two apically located rimoportulae have given rise to the two raphe slits, which in their turn acquired a new function, the directional propulsion (Round et al., 1990). Another type of processes, so-called strutted processes or fultoportulae, are found in one of the mediophycean lineages, the Thalassiosirales. Fultoportulae are located near the central annulus and/or along the valve perimeter. From these processes emerge chitin threads that stretch out into the cell exterior and link cells together into chains (Round et al., 1990). Then there are the apical pore fields, specialised structures through which mucous substances are being exuded, giving rise to mucilage pads and stalks with which some chain-forming diatoms hold on to one another and sessile diatoms hold on to various surfaces in the benthos (Round et al., 1990).

1.6 Placement of the diatoms within Stramenopile algae

Diatoms are sister group to a group of algae called Bolidophyceae and Parmales. Bolidophyceae comprise fast-swimming flagellates and Parmales are non-motile cells, which are like diatoms, encased entirely in a composite silica cell wall. The silica elements of this cell wall share several characteristics with the valves of centric diatoms, i.e., a radial pattern centre and striae perpendicular upon it, but although the frustule elements fully cover the cell, they do not show the outspoken differentiation between valves and cingular bands typical for diatoms. Diatoms and Parmales-Bolidophyceae are in their turn sister group to a variety of other brown and golden-brown micro and brown macroalgae. All of these together constitute the auxotrophic Stramenopiles, whose characteristics are the possession of two differently shaped flagella (heterokont algae). One of these flagella is long, adorned with two rows of tubular tripartite mastigonemes (stramenopilous hairs; Van

den Hoek et al., 1995) and turned forward, while the other is short, smooth and turned back. However, diatoms form the exception; only the microgametes of the centric diatoms possess a flagellum, and only one.

1.7 The sexual cycle of the diatoms, the different characteristics of the lineages

In order to escape from the aforementioned miniaturization trap (see Figure. 3), diatoms have to go through sexual reproduction to re-establish the initial cell size. In some lineages an alternative escape route exists in the form of vegetative cell enlargement, but this is not a common phenomenon among the lineages and has until now only been reported in a few lineages in Mediophyceae (Kaczmarska et al., 2022).

Sexual reproduction starts with meiosis and gamete formation, of which various modes are encountered in diatoms (Figure 3). Centrics form large non-motile macro-gametes and multiple, flagellated microgametes (oogamy). These microgametes swim to the macrogamete, which usually remains semi-enclosed in the maternal cell wall until fertilized. Instead, most of the Bacillariophyceae pennates in which the sexual cycle has been observed form non-flagellated isogametes, though behavioural differences have been reported, whereby a motile microgamete crawls in an amoeboid fashion to a nearby non-motile partner. In all cases, upon gamete fusion, a zygote is formed, which swells up by means of vacuolar expansion (and in some centric lineages subsequent partial retraction), and the formation of an organic cell wall with specialized silica platelets and bands. These bands are called properizonial or perizonial bands, depending on the lineage of diatoms. The enlarged cell confined in this compound cell wall is called an auxospore (Figure 3). Inside of this auxospore wall the cell wall elements of the initial vegetative cell are formed, and when ready, the initial cell emerges.

In Coscinodiscophyceae, the zygote swells up isometrically, and the auxospore is surrounded solely by an organic cell wall, and in some species with small silica platelets embedded within it. Inside this cell wall the initial frustule is formed. Thus, an initial global cell emerges from it, which commences dividing along its equator, thus giving rise to Petri dish shaped cells. In Mediophyceae, the zygote is

confined to swell only in particular directions by a series of often elaborately shaped bands, called properizonial bands, laid down one after another, thus giving rise to an auxospore reflecting the form of the initial non-globular cell. In some mediophycean lineages, e.g., *Chaetoceros, Trieres*, the zygote withdraws in part from the auxospore cell wall to enable the distinctive shape of these diatoms. Within the confines the frustule of the initial cell is formed. In Bacillariophyceae, the swelling zygote is confined to expand only in one dimension by a string of bands, called perizonial bands, formed and laid down one after another, to create a cigar-shaped cell. Inside this primary cell wall, another layer is formed composed of bands oriented in the apical axis and positioned above and below the cell. The frustule of the initial cell is laid down inside this elaborately formed auxospore. Of course, this description presents only the main trends; there are many lineage-specific deviations from these general patterns and research into auxospore formation is in full swing in diatoms.

Some centric diatom lineages can form resting spores, i.e., cells with heavily silicified frustules whose shapes can deviate markedly from that of the vegetative cells. Yet, these resting cells are formed from vegetative cells and retain the genetic identity of their clonal cell line. They can overcome periods unfavorable for growth, for instance, they are formed in unfavorable environmental conditions or when diseases, grazers or parasites threaten the population. Resting spores have nothing to do with auxospores; the latter are simply encapsulations of the expanded zygote and guide the formation of the initial cell. There is one known exception. In the coscinodiscophycean diatom genus *Leptocylindrus* the auxospore develops into a resting spore (Kaczmarska et al., 2022).

1.8 The evolutionary history of the diatoms

Results of paleontological and molecular phylogenetic studies agree in that Coscinodiscophyceae form the most ancient group of lineages. The last common ancestor (LCA) of one of these lineages acquired multi-polarity, thus giving rise to the mediophycean lineages. In its turn, the LCA of one of these acquired a midrib, giving rise to the various bacillariophycean lineages, and in their turn, the

LCA of one of these lineages developed the raphe, giving rise to all of the raphid pennates (Medlin, 2016).

These findings imply that the most ancestral, i.e., Coscinodiscophyceae auxospores possessed no bands to confine zygote swelling away from isodiametric inflation. The acquisition of properizonial bands in the last common ancestor of the lineage comprising Mediophyceae and Bacillariophyceae then enabled anisometric zygote swelling, and the acquisition of strings of primary perizonial bands and the secondary layer of supporting bands along the apical axis enabled the rise of elongated forms of the Bacillariophyceae.

Bacillariophyceae, and especially the raphid lineages therein, nowadays constitute the most species rich among the diatoms, but that does not mean that the non-pennate diatoms are evolutionary dead ends. Also, several lineages in Mediophyceae, such as Chaetocerotales and Thalassiosirales, have acquired novel features, such as setae and chitin threads, respectively, and these lineages are also highly diverse.

1.9 The ecology of the diatoms

The evolution of all the diatom lineages is intricately linked with the environments within which they evolved. Diatoms probably evolved in the benthos or free drifting above the sediment, and this is where many of the extant coscinodiscophycean and mediophycean lineages can be encountered, though there are several with a planktonic lifestyle. Bacillariophyceae are predominantly found on surfaces, i.e., benthic (Hudon & Legendre, 1987; Kooistra et al., 2007). Given that Bacillariophyceae form the most diverse group and predominate in the benthos, diatom species richness in the benthos is far higher than that in the plankton (Round et al., 1990). Nonetheless, a few bacillariophycean lineages have acquired a planktonic lifestyle from benthic ancestry. Examples are the araphid genus *Thalassionema* and its relatives, and the raphid genera *Pseudo-nitzschia* and *Fragilariopsis* (Kooistra et al., 2007).

Benthic diatoms dominate the microphytobenthic (MPB) communities worldwide, together with filamentous cyanobacteria. There, they colonise a variety of substrata. Based on the kind of surfaces on which they live, MPB communities have been categorized into epipelic (on soft sediments), epiphytic (on macroalgae and seagrasses), epizoic (on animals such as on the skin of marine vertebrates and on the talons of copepods), epilithic (on rocks) and epipsammic (very small cells attached on single sand grains).

Moreover, depending on the way with which benthic diatoms relate to their substratum, several distinct growth forms have been recognised (Lobban, 1985; Round, 1971; Totti et al., 2007).

Motile diatoms: these are found almost exclusively among the raphid pennates. Its cells move by means of a traction system of long, sticky polysaccharides, on one end exuded through the raphe slit and attached to the surface and then pulled along the slit in the direction opposite to that in which the cell intends to move (Round et al., 1990). A few mediophycean diatoms, such as *Toxarium*, can move actively as well, though how they do that without the traction of a raphe system still needs to be resolved (Kooistra et al., 2003; Medlin., 2008). Motile diatoms can be found in almost every sunlit benthic environment and a few even abound in the plankton (Kooistra et al., 2007). In the benthos they can occur as epipelic on unconsolidated material such as sand or mud where they can actively move onto and away from the surface, and onto any other substratum as epilithic, epiphytic and epizoic. This growth form was first reported by (Janisch, 1863) in the German Wadden Sea. Epipelic diatom communities constitute important primary producers in these intertidal ecosystems.

Second, there are the sessile diatoms. Their growth forms can be classified roughly into the following categories depending on the mechanism of attachment that involves mucilage pads or stalks exuded through specialised apical pore fields and/or rimoportulae in the valve apices and/or raphe. Benthic ecologists now widely use the following terminology to describe three different categories of attachment, namely:

- Adnate: this lifestyle includes diatoms that are firmly attached to the surface by one of their valves or by the girdle bands. Species in this group include *Amphora, Achnanthidium* and *Cocconeis* and its relatives. Their firm attachment means that these diatoms are essentially sedentary. Many of the raphid pennate lineages in this group have independently from one another become monoraphid, i.e., they possess a raphe in only one of their valves (*Cocconeis*). No raphe slits are formed in the other valve, or these slits are filled in secondarily with silica before the silica deposition vesicle releases the valve to the exterior. Adnate diatoms are found on seagrass leaves, on rocks, on the carapaces of sea turtles and on a variety of other surfaces experiencing strong water movement.
- Erect: this lifestyle includes diatoms attached to surfaces by means of mucilage pads or -stalks exuded from their apical pore fields or apical rimoportulae. They are found principally among the araphid pennates (e.g., *Gomphonema*, *Licmophora*), but also among raphid pennates (e.g., *Achnanthes, Cymbella*) and Mediophyceae (e.g., *Toxarium*), thus giving rise to ramified or bushy structures that are beautiful to observe (Round et al., 1990). The stalks allow the diatoms to stick out through the boundary layer of the surface.
- Tube-dwelling: this growth form of diatoms represents small naviculoid or nitzschioid species living in their own mucilage tube (appears as filaments), they appear mostly in the epilithic MPB communities. These tubes resemble small brown seaweeds or filamentous cyanobacterial mats. Examples are *Berkeleya rutilans, Navicula delognei* (Lobban, 1985).
- Plocon: this lifestyle presents a somewhat ill-defined and mixed category of diatoms loosely attached to surfaces by various means. These diatoms often form strings of cells holding on to one another by mucilage pads, which can also connect with surfaces. An example is the mediophycean diatom genus *Odontella*. Then there are diatoms that are often found in benthic communities but that do not occur attached to the surface. These diatoms drift freely over the sediment; their frustules are robust and way too heavily silicified for a planktonic existence. Examples are the coscinodiscophycean genera *Ellerbeckia* and *Paralia* (Round et al., 1990).

Then there are diatoms that can switch between lifestyles, occurring attached to free-floating ice as well as in the plankton. Another more exotic lifestyle is exhibited by diatoms in the surf zone (Hewson et al., 2001). These diatoms occur in blooms in the high-energy surf zone of sandy beaches, where they attach to wave-generated air bubbles, thus maintaining buoyancy. Yet, they can also sink to the sediment, especially under light stress, and thus become part of the epibenthic community. Examples are the mediophycean genus *Anaulus* and the araphid pennate genus *Asterionellopsis*.

1.10 Study of benthic diatoms, sampling, microscopy and molecular approaches

1.10.1 History: The study of benthic diatoms goes back to the early 19th century when (Greville, 1827) and (Hooker, 1833) observed such a group of diatoms sharing an epiphytic lifestyle. Since then, numerous taxonomists have explored and described the diversity of benthic diatoms. Unfortunately, most of the early studies were carried out on cleaned frustules, and therefore little information became available on the life strategies and ecology of these diatoms (reviewed in Round 1971). Only in the late 19th, early 20th century, authors paid attention to the lifestyle of benthic diatoms; for instance, (H. , Peragallo, 1888; H. Peragallo & Peragallo, 1897b) on the maritime diatoms of France, (van Heurck, 1909) and (A. Mann, 1937) on those of the Antarctic, Hustedt (1938) on the Pacific, Hustedt (1927-1965) on the taxonomy of diatoms world-wide, Hendey (1951) for England, Hendey (1959) for West Africa, and (Simonsen, 1962)on those of the Baltic.

1.10.2 Sampling: one issue when studying benthic diatoms is how to sample them. Epipsammic and epipelic diatoms can be sampled with grabs and corers, and then the surface layers can be gathered and further processed. However, the sampling procedures may whirl up the more loosely associated diatom species during the sampling. Epiphytic diatoms can be sampled by collecting seaweeds and seagrasses, but also in these cases the samples are easily disturbed, leading to loss of the more loosely attached species. Epilithic diatoms, especially those on large rock surfaces are particularly difficult

to sample because they have to be chiseled or scraped off the rocks as they are often very firmly attached to the surfaces.

1.10.3 Lab work: Isolation; There are issues with handling the collected diatoms in the lab. For the identification of the diatoms, the first step is to separate them from the sediment granule, for this purpose concentrated sulphuric and nitric acids have been used for a long. The use of these acids allows the removal of the organic material leaving the siliceous wall of the diatom which further can be used for identification and quantitative studies. Isolation of the live cells of the benthic diatoms can be achieved by using cover glasses or cellulose tissue layers but it only allows the isolation of the motile diatoms. Further separation of the epipsammic diatoms can be achieved by different techniques such as the washing of the sediment, cutting the sediment grain to which the diatom has attached, ultra-sonication to shake off the diatom from the sediment, or micro-pipetting (Round, 1971). These techniques lead to the loss of cells. So, many researchers try to adjust the sampling period based on the peak of the occurrence to obtain a maximum number of cells. Further, monoclonal cultures can be established using the micropipette for cell isolation and the isolated cells grown up in the media such as f/2 (Guillard, 1975; Guillard & Ryther, 1962).

Counting: As compared to phytoplankton, separation of diatom cells from the sediment is technically difficult. In the past, taxonomists used to observe diatoms cells by directly placing the diluted sediment in the chamber (Cibic et al., 2007). This was tedious work as sand and clay particles cover the cells creating difficulties in the correct cell counting. Moreover, this method imposes to analyze very low sample volumes, due to the sediment disturb, causing overestimation of cell abundances. The main problem is to establish a method that allows the elimination of only silt and clay particles. Also, few methods do not allow the separation between the living and dead cells of diatoms for the correct quantitative analysis. For examples using of strong-acid (e.g., HNO_3 or H_2SO_4) or weak (H_2O_2) cleaning can cause the destruction of the fragile ones and can favor the sturdier frustules. Moreover, these techniques do not allow to identify living cells from empty frustules, that are

abundant in the sediment (de Jonge, 1979; Vilhena et al., 2021). Further density gradient methods using the silica-based solvents like Percoll and Ludox HS-40 have been proved to be the more efficient approach for the extraction of benthos from the sediment (Méléder et al., 2007). These solutions are denser than the microbenthos but distinctly lighter than the sediment grain which separates the diatom cells from sediment at much extent.

1.10.4 Microscopic observation and identification; Another issue is that taxonomic identification of many diatoms is based solely on morphological characters as observed in light microscopy. The reason is that diatoms have been studied and described from the late 18th century onwards (e.g., (Müller, 1773), but during most of that time the only tool available to taxonomists was the light microscope (LM), revealing only the shape, ornamentation and, in larger diatoms, the striature of valves and cingular bands. Scanning and transmission electron microscopy (SEM, TEM) can uncover ultrastructural details of the frustule elements, such as the shape of perforations and their occlusions in the striae as well as the fine structure of various valve processes invisible in LM, revealing a wealth of additional characters for taxonomic identification. Yet, these tools became accessible only since the 1960s (see Round et al., 1990).

Molecular tools were pioneered in diatoms only since the late 1980s (Medlin et al., 1988) but have since then been applied widely (Evans et al., 2007; Jahn, 2007; Mann et al., 2010; Theriot et al., 2015; Witkowski et al., 2016). Nowadays, state-of-the-art diatom taxonomic studies integrate information from LM, EM and DNA marker sequences to characterize new species (e.g., Mucko et al., 2020), to explore cryptic diversity (e.g., Kollár et al., 2019) and to reassess taxa previously described morphologically now also by means of reference DNA sequences (Kermarrec, 2011).

1.10.5 Molecular approaches: Molecular characterization and identification of species is done usually by means of species-specific sequence differences on taxonomically discriminative DNA sequences. Widely applied examples of such molecular markers are of the nuclear encoded 18S and 28S rRNA genes and the ITS rDNA regions in between them and the plastid-encoded *rbc*L (ribulose

1,5 bisphosphate carboxylase/oxygenase) and the mitochondrial COX1 (cytochrome C-oxidase subunit 1). Flanking primer regions are conserved across the eukaryotic diversity to enable specific PCR-amplification of the marker and sequencing of the resulting PCR products. The obtained sequences are used to identify cultured strains and to infer phylogenetic relationships among the uncovered species. Among markers, the 18S rRNA gene and the *rbc*L are favoured for phylogenetic purposes because of their comprehensive coverage in reference databases, their universally conserved functions and their resolution power across different taxonomic levels. The 18S and 28S rRNA genes and the *rbc*L are appropriate at resolving relationships among closely related species as well as among higher diatom taxa and even between diatoms and the other lineages in the stramenopile algae (e.g.,Bruder & Medlin, 2007), whereas COX1 and the ITS regions are ideal for resolving relationships among very closely related taxa. Although, rbcL evolves slightly faster than the 18S rRNA gene, it potentially is a good barcode marker for the identification of closely related benthic pennate diatom. Yet, it has been applied less widely among diatoms because (and therefore) the taxonomic coverage of its reference database is less comprehensive.

A DNA barcode is comparable to a supermarket barcode, which uniquely associates with a particular product. Basically, a DNA barcode can be used to rapidly and easily assign a specimen to a species. DNA barcodes contain enough information to identify millions of species in the community (Hebert et al., 2003). And if this target sequence (i.e., barcode) differs enough from the reference sequences then the species is considered as new and added to the database/ sequence library. Besides this barcoding can also be used to explore hidden diversity (Evans et al., 2007, 2008; Moniz & Kaczmarska, 2009, 2010).

Valentini et al. (2009) explained different criteria for an ideal barcode, which includes: 1) a barcode marker should be identical, or at least highly similar, among individuals of the same species but different between those of different species; 2) the barcode should be standardizable in the sense that the same DNA region should be applicable across taxonomic groups; 3) the barcode should have

enough phylogenetic information so individual taxa can be easily designated; 4) barcode marker regions should be flanked by ultra-conserved primer sites to guarantee highly reliable DNA amplification and sequencing; and 5) the barcode should be able to be amplified from environmental DNA. The 18S rRNA gene I have used for my study is expected to be adequate for these purposes. The 18S rRNA gene, or specifically the V4 region therein, is widely used for environmental metabarcoding, also of benthic communities. So, the obtained barcodes will be useful for those studies.

1.11 Main issues in the taxonomic study of benthic diatoms

Descriptions based solely on overall valve shape observed in LM are imprecise for two reasons; one of these is morphological plasticity. Overall cell shape can change markedly during the vegetative part of the diatom's life cycle; cell size decreases gradually, and overall valve shape can change markedly with ongoing mitotic divisions. Miniaturized cells are particularly cumbersome to identify accurately. External abiotic and biotic factors also affect overall cell morphology (Cerino et al., 2005; Ligowski et al., 2012; Mann & Chepurnov, 2004). Changes in the nutrient concentration of Si, P, and N have been demonstrated to result in morphological changes (Marchetti & Harrison, 2007; Trobajo et al., 2011) and so have changes in the salinity (Balzano et al., 2011).

The other reason is cryptic diversity. Descriptions based solely on overall valve shape observed in LM also seriously underestimate species diversity. Species defined exclusively by their morphology are composed usually of cryptic species complexes, i.e., groups of morphologically indistinguishable but ultra-structurally, biologically and genetically distinct taxa. Cryptic species have been uncovered in almost any morphologically defined species (morphospecies) investigated. The following citations provide examples of such species complexes in benthic diatoms: *Berkeleya rutilans* (Hamsher & Saunders, 2014), *Eunotia bilunaris* (Vanormelingen et al., 2007, 2008), *Gomphonema parvulum* (Abarca et al., 2014; Kermarrec et al., 2013), *Hantzschia amphioxis* and *Pinnularia borealis* (Souffreau et al., 2013), *Navicula cryptocephala* (Poulíčková et al., 2010), *Nitzschia palea* (Trobajo

et al., 2009, 2010), *Sellaphora pupula* (Evans et al., 2008). The same is observed among planktonic centric: e.g., *Chaetoceros socialis* (Gaonkar et al., 2017); *Skeletonema costatum* (Sarno et al., 2005, 2007), *Pseudo-nitzschia delicatissima* and *P. pseudodelicatissima* (Amato & Montresor, 2008).

1.12 The aims of my thesis research

In my thesis I have aimed at exploring the diatom diversity in the benthos of two locations along the Italian coast, one in the Adriatic Sea and one on the opposite side of the peninsula, on the Tyrrhenian side. The reasons for choosing these two sides are the contrasting marine conditions at these geographically relatively proximal sides, and the easy access to sampling and maintenance facilities at the Polytechnic University of Marche, Ancona and the Stazione Zoologica Anton Dohrn, Naples. In addition, my supervisors have ample experience in diatom taxonomy, culture methods and molecular biological approaches.

In **Chapter 2,** I explore the diatom diversity through the seasons at ecologically contrasting sites in each of the two locations by means of light microscopical analysis of samples taken at these sites. Light microscopical observation allows for rapid characterization of community samples composed of numerous different species. However, identification down to the species level has its limitations. Nonetheless, the results of these observations enable the selection of cells to be isolated and grown up into monoclonal strains for further research.

In **Chapter 3,** I describe the isolation of cells from these samples, bringing them in monoclonal culture and explore the obtained culture strains by means of LM observation and by comparing marker DNA sequences obtained from these cultures with information in GenBank and with taxonomically verified reference sequences. For selected strains I then obtain ultrastructural information by means electron microscopic observation and evaluate based on all the obtained information the identity of the examined strains.

In the **Chapter 4**, I will provide the description and micrographs of the taxa that were characterized using the scanning electron microscopy.

In the **Chapter 5,** I will then present my conclusions, outlook and impact of my results. A major outcome forms a set of barcode sequences of taxonomically verified strains of benthic diatoms common in the studied sites.

Chapter 2. Seasonal variability of epipelic microphytobenthos community in two subtidal areas of the N Adriatic Sea

2.1 Abstract

To study the biodiversity and seasonality of benthic diatoms, two areas of N Adriatic Sea were investigated. Sediment samples were collected in four seasons at two stations located at ca. 1 nM from the coast (11–12 m depth). Diatom cells were separated from sediment using the density centrifugation method with Ludox HS-40. Total benthic diatoms' abundance ranged from 4,640 to 77,727 cells/cm^2 and biomass ranged from 0.55 to 3.70 μg C/cm^2. Benthic diatoms expressed a marked seasonal behaviour, with maximum abundance, biomass and biodiversity in spring and minimum in summer. The motile life forms like *Navicula, Nitzschia, Fallacia, and Psammodictyon* were dominant at both stations. This study highlighted that no marked spatial variability between the two stations resulted in similar diversity and seasonal trend. Given the ecological importance of benthic diatoms, further studies on their communities in subtidal areas are required to increase the knowledge about their diversity and variability in the long-term monitoring programs.

2.2 Introduction

Microphytobenthos (MPB) include microalgal communities living on benthic substrata. They are composed of unicellular eukaryotic algae (mainly diatoms) and cyanobacteria (Admiraal et al., 1984; MacIntyre et al., 1996; Underwood & Barnett, 2006). MPB play a key role in marine food web because of the significant primary production (globally- ca. 500 million tons C year−1) and biogeochemistry in aquatic ecosystems (Cahoon, 1999; Pinckney, 2018). Benthic diatoms communities have traditionally been divided into different groups according to the substrata they are associated with, i.e., epipelon (free living on sediment), epipsammon (attached to sand grains), epilithon (rocks, artificial substrata), epiphyton (algae, plants) and epizoon (animals) (Round, 1971).

Diatoms are the most important group of eukaryotic microalgae and include around 200,000 species (estimated up to 10^6 species). The majority of diatom diversity is expressed by benthic diatoms which represent around 90% of the total species number. Benthic diatoms have been traditionally subdivided in growth forms (Round et al., 1990): 'motile' comprising biraphid pennates with high motility (e.g., *Navicula* and *Nitzschia*); adnate' including diatoms living attached to the substratum by one valve face and having limited motility. They include both monoraphid (e.g., *Cocconeis*) and biraphid (*Amphora*) diatoms. 'Erect' diatoms are attached to surfaces by means of mucilage pads, stalks or peduncles exuded from their apical pore fields or apical rimoportulae. They include mainly araphid pennates (e.g., *Gomphonema*, *Licmophora*), but also raphid ones (e.g., *Achnanthes*, *Cymbella*). 'Tube-dwelling' diatoms are *small* naviculoid or nitzschioid species living in their own mucilage tube (appears as filaments). 'Plocon' identify a category of diatoms lying on substrata because of their frustules too heavily silicified for a planktonic existence (e.g., *Odontella*, *Paralia*) (Round et al., 1990).

Biofilm of the epipelic MPB plays important role in the habitat ecology because of sediment stabilization (Miller et al., 1996; Underwood & Paterson, 2003) and the exchange between sediment and water column of oxygen, silicon, and carbon (Armbrust, 2009). Several studies have addressed the influence of environmental parameters on epipelic MPB abundance, biomass and community

composition. The combination of environmental factors like temperature, oxygen saturation, silicate concentration, and salinity determine the seasonal succession and community structure (Cochero et al., 2015; Hafner et al., 2018; Underwood & Barnett, 2006). In the Mediterranean Sea, the annual maximum of MPB biomass is generally reported in spring and the minimum in summer (Barranguet et al., 1998; Blackford, 2002; Cibic et al., 2012; Facca & Sfriso, 2007; Franzo et al., 2015; Méléder et al., 2007). Indeed, the same was reported for epilithic (Pennesi & Danovaro, 2017), epiphytic (Car et al., 2012; de Stefano et al., 2000), epizoic (Romagnoli et al., 2007, 2014).

The majority of studies regarding the epipelic communities are referred to the intertidal areas where it is convenient to sample during low tide (Barranguet et al., 1998; Franzo et al., 2015; Underwood & Barnett, 2006). In this zone, high abundances, and biodiversity of MPB have been reported because of the optimal environmental conditions such as temperature and irradiance level. In the subtidal areas, where light or photosynthetically available radiation (PAR) was found to be the most relevant limiting factor for the growth of MPB many studies reported high biomass even at subtidal depth (Longphuirt et al., 2006, 2007; Totti, 2003). Regarding nutrients, despite they are present with high concentration in bottom sediments, some studies highlighted that they could limit the MPB growth. Totti (2003) indicated that in the northern Adriatic Sea the abundance and community structure of the MPB was influenced by the plume of the river Po. In the Gulf of Trieste, Si and P appeared to co-limit the abundance of MPB and, biomass of the MPB was inversely proportional to total nitrogen (Blasutto et al., 2005; Cibic et al., 2007; Franzo et al., 2015), whereas positive correlation was found between the abundance of MPB and ammonium, suggesting the preference for the ammonium for the MPB growth (Welker et al., 2002). The texture of the sediment also affects the community structure and biomass production; in sandy sediments, relatively lower biomass production has been reported than in muddy ones due to the different nutrient concentrations (Barranguet et al., 1998).

The northern Adriatic Sea (NAS) is highly influenced by the riverine waters which contribute the high content organic and inorganic nutrients. Hence, it is one of the most productive areas in the Mediterranean Sea (Campanelli et al., 2011; Cozzi & Giani, 2011; D'Ortenzio & Ribera D'Alcalà,

2009). It has been deeply investigated for planktonic communities, where several long-term data sets are available (Aubry et al., 2012; Neri et al., 2022; Totti et al., 2019), whereas studies on microphytobenthic communities are lesser and limited to shorter periods.

Despite the ecological importance of MPB in marine ecosystems, the MPB communities are poorly known, in terms of seasonal cycle and interannual variability, as they are not regularly monitored as are planktonic ones both by environmental agencies and by research institutions (no LTER sites involving MPB do exist at all).

In the Adriatic Sea, several studies investigated the composition, abundance and biomass of the MPB communities of epipelic (Cibic et al., 2007, 2012; Totti, 2003; Welker et al., 2002), epilithic (Car et al., 2020, 2021; Munda, 2005; Pennesi & Danovaro, 2017; Totti et al., 2007) and epiphytic (Accoroni et al., 2016) communities, reporting results sometimes conflicting.

This study aims to describe the seasonal variability and composition of the epipelic diatom communities in two subtidal areas in the northern Adriatic Sea as well as their relationships with environmental conditions.

2.3 Materials and Methods

2.3.1 Study area

Sediment samples were collected in the northern Adriatic Sea at two stations along the Marche region coast: Senigallia (SG) (N43°45.296' E13°35.629') located at 1.2 nM from the coast (bottom depth 12 m) and Portonovo (PN) (N43°34.761' E13°35.100') located at 1 nM (bottom depth 11 m) (Figure. 5).

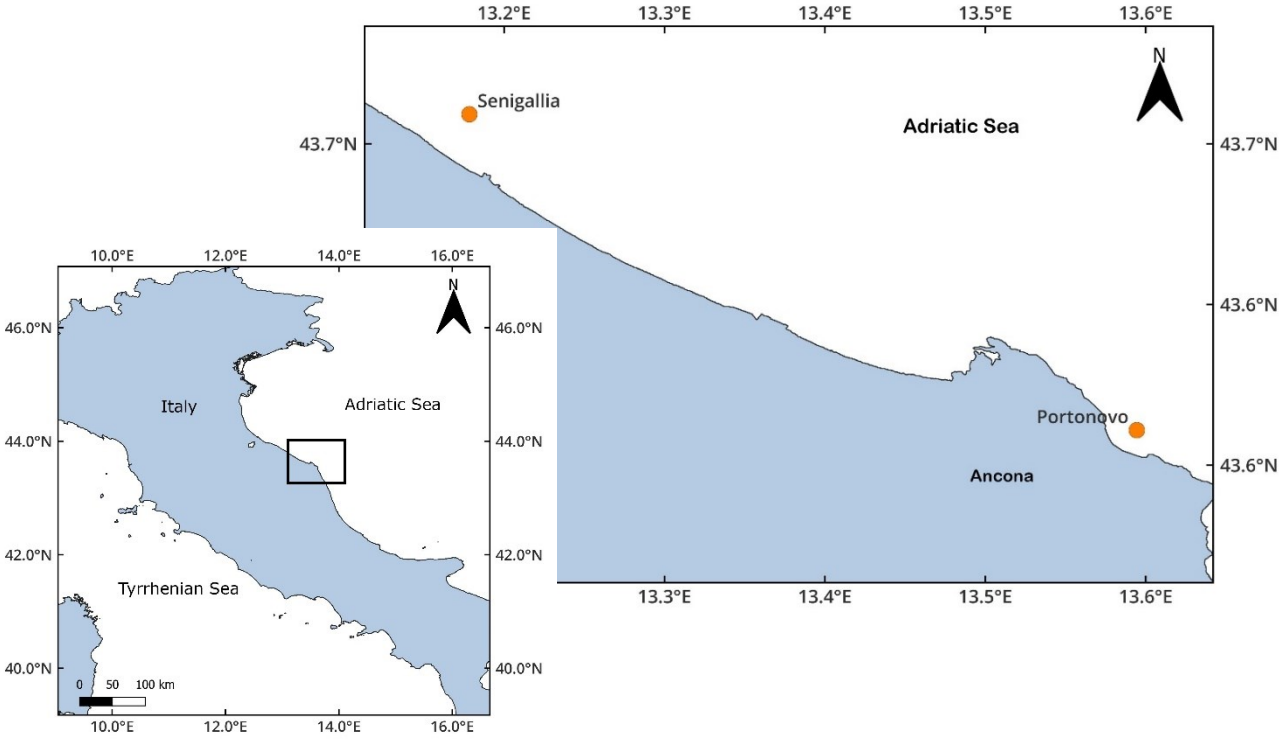

Figure. 5: Sampling stations near Ancona.

2.3.2 Environmental parameters

Temperature, salinity, pH, fluorescence and turbidity data were acquired by a (CTD) SeaBird Electronic SBE 911plus. Water samples for determination of dissolved inorganic nutrients (nitrite-NO_2, nitrate-NO_3, ammonia-NH_4, -orthophosphate-PO_4 and orthosilicate-$Si(OH)_4$) analysis were collected by Niskin bottles at surface and close to the bottom. Water samples for nutrient analysis were filtered (GF/F Whatman, 0.7 μm), and stored at −22 °C in polyethylene vials until analysis. Nutrient analysis was carried out using an autoanalyzer QUAATRO Technicon. Dissolved Inorganic

Nitrogen (DIN) concentration is intended as the sum of NO_2, NO_3 and NH_4 concentrations. The chlorophyll-a concentration was derived from fluorescence data.

2.3.3 Sediment sampling

Sediment samples were collected using "bottom grabs/Peterson grab" with a seasonal frequency in May (spring), July (summer), October (autumn) 2020, and January (winter) 2021. In each station bottom grab was lowered three times to collect samples in 3 replicates.

For each grab, a syringe with diameter of 2 cm was used to collect the top 1 cm of undisturbed sediment (about 10 ml of sediment) that was then placed into a sterile 50 ml plastic Falcon tube for diatom counting and identification. This sample was stored at +4 °C until the diatom extraction procedure. Another syringe sample was collected by the same grab for cell isolation (results will be reported in a separate paper).

2.3.4 Sediment grain size analysis

One sediment sample was also collected in each station for grain size and soil texture analysis which was carried out using the Mastersizer v3.81(Malvern Instruments Ltd.). At both the stations sediment structure was very fine sand (63−125 um).

2.3.5 Microphytobenthos extraction

Diatom cells were separated from sediment using the density centrifugation method with Ludox HS-40 Colloidal silica (Méléder et al., 2007). This procedure allows the separation of organic and mineral fractions of sediment based on their different densities, i.e.,~1.0 $g.cm^{-3}$ and ~2.5 $g.cm^{-3}$, respectively, on a Ludox HS-40 Colloidal silica, which has the density of ~1.3 g cm^{-3}. A mixture composed by 30 ml of Ludox and 5 ml of sediment was vigorously shaken and ultra-sonicated for 10 mins to detach diatom cells from sand grains. After this, centrifugation at 4500 rpm/15 mins was carried out to suspend diatom cells in the supernatant. This supernatant with diatoms centrifuged with water to get diatom cells in the pellet at 1300 rpm/15 mins. To eliminate Ludox completely, the pellet was

resuspended in distilled water and centrifuged at 1300 rpm/15 mins and rinsed several times. At the end, pellet (cells) was suspended in 10 ml distilled water with 400 µl 20% formaldehyde and stored in at + 4 °C for (i) counting at LM and (ii) cleaning treatment and SEM analysis.

2.3.6 Identification and counting

To identify and count the microalgae, fixed samples were homogenized, and then subsamples (variable volume from 0.1 to 4 ml) were taken with a pipette and settled overnight in a cylinder /chamber Utermöhl apparatus filled with 0.2% solution of formalin in filtered seawater.

The sample was then observed with a phase contrast inverted microscope (Zeiss Axiovert 135). Counting was carried out at 400x magnification in 30 random fields. Then, the whole chamber was analysed at 200x for a better estimation of larger and rarer species. Each cell was measured under light microscope to calculate the biovolume approximating species shapes to geometrical models (Hillebrand, 1999). Carbon content was calculated from mean cell bio volumes using (Menden-Deuer & Lessard, 2000). Identification was made at the lowest possible taxonomical level. In cases where cell identification was uncertain because of the small size or the indistinct morphology, cells were identified as undetermined pennate 1, pennate 2 and so on; then these taxa were analyzed using scanning electron microscope.

Diatom taxa were annotated according to their growth form: adnate, plocon, motile or erect (Round et al., 1990).

2.3.7 Cleaning and SEM

Subsamples (5 ml) were treated with nitric/sulfuric acids for SEM observation. Samples were first centrifuged at 3500 rpm for 10 mins to collect the pellet. Pellet was washed three times with distilled water to eliminate salt. To this pellet, one volume of 65% HNO_3 and 4 volumes of 98% H_2SO_4 (1:1:4, sample: HNO_3: H_2SO_4) were added under fume hood. This mixture was boiled till the fumes becomes colourless. Cooled down mixture was centrifuged at 3500 rpm for 30 mins and rinsed several times

with distilled water till pH was neutral. Cleaned diatom material was stored in distilled water with few drops of acetic acid to avoid the growth of fungi, bacteria and the dissolution of silica.

Before the SEM observation, one or few drops of the cleaned material were mounted on a nucleopore polycarbonate filter (0.4 μm), fixed on a metal stub and left to air dry completely. Then, this stub was sputter coated with a thin layer of gold-palladium. Stubs were observed using a scanning electron microscope FE-SEM Zeiss Supra 40.

2.3.8 Statistical analysis

To identify taxa that characterized the different seasons, the Indicator Value (IndVal) was applied, which combines the relative abundance of a species with its relative frequency of occurrence in a given period (Dufrêne & Legendre, 1997).

Non-Metric Multidimensional Scaling (NMDS) was performed on abundances and biomass of the diatom growth forms and environmental parameters, using the metaMDS function from the R vegan package (Oksanen et al., 2022) and setting the auto transform as true, to highlight the relationship between seasonal abundances of the four growth forms and environmental parameters for the two stations.

For each season, Shannon diversity index (H') (Shannon, 1948) was calculate using the diversity function available in the R vegan package (Oksanen et al., 2022). To test for significant differences between the two stations, two-sample Wilcoxon tests was calculated, using the Wilcox.test function in the stats package (R Core Team, 2021). The R software (R version 4.1.1, R Core Team, 2021) was used for this analysis.

Co-occurrence analysis was performed on presence-absence data using the cooccur package in R. Statistically significant pair-wise species co-occurrences (positive, negative or random associations) are calculated through the use of a probabilistic model (Veech, 2013) which compares the observed and the expected co-occurrences (Griffith et al., 2016; Veech, 2013). The R software (R version 4.1.1, R Core Team, 2021) was used for these analyses.

2.4 Results

2.4.1 Environmental variables

Variations in bottom temperature showed the typical trend (Figure. 6) with high temperature in summer (at bottom around 23° in PN and 21°C in SG) and low temperature (8-10°C) in winter. The autumn and spring had mild temperatures with values between 15 and 18°C. In all seasons, bottom temperature at PN station was slightly higher than at SG. At both stations salinity ranged between 35 and 38 in all the seasons (Figure. 7) and pH values were around 8. At SG, chlorophyll maximum was observed in winter (3.08 mg/m^3), while at PN in autumn (2.12 mg/m^3) (Figure. 8). Turbidity was highest in spring at both stations, with values around 4–6 NTU (Figure. 9) (Supplementary material Table 1).

The seasonal trend of DIN (Figure 10 a,b) was quite different between the two stations: in SG station the DIN showed the minimum value (2.11 μM) in spring and the maximum (18.04 μM) in winter, whereas in PN the minimum (5.70 μM) was observed in autumn and the maximum (13.41 μM) in summer. At both stations, nitrates represented the higher fraction of DIN except in spring and summer when the ammonia prevailed.

Phosphate concentration at SG station was maximum in autumn (0.31 μM) and minimum in spring and summer (0.06 μM), while at PN the maximum was in summer and winter (0.1 and 0.14 μM, respectively) and minimum in the spring and autumn (0.07 and 0.08 μM, respectively) (Figure. 11).

Silicate concentration at SG was maximum in summer and autumn (19.10 and 17.29 μM, respectively) and minimum in spring and winter (9.19 and 4.90 μM, respectively), whereas at PN silicate concentration was comparable in all seasons with a slight decrease in autumn (5.64 μM) (Figure. 12).

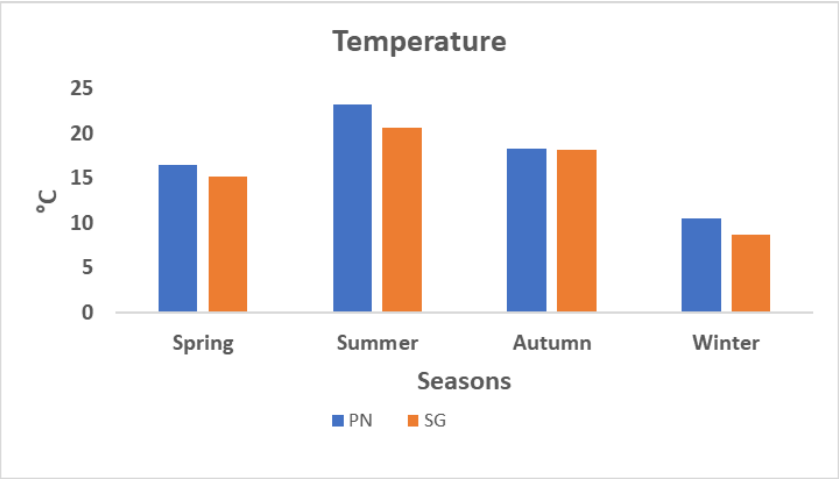

Figure. 6. Temperature concentrations near the bottom at both stations in the different seasons

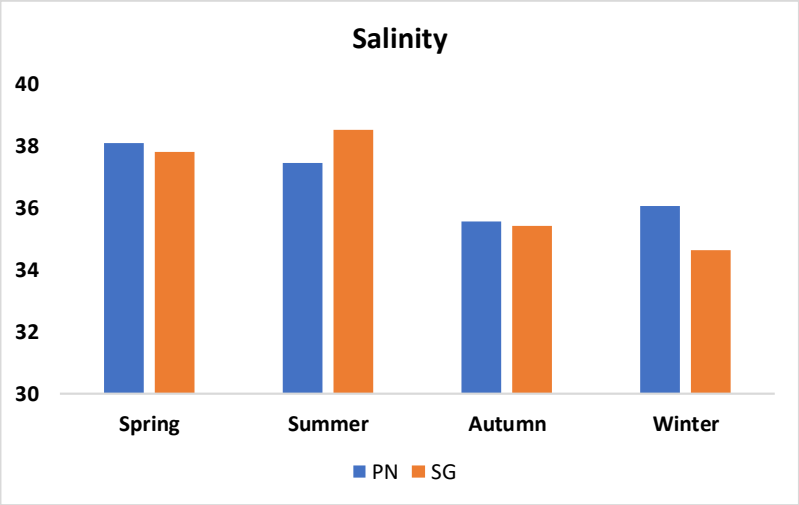

Figure. 7. Salinity concentrations near the bottom at both stations in the different seasons

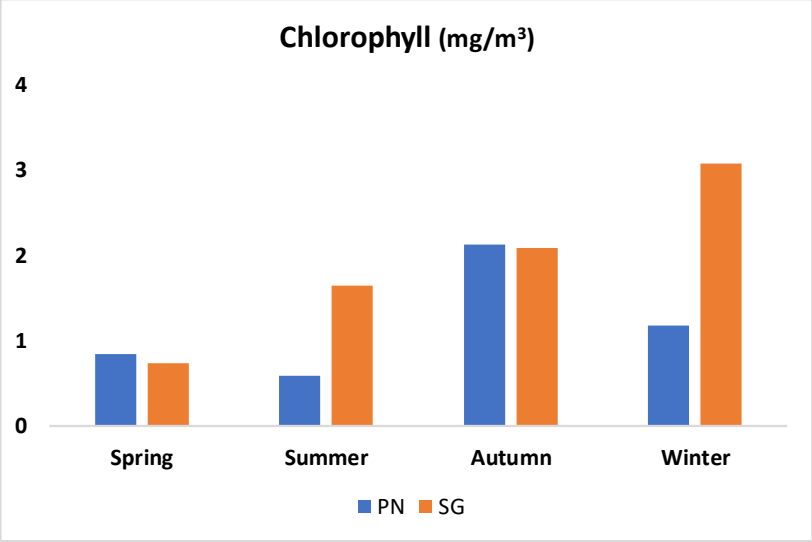

Figure. 8. Chlorophyll concentrations near the bottom at both stations in the different seasons

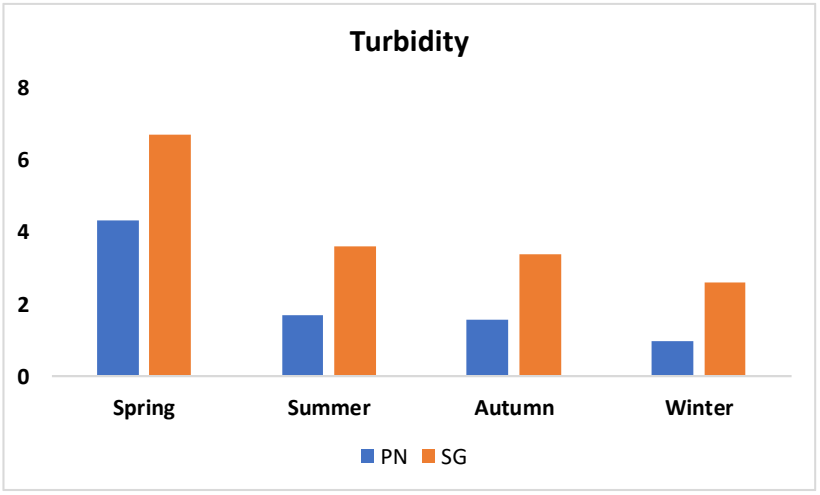

Figure. 9. Turbidity measurements in the water column at both stations in the different seasons

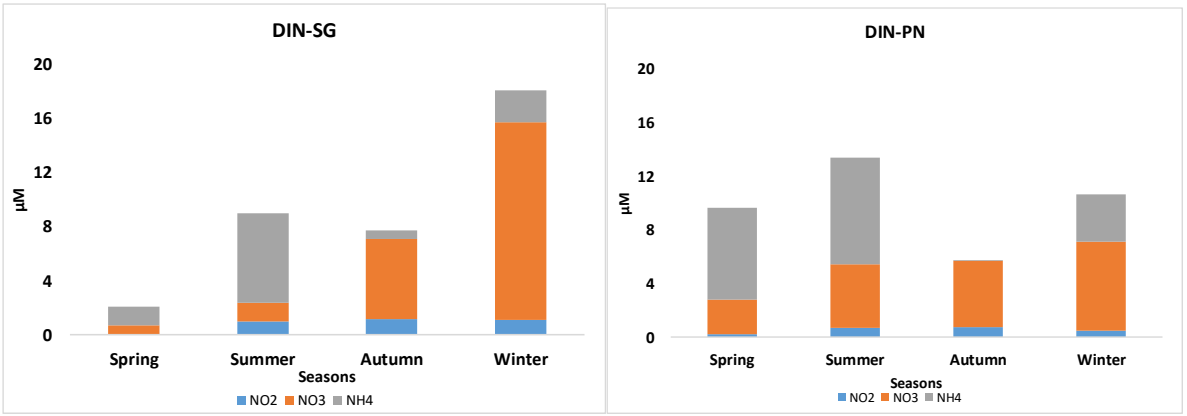

Figure. 10: DIN concentrations divided in nitrate, nitrite and ammonia near the bottom at both stations in the different seasons a) SG b) PN.

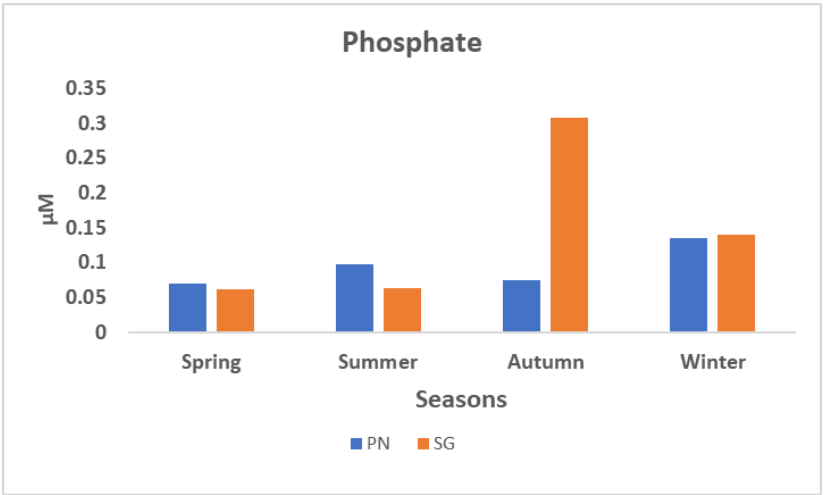

Figure. 11: Phosphate concentrations near the bottom at both stations in the different seasons.

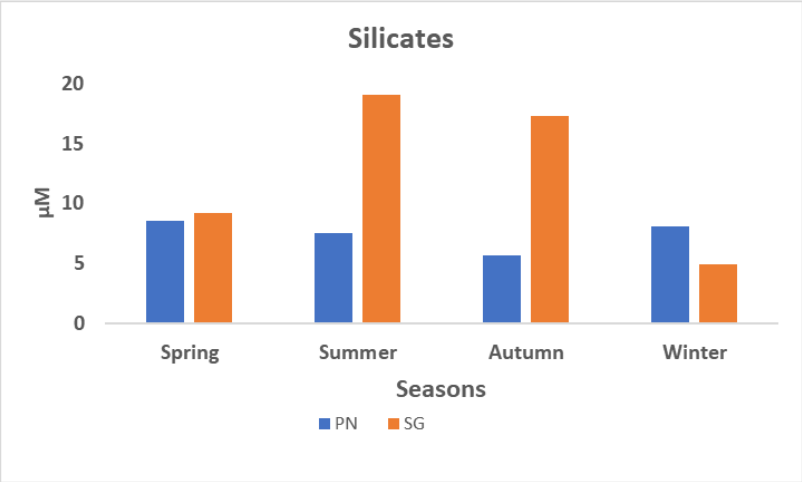

Figure. 12: Silicates concentrations near the bottom at both stations in the different seasons

2.4.2 Taxonomic composition

The full list of taxa is presented as supplement (Table S2) and their detailed morphological illustrations in Chapter 4. In total 118 taxa of diatoms were found, 51 of them identified to the species/subspecies level (Supplementary Table S2). Among them, the richest families were Naviculaceae (15 taxa), Bacillariaceae (12 taxa) and Catenulaceae (8 taxa). Among them, *Amphora, Navicula* and *Nitzschia* genera were dominant throughout the year at both stations, while genera like *Cocconeis, Fallacia* and *Odontella* were also observed in all the sampling though the specific diversity was lower. In regard to growth forms, 14 species were adnate, 72 were motile, and 23 were plocon and 5 erect while 4 were araphid. Detailed contribution of these growth forms to abundance and biomass is showed and discussed further. Abundance and biomass data are provided in the supplementary table 3 and 4.

2.4.3 Benthic diatoms' abundance and biomass

At both stations, the maximum cell abundance was found in spring (77,727 cells/cm^2 in PN and 69,506 cells/cm^2 in SG) and the minimum in summer (4,640 cells/cm^2 in PN and 7,225 cells/cm^2 in SG). However, in SG no significant differences were observed among seasons, whilst in PN only spring cell density (77,727 ± 30,445 cells/cm^2) was found to be significantly higher ($p < 0.05$) than summer one (12,660 ± 3,545 cells/cm^2) (Figure. 13).

In autumn, the MPB was slightly more abundant in SG station 26,277 cells/cm^2 than PN station 15,705 cells/cm^2. In winter cell density was 10,467 cells/cm^2 at SG and 12,660 cells/cm^2 at PN station. In both stations, MPB abundance did not significantly differ between the autumn and winter.

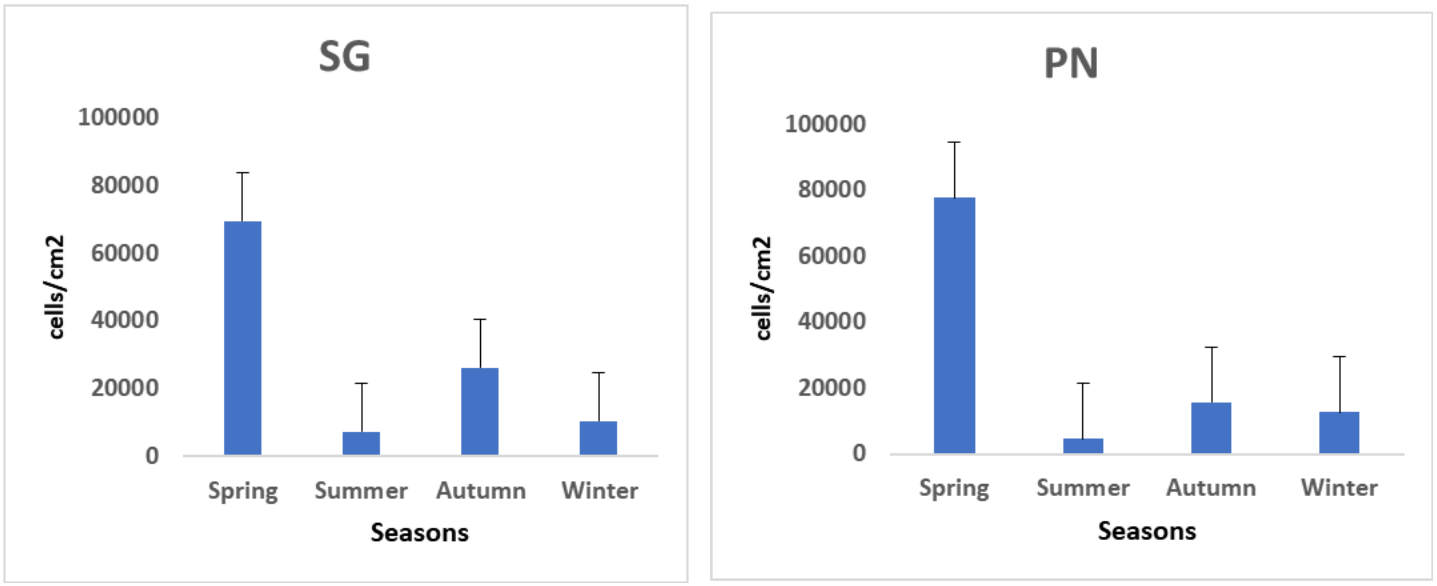

Figure. 13: Total diatoms' abundance (cells/cm^2) at Senigallia (SG) and Portonovo (PN) stations.

At both stations, microphytobenthos biomass (Figure. 14) was maximum in spring (3.70 and 3.43 µg C/cm^2 at SG and PN stations, respectively), and minimum in summer (0.55 and 0.59 µg C/cm^2 at SG and PN stations, respectively. In autumn, biomass was nearly similar at the two stations: 2.18 and 2.71 µg C/cm^2 at SG and PN, respectively. Biomass was 0.78 µg C/cm^2 at SG and 1.60 µg C/cm^2 at PN in winter. No significant difference was found among seasons for both the stations.

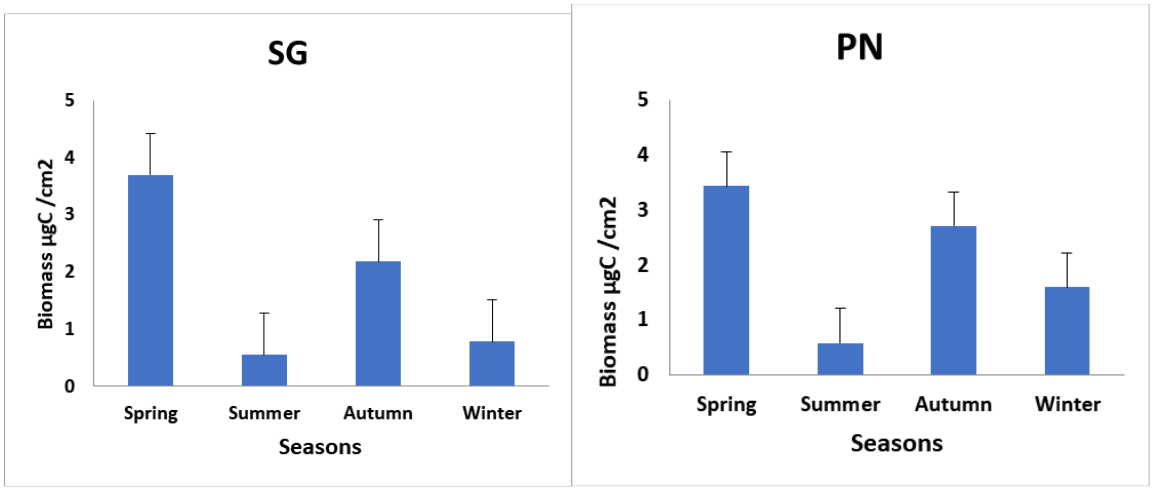

Figure. 14: Total diatoms' biomass (µg C/cm^2) at Senigallia (SG) and Portonovo (PN) stations.

At both stations, the community composition of benthic diatoms showed that the motile growth forms were the most represented in terms of abundance followed by the adnate, except than in summer at SG station, when adnate diatoms were dominating. The importance of adnate diatoms decreased in autumn and winter when motile forms were markedly dominant. Motile diatoms trend paralleled that of total community, with maximum in spring and minimum in summer. The most abundant motile taxa were *Diploneis* and *Navicula* while *Amphora* was the most important adnate genus. Plocon forms were mainly represented by Biddulphiaceae (*Odontella* and *Biddulphia* species). Their contribution was minimum in spring in both station; in PN station their contribution was higher than that of adnate in autumn and winter. In both stations the contribution of erect diatoms (*Tabularia*, *Rhaponeis* and *Achnanthes*) was very low (Figure. 15).

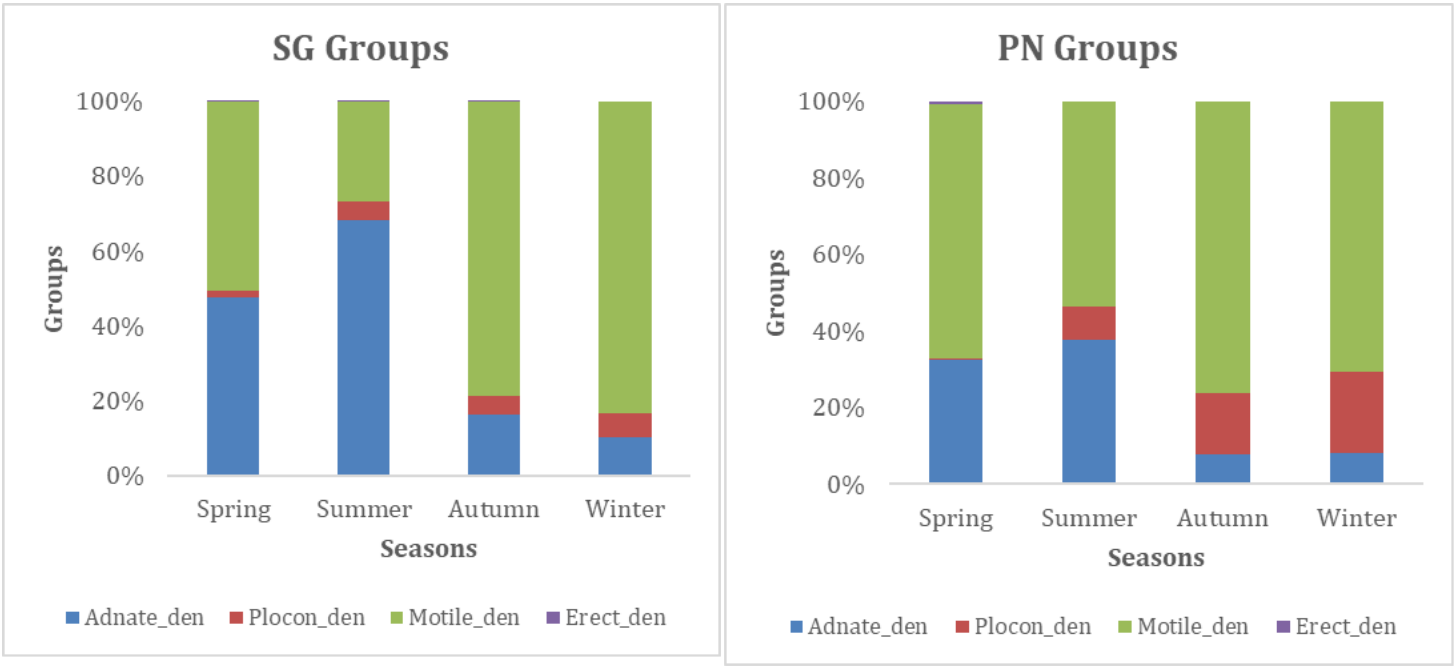

Figure. 15: Percent abundance of different diatom growth forms in the two sampling stations.

At SG, the abundance of adnate forms was significantly higher in spring (33,160 ± 13,135 cells/cm^2) than in winter (1,081 ± 545 cells/cm^2, $p<0.05$). At PN the abundance of motile diatoms was significantly higher in spring (51,646 ± 19,320 cells/cm^2) than in summer (2,491 ± 417 cells/cm^2, $p<0.05$).

The community composition in terms of biomass showed that in spring the community was dominated by adnate forms (mainly *Amphora*) followed by motile (*Diploneis*, *Navicula*) and by taxa belonging to plocon (Biddulphiales) at both stations. During summer, the contribution to the biomass of plocon increased in both stations and at PN it was higher than that of adnate (Figure. 16). In autumn, plocon showed the maximum percent biomass at both stations, followed by motile and adnate. In winter, plocon was still the maximum contributor to the biomass at PN station, while at SG station plocon and motile forms showed comparable values. At both stations, erect forms gave a minimum contribution to diatom biomass (Figure.16).

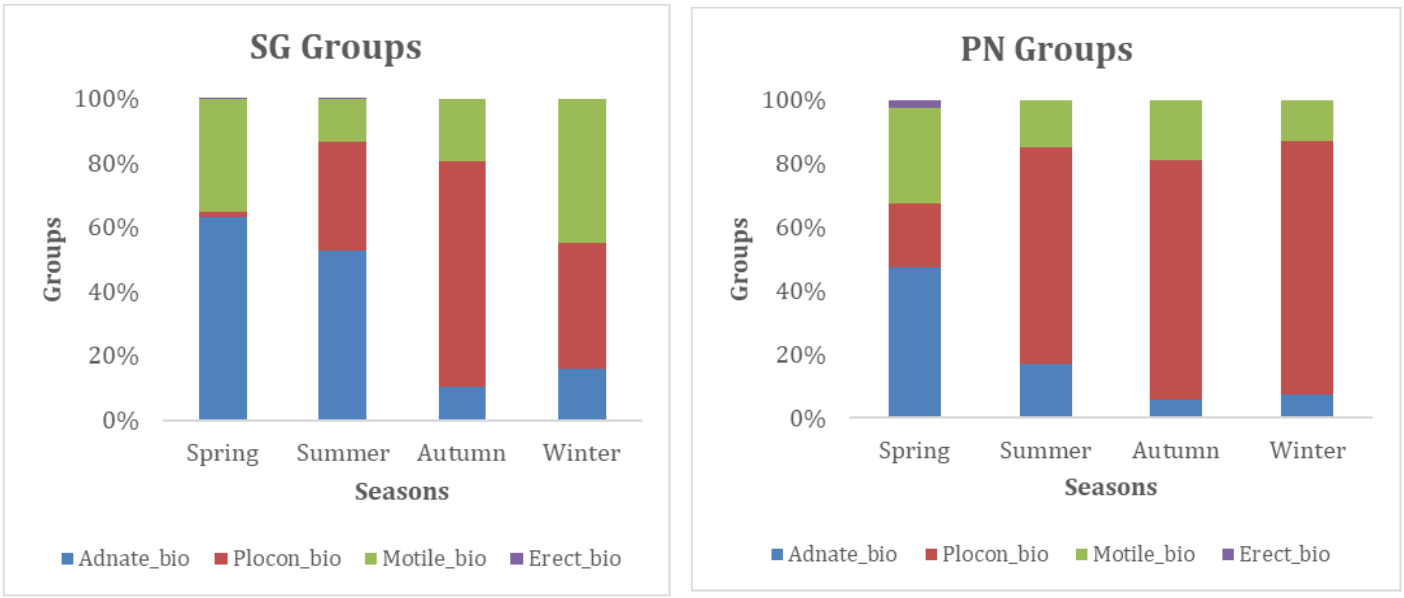

Figure. 16: Percent biomass of different diatom growth forms in the two sampling stations.

In both stations, the biomass of motile form was significantly higher in spring (1.31 ± 0.68 and 1.04 ± 0.37 µg C/cm^2, respectively, $p<0.05$) than in summer (0.07 ± 0.03 and 0.08 ± 0.02 µg C/cm^2, respectively, $p<0.05$). Furthermore, at SG station, a significantly higher biomass of plocon was observed in autumn (1.53 ± 0.4 µg C/cm^2) than in spring (0.06 ± 0.008 µg C/cm^2, $p<0.05$).

2.4.4 Community composition

Indicator Value analysis (IndVal) was performed for four seasons to highlight the indicator species of the season irrespective of stations. IndVal analysis showed that in the spring adnate forms like *Amphora* cf. *proteus, Amphora copulata*, and motile forms like *Fallacia* cf. *forcipata and Surirella* sp. were indicative. In the summer, motile form, *Navicula distans* was only indicative of this season. The plocon form diatoms were indicative for autumn and winter, *Cyclotella striata* in autumn and *Odontella* sp. 2 in winter.

Table 1: List of MPB taxa characterized by the highest IndVal for each season calculated for the top layer of sediment irrespective of stations. Significant p values are expressed like following: $p < 0.05$ *, $p < 0.01$ **, at $p < 0.001$ ***. The shades of colour are proportional to the IndVal values, from dark green to white, in decreasing order.

Species name	Spring	Summer	Autumn	Winter
Fallacia cf. *forcipata (*Greville) Stickle & D.G.Mann	96.075**	1.418	1.042	1.465
Surirella sp.	95.244*	0.679	0.94	2.797
Amphora cf. *proteus* W.Gregory	80.378***	8.631	7.809	3.182
Amphora copulata (Kützing) Schoeman & R.E.M.Archibald 1986	78.209**	16.005	5.162	0.625
Pleurosigma cf. *latum* Cleve	43.832	6.113	10.954	36.044
Amphora cf. *graeffei* Grunow	31.429	0.476	0	8.333
Nitzschia longissima (Brébisson) Ralfs	0.829	95.907*	0.372	0.2
Navicula distans (W.Smith) Brébisson	2.454	94.594***	0.455	1.337
Navicula sp. 2	24.186	65.055	7.494	1.178
Psammodictyon panduriforme (W.Gregory) D.G.Mann	33.891	59.789	1.962	2.644
Campylodiscus sp.	16.071	47.768	0.558	0.446
Nitzschia cf. *sigma* (Kützing) W.Smith	2.759	39.395	10.284	0.089
Diploneis weissflogiopsis Lobban & Pennesi	3.835	29.115	1.47	6.616
Gyrosigma cf. *balticum* (Ehrenberg) Rabenhorst	0	23.043	8.986	0
Thalassiosira sp. 1	0.013	0.439	82.505	0.013
Cyclotella striata Prasad	0.148	3.552	60.785*	16.721
Pennate sp. 9	0	2.174	40.217	1.087
Halamphora coffeiformis (C.Agardh) Mereschkowsky	9.942	0.488	28.432	26.76
Cocconeis sp.	14.957	2.564	27.436	11.026
Navicula sp. 4	0.99	5.961	24.81	23.947
Odontella sp. 2	4.387	0.105	0	60.871**
Ralfsiella smithii (Ralfs) P.A.Sims, D.M.Williams & Ashworth	2.155	9.926	7.613	45.063
Odontella sp. 1	10.577	0.321	3.205	37.821
Tryblionella cf. *marginulata* (Grunow) D.G.Mann	0	18.106	9.053	33.705
Coscinodiscus sp. 1	5.983	3.675	1.709	11.88
Caloneis sp.	7.884	5.788	0	8.25

The Shannon diversity index (Figure. 17) showed no significant differences between the two stations, in all the seasons ($p>0.05$), although lower values were found in winter compared to the other seasons.

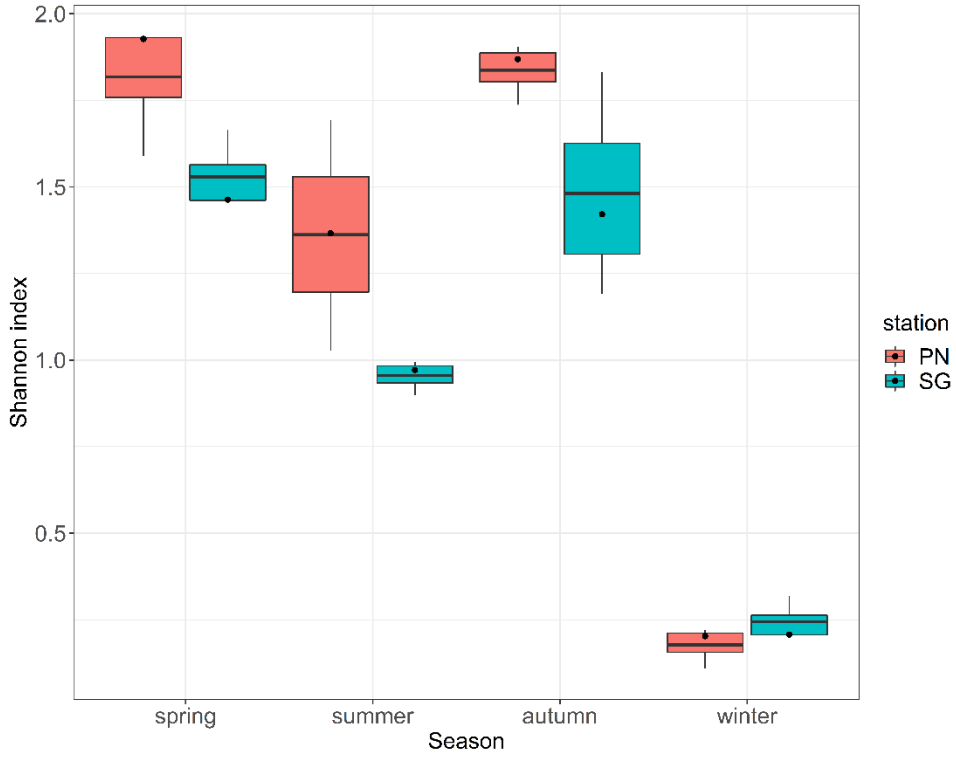

Figure. 17: Shannon's index (H') in the four seasons at two stations

Observing the NMDS (Figure. 18), it seems that the seasonal abundances were mainly related to temperature and nutrients (i.e., DIN, phosphate and silicates). The two stations did not differ each other, while considering the seasons, spring and summer were clearly separated. These results were confirmed by the PERMANOVA as no significant differences were found between stations ($p>0.05$), while significant differences were found between seasons ($p<0.001$).

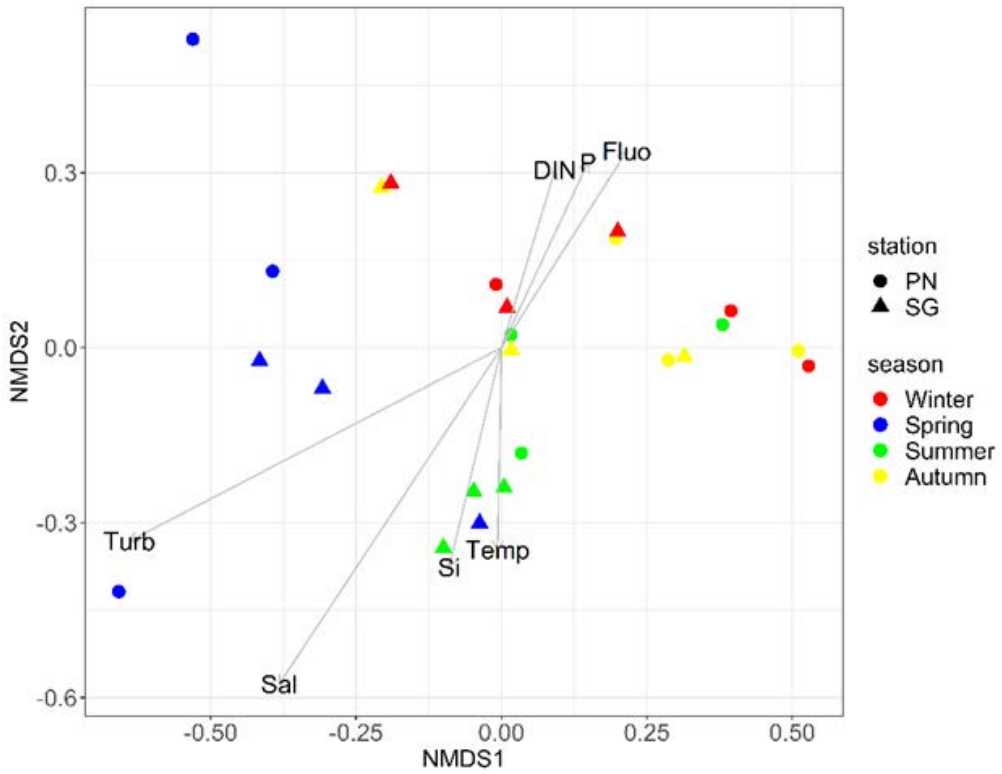

Figure. 18: NMDS was performed on the seasonal abundances of the four growth forms and environmental parameters for the two stations. [The points represent the abundances, while the arrows represent the environmental parameters fitted on the NMDS.]

2.4.5 Species co-occurrence

In this analysis, the 51.41 and 44.98% of the total species pair combinations of SG and PN respectively were removed from the total of species pairing, because of the low pair combination (<1), that means that the pairing was not relevant. In the SG station, the 92.7% were random, 4.8% was unclassifiable, and the remaining 2.5% was non-random (1% and 1.45% for positive and negative co-occurrences, respectively). The taxa involved in non-random pair associations are showed in (Figure. 19A). In the PN station, 95.2% were random, 2.8% were unclassifiable and 2% was non-random (0.8% and 1.2% for positive and negative co-occurrences, respectively). The taxa that resulted involved in positive and negative co-occurrences are showed in (Figure. 19B).

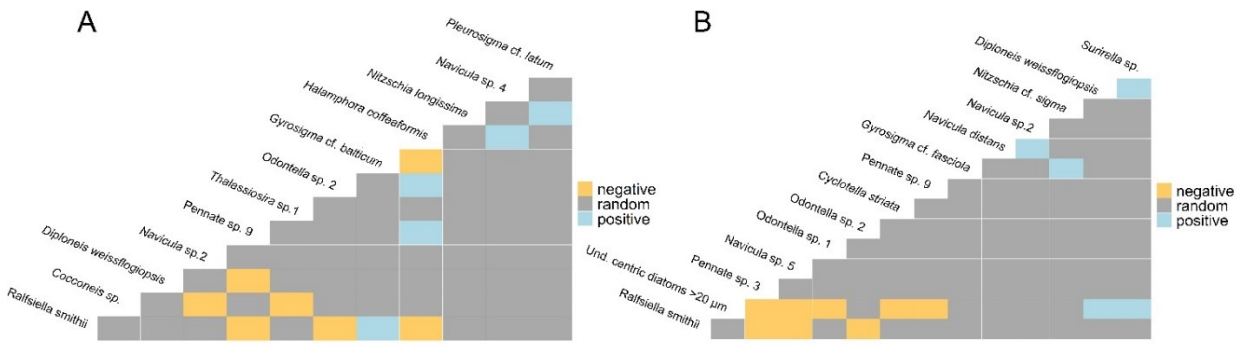

Figure.19: Species co-occurrence at stations A) SG B) PN stations

2.5 Discussion

The present study is an attempt to investigate the seasonal abundance and biomass of epipelic diatoms in two distinct sites of the Adriatic coastal area. The two sites have a similar granulometric composition and the same depth, and, although unfortunately in this study we did not measure the light penetration, we assume that the light conditions in both areas were comparable. Even though one of the sites- Senigallia is partly affected by mussel cultivation nearby, results did not show important differences in the seasonal variability of nutrient concentrations and diatom abundance and biomass with respect to the site-Portonovo. The annual cycle of epipelic diatoms abundances at the two stations was comparable, with maximum values in spring, followed by a summer decline and a further increase in autumn.

The abundance values observed in this study are of the same order of magnitude as those reported in previous studies in the Adriatic Sea by (Franzo et al., 2015), (Rogelja et al., 2016), (Tolomio et al., 2002), and (Welker et al., 2002). On the contrary, abundances found in this study were lower than (T. Cibic et al., 2007, 2012), (Sdrigotti et al., 1999), (Tolomio et al., 1999) and (Facca & Sfriso, 2007), (Facca et al., 2002), and higher than (Totti, 2003).

We should also notice that such differences could be explained by the depth of sampled sediment, and by the method of analysis such as direct counting after dilutions of the sediment, separation of diatom cells using gradient centrifugation.

Table 2: Summary of benthic diatom abundances from different sites in the Mediterranean Sea

References	cells/cm^2	Location/(Bottom depth)
This study	**4,640 -77,727**	**Ancona (11-12 m)**
Cibic et al 2007	19,600 - 106,400	Gulf of Trieste/(17m)
Cibic et al., 2012	10,911 - 106,505	Gulf of Trieste/(17-21m)
Facca et al., 2002a	700,000 - 10,400,000	Venice lagoon/ (0.8, 1, 1.1m)
Facca et al., 2007	260,000 - 5,650,000	Venice lagoon/(1-1.2m)
Franzo et al.,2015	9,900 - 111,600	Emilia-Romagna coast (N Adriatic Sea)/ (13- 50m)
Rogelja et.al. 2016	1,617 - 20,045	gas and thermal vents in the Aeolian Islands (Tyrrhenian Sea, Italy)/ (11-21m)
Sdrigotti et.al. 1999	22,333 - 1,495,500	Gulf of Trieste/(12-13m)
Totti, 2003	728 - 9,278	N Adriatic sea/(14 to 66m)
Tolomio et al., 1999	200,000 - 1,800,000	South basin of venice lagoon
Tolomio et al., 2002	1,800 - 70,000	South basin of venice lagoon
Welker et al., 2002	1,434 - 57,992	Gulf of Trieste (N Adriatic Sea)/20m

2.5.1 Seasonal cycle

In our study at both stations, we observed the highest diatom abundance and biomass values in spring and the minimum in summer. This cycle partly differed from what reported in other Mediterranean areas, where the maximum biomass was generally observed in the spring and summer and the minimum from autumn to winter (Cibic et al., 2007, 2012; Méléder et al., 2007). In summer the minimum values are reported for the northern Adriatic by (Facca et al., 2002) and (Franzo et al., 2015). The maximum in spring has been generally related to the increasing photoperiod and light intensity, considering that the light represents the most common limiting factor for the MPB growth (Welker et al., 2002). Although the grazing pressure has not been measured in this study, we hypothesize that the sudden decrease in cell abundance in the summer could be related to the grazing effect, considering that meiofauna which represents the major consumer of MPB (Schratzberger & Ingels, 2018) typically increase in summer (Balsamo et al., 2010). Particularly in the subtidal areas, there is a high possibility of cells being washed away, resulting in the downward migration of epipelic cells, which ultimately saves them from the grazers (Bennett et al., 2000; Smith & Underwood, 1998).

2.5.2 Environmental factors and nutrient ratios

Nutrients like phosphates, nitrogen and silicates can also affect the abundance and biomass of the diatoms. In the past, it was assumed that MPB had an abundant supply of nutrients from the sediment pore water. Although this pore water contains a higher amount of nutrients than the overlying water column, a correlation between nutrients in the bottom-overlaying water and the MPB abundance was also found (Welker et al. 2002, 2007). It was observed that, whenever ratios between nutrients in the water column are unbalanced, the MPB growth was determined by the limiting nutrient. For instance, it is obvious that silica is the most important nutrient for the diatom cell to build its frustule and its depletion ultimately reduces the cell metabolism. The optimal nutrient ratio (Si:N:P) for diatoms is 16:16:1 (Brzezinski, 1985; Hillebrand & Sommer, 1997).

At both stations and in all seasons, the high N: P ratio highlighted the strong P limitation, that have been the typical condition of the Adriatic Sea (Grilli et al., 2020), but it is assumed that diatoms, as other microalgae can also exploit the organic P sources, making the estimation of P limitation more complex. Currently the most important source of Si in the Mediterranean Sea are riverine waters and groundwater discharges (Sospedra et al., 2018). At station SG, the Si concentration was higher than the DIN one in all the seasons, except winter, likely because of the seasonal bloom of the planktonic diatom *Skeletonema marinoi*, reaching abundances up to 10^6-10^7 cells/l and during which the concentration of Si typically decreases, as it is rapidly uptaken by phytoplankton. At the PN station, where the impact of riverine waters is modest, DIN is higher than Si in all the seasons, suggesting that the Si can be limiting factor.

Interestingly, in both stations, we noted a higher ammonium concentration than the nitrite and nitrate ones in spring and summer, even though we observed the highest and lowest MPB abundance respectively. As diatoms typically prefer ammonium over nitrites and nitrates (Welker et al., 2002)

this, coupled with the increased daylight period, could have enhanced the spring MPB growth, whereas in summer the grazing pressure could have caused the decrease.

2.5.3 Community composition

Motile forms were dominant at all the seasons, as already reported by Totti (2003) in the northern Adriatic Sea. The abundance of motile forms could be explained by their high ability to move across the sediment in which they are the better competitors for nutrients and light (DeNicola & McIntire, 1990; Lange et al., 2011). Interestingly, even though motile were abundant in all the seasons, their contribution to biomass was low, considering that they were mainly composed by small pennate forms. Adnate were the second group in terms of abundances and showed their maximum in spring, while in other seasons low values were observed. Among the adnate, only *Amphora* species were observed, while the presence of *Cocconeis* was negligible, as it commonly lives as epiphyte (de Stefano et al., 2000), epilithic (Car et al., 2020, 2021; Totti et al., 2007) or epizoic (Romagnoli et al., 2007; Totti et al., 2009) modes. The almost negligible presence of erect diatoms was expected, as they need solid substratum to attach. Plocon diatoms represented a major contributor to diatom biomass, given the high biovolumes of the centric benthic species, as those belonging to Biddulphiales. Their contribution was minimum in spring, when the maximum of MPB abundance was observed.

Diatoms resulting significantly indicators of spring and summer belong to motile and adnate growth forms (the latter only for spring), while those indicator of autumn and winter belong to plocon. In diatom studies growth forms has been applied mostly to describe community structure (e.g., Hudon & Legendre, 1987; Pringle, 1990). This could suggest the importance of growth forms in the community composition and seasonal dominance of the taxa.

In both stations, the co-occurrence analysis showed that in the microphytobenthos community the majority of the interactions were random. These positive and negative interactions between different diatom taxa suggest that they play important role in the formation of the communities in different

environmental conditions, independently of if they are indicator or not of a particular season of a station.

2.6 Conclusions

In conclusion, this study provides important results in terms of the quantitative distribution (abundance and biomass), community structure and taxonomic composition about the marine epipelic diatoms in the subtidal sediments of the Adriatic Sea. The motile forms like *Navicula, Nitzschia, Fallacia, Psammodictyon* were dominant at both stations. Benthic diatoms express a marked seasonal behaviour, with maximum abundance, biomass and biodiversity in spring. The seasonal species composition was also highlighted, indicating that an increase of big sized centrics (*Odontella*) belonging to plocon was highlighted in autumn causing an increase of biomass. This study highlighted that there was no marked spatial variability between the two stations that resulted similar in terms of diversity and seasonal trend. Given the ecological importance of MPB, further studies on benthic diatom communities in subtidal areas are required to increase the knowledge about their diversity and variability, and it would be recommended that the study of microphytobenthic communities would be inserted in the long-term monitoring programs.

Chapter 3. **Identification of benthic diatoms isolated from the Adriatic and Tyrrhenian Seas: integrating morphological and molecular approaches**

3.1 Abstract

Benthic diatom diversity at different sites located on the Northern Adriatic and Tyrrhenian coasts was analysed with and integrative approach based on a combination of morphological and molecular methods. In total 59 unialgal strains were established and cultivated. All strains were tentatively identified by light microscopy and sequenced for the 18S rRNA. The BLAST search indicated that most of the strains showed low similarity with reference sequence available on the GenBank. All 18S RNA gene sequences were then placed in a tree containing 541 partial sequences of the 18S rRNA gene in order to analyse their phylogenetic relationships. Finally, 13 strains that showed a questionable position in the tree, were analyzed at SEM and TEM for detailed ultrastructural analysis and species identification. In this study, only four strains were identified at the species level with a 100% similarity with reference sequences of 18S rRNA that was in agreement with the morphological identification. This study confirms that there is a need to use a polyphasic approach in the study of benthic diatom diversity in order to improve reference databases with reliable morphological and molecular data on high number of species.

3.2 Introduction

Microphytobenthic communities play an important role in the aquatic ecosystem for their high contribution to primary production and their role in the food webs and in the biogeochemical cycles (H. L. MacIntyre et al., 1996; Miller et al., 1996). A major part of these communities is dominated by benthic diatoms (Bacillariophyta). They are more diverse than planktonic diatoms in terms of number of species and life forms (Round et al., 1990). For the better understanding of the impact and applications of benthic diatoms it is important to know their taxonomy in detail. However, different taxonomist used various systems to classify diatoms based on the morphological characters and reproduction systems. Now it is crucial to combine morphological and molecular approaches to assess the role and functioning of common species in benthic diatom communities. In addition, molecular approaches also help to resolve the evolutionary position of the particular taxa.

Many studies have focused on the species composition of benthic diatom assemblages. Yet, the classification of benthic diatoms based solely on morphology still remains challenging and problematic. This is partly because of their often-small size and simple forms as compared to planktonic ones. Moreover, it often is not clear if small differences with the type material are because the frustules of the examined specimens belong to different species or result from morphological plasticity in response to environmental variation. In recent years, scientists have used a so-called polyphasic approach to identify new species (Mucko et al., 2020a) and pseudo-cryptic diversity in morphologically defined species (Kollár et al., 2019), often by re-examining taxa traditionally described by means of light microscopy with more sophisticated morphological (scanning and transmission electron microscopy) and molecular means (Kermarrec et al., 2011). The use of molecular markers such as the 18S rRNA-gene along with *rbc*L (Ribulose 1,5 bisphosphate carboxylase/oxygenase), COX1 (Cytochrome C-oxidase subunit 1) and ITS rDNA has enhanced the research interest in the area of phylogeny, evolution and taxonomy of diatoms (Evans et al., 2007; Jahn, 2007; Mann et al., 2010; Theriot et al., 2015; Witkowski et al., 2016). Further, the 18S rRNA-

gene has been widely used in the interest of metabarcoding purposes to assess community structure of benthic diatoms.

Many studies have used combined morphological - molecular approaches to identify and compare species (Alverson & Theriot, 2005; Bruder & Medlin, 2008a; Kooistra et al., 2003; Kulikovskiy et al., 2019; Pennesi et al., 2012; Pennesi & Danovaro, 2017; Skibbe et al., 2018; Stachura-Suchoples et al., 2016; Zgrundo et al., 2013). Along the Mediterranean coasts, only few detailed taxonomy studies have been carried out on benthic diatoms collected from the natural (Akcaalan et al., 2022; Cibic, 2010; Çolak Sabanci, 2011; Facca & Sfriso, 2007; Kaleli et al., 2020; Pérez-Burillo et al., 2022; Sabanci, 2012; Totti, 2003) and artificial substrata (Munda, 2005; Pennesi & Danovaro, 2017; Totti et al., 2007). Recently, Álvarez-Blanco (2014) published a book on the taxonomic study of the coastal benthic diatoms collected from seven northern Mediterranean sites (Italy, Spain, Greece, Turkey) in the spring of 2010. This study reported around 120 taxa (belonging to 73 different genera) with eight new records for the Mediterranean Sea. Considering the importance of the diatoms in the environment, a molecular taxonomic study will enable me to compare findings based on morphology with molecular data. Therefore, in this chapter, I combined morphological and molecular approaches to identify and characterize the benthic diatoms and also provide sequences that will be useful for following taxonomic and ecological studies..

3.3 Materials and methods

3.3.1 Study area

Sampling stations were chosen on two sides of the Italian peninsula: two on the Adriatic side near Ancona, and eleven on the Tyrrhenian side near Naples (Figure. 20, Table 1).

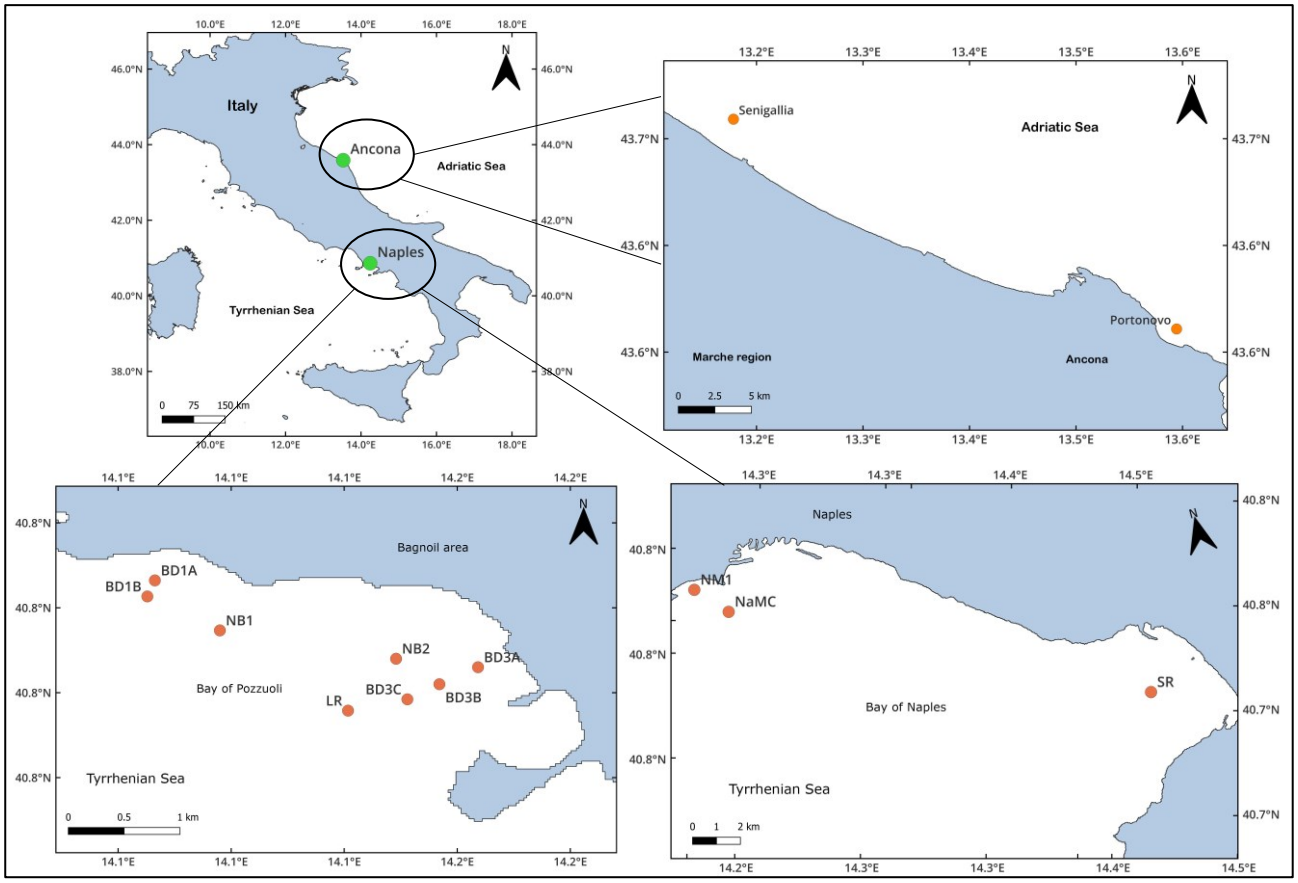

Figure. 20: Sampling stations in the Adriatic and Tyrrhenian Seas.

The two Adriatic stations were located in front of Senigallia (SG) and Portonovo (PN), in the lower part of the northern Adriatic basin, that is a highly productive area experiencing moderate to high input of riverine waters (mainly the river Po), that affect both the trophic state and the circulation regime (Campanelli et al., 2011; Cozzi & Giani, 2011; D'Ortenzio & Ribera D'Alcalà, 2009). SG is the coastal station of the LTER (i.e. Long Term Ecological Research)-Senigallia-Susak transect,

where physico-chemical parameters and phytoplankton are recorded since 1988 (Neri et al., 2022; Totti et al., 2019). PN station is located in the coastal area in front of the Conero Riviera and has been sampled since 2007.

The Tyrrhenian stations comprise the LTER station NEREA near the mouth of the river Sarno, two stations near the city of Naples of which one is the LTER station MareChiara, and nine stations in the Bay of Pozzuoli (Figure. 21, Table 3). The purpose of selecting many stations near Naples was to increase the diversity database by isolating many strains at sites under influence of contrasting ecological conditions and different intensities of human impact. For instance, the Bay of Pozzuoli has been contaminated strongly with heavy metals by the -now closed- Bagnoli steel smelters while the station near the mouth of the Sarno river is impacted by intermittent high levels of nutrients as this river is the most polluted in the world (Montuori et al., 2013).

Table 3: The sampled stations along the Adriatic and Tyrrhenian coasts and the strains collected from material sampled at these stations.

Station	**Location**	**Coordinates (N, E)**	**Depth (m)**	**Sampling Date**	**Strains**	**No of strains**
BD1A	Pozzuoli Bay	40.8179,14.1279	10	21-10-2019	BD1, BD2, BD3, BD4, BD5, BD6, BD7	7
BD1B	Pozzuoli Bay	40.8162,14.1271	20	21-10-2019	BD8, BD9, BD10, BD11	4
BD3A	Pozzuoli Bay	40.8087,14.1622	10	21-10-2019	BD12	1
BD3B	Pozzuoli Bay	40.8069,14.1622	20	21-10-2019	BD13	1
BD3C	Pozzuoli Bay	40.8053,14.1547	40	21-10-2019	BD15, BD16	2
LR	Pozzuoli Bay	40.8041,14.1484	55	05-12-2018	LR13, LR26, LR34, LR40, LR43	5
NB1	Pozzuoli Bay	40.8126,14.1348	30	21-09-2020	NB11	1
NB2	Pozzuoli Bay	40.8096,14.1535	19.7	21-09-2020	NB21, NB22, NB23, NB29	4

NM1	Bay of Naples	40.8272,14.235	20	21-09-2020	NM11, NM12, NM14, NM17	4
NaMC (LTER MC)	Bay of Naples	40.8123,14.2486	75	07-07-2020	NaMC2, NaMC3	2
SR	Bay of Naples (Sarno river mouth)	40.72, 14.44	12-13	09-07-2021	SRA, SRD	2
PN	Ancona	43.5795, 13.585	12-13	4 different season sampling (2020-2021) May (spring), July (summer), October (autumn) 2020, and January (winter) 2021	PN11, PN12, PN21, PN23, PN31, PN4A, PN4Am, PN4B, PN4BA, PN4C, PN4DP, PN4E, PN4F, PN4G	14
SG (LTER Senigallia-Susak transect)	Ancona	43.7565, 13.2105	50	4 different seasons (2020-2021) May (spring), July (summer), October (autumn) 2020, and January (winter) 2021	SG11, SG12, SG22, SG23, SG27, SG31, SG34, SG35, SG4A, SG4C, SG4D, SG4E	12

The isolations of strains prior to 2020 were carried out by Angela Pelusi.

3.3.2 Sediment sampling

Ancona sampling

At both stations, sediment samples were collected using "bottom grabs/Peterson grab" (Figure. 21a) in May (spring), July (summer), October (autumn) 2020, and January (winter) 2021. At each station, the bottom grab was lowered three times to collect three replicate samples. For each grab, a syringe with diameter of 2 cm was used to collect the top 1 cm of undisturbed sediment (about 10 ml of sediment) (Figure. 21b) that was then placed into a sterile 50 ml plastic Falcon tube for diatom biodiversity analysis (results will be reported in Chapter 3). These samples were stored at 4 °C until

the diatom extraction procedure to analyse the abundance and biomass (this part has been covered in the Chapter 2). Another syringe sample was collected from the same grab for cell isolation. Diatom cell isolation was carried out immediately after sediment collection.

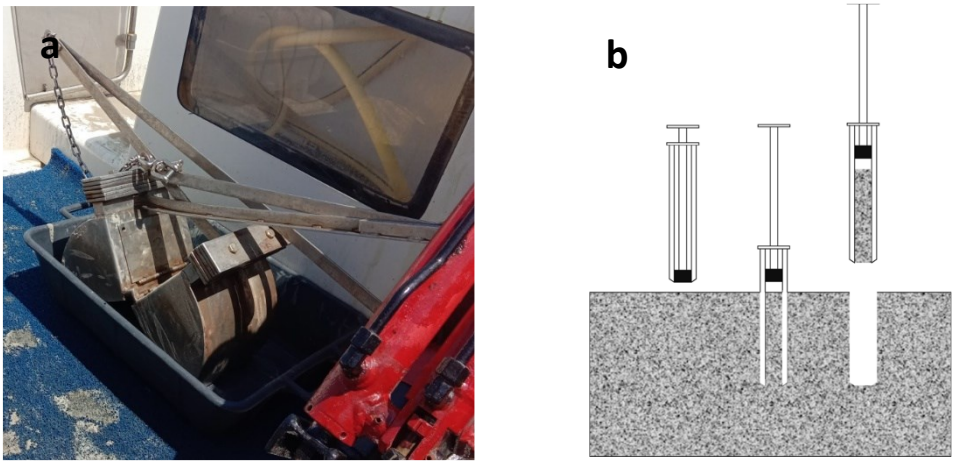

Figure. 21: a; Bottom grab, b; use of syringe to collected upper 1 cm of the sediment.

Naples sampling

The first sampling was done in October 2019 in the Bagnoli area. The surface sediment samples were collected at two (BD1 and BD3) sites with a box-corer (Figure. 22). BD1 was approximately 2.5 km away from the ex-industrial plant, and therefore, represent a lower level of contamination while BD3 was situated within the internal area so that it would reflect the most impacted areas. At both the stations sediment samples were collected from different water depths following: BD1A & BD3A; 10 m, BD1B & BD3B; 20 m, BD3C; 40m. Sediments were collected in three replicates for both morphological and molecular benthic foraminiferal analyses by independent deployments of the box-corer at all the stations. The sediments from only the first deployment were sub-sampled for geochemical and grain-size analyses. Only the uppermost part of the sediment (1 cm) was sampled and used for cell isolation and cultivation, grain-size, and geochemical analyses.

The second sampling was carried out in July and September 2020. Sediment samples were collected using same method of box corer across the Pozzuoli Bay (NB1 and NB2), Naples Gulf (NM1 near

the Castle dell'Ovo and NaMC close to the LTER-MC station) and near Sarno river mouth (SR) (Table 3).

Figure. 22: Different box corer used at Naples stations.

3.3.3 Cell isolation and maintenance

To isolate diatom cells from the sediment, a coverslip was floated onto the sediment after the material has settled in the petri dish. Living motile diatom cells actively adhered to the lower surface of the coverslip under the water (Figure 23 a & b). This coverslip was observed under the microscope and washed with sterile f/2 medium (Guillard & Ryther, 1962) in the petri dish and kept in a photo incubator for diatom cells to grow. Also, diatom cells which were attached to sediment grains and not able to move on the coverslip were picked under microscope delicately.

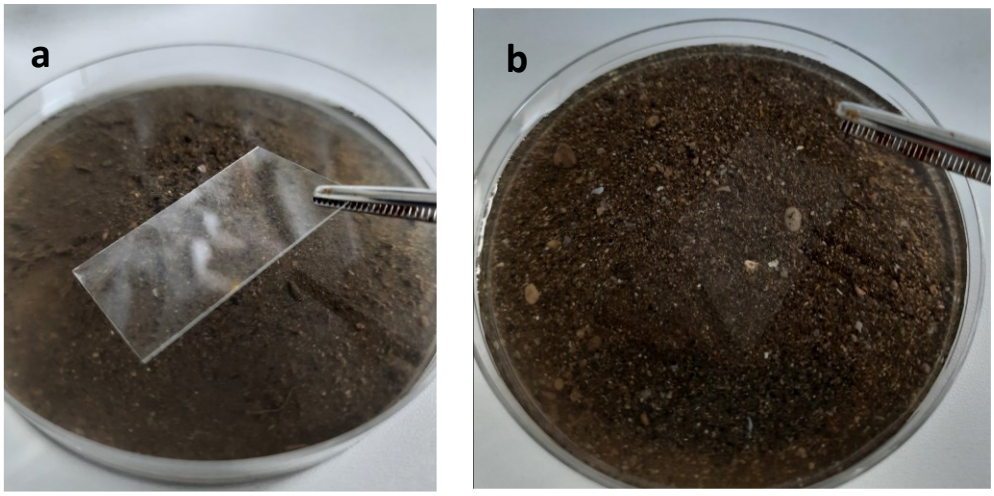

Figure. 23: a & b; Diatom cells isolation using glass coverslip.

To obtain monoclonal diatom strains, single cells were picked using a drawn-out Pasteur pipette under an inverted microscope (Figure. 24a). Each cell was placed in a single well of a micro titre plate (Figure. 24b). This well plate was kept in a photo incubator to enable growth of the isolated microalgae. Cultures were maintained in a liquid f/2 medium. To make cultures bacteria-free, diatoms were grown on f/2 agar (1%) plates. Diatoms colonies growing on the agar plates were observed under microscope and a single, isolated colony was picked with the help of wire loop and transferred to liquid f/2 medium.

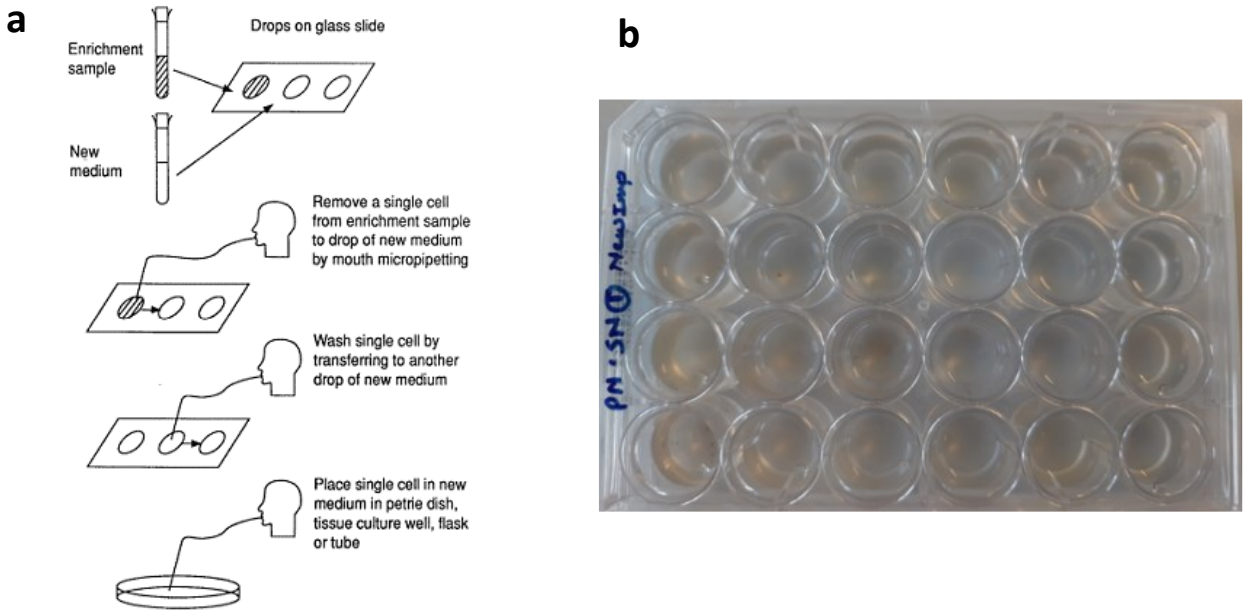

Figure. 24: a; single cell picking using the micropipette under inverted microscope, b; Microwell plate with single cell in the single well.

3.3.4 Morphological observations

Light microscopy

Live culture material of diatom strains was observed under a Zeiss Axiovert 25 microscope equipped with the camera Canon EOS 6D for PN, SG, NM, NB and NaMC samples, while Axiophot light

microscopes (Carl Zeiss, Oberkochen, Germany) and a Zeiss Axiocam digital camera (Carl Zeiss, Oberkochen, Germany) was used for SR, LR and BD samples. Cell measurements were taken directly in the acquired images. Due to the Covid-19 emergency some cultures isolated in 2020 and 2021 were observed a long time after their isolation and appeared small and deformed.

Electron microscopy

For transmission and scanning electron microscopy (TEM and SEM) observations, clean diatom frustules were obtained after removal of the organic matter with nitric and sulfuric acids (modified from Round et al., 1990), as follows. Cultures were centrifuged at 3000-3500 rpm for 10 min and the supernatant was removed without disturbing the pellet. This pellet was washed at least 3 times with distilled water to eliminate salt. In this pellet, 1 volume of 65% HNO_3 and 4 volumes of H_2SO_4 (1:1:4, sample: HNO_3: H_2SO_4) were added under the fume hood. This mixture was boiled for a few seconds and the procedure was repeated. After cooling this mixture for about 30 minutes, it was centrifuged at 3500 rpm for 30 min. Pellet was rinsed with distilled water several times to remove residual acid. In the end, pH was checked for a neutral value. Cleaned diatom material was stored in the distilled water with a few drops of acetic acid to avoid the growth of fungi and bacteria and the dissolution of silica.

For SEM observations, cleaned diatom material was mounted on metal stubs with sticky nucleopore polycarbonate discs and appropriate filters (1.3 to 5 µm) according to the cell sizes. One or few drops of the cleaned material were mounted on stubs and left to air dry completely. Before SEM observation stubs were sputter-coated with a thin layer of gold-palladium and observed with a JEOL JSM-6500F SEM (JEOL-USA Inc., Peabody, MA, USA). For TEM observations, cleaned material was mounted on Formvar-coated grids and observed with a Philips 400 TEM (Philips Electron Optics BV, Eindhoven, Netherlands). Available literature (Hustedt, 1938; H. , Peragallo, 1888; H. Peragallo & Peragallo, 1897; van Heurck, 1909) Álvarez-Blanco, 2014; Hendey, 1964; Krammer, 1991; D. G.

Mann, 1982; Round et al., 1990; Simonsen, 1962) was consulted for the morphological identification. Strains that could not be matched with the published literature down to the species-level were treated as undetermined species and named by their generic name followed by 'sp.' Terminology of morphological features of the frustules followed (reference) (Ross et al., 1979; Ross & Sims, 1972).

3.3.5 Molecular analysis

DNA extraction (CTAB protocol)

The medium in the cell culture was removed by centrifugation at 4500g/10 mins. To the cell pellet was added 500 µl CTAB, 1 µl beta-mercapto-ethanol and 4 µl RNase solution. Then the mixture was incubated for ca. 1 hour at 65 °C and shaken for 10 sec every 15 min, using a vortex. After cooling, 500 µl of chloroform:isoamyl alcohol (24:1) was added to the mixture and the liquids mixed thoroughly by rapid inverting movements. Centrifugation at 14000 rpm for 10 min was carried out and upper watery supernatant collected carefully, avoiding the milky interphase, and transferred into a new tube. The chloroform: iso-amyl alcohol treatment and centrifugation steps were repeated once. The supernatant was transferred to a new tube and an equal volume of ice-cold isopropanol added. The tubes were inverted gently and kept at -20 °C for at least one hour to precipitate the DNA. Then, centrifugation was carried out at 14000 rpm for 30 min. Pellet (DNA on the centrifugal side) was washed with 500 µl of 75% ethanol (kept in the freezer). 25-40 µl of double distilled water was added to the dried DNA pellet to enable it to dissolve completely. The extracted DNA was kept for long-term storage at -20 °C.

PCR amplification and sequencing

PCR amplification of the 18S rRNA gene was performed using as primers the Ch-300F 5'-ATTAGGGTTTGATTCCGGAGAGG-3' (Gaonkar et al., 2018). and the 1147R 5'-AGTTTCAGCCTTGCGACCATAC-3' (Alverson et al., 2007). These primers produced a PCR

product with a length of approximately 550 bp. Single 25 µl PCR reaction mixture contained 5 µl of 'extra' buffer, 2.5 µl of 10x dNTPs, 1 µl of each forward (300F) and reverse primer (1147R), 0.25 µl TAQ polymerase, 14.25 µl of water and 1 µl of DNA solution. Following PCR conditions were used, Initial denaturation at 95 °C for 2 min, followed by 35 cycles of denaturation at 95 °C for 20 s, annealing at 56 °C for 30 s, and extension at 72 °C for 1 min, and then a final extension at 72 °C for 7 min.

PCR products were purified using low melting agarose TAE (Tris-acetate-EDTA) buffer gel electrophoresis, excision of the target band under low UV light, and subsequent purification using DNA Isolation Spin Kit Agarose (PanReac Applichem GmbH, Darmstadt, Germany) following manufacturer's instructions. The obtained PCR products were sequenced using the BigDye Terminator Cycle Sequencing technology (Applied Biosystems, Foster City, CA, USA), purified using a 'Biomek FX' (Beckman Coulter, Fullerton, CA, USA) robotic station, and analysed on an Automated Capillary Electrophoresis Sequencer '3730 DNA Analyzer' (Applied Biosystems). Forward and reverse sequences were combined into contigs and aligned using BioEdit v7.0.0 (Hall, 1999). Any site showing an ambiguity in the forward and reverse sequence was recorded as such, if the surrounding sites read without difficulties.

Sequence alignment and phylogenetic analysis

For phylogenetic analysis, 18S rRNA gene sequences were retrieved from the GenBank (www.ncbi.nlm.nih.gov) and Matt Ashworth (personal communication). After excluding sequences of uncultured material, 541 partial sequences of the 18S rRNA gene were aligned using Se-Al application and corrected manually. Sequences of 30 Mediophyceae were used as an outgroup.

The phylogeny was inferred by using the Maximum Likelihood (ML) method and Kimura 2-parameter model (Kimura M., 1980) as base substitution model. Initial trees for the heuristic search

in ML were obtained automatically by applying the Neighbor-Joining algorithm to a matrix of pairwise distances estimated using the Maximum Composite Likelihood (MCL) approach, and then selecting the topology with superior log likelihood value. The analysis involved 541 nucleotide sequences. There were a total of 1897 positions in the final dataset. Evolutionary analyses were conducted in MEGA X (Kumar S., 2018).

3.4 Results

3.4.1 Light microscopical observations

In total 59 strains were isolated from all 13 stations and the numbers of strains isolated from each station (abbreviations, see Table 3) are as follows: BD-15, LR-5, NaMC-2, NB1-1, NB2-4, NM-4, SR-2, PN-14, SG-12. Light microscopic observations allowed identification of most of the strains down to the genus-level. (LM photos are provided in the supplementary material of chapter 3). A total of 13 strains are marked as 'undetermined' which were not identified. Strains were provided with species name based on LM observation (Table 4).

Table 4: Strains isolated from all the stations in Adriatic and Tyrrhenian Seas, with their collection date (DD-MM-YY).

Species name based on LM	**LM plate number (Suppl. material of Chapter 3)**	**Strain Code**	**Station**	**Sampling date**
Amphiprora sp.	Plate 1, a	PN4Am	PN	19-01-21
Amphiprora sp.	Plate 1, b	PN4C	PN	19-01-21
Amphora sp.	Plate 1, c	BD10	BD1B	21-10-19
Amphora sp.	Plate 1, d	NM14	NM	21-09-20
Amphora sp.	Plate 1, e	PN4B	PN	19-01-21
Amphora sp.	Plate 1, f	SG31	SG	19-10-20
Amphora sp.	Plate 1, g	SRA	SR	9-7-21

Amphora sp.	Plate 1, h	SRD	SR	9-7-21
Bacillaria sp.	Plate 2, a	NM12	NM	21-09-20
Bacillaria sp.	Plate 2, b	PN4BA	PN	19-01-21
Dimeregramma or *Plagiogramma* sp.	Plate 2, c	BD2	BD1A	21-10-19
Dimeregramma or *Plagiogramma* sp.	Plate 2, d	BD11	BD1B	21-10-19
Dimeregramma or *Psammogramma* sp.	Plate 2, e	BD4	BD1A	21-10-19
Dimeregramma, Plagiogramma or *Psammogramma* sp.	Plate 2, f	BD15	BD3C	21-10-19
Diploneis sp.	Plate 3, a	PN4DP	PN	19-01-21
Gyrosigma or *Pleurosigma* sp.	Plate 3, b	NB29	NB2	21-09-20
Halamphora or *Amphora* sp.	Plate 3, c	NM17	NM	21-09-20
Nanofrustulum sp.	Plate 3, d	BD9	BD1B	21-10-19
Nanofrustulum sp.	Plate 3, e	LR13	LR	5-12-18
Nanofrustulum sp.	Plate 3, f	LR26	LR	5-12-18
Navicula sp.	Plate 4, a	NM11	NM	21-09-20
Navicula sp.	Plate 4, b	PN4A	PN	19-01-21
Nitzschia longissimi	Plate 4, c	PN4F	PN	19-01-21
Nitzschia longissimi	Plate 4, d	SG35	SG	19-10-20
Nitzschia longissima	Plate 4, e	SG4C	SG	19-01-21
Nitzschia sp.	Plate 4, f	BD3	BD1A	21-10-19
Nitzschia sp.	Plate 4, g	BD6	BD1A	21-10-19
Nitzschia sp.	Plate 5, a	LR40	LR	5-12-18
Nitzschia sp.	Plate 5, b	LR43	LR	5-12-18
Nitzschia sp.	Plate 5, c	NaMC3	NaMC	7-7-20
Nitzschia sp.	Plate 5, d	NB21	NB2	21-09-20
Nitzschia sp.	Plate 5, e	NB22	NB2	21-09-20
Nitzschia sp.	Plate 5, f	NB23	NB2	21-09-20
Nitzschia sp.	Plate 6, a	PN11	PN	28-05-20
Nitzschia sp.	Plate 6, b	PN21	PN	20-07-20
Pleurosigma sp.	Plate 6, c	PN4G	PN	19-01-21
Pleurosigma sp.	Plate 6, d	SG11	SG	28-05-20
Pleurosigma sp.	Plate 6, e	SG4A	SG	19-01-21
Psammodictyon sp.	Plate 6, f	BD1	BD1A	21-10-19
Psammodictyon sp.	Plate 7, a	BD8	BD1B	21-10-19
Psammodictyon sp.	Plate 7, b	BD12	BD3C	21-10-19
Psammodictyon sp.	Plate 7, c	BD13	BD3B	21-10-19
Psammodictyon sp.	Plate 7, d	NaMC2	NaMC	7-7-20

Psammodictyon sp.	Plate 7, e	NB11	NB1	21-09-20
Psammodictyon sp.	Plate 7, f	PN12	PN	28-05-20
Psammodictyon sp.	Plate 7, g	PN4E	PN	19-01-21
Psammodictyon sp.	Plate 7, h	SG12	SG	28-05-20
Psammodictyon sp.	Plate 8, a	SG22	SG	20-07-20
Psammodictyon sp.	Plate 8, b	SG4E	SG	19-01-21
Tabularia sp.	Plate 8, c	SG4D	SG	19-01-21
Undetermined	Plate 8, d	BD5	BD1A	21-10-19
Undetermined	Plate 8, e	BD16	BD3C	21-10-19
Undetermined	Plate 8, f	LR34	LR	5-12-18
Undetermined	Plate 8, g	PN23	PN	20-07-20
Undetermined	Plate 8, h	PN31	PN	19-10-20
Undetermined	Plate 9, a	SG23	SG	20-07-20
Undetermined	Plate 9, b	SG27	SG	20-07-20
Undetermined	Plate 9, c	SG34	SG	19-10-20
Undetermined	Plate 9, d	BD7	BD1A	21-10-19

3.4.2 Molecular results

Partial 18S rRNA gene sequences were obtained for all of the 59 strains considered in this study. Many of their strains could not be identified with the light microscopy because of insufficient resolution of the frustule characters. Searches with BLASTn function in NCBI GenBank using the obtained sequences as query allowed identification of the vast majority of the obtained sequences down to the species-level within the 97.5% similarity level (Table 5). The query sequences were assigned to 23 genera and 43 species based on the name associated with the GenBank sequence accession number with nearest hit (% similarity with that nearest hit).

Table 5: Species name based on morphological and molecular identification

Strain code	**Species name based on LM**	**Species name based on partial 18S rRNA gene sequence**	**% similarity of partial 18S query with GenBank accession number of nearest sequence**
BD1	*Psammodictyon* sp.	*Psammodictyon* sp.	98.88%, JQ885984.2
BD2	*Dimeregramma* or *Plagiogramma* sp.	*Plagiogramma appendiculatum*	99.59%, KJ577867
BD3	*Nitzschia* sp.	*Nitzschia* sp.	97.92%, KT943641

BD4	*Dimeregramma* or *Psammogramma* sp.	*Neofragilaria nicobarica*	98.10%, AB433340
BD5	Undetermined	cf. *Delphineis* sp.	98.09%, JX413544
BD6	*Nitzschia* sp.	*Nitzschia volvendirostrata*	99.51%, MW327187
BD7	Undetermined	cf. *Gedaniella flavovirens*	98.73%, MF093136
BD8	*Psammodictyon* sp.	*Psammodictyon* sp.	99.18%, MH063501
BD9	*Nanofrustulum* sp.	*Nanofrustulum shiloi*	99.32%, KU851875
BD10	*Amphora* sp.	*Amphora* sp.	97.24%, OP304755
BD11	*Dimeregramma* or *Plagiogramma* sp.	*Plagiogramma marginalis*	96.47 %, MN473922
BD12	*Psammodictyon* sp.	*Psammodictyon constrictum*	100%, KX981851
BD13	*Psammodictyon* sp.	*Psammodyction* sp.	99.71%, JQ885984
BD15	*Dimeregramma*, *Plagiogramma* or *Psammogramma* sp.	*Dimeregramma* sp.	99.71%, KF701597
BD16	Undetermined	*Berkeleya fennica*	95.78%, KY320346
LR13	*Nanofrustulum* sp.	*Nanofrustulum shiloi*	99.83%, AF525658
LR26	*Nanofrustulum* sp.	*Nanofrustulum shiloi*	99.27%, AF525658
LR34	Undetermined	cf. *Rhaphoneis*	93.86%, MZ687551
LR40	*Nitzschia* sp.	*Nitzschia* adh*aerens*	100%, MH734167
LR43	*Nitzschia* sp.	*Nitzschia traheaformis*	100%, KT943644
NaMC2	*Psammodictyon* sp.	*Psammodictyon* sp.	99.81%, JQ885984
NaMC3	*Nitzschia* sp.	*Nitzschia traheaformis*	100%, KT943644
NB11	*Psammodictyon* sp.	*Psammodictyon* sp.	100%, JQ885984
NB21	*Nitzschia* sp.	*Nitzschia traheaformis*	100%, KT943644
NB22	*Nitzschia* sp.	*Nitzschia* sp.	99.68%, KY045849
NB23	*Nitzschia* sp.	*Nitzschia traheaformis*	99.52%, KT943644
NB29	*Gyrosigma* or *Pleurosigma* sp.	*Gyrosigma acuminatum*	95.34%, KM999005
NM11	*Navicula* sp.	*Seminavis* sp.	99.51%, KY320398

NM12	*Bacillaria* sp.	*Bacillaria* sp.	99.67%, KY320377
NM14	*Amphora* sp.	*Amphora eunotia*	*98.13%, KC222326*
NM17	*Halamphora* or *Amphora* sp.	*Halamphora coffeiformis*	99.53%, MT259194
PN11	*Nitzschia* sp.	*Nitzschia traheaformis*	100%, KT943642
PN12	*Psammodictyon* sp.	*Psammodictyon panduriforme*	100%, KY054991
PN21	*Nitzschia* sp.	*Nitzschia traheaformis*	100%, KT943642
PN23	Undetermined	*Astartiella marksii*	100%, MT982905
PN31	Undetermined	*Schizostauron trachyderma*	99.69%, MT982916
PN4A	*Navicula* sp.	*Navicula* sp.	99.80%, MH063477
PN4Am	*Amphiprora* sp.	*Entomoneis* cf. *alata*	99.83%, MF000610
PN4B	*Amphora* sp.	*Amphora* sp.	99.38%, MH017634
PN4BA	*Bacillaria* sp.	*Bacillaria paxillifera*	99.79%, KT861008
PN4C	*Amphiprora* sp.	*Entomoneis paludosa*	99.85%, AY485468
PN4DP	*Diploneis* sp.	*Diploneis* sp.	96.19%, KX981839
PN4E	*Psammodictyon* sp.	*Psammodictyon* sp.	99.81%, KT861018
PN4F	*Nitzschia longissima*	*Cylindrotheca closterium*	99.36%, KJ671694
PN4G	*Pleurosigma* sp.	*Pleurosigma planktonicum*	99.37%, AY485514
SG11	*Pleurosigma* sp.	*Pleurosigma* sp.	99.21%, MW805713
SG12	*Psammodictyon* sp.	*Psammodictyon* sp.	99.84%, KT861018
SG22	*Psammodictyon* sp.	*Psammodictyon* sp.	99.84%, KT861018
SG23	Undetermined	*Nitzschia pusilla*	99.84%, MN750475
SG27	Undetermined	*Nitzschia* sp.	100%, MH040327
SG31	*Amphora* sp.	*Amphora* sp.	99.85%, MW327163
SG34	Undetermined	*Astartiella marksii*	100%, MT982905
SG35	*Nitzschia longissima*	*Cylindrotheca closterium*	99.31%, KJ671694
SG4A	*Pleurosigma* sp.	*Pleurosigma planktonicum*	99.85%, AY485514

SG4C	*Nitzschia longissima*	*Cylindrotheca closterium*	99.37%, KJ671694
SG4D	*Tabularia* sp.	*Fragilariophyceae* sp.	99.82%, MG684377
SG4E	*Psammodictyon* sp.	*Psammodictyon* sp.	99.82%, KT861018
SRA	*Amphora* sp.	*Amphora eunotia*	99.20 %, KC222326
SRD	*Amphora* sp.	*Amphora pediculus*	99.53%, AM501960

To validate the GenBank-based identification, the query sequences were aligned with a database of taxonomically validated sequences, and a phylogenetic tree inferred from the aligned sequences. The resulting maximum likelihood tree inferred from 541 sequences comprised 511 ingroup sequences of pennate diatoms (of which the 59 from the present study) and 30 outgroup sequences of bi- and multipolar centric diatoms (Mediophyceae) (Figure. 25). Many of the ramifications were not well-resolved, showing bootstrap values below 50% because of the large number of sequences relative to the number of phylogenetically informative sites in the alignment.

3.4.3 Phylogenetic tree analysis

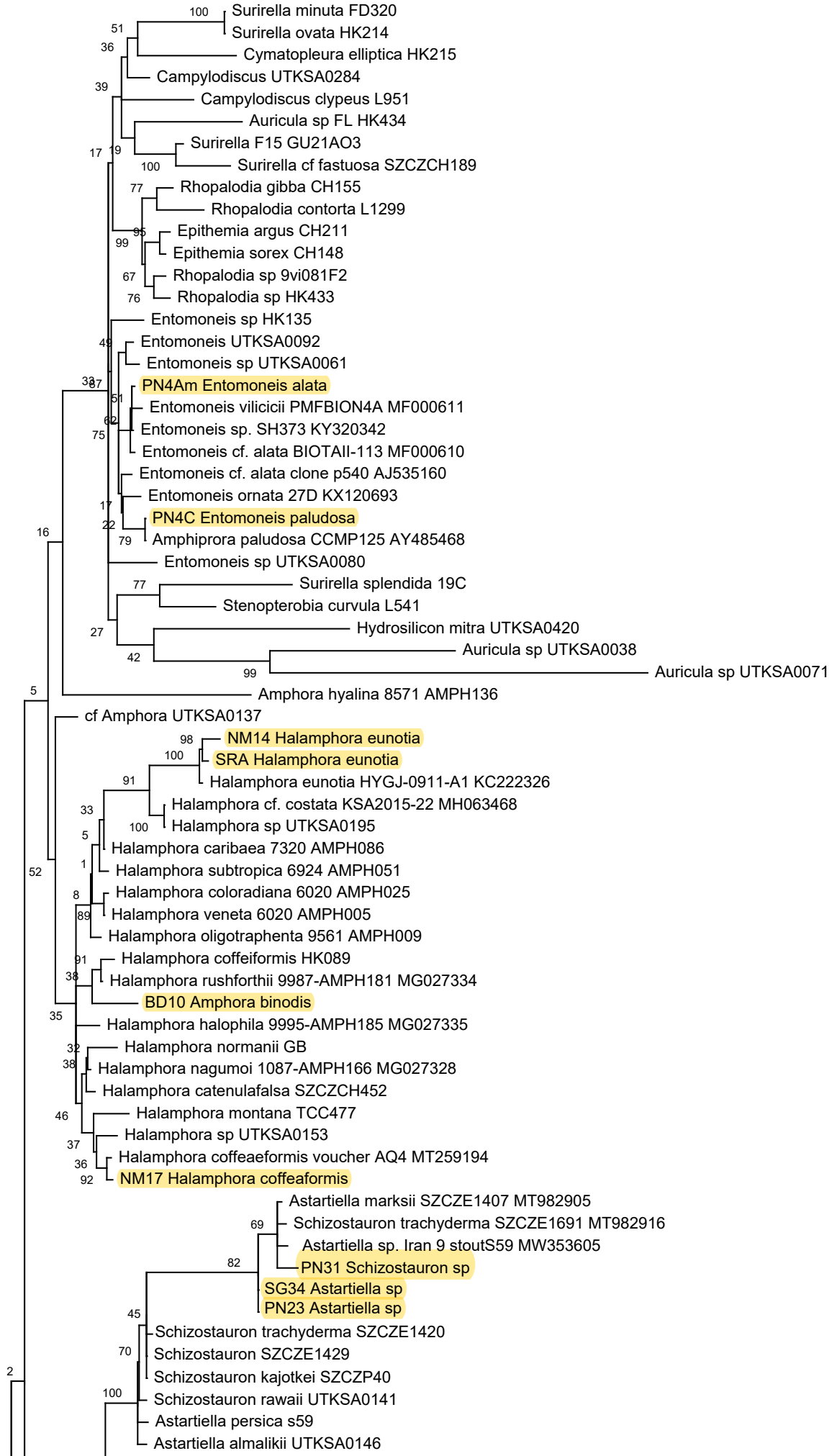
Surirella minuta FD320
Surirella ovata HK214
Cymatopleura elliptica HK215
Campylodiscus UTKSA0284
Campylodiscus clypeus L951
Auricula sp FL HK434
Surirella F15 GU21AO3
Surirella cf fastuosa SZCZCH189
Rhopalodia gibba CH155
Rhopalodia contorta L1299
Epithemia argus CH211
Epithemia sorex CH148
Rhopalodia sp 9vi081F2
Rhopalodia sp HK433
Entomoneis sp HK135
Entomoneis UTKSA0092
Entomoneis sp UTKSA0061
PN4Am Entomoneis alata
Entomoneis vilicicii PMFBION4A MF000611
Entomoneis sp. SH373 KY320342
Entomoneis cf. alata BIOTAII-113 MF000610
Entomoneis cf. alata clone p540 AJ535160
Entomoneis ornata 27D KX120693
PN4C Entomoneis paludosa
Amphiprora paludosa CCMP125 AY485468
Entomoneis sp UTKSA0080
Surirella splendida 19C
Stenopterobia curvula L541
Hydrosilicon mitra UTKSA0420
Auricula sp UTKSA0038
Auricula sp UTKSA0071
Amphora hyalina 8571 AMPH136
cf Amphora UTKSA0137
NM14 Halamphora eunotia
SRA Halamphora eunotia
Halamphora eunotia HYGJ-0911-A1 KC222326
Halamphora cf. costata KSA2015-22 MH063468
Halamphora sp UTKSA0195
Halamphora caribaea 7320 AMPH086
Halamphora subtropica 6924 AMPH051
Halamphora coloradiana 6020 AMPH025
Halamphora veneta 6020 AMPH005
Halamphora oligotraphenta 9561 AMPH009
Halamphora coffeiformis HK089
Halamphora rushforthii 9987-AMPH181 MG027334
BD10 Amphora binodis
Halamphora halophila 9995-AMPH185 MG027335
Halamphora normanii GB
Halamphora nagumoi 1087-AMPH166 MG027328
Halamphora catenulafalsa SZCZCH452
Halamphora montana TCC477
Halamphora sp UTKSA0153
Halamphora coffeaeformis voucher AQ4 MT259194
NM17 Halamphora coffeaformis
Astartiella marksii SZCZE1407 MT982905
Schizostauron trachyderma SZCZE1691 MT982916
Astartiella sp. Iran 9 stoutS59 MW353605
PN31 Schizostauron sp
SG34 Astartiella sp
PN23 Astartiella sp
Schizostauron trachyderma SZCZE1420
Schizostauron SZCZE1429
Schizostauron kajotkei SZCZP40
Schizostauron rawaii UTKSA0141
Astartiella persica s59
Astartiella almalikii UTKSA0146

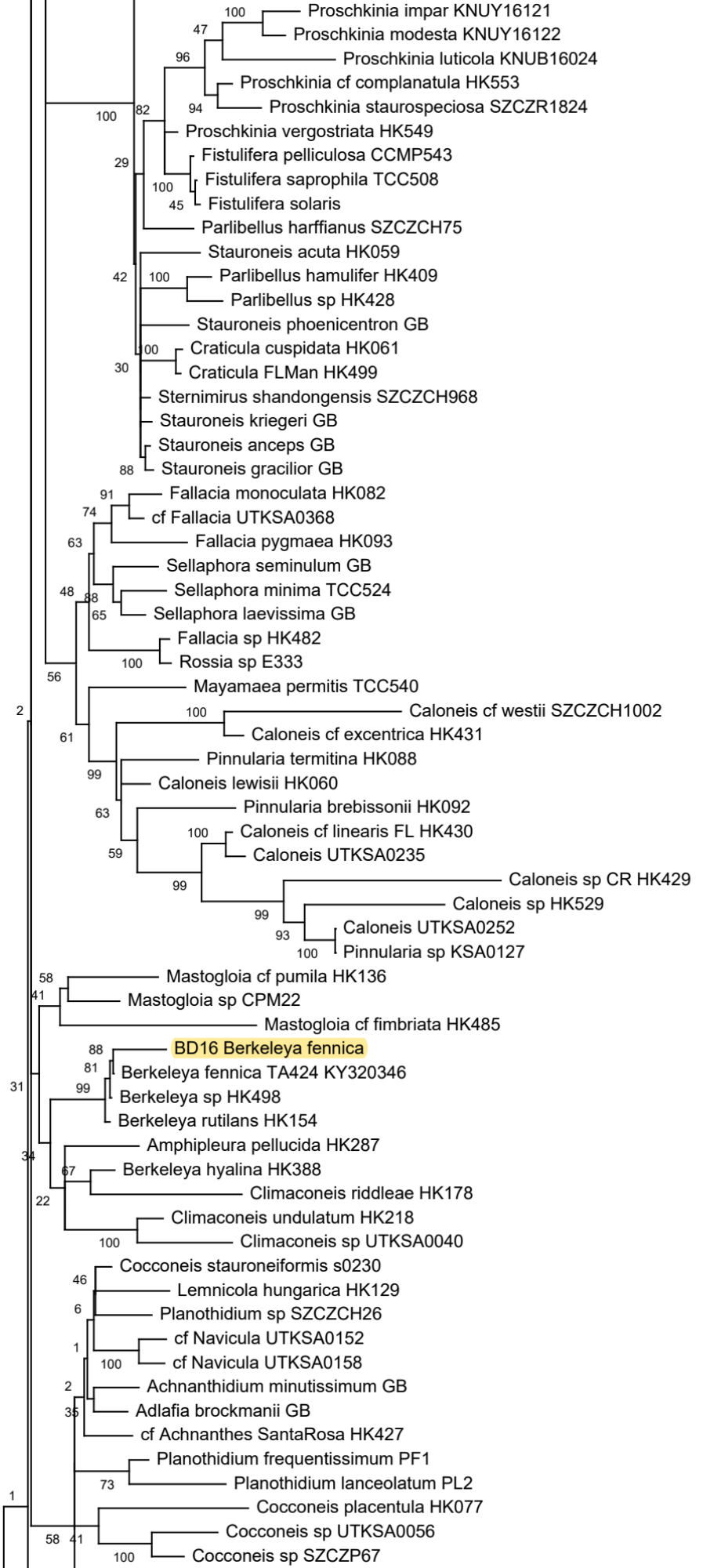
Proschkinia impar KNUY16121
Proschkinia modesta KNUY16122
Proschkinia luticola KNUB16024
Proschkinia cf complanatula HK553
Proschkinia staurospeciosa SZCZR1824
Proschkinia vergostriata HK549
Fistulifera pelliculosa CCMP543
Fistulifera saprophila TCC508
Fistulifera solaris
Parlibellus harffianus SZCZCH75
Stauroneis acuta HK059
Parlibellus hamulifer HK409
Parlibellus sp HK428
Stauroneis phoenicentron GB
Craticula cuspidata HK061
Craticula FLMan HK499
Sternimirus shandongensis SZCZCH968
Stauroneis kriegeri GB
Stauroneis anceps GB
Stauroneis gracilior GB
Fallacia monoculata HK082
cf Fallacia UTKSA0368
Fallacia pygmaea HK093
Sellaphora seminulum GB
Sellaphora minima TCC524
Sellaphora laevissima GB
Fallacia sp HK482
Rossia sp E333
Mayamaea permitis TCC540
Caloneis cf westii SZCZCH1002
Caloneis cf excentrica HK431
Pinnularia termitina HK088
Caloneis lewisii HK060
Pinnularia brebissonii HK092
Caloneis cf linearis FL HK430
Caloneis UTKSA0235
Caloneis sp CR HK429
Caloneis sp HK529
Caloneis UTKSA0252
Pinnularia sp KSA0127
Mastogloia cf pumila HK136
Mastogloia sp CPM22
Mastogloia cf fimbriata HK485
BD16 Berkeleya fennica
Berkeleya fennica TA424 KY320346
Berkeleya sp HK498
Berkeleya rutilans HK154
Amphipleura pellucida HK287
Berkeleya hyalina HK388
Climaconeis riddleae HK178
Climaconeis undulatum HK218
Climaconeis sp UTKSA0040
Cocconeis stauroneiformis s0230
Lemnicola hungarica HK129
Planothidium sp SZCZCH26
cf Navicula UTKSA0152
cf Navicula UTKSA0158
Achnanthidium minutissimum GB
Adlafia brockmanii GB
cf Achnanthes SantaRosa HK427
Planothidium frequentissimum PF1
Planothidium lanceolatum PL2
Cocconeis placentula HK077
Cocconeis sp UTKSA0056
Cocconeis sp SZCZP67

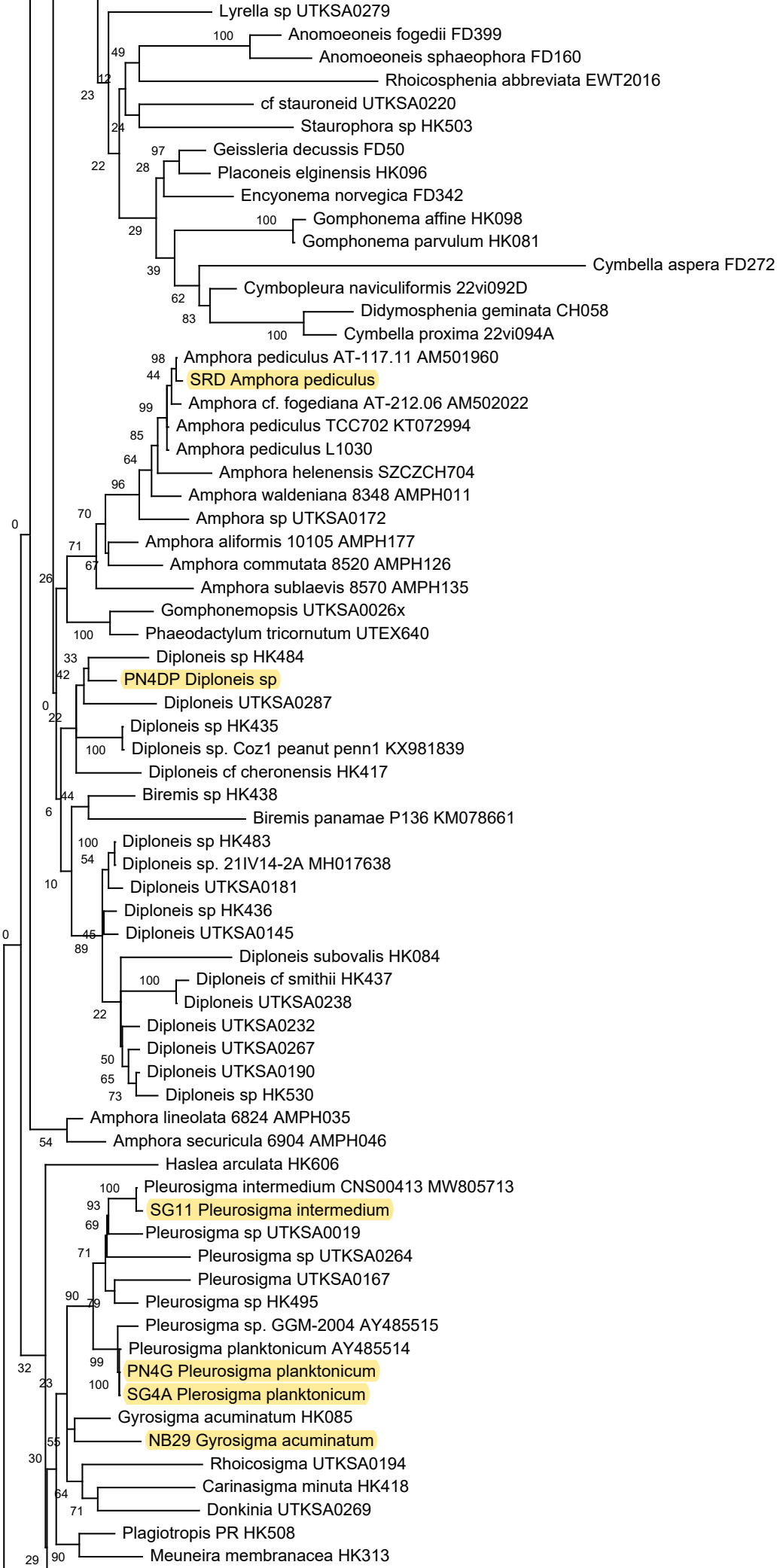
Lyrella sp UTKSA0279
Anomoeoneis fogedii FD399
Anomoeoneis sphaeophora FD160
Rhoicosphenia abbreviata EWT2016
cf stauroneid UTKSA0220
Staurophora sp HK503
Geissleria decussis FD50
Placoneis elginensis HK096
Encyonema norvegica FD342
Gomphonema affine HK098
Gomphonema parvulum HK081
Cymbella aspera FD272
Cymbopleura naviculiformis 22vi092D
Didymosphenia geminata CH058
Cymbella proxima 22vi094A
Amphora pediculus AT-117.11 AM501960
SRD Amphora pediculus
Amphora cf. fogediana AT-212.06 AM502022
Amphora pediculus TCC702 KT072994
Amphora pediculus L1030
Amphora helenensis SZCZCH704
Amphora waldeniana 8348 AMPH011
Amphora sp UTKSA0172
Amphora aliformis 10105 AMPH177
Amphora commutata 8520 AMPH126
Amphora sublaevis 8570 AMPH135
Gomphonemopsis UTKSA0026x
Phaeodactylum tricornutum UTEX640
Diploneis sp HK484
PN4DP Diploneis sp
Diploneis UTKSA0287
Diploneis sp HK435
Diploneis sp. Coz1 peanut penn1 KX981839
Diploneis cf cheronensis HK417
Biremis sp HK438
Biremis panamae P136 KM078661
Diploneis sp HK483
Diploneis sp. 21IV14-2A MH017638
Diploneis UTKSA0181
Diploneis sp HK436
Diploneis UTKSA0145
Diploneis subovalis HK084
Diploneis cf smithii HK437
Diploneis UTKSA0238
Diploneis UTKSA0232
Diploneis UTKSA0267
Diploneis UTKSA0190
Diploneis sp HK530
Amphora lineolata 6824 AMPH035
Amphora securicula 6904 AMPH046
Haslea arculata HK606
Pleurosigma intermedium CNS00413 MW805713
SG11 Pleurosigma intermedium
Pleurosigma sp UTKSA0019
Pleurosigma sp UTKSA0264
Pleurosigma UTKSA0167
Pleurosigma sp HK495
Pleurosigma sp. GGM-2004 AY485515
Pleurosigma planktonicum AY485514
PN4G Pleurosigma planktonicum
SG4A Plerosigma planktonicum
Gyrosigma acuminatum HK085
NB29 Gyrosigma acuminatum
Rhoicosigma UTKSA0194
Carinasigma minuta HK418
Donkinia UTKSA0269
Plagiotropis PR HK508
Meuneira membranacea HK313

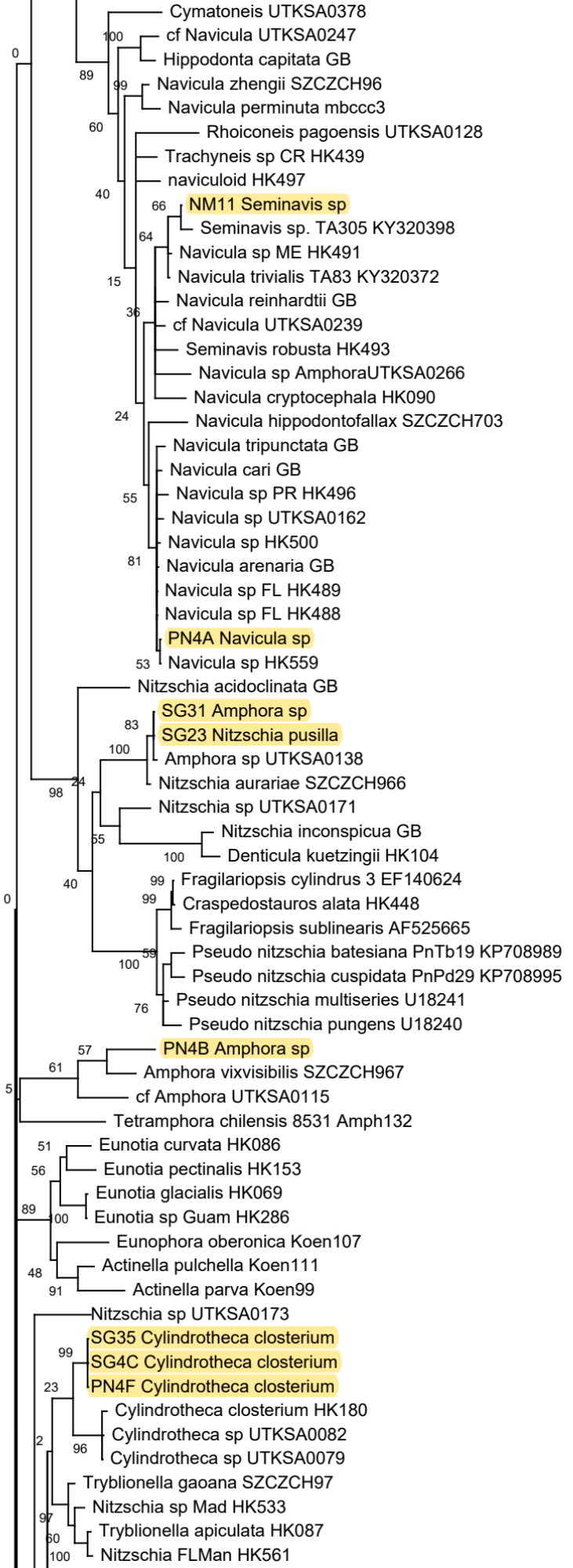
Cymatoneis UTKSA0378
cf Navicula UTKSA0247
Hippodonta capitata GB
Navicula zhengii SZCZCH96
Navicula perminuta mbccc3
Rhoiconeis pagoensis UTKSA0128
Trachyneis sp CR HK439
naviculoid HK497
NM11 Seminavis sp
Seminavis sp. TA305 KY320398
Navicula sp ME HK491
Navicula trivialis TA83 KY320372
Navicula reinhardtii GB
cf Navicula UTKSA0239
Seminavis robusta HK493
Navicula sp AmphoraUTKSA0266
Navicula cryptocephala HK090
Navicula hippodontofallax SZCZCH703
Navicula tripunctata GB
Navicula cari GB
Navicula sp PR HK496
Navicula sp UTKSA0162
Navicula sp HK500
Navicula arenaria GB
Navicula sp FL HK489
Navicula sp FL HK488
PN4A Navicula sp
Navicula sp HK559
Nitzschia acidoclinata GB
SG31 Amphora sp
SG23 Nitzschia pusilla
Amphora sp UTKSA0138
Nitzschia aurariae SZCZCH966
Nitzschia sp UTKSA0171
Nitzschia inconspicua GB
Denticula kuetzingii HK104
Fragilariopsis cylindrus 3 EF140624
Craspedostauros alata HK448
Fragilariopsis sublinearis AF525665
Pseudo nitzschia batesiana PnTb19 KP708989
Pseudo nitzschia cuspidata PnPd29 KP708995
Pseudo nitzschia multiseries U18241
Pseudo nitzschia pungens U18240
PN4B Amphora sp
Amphora vixvisibilis SZCZCH967
cf Amphora UTKSA0115
Tetramphora chilensis 8531 Amph132
Eunotia curvata HK086
Eunotia pectinalis HK153
Eunotia glacialis HK069
Eunotia sp Guam HK286
Eunophora oberonica Koen107
Actinella pulchella Koen111
Actinella parva Koen99
Nitzschia sp UTKSA0173
SG35 Cylindrotheca closterium
SG4C Cylindrotheca closterium
PN4F Cylindrotheca closterium
Cylindrotheca closterium HK180
Cylindrotheca sp UTKSA0082
Cylindrotheca sp UTKSA0079
Tryblionella gaoana SZCZCH97
Nitzschia sp Mad HK533
Tryblionella apiculata HK087
Nitzschia FLMan HK561

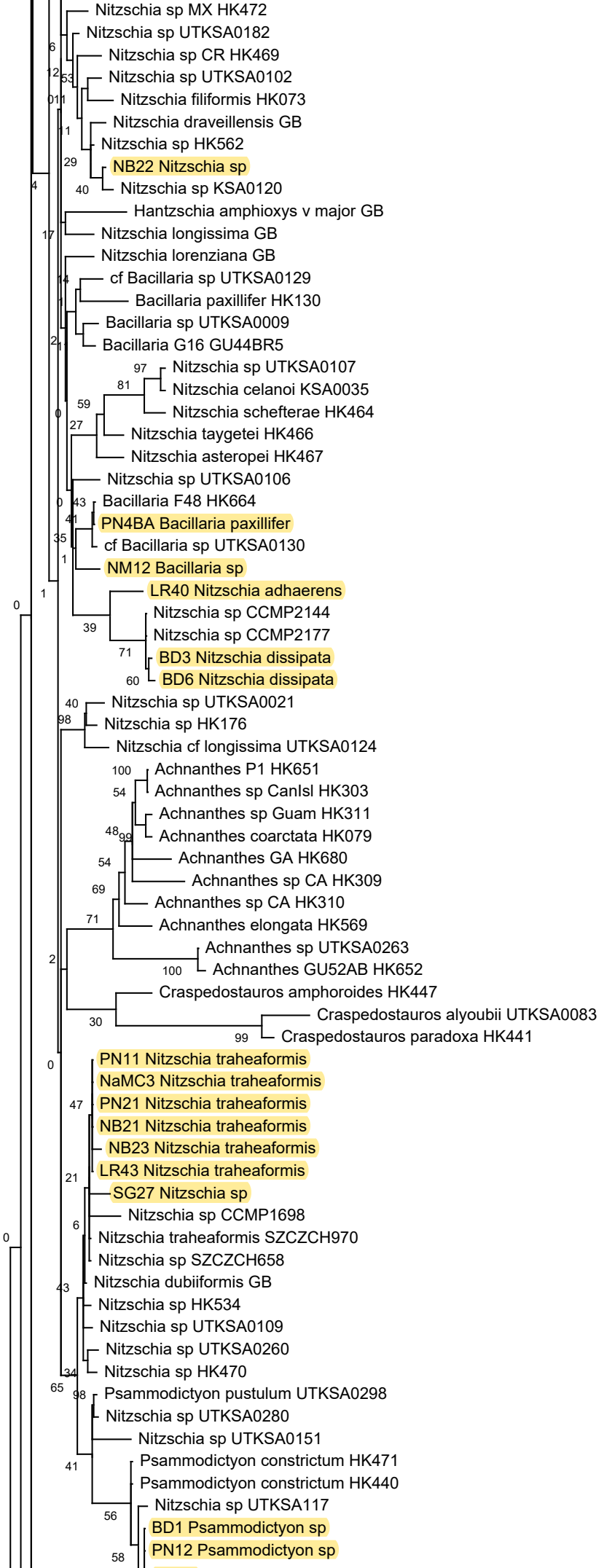
Nitzschia sp MX HK472
Nitzschia sp UTKSA0182
Nitzschia sp CR HK469
Nitzschia sp UTKSA0102
Nitzschia filiformis HK073
Nitzschia draveillensis GB
Nitzschia sp HK562
NB22 Nitzschia sp
Nitzschia sp KSA0120
Hantzschia amphioxys v major GB
Nitzschia longissima GB
Nitzschia lorenziana GB
cf Bacillaria sp UTKSA0129
Bacillaria paxillifer HK130
Bacillaria sp UTKSA0009
Bacillaria G16 GU44BR5
Nitzschia sp UTKSA0107
Nitzschia celanoi KSA0035
Nitzschia schefterae HK464
Nitzschia taygetei HK466
Nitzschia asteropei HK467
Nitzschia sp UTKSA0106
Bacillaria F48 HK664
PN4BA Bacillaria paxillifer
cf Bacillaria sp UTKSA0130
NM12 Bacillaria sp
LR40 Nitzschia adhaerens
Nitzschia sp CCMP2144
Nitzschia sp CCMP2177
BD3 Nitzschia dissipata
BD6 Nitzschia dissipata
Nitzschia sp UTKSA0021
Nitzschia sp HK176
Nitzschia cf longissima UTKSA0124
Achnanthes P1 HK651
Achnanthes sp CanIsl HK303
Achnanthes sp Guam HK311
Achnanthes coarctata HK079
Achnanthes GA HK680
Achnanthes sp CA HK309
Achnanthes sp CA HK310
Achnanthes elongata HK569
Achnanthes sp UTKSA0263
Achnanthes GU52AB HK652
Craspedostauros amphoroides HK447
Craspedostauros alyoubii UTKSA0083
Craspedostauros paradoxa HK441
PN11 Nitzschia traheaformis
NaMC3 Nitzschia traheaformis
PN21 Nitzschia traheaformis
NB21 Nitzschia traheaformis
NB23 Nitzschia traheaformis
LR43 Nitzschia traheaformis
SG27 Nitzschia sp
Nitzschia sp CCMP1698
Nitzschia traheaformis SZCZCH970
Nitzschia sp SZCZCH658
Nitzschia dubiiformis GB
Nitzschia sp HK534
Nitzschia sp UTKSA0109
Nitzschia sp UTKSA0260
Nitzschia sp HK470
Psammodictyon pustulum UTKSA0298
Nitzschia sp UTKSA0280
Nitzschia sp UTKSA0151
Psammodictyon constrictum HK471
Psammodictyon constrictum HK440
Nitzschia sp UTKSA117
BD1 Psammodictyon sp
PN12 Psammodictyon sp

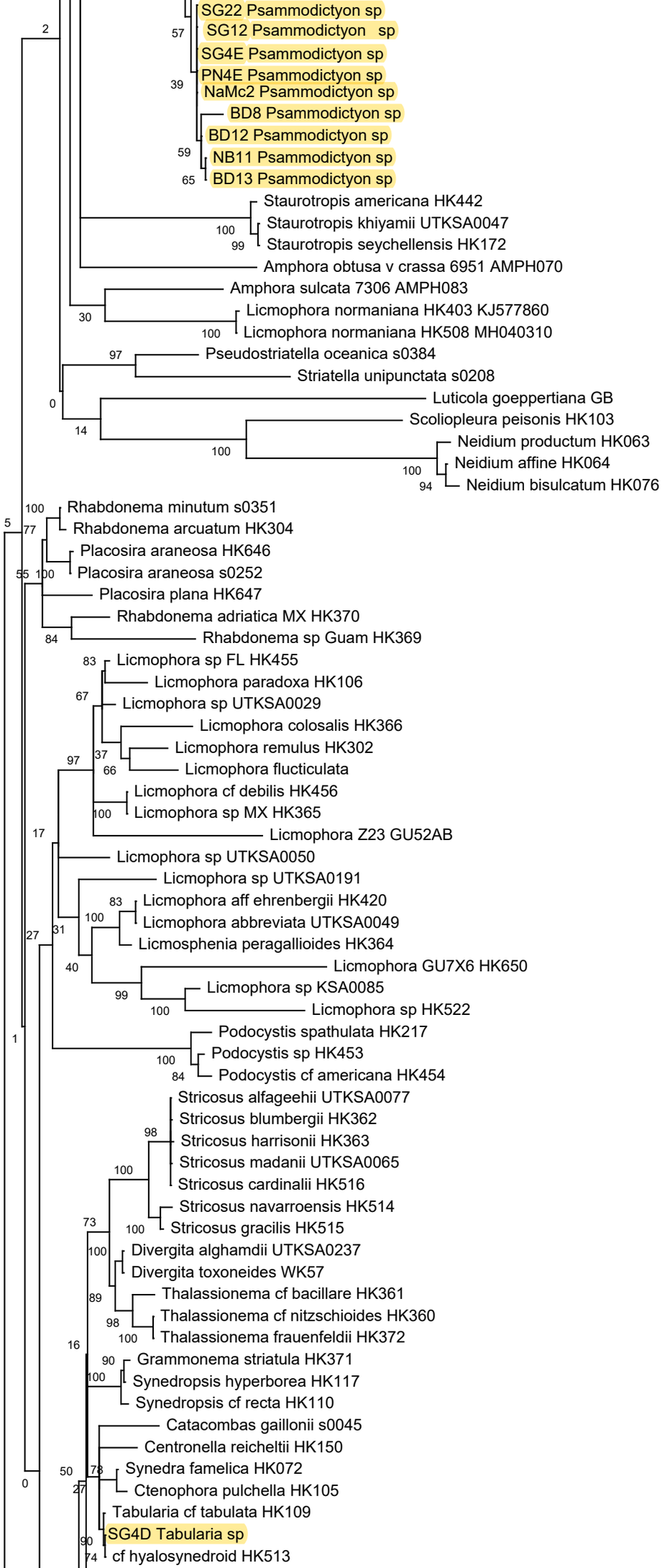
SG22 Psammodictyon sp
SG12 Psammodictyon sp
SG4E Psammodictyon sp
PN4E Psammodictyon sp
NaMc2 Psammodictyon sp
BD8 Psammodictyon sp
BD12 Psammodictyon sp
NB11 Psammodictyon sp
BD13 Psammodictyon sp
Staurotropis americana HK442
Staurotropis khiyamii UTKSA0047
Staurotropis seychellensis HK172
Amphora obtusa v crassa 6951 AMPH070
Amphora sulcata 7306 AMPH083
Licmophora normaniana HK403 KJ577860
Licmophora normaniana HK508 MH040310
Pseudostriatella oceanica s0384
Striatella unipunctata s0208
Luticola goeppertiana GB
Scoliopleura peisonis HK103
Neidium productum HK063
Neidium affine HK064
Neidium bisulcatum HK076
Rhabdonema minutum s0351
Rhabdonema arcuatum HK304
Placosira araneosa HK646
Placosira araneosa s0252
Placosira plana HK647
Rhabdonema adriatica MX HK370
Rhabdonema sp Guam HK369
Licmophora sp FL HK455
Licmophora paradoxa HK106
Licmophora sp UTKSA0029
Licmophora colosalis HK366
Licmophora remulus HK302
Licmophora flucticulata
Licmophora cf debilis HK456
Licmophora sp MX HK365
Licmophora Z23 GU52AB
Licmophora sp UTKSA0050
Licmophora sp UTKSA0191
Licmophora aff ehrenbergii HK420
Licmophora abbreviata UTKSA0049
Licmosphenia peragallioides HK364
Licmophora GU7X6 HK650
Licmophora sp KSA0085
Licmophora sp HK522
Podocystis spathulata HK217
Podocystis sp HK453
Podocystis cf americana HK454
Stricosus alfageehii UTKSA0077
Stricosus blumbergii HK362
Stricosus harrisonii HK363
Stricosus madanii UTKSA0065
Stricosus cardinalii HK516
Stricosus navarroensis HK514
Stricosus gracilis HK515
Divergita alghamdii UTKSA0237
Divergita toxoneides WK57
Thalassionema cf bacillare HK361
Thalassionema cf nitzschioides HK360
Thalassionema frauenfeldii HK372
Grammonema striatula HK371
Synedropsis hyperborea HK117
Synedropsis cf recta HK110
Catacombas gaillonii s0045
Centronella reicheltii HK150
Synedra famelica HK072
Ctenophora pulchella HK105
Tabularia cf tabulata HK109
SG4D Tabularia sp
cf hyalosynedroid HK513

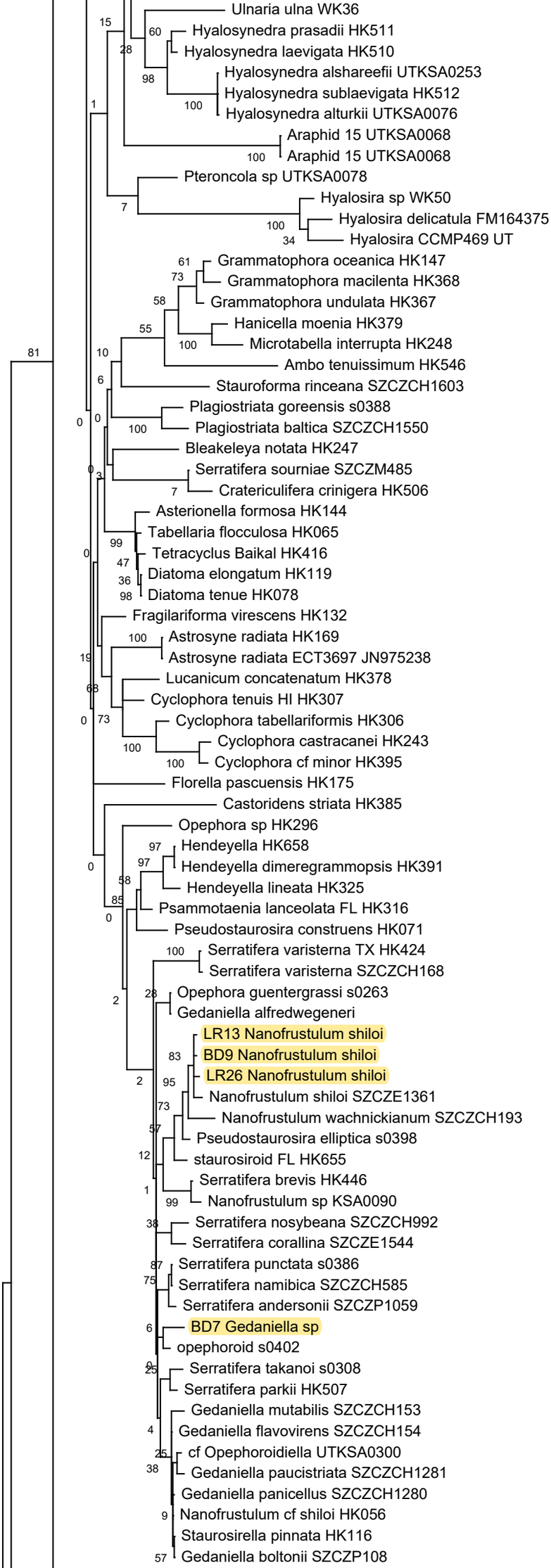
Ulnaria ulna WK36
Hyalosynedra prasadii HK511
Hyalosynedra laevigata HK510
Hyalosynedra alshareefii UTKSA0253
Hyalosynedra sublaevigata HK512
Hyalosynedra alturkii UTKSA0076
Araphid 15 UTKSA0068
Araphid 15 UTKSA0068
Pteroncola sp UTKSA0078
Hyalosira sp WK50
Hyalosira delicatula FM164375
Hyalosira CCMP469 UT
Grammatophora oceanica HK147
Grammatophora macilenta HK368
Grammatophora undulata HK367
Hanicella moenia HK379
Microtabella interrupta HK248
Ambo tenuissimum HK546
Stauroforma rinceana SZCZCH1603
Plagiostriata goreensis s0388
Plagiostriata baltica SZCZCH1550
Bleakeleya notata HK247
Serratifera sourniae SZCZM485
Cratericulifera crinigera HK506
Asterionella formosa HK144
Tabellaria flocculosa HK065
Tetracyclus Baikal HK416
Diatoma elongatum HK119
Diatoma tenue HK078
Fragilariforma virescens HK132
Astrosyne radiata HK169
Astrosyne radiata ECT3697 JN975238
Lucanicum concatenatum HK378
Cyclophora tenuis HI HK307
Cyclophora tabellariformis HK306
Cyclophora castracanei HK243
Cyclophora cf minor HK395
Florella pascuensis HK175
Castoridens striata HK385
Opephora sp HK296
Hendeyella HK658
Hendeyella dimeregrammopsis HK391
Hendeyella lineata HK325
Psammotaenia lanceolata FL HK316
Pseudostaurosira construens HK071
Serratifera varisterna TX HK424
Serratifera varisterna SZCZCH168
Opephora guentergrassi s0263
Gedaniella alfredwegeneri
LR13 Nanofrustulum shiloi
BD9 Nanofrustulum shiloi
LR26 Nanofrustulum shiloi
Nanofrustulum shiloi SZCZE1361
Nanofrustulum wachnickianum SZCZCH193
Pseudostaurosira elliptica s0398
staurosiroid FL HK655
Serratifera brevis HK446
Nanofrustulum sp KSA0090
Serratifera nosybeana SZCZCH992
Serratifera corallina SZCZE1544
Serratifera punctata s0386
Serratifera namibica SZCZCH585
Serratifera andersonii SZCZP1059
BD7 Gedaniella sp
opephoroid s0402
Serratifera takanoi s0308
Serratifera parkii HK507
Gedaniella mutabilis SZCZCH153
Gedaniella flavovirens SZCZCH154
cf Opephoroidiella UTKSA0300
Gedaniella paucistriata SZCZCH1281
Gedaniella panicellus SZCZCH1280
Nanofrustulum cf shiloi HK056
Staurosirella pinnata HK116
Gedaniella boltonii SZCZP108

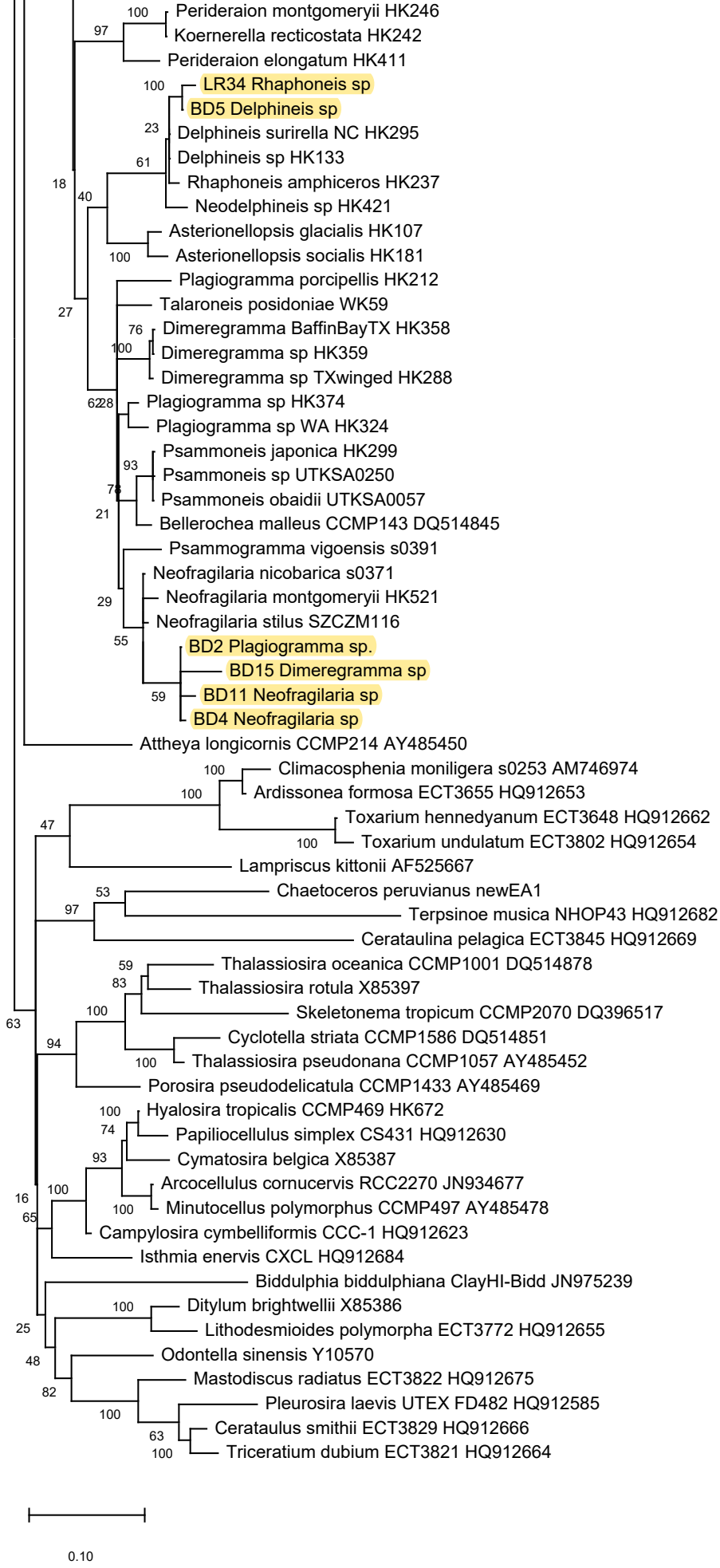
Perideraion montgomeryii HK246
Koernerella recticostata HK242
Perideraion elongatum HK411
LR34 Rhaphoneis sp
BD5 Delphineis sp
Delphineis surirella NC HK295
Delphineis sp HK133
Rhaphoneis amphiceros HK237
Neodelphineis sp HK421
Asterionellopsis glacialis HK107
Asterionellopsis socialis HK181
Plagiogramma porcipellis HK212
Talaroneis posidoniae WK59
Dimeregramma BaffinBayTX HK358
Dimeregramma sp HK359
Dimeregramma sp TXwinged HK288
Plagiogramma sp HK374
Plagiogramma sp WA HK324
Psammoneis japonica HK299
Psammoneis sp UTKSA0250
Psammoneis obaidii UTKSA0057
Bellerochea malleus CCMP143 DQ514845
Psammogramma vigoensis s0391
Neofragilaria nicobarica s0371
Neofragilaria montgomeryii HK521
Neofragilaria stilus SZCZM116
BD2 Plagiogramma sp.
BD15 Dimeregramma sp
BD11 Neofragilaria sp
BD4 Neofragilaria sp
Attheya longicornis CCMP214 AY485450
Climacosphenia moniligera s0253 AM746974
Ardissonea formosa ECT3655 HQ912653
Toxarium hennedyanum ECT3648 HQ912662
Toxarium undulatum ECT3802 HQ912654
Lampriscus kittonii AF525667
Chaetoceros peruvianus newEA1
Terpsinoe musica NHOP43 HQ912682
Cerataulina pelagica ECT3845 HQ912669
Thalassiosira oceanica CCMP1001 DQ514878
Thalassiosira rotula X85397
Skeletonema tropicum CCMP2070 DQ396517
Cyclotella striata CCMP1586 DQ514851
Thalassiosira pseudonana CCMP1057 AY485452
Porosira pseudodelicatula CCMP1433 AY485469
Hyalosira tropicalis CCMP469 HK672
Papiliocellulus simplex CS431 HQ912630
Cymatosira belgica X85387
Arcocellulus cornucervis RCC2270 JN934677
Minutocellus polymorphus CCMP497 AY485478
Campylosira cymbelliformis CCC-1 HQ912623
Isthmia enervis CXCL HQ912684
Biddulphia biddulphiana ClayHI-Bidd JN975239
Ditylum brightwellii X85386
Lithodesmioides polymorpha ECT3772 HQ912655
Odontella sinensis Y10570
Mastodiscus radiatus ECT3822 HQ912675
Pleurosira laevis UTEX FD482 HQ912585
Cerataulus smithii ECT3829 HQ912666
Triceratium dubium ECT3821 HQ912664
0.10

Figure. 25 Phylogenetic Tree: Maximum likelihood tree of 541 sequences of pennate diatoms and outgroup in centric diatoms; log likelihood -67753.92. The percentage of trees in which the associated taxa clustered together is shown next to the branches. Bootstrap support is shown next to the branches. The tree has been drawn to scale, with branch lengths measured in the number of substitutions per site. Sequences obtained in this study are marked yellow.

The tree showed that 55 of the 59 strains were recovered in a clade with reference sequences of conspecific or congeneric species in accordance with expectations based on the morphological observations (Table 2). While sequences of the remaining strains were recovered near reference sequences inconsistent with expectations based on morphology.

For the following strains, the morphological classification was inconsistent with results of Blast and phylogenetic position according to the 18S rRNA gene sequence: BD2, BD11 and BD4 which were identified as *Dimeregramma* species with LM showed *Plagiogramma* sp., *Plagiogramma marginalis*, *Neofragilaria nicobarica* respectively. NM11 strain identified as *Navicula* sp.in the LM resulted in the *Seminavis* sp. with the gene sequencing. The strains PN4F, SG35 and SG4C that were identified

as *Nitzschia longissima* in LM resulted to be *Cylindrotheca closterium* based on V4 18S rRNA sequence.

A total of 13 strains out of the 59 investigated in this study were selected for ultrastructural analysis in electron microscopy (SEM & TEM) to confirm species identification in cases in which LM and 18S rRNA gene have provided uncertain or conflicting results (Table 5). The morphological description of these strains has been provided below.

Table (): Morphometrics and molecular comparison of the selected isolated strains. (Species name and sequence identity of the closest relative found in the GenBank using BLASTn). AA: Apical Axis, TA: Transapical axis, TS: Transverse striae in 10 µm, F: Fibulae

Species Name (Morphological identified)	**Strain no.**	**Morphometrics**				**Ref. (which confirms the species morphologically)**	**BLASTn of 18S rDNA**	
		AA	**TA**	**TS**	**F**		**Species name**	**Identity %**
Nitzschia traheaformis	PN11	44-47	4-5	35-38	15-17	(Witkowski et al., 2016)	*Nitzschia traheaformis*	100
Nitzschia traheaformis	NaMC3	41-44	5-6	34-36	12-15	(Witkowski et al., 2016)	*Nitzschia traheaformis*	100
Nitzschia adhaerens	LR40	32.48	2.25	49	23	(Mucko et al., 2020b)	*Nitzschia adhaerens*	100
Psammodictyon panduriforme	PN12	19-22	6-7	29-30	15	(Round et al., 1990)	*Psammodictyon panduriforme*	100
Psammodictyon sp.	NaMC2	10-13	5-6	28-31	9-12	(Round et al., 1990)	*Psammodictyon* sp.	99.81
cf. *Dimeregramma* sp.	BD2	-	-	-		(Round et al., 1990)	*Plagiogramma appendiculatum*	99.59
Nanofrustulum shiloi	BD9	6.5-7.65	2-3	20		(Round et al., 1999)	*Nanofrustulum shiloi*	99.32
cf. *Gedaniella* sp.	BD7	-	-	-		(LI et al., 2018)	*Gedaniella* cf. *flavovirens*	98.73

cf. *Psammogramma* sp.	BD4	14.6-15.4	4.3-4.5	20		(Sato et al., 2008)	*Neofragilaria nicobarica*	98.10
Nitzschia sp. *dissipata*	BD3	10.45-11	4	49-50	10	(Rimet et al., 2011)	*Nitzschia* sp.	97.92
Amphora binodis	BD10	22.8	3.7	22		(Gregory, 1857b)	*Amphora* sp.	97.24
cf. *Dimeregramma* sp.	BD11	-	-	-		(Round et al., 1990)	*Plagiogramma marginalis*	96.47
Diploneis weissflogiopsis	PN4DP	32-42	8.5-12.22	11-12		(Pennesi et al., 2017a)	*Diploneis* sp.	96.19

3.4.4 Morphology based identification of the 13 selected strains using electron microscopy

In the below text the following abbreviations are applied: AA: Apical Axis, TA: Transapical Axis, TS: Transapical striae

1. **PN11 and NaMC3 *Nitzschia traheaformis*** Witkowski

   PN11:

   Sequence information: *Nitzschia traheaformis,* 100%, KT943642

   Locality: Ancona, station Portonovo

   Morphometric data: AA: 44-47 µm, TA: 4-5 µm, TS in 10 µm: 35-38, F in 10 µm: 15-17

2. **NaMC3:**

   Sequence information: *Nitzschia traheaformis*, 100%, KT943644

   Locality: Gulf of Naples, station NaMC

   Morphometric data: AA: 41-44 µm, TA: 5-6 µm, TS in 10 µm: 34-36, F in 10 µm: 12-15

Cells solitary, linear to lanceolate, with cuneate, slightly capitate apices. Valves constricted in the centre on the raphe side where the opposite side is nearly straight. Raphe strongly eccentric in marginal canal (Figure. 26b). External view has central nodule (Figure. 26d), while terminal part is hooked (Figure. 26c). In the internal view central part of the raphe shows simple endings. Fibulae forms simple arches bridging in two sides of valves, other than centre part more less evenly distributed

(Figure. 26a). Transverse striae parallel throughout with circular areolae (Figure 26d). Few areolae are absent in the central part on the smaller side of the valve (Figure. 26d). Girdle bands are open with 1 to 2 rows of the round poroids. Also, molecular analysis done by (Witkowski et al., 2016) confirmed the same species as *N. traheaformis*.

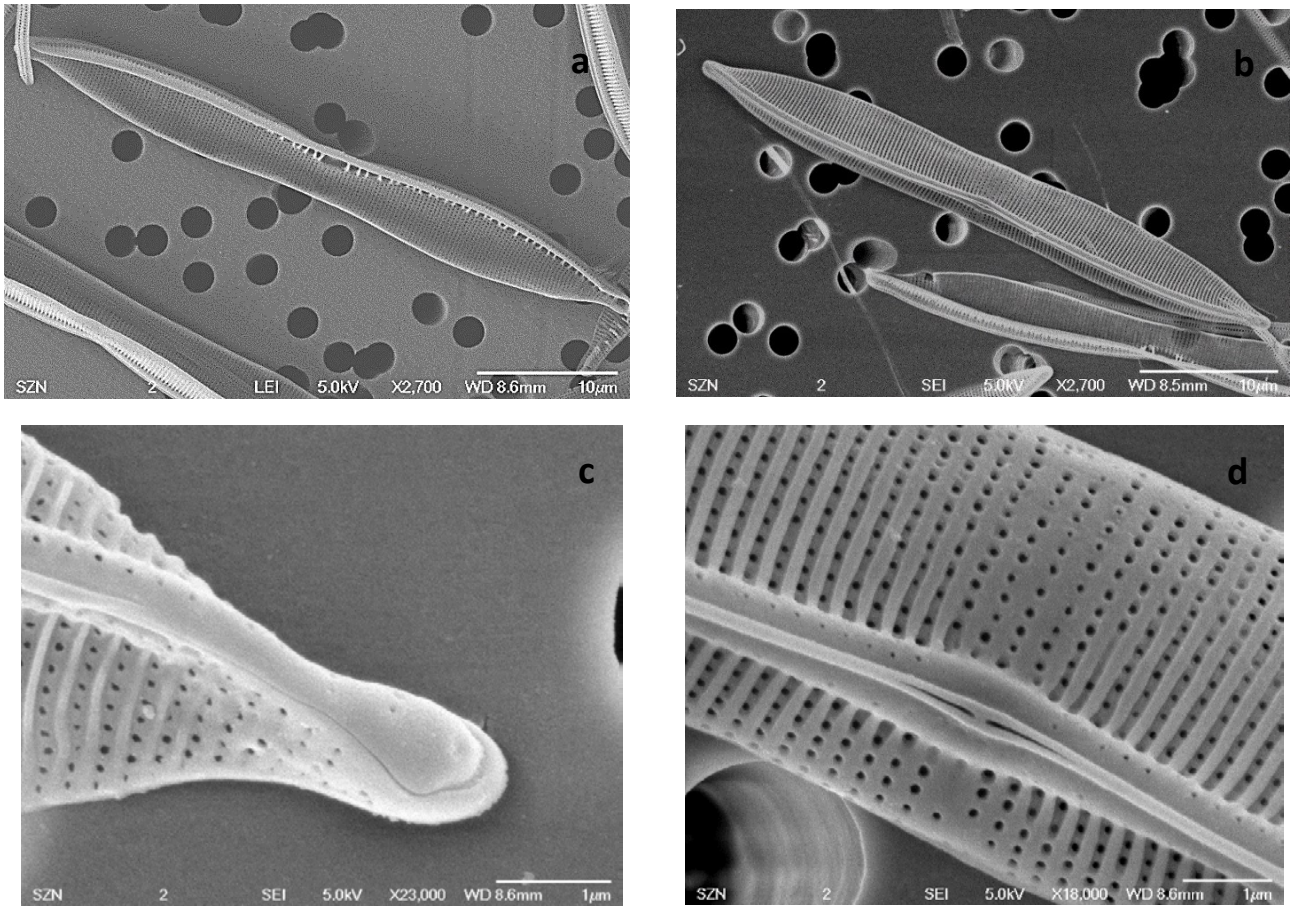

Figure. 26: *Nitzschia traheaformis* a; internal valve view, b; external valve view, c; terminal of external valve, d; central nodule on external valve

3. LR40 *Nitzschia adhaerens* Mucko & Bosak

Sequence information: Nitzschia adhaerens, 100%, MH734167

Locality: Pozzuoli Bay, station LR

Morphometric data: AA: 32.48 um, TA: 2.25 um, TS in 10 µm: 49, F in 10 µm: 23, poroids in 1 µm: 6.

Valves lanceolate, apices cuneate in valve view (Figure. 27a) and apparently very slightly spathulate (broad, rounded ends) in girdle view (Figure. 27c). Raphe keel narrow, discrete and elevated about valve face (Figure. 27c) (i.e., there is an abrupt transition from valve face to keel, almost central). Terminal raphe fissures curved (Figure. 27c). External raphe end to end. Very fine and delicate transverse striae, not resolvable in LM. Uniseriate striae of tiny round to rectangular areolae; the areolae (5–6 in 1 μm) occluded by finely perforated hymens (Figure. 27d). Each uniseriate transapical stria ends up by two areolae within the keel (Figure. 27c). Virgae flat, never bifurcating (Figure. 27d). Fibulae relatively dense, regularly spaced throughout keel (Mucko et al., 2020a).

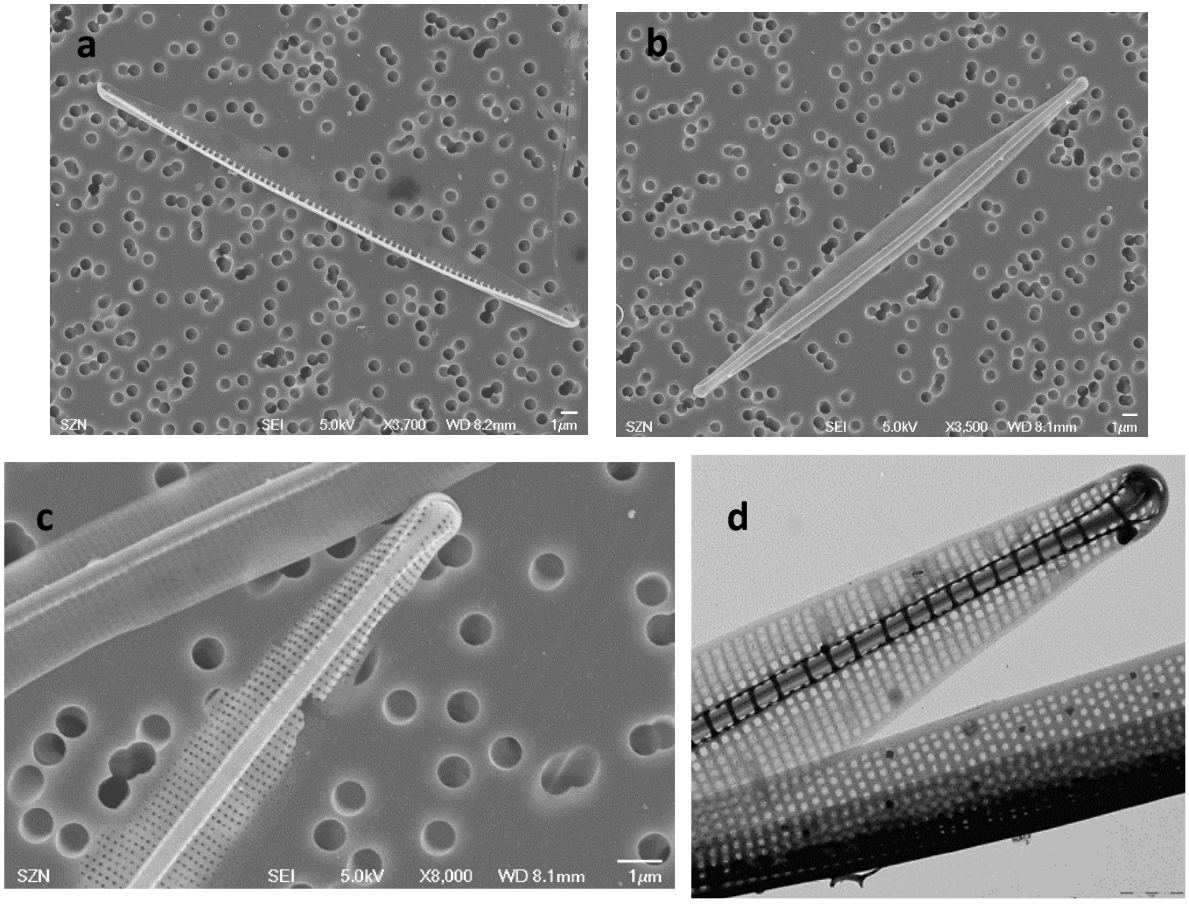

Figure. 27: *Nitzschia* a*dhaerens* a; internal valve view, b; external valve view, c; terminal of external view, d; TEM of external valve view

4. PN12 ***Psammodictyon panduriforme*** D.G.Mann

Sequence information: *Psammodictyon panduriforme,* 100%, KY054991

Locality: Ancona, station Portonovo

Morphometric data: AA:19–22 µm, TA: 6–7 µm, TS in 10 µm: 29–30, F in 10 µm: 15

Cells panduriform with apiculate apices in valve view (Figure. 28a). Raphe submarginal, keeled and internally composed by simple rib-like fibulae. Internally raphe endings terminate in very small helictoglossae (Figure. 28b) while external terminal end shows hooked structure pointing outside (Figure 28c). External central raphe endings not continuous/ disrupted, nodule present (Figure 28d). Striae uniseriate, consisting of quadrangular to roundish loculate areolae externally. Internally areolae opening in the bipinnate (Figure. 28b) while externally exhibiting large perforations. Open girdle bands generally exhibit 2 to 3 rows of poroids.

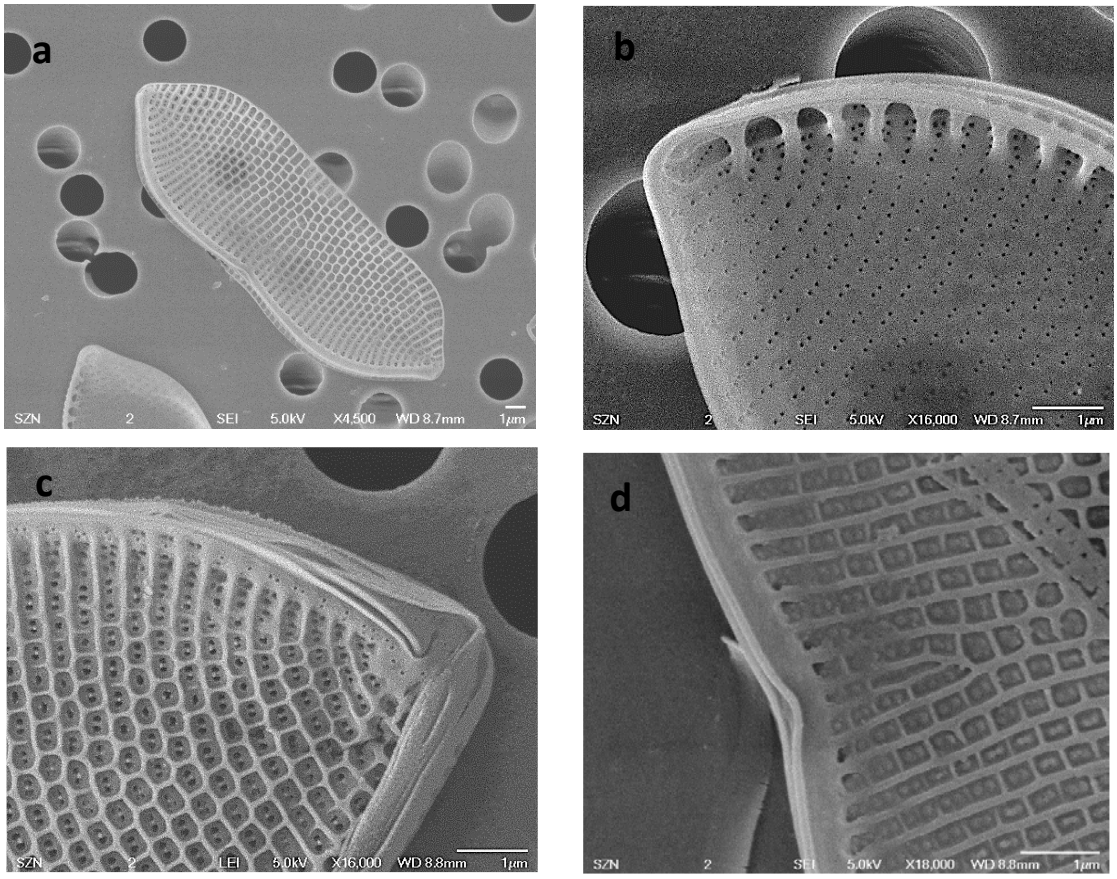

Figure. 28: *Psammodictyon panduriforme* a; external valve view, b; terminal of internal valve, c; terminal of external valve, d; central nodule on external valve

5. NaMC2: *Psammodictyon* sp.

Sequence information: *Psammodictyon* sp. 99.81%, JQ885984

Locality: Gulf of Naples, station NaMC

Morphometric data: AA: 10–13 µm, TA: 5–6 µm, TS in 10 µm: 28–31, F in 10 µm: 9–12

Cells panduriform with apiculate apices in valve view (Figure. 29a). Raphe submarginal, keeled and internally composed by simple rib-like fibulae. Internally raphe endings terminate in very small helictoglossae (Figure. 29b) while external terminal end shows hooked structure (Figure. 29c) pointing inside. On the external valve, the central structure of the raphe shows an elevated central nodule (Figure. 29d). Striae uniseriate, consisting of quadrangular to roundish areolae externally. In the internal valve, bi- to quadri-porate areolae were visible, while in the external valve large perforations were observed. Open girdle bands generally with 2 to 3 rows of poroids.

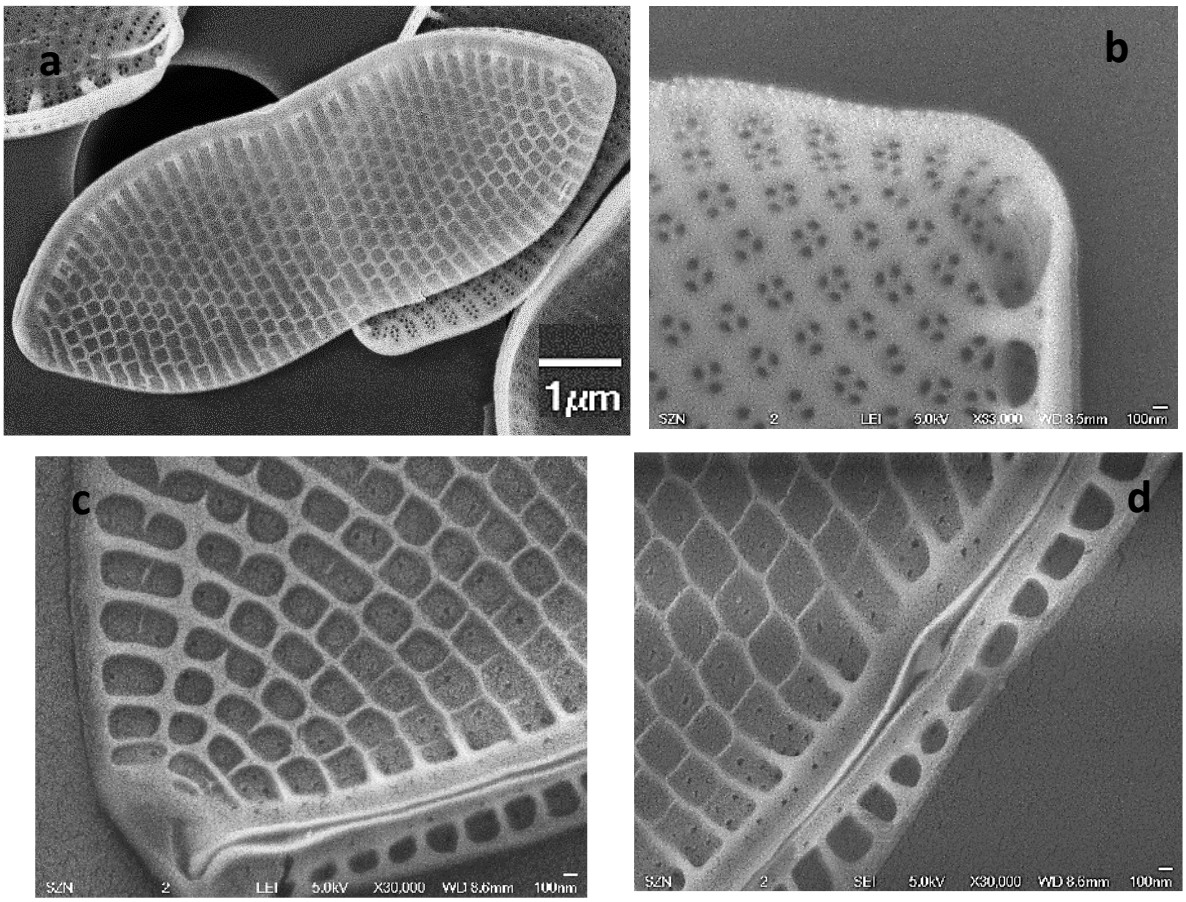

Figure. 29: *Psammodictyon* sp. a; external valve view, b; terminal of internal valve, c; terminal of external valve, d; central nodule on external valve

6. BD2: *Dimeregramma* sp.

Sequence information: Plagiogramma appendiculatum, 99.59%, KJ577867

Locality: Pozzuoli Bay, station BD1A

Measurements of the cells are not feasible as the culture was old and has compromised size and shape. In LM, cells are rectangular and attached to each other with apices forming a filament (Plate. 2c).

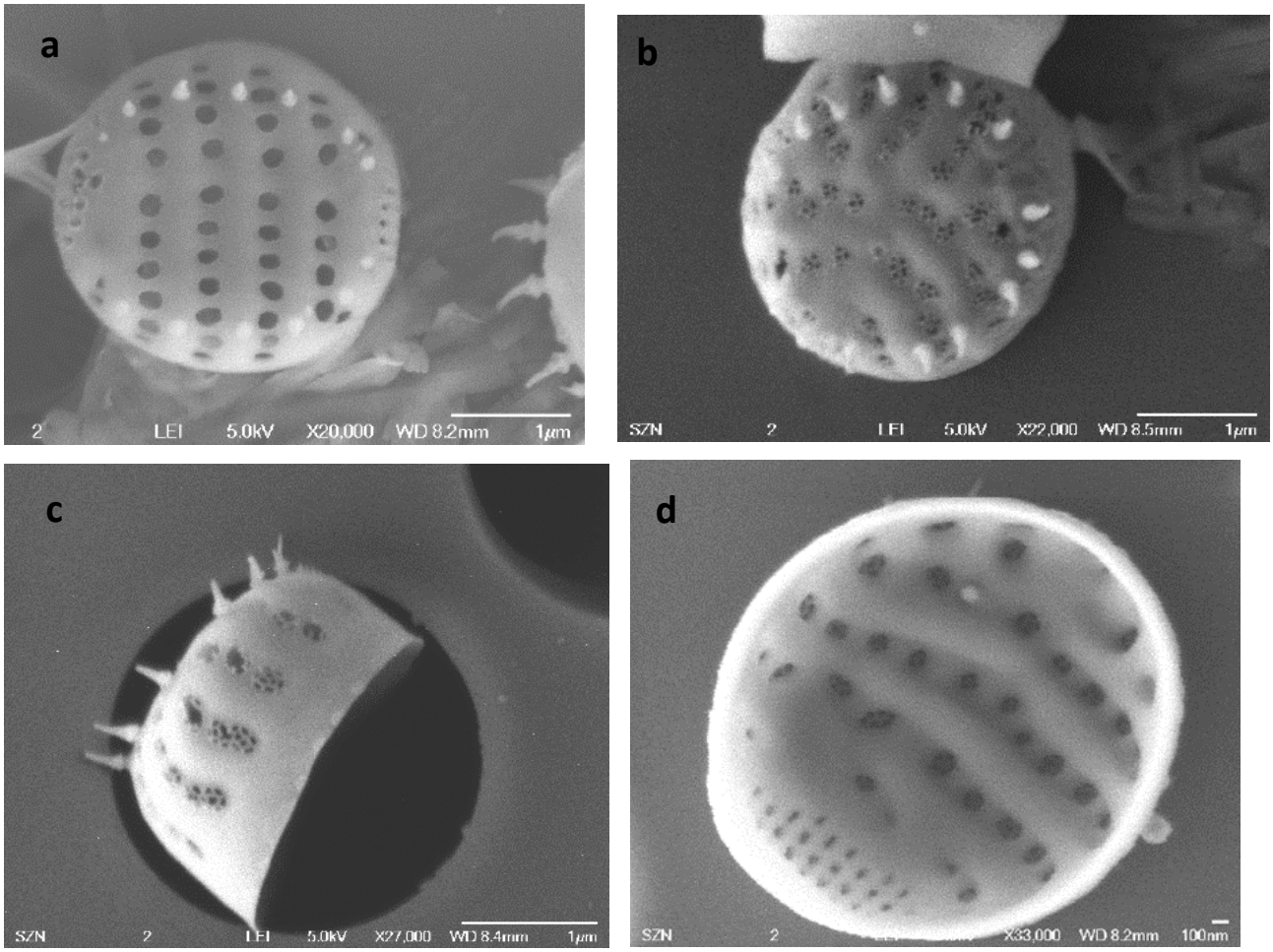

Figure. 30: *Dimeregramma* sp.: a; external valve view in which sternum is slightly visible; b; external valve view showing perforations in areolae: c; side view of external valve with spines, d; internal valve view.

As the cultures were old, cells were not in good state while taking photographs (shape of the valve has changed from elongated to circular). Valves are deep (Figure. 30c). Uniseriate striae containing round areolae. Areolae arranged in a single line have cribra internally and externally. Spines are present on the margin and bifurcating (in some places) (Figure. 30c). Apical pore field observed at both ends (Figure. 30a). The sternum is slightly visible, while in in the genus *Dimeregramma* it is clearly distinct.

7. **BD9 *Nanofrustulum shiloi*** (J.J.Lee, Reimer & McEnery) Round, Hallsteinsen & Paasche

Sequence information: Nanofrustulum shiloi, 99.32%, KU851875

Locality: Pozzuoli Bay, station BD1B

Morphometric data: AA: 2–6 µm, TA: 2– 3 µm, TS in 10 µm: 15.

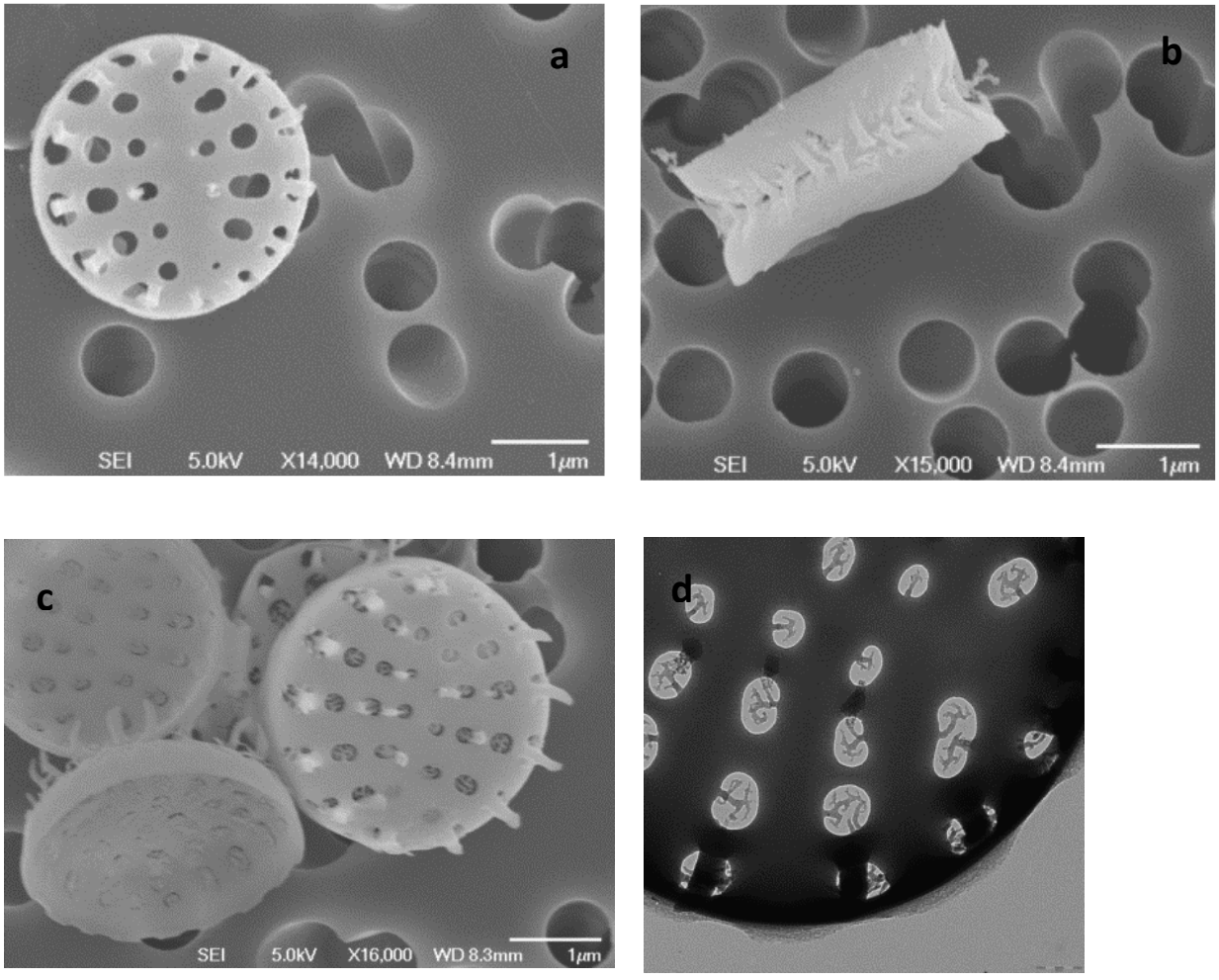

Figure. 31: *Nanofrustulum shiloi* a; external valve view, b; girdle valve view showing interlocking of copulae, c; external valve with spines and perforations of areolae, d; TEM showing hymen in the areolae.

Cells in short chains, linked by interlocking marginal spines (Figure. 31b). Valves circular to slightly oval (Figure. 31a). Valve surface flat or slightly domed, mantle curved or vertical. Areolae radiating and forming striae from a central elongate sternum - not from a central annulus. Areolae somewhat variable - round to radially elongate, especially towards the mantle (Figure. 31a). Vela on the inside of the valve (Figure. 31d). Central valve faces often with small warts or spines, sometimes almost plain (Figure. 31c). Marginal spines located peripherally across the areolar rows, usually simple but often with a basal, downwardly projecting spinule (Figure. 31a, c). Areolae continuing (as single, or more rarely, double) openings below the spines. Valvocopula split segments and copulae a series of interlocking segments, without areolae but some with fimbriate edge (Figure. 31b).

8. BD7 *Gedaniella*

Sequence information: cf. *Gedaniella flavovirens,* 98.73%, MF093136

Locality: Pozzuoli Bay, station BD1A, depth (10m), 21/10/2019

The culture was observed long after isolation, so the size and shape changed and it was not possible to measure cells.

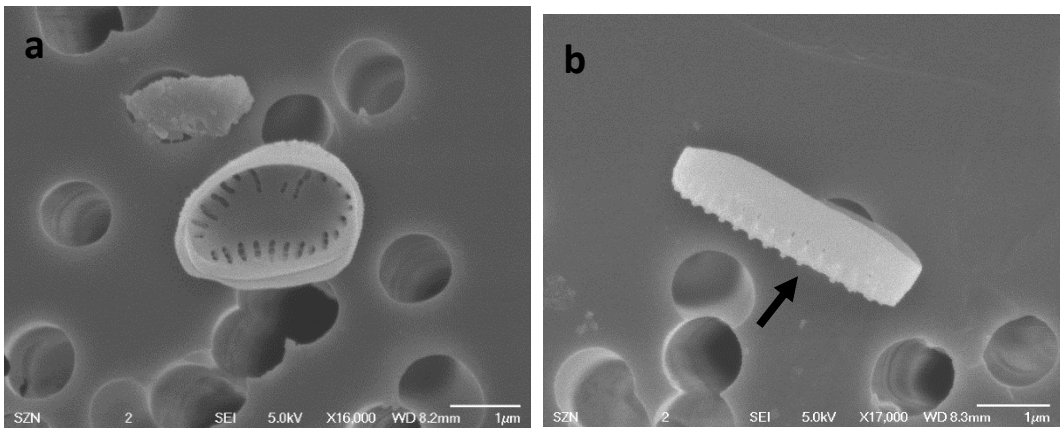

Figure. 32: *Gedaniella* sp. a; internal valve view, b; side valve view

In light microscopy one or two chloroplasts were observed. Frustules rectangular in girdle view, forming ribbon-like, valve face to valve face colonies or as radiate colonies by contact of apical pore fields, rarely solitary. Valves heteropolar, lanceolate, elliptical or ovate. Transverse striae uniseriate, alternate, composed of areolae variable in number within a single stria. Shape of areola varies, from round to tetragonal to apically elliptical. Areolae occluded with branched volae, in most cases, with rods originating from vimines (a silica connection between adjacent areolae, separating areolae within a stria) and parallel to transapical axis (Figure. 32a). Marginal spines present (Figure. 32b). Apical pore fields heteropolar, with absent or small head apical pore fields. No rimoportulae. Spines, which is the characteristic feature of *Gedaniella boltoni*, can be noticed in one picture (Figure. 32b).

9. BD4 cf. *Psammogramma*

Sequence information: Neofragilaria nicobarica, 98.10%, AB433340

Locality: Pozzuoli Bay, station BD1A, depth (10m), 21/10/2019

Morphological measurements: AA: 14.6–15.4 µm, TA: 4.3–4.5 µm, Striae in 10 µm: 20

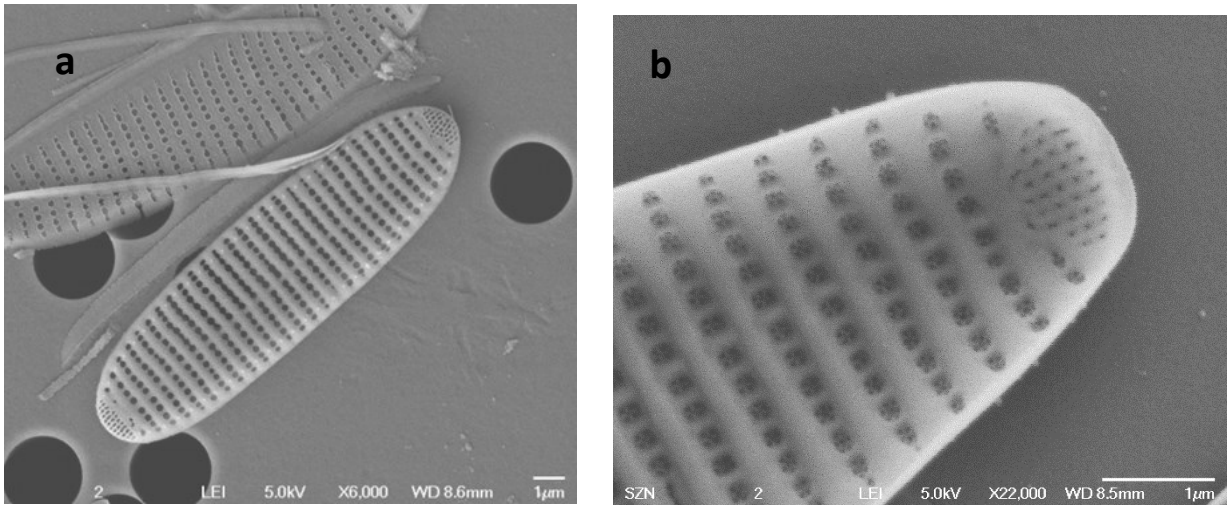

Figure. 33: cf. *Psammogramma* sp. a; external valve view, b; internal valve view showing perforations in areolae

In LM, cells attached to each other in single straight line. Chloroplast 2. Cells rectangular in girdle view. 5–10 plain and open girdle bands interlacing with each other. Valves elliptical, with rounded face without an abrupt mantle. Granules present on the valve face-mantle junction (Figure. 33b). Uniseriate striae with round areolae containing fine rotae (Figure. 33b) (rotae not observed from valve exterior but from the interior). Apical pore field obscured externally (Figure. 33b) but internally well arranged (Figure. 33b). Indistinct Sternum. Rimoportula absent. (Sato et al., 2008).

10. BD3: ***Nitzschia dissipata*** (Kützing) Rabenhorst

Sequence information: Nitzschia sp., 97.92%, KT943641

Locality: Pozzuoli Bay, station BD1A

Morphometric data: AA: 10.45–11 µm, TA: 4 µm, TS in 10µm: 49–50, F in 10µm: 10.

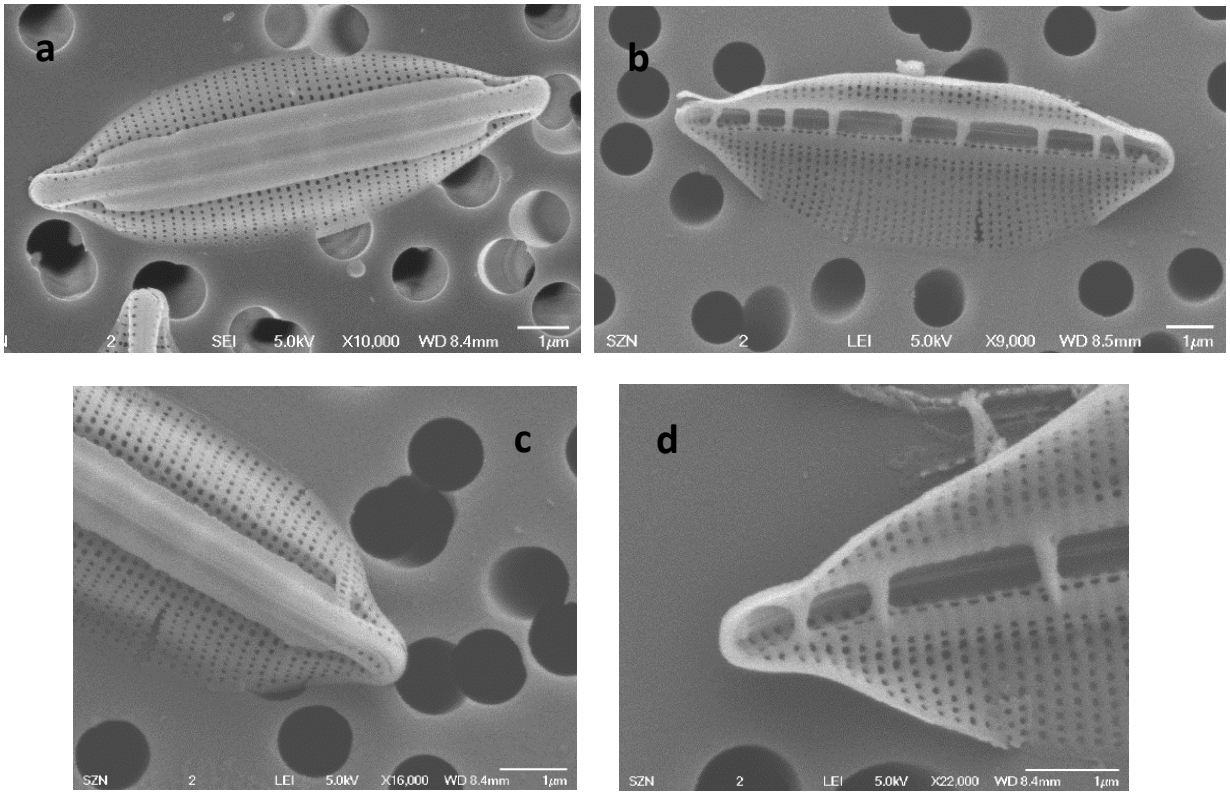

Figure. 34: *Nitzschia dissipata* a; external valve view, b; internal valve view, c; terminal end of external valve, d; terminal end of internal valve

Valve lanceolate expanded in the centre. Poles slightly rostrate (Figure. 34a). Uniseriate striae interrupted by lateral sternum in the internal valve with small and round areolae (Figure. 34b).

Conopeum present on the external valve with single row of poroids on both the sides of the raphe (Figure. 34a). Raphe slightly eccentric (Figure. 34b), continuous from pole to pole. Terminal fissure present at both ends turned towards distal side (Figure. 34c). Internally raphe endings terminate in very small helictoglossae (Figure. 34d). Fibulae coarse and less, unevenly distributed (Figure. 34b).

11. BD10 *Amphora binodis* var *bigibba* W. Gregory

Sequence information: *Amphora* sp. 97.24%, OP304755

Locality: Pozzuoli Bay, station BD1B

Morphological measurements: AA: 22.88 µm, TA: 3.7 µm in the wide region, 2.5 µm in the centre constricted, TS in 10 µm: 22 on the dorsal side.

Valves linear with rounded apices, markedly constricted in the centre, transverse striae delicate, forming visible divisions (interrupted in the centre) (Figure. 35a). Ventral margin straight, often convex in the central part. Raphe hooked on the external terminal side, in the centre curved in the same direction (Figure. 35b). Internal side of the valve contains central nodule (Figure 35a). In the records, *Amphora binodis* measures 44 to 60 µm in apical length with 13–15 TS in 10 µm. Instead var *bigibba* (Grun) is smaller in size and with finer striae. Therefore, this strain is confirmed as *A. binodis* var *bigibba.*

The specimen differs from *Amphora binodis,* which is taller, measuring 44 to 60 µm in length, and exhibiting fewer (13–15) TS in 10 µm. (Gregory, 1857a).

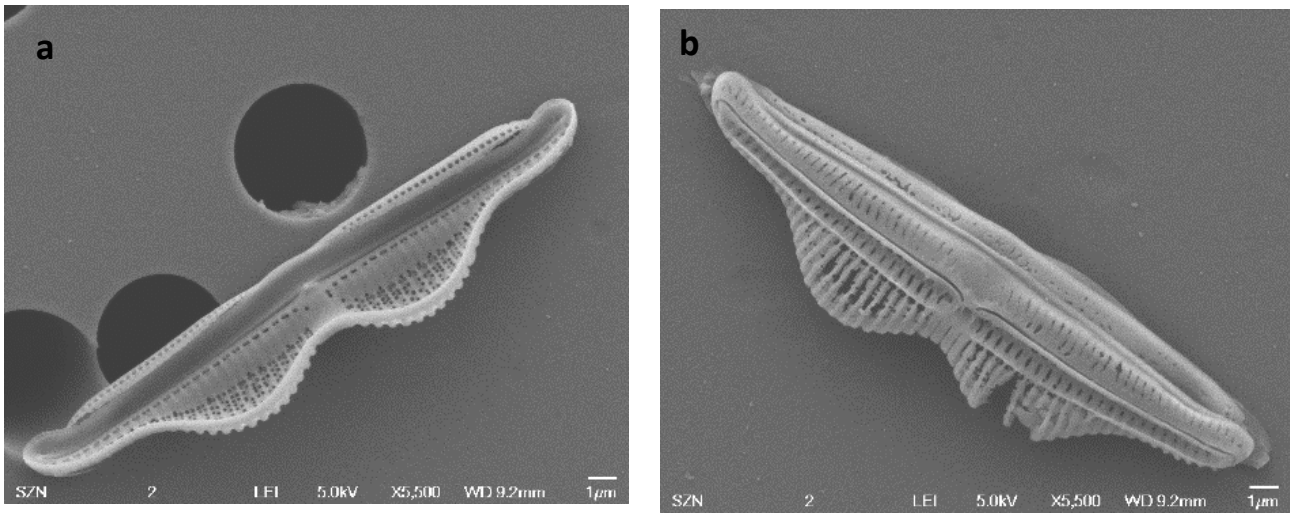

Figure. 35: *Amphora binodis* a; Internal valve view, b; external valve view.

12. BD 11 *Dimeregramma* sp.

Sequence information: Plagiogramma marginalis, 96.47 %, MN473922

Locality: Pozzuoli Bay, station BD1B

Morphometric data were not reliable as the culture was old and cells has reduced in size.. Valves linear or elliptical, distinct narrow sternum externally (Figure. 36a). Frustules strongly incised beneath the poles. Robust uniseriate striae with rounded areolae (Figure. 36a). Mantles are shallow. Spines are present around the edge of valves (Figure. 36c). Apical pore plate present, ornamented externally (Figure. 36a,c) and plain inside (Figure. 36b). Cribra were not visible. Cingular bands plain and closed (Figure. 36d).

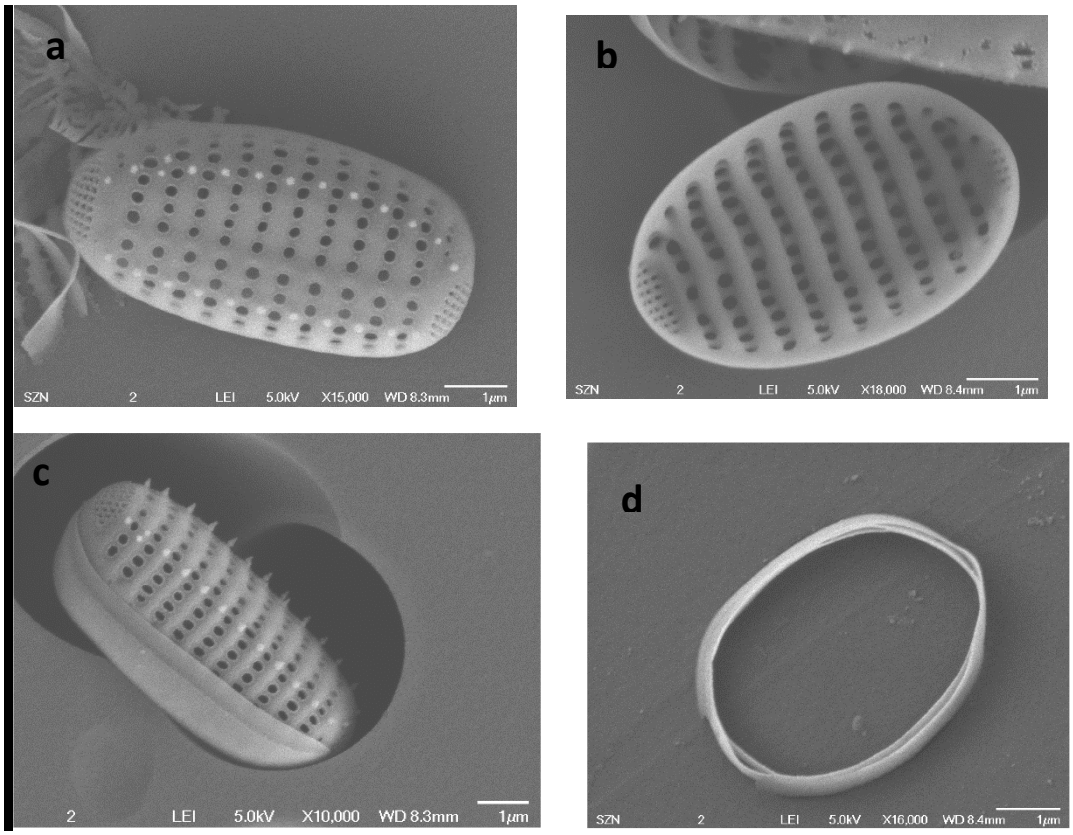

Figure. 36: *Dimeregramma* sp. a; external valve view, b; internal valve view, c; side view showing spines around the valve edge, d; girdle bands.

13. PN4DP: *Diploneis weissflogiopsis* Lobban & Pennesi

Sequence information: *Diploneis* sp. 96.19%, KX981839

Locality: Ancona, station Portonovo, depth (12–13 m), 19/01/2021

Morphological measurements: AA: 32–42 µm, TA at widest point: 8.5–12.22 µm, TA at centre: 4 to 6 µm, TS in 10 µm: 11 to 12,

Valves panduriform, with rounded apices. Externally, the raphe consists of two straight branches ending in deep central pores and terminal fissures bent towards the same side (Figure. 37a). Raphe-sternum narrow and depressed central area constrained by two triangular spines and four pores

(arrow). A pair of modified striae extend from these spines to the valve margin with one loculus in the middle of each. Two more pairs of modified areolae adjacent, each with one loculus, giving the series of three single foramina seen internally (Figure. 37b). Externally, strongly silicified valve surface shows virgae and vimenes. Internal raphe fissures sunken relative to the longitudinal canals and central nodule, ending co-axially in a raised central nodule and in slightly raised helictoglossae at poles. Parallel longitudinal canals present with a row of large round areolae which opens externally only. Radiate transapical striae, composed of transapically elongated areolae (Figure. 37a) externally and roundish foramina internally (Figure. 37b).

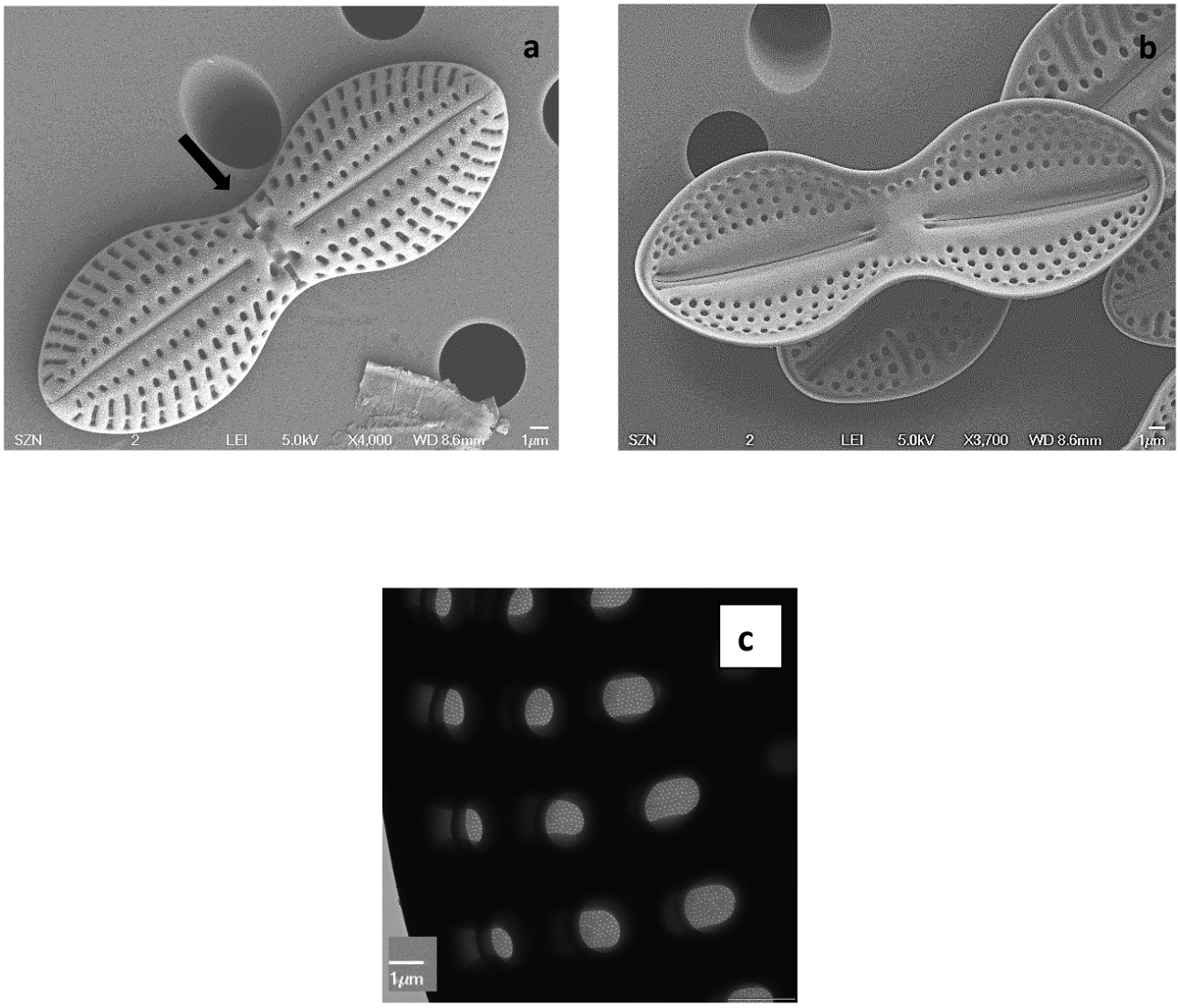

Figure. 37: *Diploneis weissflogiopsis* a; external view (arrow showing the central region characteristic of species), b; internal view, c; ultrastructure of the areolae.

3.5 Discussion

Most of the diatom strains isolated in this study can be identified to the genus level by means of LM alone. 18S rRNA gene sequences enable species level identification for many strains though this identification is not always reliable in case of hits with GenBank sequences below 97.5%. In the phylogenetic tree of 18S rRNA, despite of the morphological differences, some diatom sequences showed a high similarity (>99%) to sequences of other species than the expected one. This can be due the deposition in GenBank of misidentified species or to low resolution of the 18S rRNA gene (Mann et al., 2010; Moniz & Kaczmarska, 2010). Although there are many studies carried out to understand the particular taxonomic or phylogenetic issues regarding the marine benthic diatoms those were restricted to smaller, closer clades and particular genera with limited geographic sampling (Ashworth et al., 2012, 2013; Kooistra et al., 2003; Sato, Watanabe, et al., 2008b). Here I am trying to represent many clades of the benthic diatoms sampled in the different seasons and different stations accompanying the metadata, LM and SEM of the selected strains across the tree.

Out of the 13 selected strains for the morphological and molecular comparison (Table 4), the matching (100%) of morphological and molecular identities was obtained only in three strains which are PN11 and NAMC3 as *Nitzschia traheaformis* and LR40 as *Nitzschia adhaerens*.

The two *Psammodictyon* strains PN12 and NaMC2 are very close each other in the phylogenetic tree. However, they show different morphological characters as visible in the electron microscopy (Figure. 28 & 29.). Both these strains are close to *P. panduriforme* in terms of shape, raphe position and external areolae structure. These strains have morphological characters similar to those of the original species, but they have smaller size and denser number of striae (29–30 in 10 µm while in original species 17–20 in 10 µm).

The two strains differ each other for the size and the shape of the cells. In particular, NaMC2 is smaller and has blunt ends while PN12 has ends slightly apiculate. The arrangement of the areolae in the internal valve face is different: in the strain NaMC2 the areolae show bi-quadripored openings (Figure. 29b) while in the PN12 the openings were bipored (Figure.28b). This match with the description of *P. panduriforme* (Round et al., 1990) that report a variability in the number of areolae openings. Also, in the case of the raphe structure, external central nodule is clearly visible in both strains. Though morphologically both strains are quite close to the species *panduriforme* (Round 1990), the strain NaMC2 was smaller than the original *P. panduriforme* description in which valve size range from 95 to 140 µm in length, and from 33 to 36 µm in width, and the number of transapical striae in 10 µm (17–20) is lower than that observed in our strains (28–31). Valve undulation is less pronounced in both strains than in the original description (Round 1990). Although the external terminal ends of the raphe are hooked in both strains, in the case of NaMC2 the hook it is turned inwards, while in the PN12 it turns outwards. In the original description, Round et al. (1990) don't mention the direction of the hook.

Also, in the BLASTn result, the strain which showed 100% identity for PN12 is named as *Psammodictyon panduriforme* (KY054991) and was submitted directly to GenBank without any morphological data. The strain NaMC2 shows the highest identity with a reference sequence of *Psammodictyon* sp. (99.81%, JQ885984) for which no morphological data are available. Although PN12 match with the species *P. panduriforme,* the number of the striae is higher (29-30) than in the original description (17–20). The GenBank comparison, confirmed that NaMC2 belongs to the genus *Psammodictyon* but not to the species, letting to hypothesize that it could be a variety of the *panduriforme* species or even a new species. Further, the use of a more sensitive marker such as *rbc*L will give more information on strain identity and relationships.

The strain BD2 is 99.59% similar to a sequence of *Plagiogramma appendiculatum*. In the phylogenetic tree (Figure. 25), this strain is closer to *Psammogramma*, *Neofragilaria and*

Plagiogramma and distant from *Dimeregramma*. BD2 resulted in the *Plagiogramma* sp. basing on the sequencing level (GenBank). However, from a morphological point of view, it lacks the main distinguishing character of the genus *Plagiogramma,* which is the presence of a 'fascia' in the centre of the valve face, where striae are absent (Figure. 30a). Also, *Plagiogramma* has large, elliptical areolae with cribra, while in the BD2 strain the areolae are small and round. These differences show that our strain does not belong to the genus *Plagiogramma* but to *Dimeregramma*, as shown by single line arrangement of areolae with cribra, presence of short spines at the edge of valve face, apical pore field, sternum and absence of the rimoportula. However, we have to notice that that the strain BD2 was morphologically modified as it was maintained for a long period in the laboratory conditions.

The identity of the strain BD9 was confirmed as *Nanofrustulum shiloi* both by the morphology and the sequencing results (99.32% in the BLASTn). In the phylogenetic tree (Figure. 25) this strain is in the correct clade of *Nanofrustulum shiloi* SZCZE1361. Round et al. (1999) established this genus and compared it with "fragilarioid" taxa like *Fragilaria*, *Opephora* and *Pseudostaurosira*. One of the main distinguishable characters of this genus is the presence of segmented scale-like copulae, which can be clearly noticed in our strain, and the downwardly direct spinula on the spine (Figure. 31c). In this case the V4 region of 18S rRNA was good for species identification.

The strain BD7, which is 98.73% similar to a sequence of *Gedaniella* sp. available in GenBank, in the phylogenetic tree, it forms a single branch that is distantly related to other strains of the genus *Gedaniella*, *Opephora* and *Pseudostaurosira.* However, comparing the morphology, our strain possesses marginal spines that are absent in *Opephora* (Figure. 32b). The strain BD7 differs also from the genus *Pseudostarosira* for the absence of apical pore field that is present in *Pseudostaurosira*. (Li et al., 2018) established the genus *Gedaniella* basing on some distinguished morphological characters like presence of volae. In the BD7 'volae' can be observed (Figure. 32a). These differences render BD7 closer to *Gedaniella* genus, although the low resolution of the 18S rRNA and the morphological deterioration due to age of culture makes difficult to confirm the identification.

The strain BD4 showed 98.10% similarity with *Neofragilaria nicobarica.* In the phylogenetic tree this strain is close to *Neofragilaria* and *Psammogramma* genera. In *Neofragilaria* species, cells attach to each other with one valve apex making zig-zag colonies, while in the strain BD4 sister cells are attached to each other by valve face forming a filament (LM Figure. Plate 1a, in the supplementary material for Chapter 3). Moreover, in *Neofragilaria* the sternum is zig-zig shaped and possesses small granules (C. L. Li et al., 2015; Williams & Round, 1987) which are not noticeable in this strain. Also, the typical ornamentation on the apical slit is absent here. On the other hand, the elliptical valves, the indistinct sternum, the round areolae with fine rotae and the presence of the granules in the valve face-mantle junction suggest this strain belongs to genus *Psammogramma.*(Sato et al., 2008).

The strain BD11, identified as *Plagiogramma marginalis* in the BLASTn (96.47%), does not possess the 'fascia', which is a morphological character typical of *Plagiogramma*, suggesting that it does not belong to *Plagiogramma* genus. Instead BD11 seems closer to the *Dimeregramma* genus having a round valve shape and round areolae with cribra.

The morphological complexity of the *Plagiogrammaceae* family makes problematic species identification. These araphid diatoms lack some of the features of araphid diatoms, like parallel striae, apical rimoportulae and a prominent sternum. This creates chaos in the correct identification and positioning of these taxa in the phylogenetic tree. At molecular level, resolution of the more sensitive markers like rbcL could provide useful information, but for the araphid pennates, the availability of data for this marker in the databases is random and punctiform, which ultimately makes scientists to rely mainly on the morphological data.

The three strains BD3, BD10 and PN4DP could not be identified at the species level with the 18S rRNA sequencing, but morphological analyses allowed species identification. Morphological analyses of the strain BD3 allow its identification as *Nitzschia dissipata* ((Kützing) Rabenhorst 1860). Though the species was originally described and mainly reported from freshwater and brackish environment (Jahn & Lange-Bertalot, 2001; Mann, 1984; Rimet et al., 2011; Stancheva et al., 2007),

there are many reports of this species in the marine environment, particularly in the Mediterranean Sea (Beltrami et al., 2010; Cibic et al., 2007; Mucko et al., 2020b; Tolomio et al., 2002). *Nitzschia* is one of the most species-rich genera, with almost 899 species described to date and has a lively history of taxonomic changes. Revision of the three groups *Spathulatae*, *Dissipatae*, and *Sigmoideae,* which were placed next to each other in the phylogenetic tree by Grunow (1880), showed that they formed a single group for the presence of conopea near the raphe (Mann, 1984). Phylogenetic observation of *N. dissipata* (section *Dissipatae*) which has been paired with the section *Spathulatae* showed that its position was usually basal or outside of the nitzschioid lineages and never well supported (Krammer & Lange-Bertalot, 1997; Rimet et al., 2011). To resolve this classification and controversy between these two sections *Dissipatae* and *Spathulatae*, it is needed to find and add more strains of *Nitzschia* with a conopeum near the raphe.

Morphological characters observed in the strain BD10 suggest its attribution to the species *Amphora binodis* described by Gregory in 1857. Cells are smaller than the originally description of the species but match the variety *bigibba*. Position of this strain in the phylogenetic tree is near the clade of genus *Halamphora.* This could be because *Amphora* is one of the largest and dominant genus in the diatom classification and *Halamphora* was included in this genus until it was erected as new genus (Mereschkowsky, 1903; Stepanek, 2019). In the GenBank there is no sequence data available for this species even for sensitive markers like rbcL and ITS. This again suggests the need to improve databases of the benthic pennate diatoms and integrative approach of the identification.

The similarity of the strain PN4DP with a sequence of *Diploneis* sp. is remarkably low (96.19%), but its morphological characters confirm the species *Diploneis weissflogiopsis* (Pennesi et al., 2017b). This species was described by Pennesi and co-authors in 2017 from the Adriatic Sea but the description was based exclusively on morphological data. *Diploneis weissflogiopsis* often is confused with *D. weissflogii* and *D. claustra* in LM because of the comparable morphometrics, valve outline, raphe fissure, areolae size and shape. Only ultrastructural studies can confirm the species

identification. *D. weissflogiopsis* has 3 foramina while in *D. claustra* there is one foramen. Externally, the central part of the valve is dimpled (ribbon-like structure) in *D. weissflogiopsis*, while it is flat in *D. weissflogii.* Also, the valve interior of *D. weissflogii* shows a single areola in the centre along the margin while in our strain three areolae are present on both margins. And overall, *D. weissflogiopsis* lacks pores at the apical ends internally, while they are present in *D. weissflogii*.

Three strains (BD7, BD4 and BD11) had BLASTn identity percentage less than 99% and showed even a difference in the morphological identification. These strains cannot confirm species identification even with the electron microscopy and should be studied further. Nevertheless, strains like BD3, BD10 and PN4DP despite of the low percent identity, were identified at the species level based on the ultrastructure.

3.6 Conclusions

In the conclusion, comprehensive comparison between molecular and morphological approach to identify and characterize diatoms highlights the limited GenBank data availability for the pennate benthic diatoms. In this study, only four strains (PN11, NaMC3, LR40 and PN12) were identified at the species level with a 100% identity for 18S rRNA, and the molecular identification matched with the morphological one. For six strains (NaMC2, BD9, BD7, BD3, BD10 and PN4DP) sequencing allowed the identification at the genus level but not at species level, and only morphological characters successfully confirmed the species. In the remaining three strains (BD2, BD4 and BD11) molecular identification does not correspond to morphological characters even at the genus level. In the overview low percentage sequence identity in the GenBank suggests that the V4 region in the 18S rRNA is not the best marker to identify benthic pennate diatoms even at the genus level and highlights the need to enrich these reference databases further. However, this study suggest that more effort should be taken to construct a reliable database containing polyphasic taxonomic data for diatom identification and classification.

Chapter 4. **Description of taxa**

On the basis of their morphology diatoms have been classified in different ways by different taxonomist. They have divided diatoms into two or three major groups, based on the morphometrics such as organization of the pattern of striae on the valve and position of raphe. Round et al. (1990) divided the diatoms into three classes based on the valve organization: Coscinodiscophyceae (centrics), Fragilariophyceae (araphid pennates) and Bacillariophyceae (raphid pennates). Later in 1995, Van den Hoek et al. proposed only two major groups of diatoms, Centrales (Coscinodiscophyceae) and Pennales (Fragilariophyceae and Bacillariophyceae).

Further as discussed in the Chapter 1, depending on how benthic diatoms relate to their substratum, several distinct growth forms have been recognised (Round 1971, Lobban 1985, 1990, Totti et al., 2007) like adnate, motile, plocon and erect.

In this chapter, I am describing the number of taxa which are found in the SEM observations in samples collected from Portonovo (PN) and Senigallia (SG). Some taxa are missing from the floristic list because electron microscopy needs more extensive work and few taxa are not providing all the morphological characters useful for identification. Also, for many taxa only internal or external valve has been observed which has increased the complexity in the description of correct taxa.

Terminology used in the description of the cell wall, raphe structure, valve outline and other features follows the definitions gathered in Cox (1996), Krammer & Lange-Bertalot (2000b) and Round et al. (1990).

For each taxon entry the following information is given (fields in bold):

- Name and author
- Micrographs – plate and number SEM micrographs
- Basionym

- References
- Morphometric

  Frustule geometry- shape of the valve

  AA: Transapical Axis - valve length (in μm), For radial centrics the diameter is given.

  PA: Pervalvar Axis- in μm

  TA: Apical Axis- valve width (in μm)

  TS: Transapical striae. For centric diatoms, the number of areolae and/or striae was noted.

  F: Fibulae

  Processes/other features – remarks (e.g. number and/or arrangement) on rimoportulae and fultoportulae of centric and pennate diatoms.

Description – a morphological description was added of taxa that were observed in the images, for the further detailed information of the taxa references given should be consulted.

1. *Amphora arenicola* Grunow ex Cleve, Plate.1, a-c

   Ref: Cleve, 1895; Witkowski et al., 2000

   AA: 38.75 - 41.48 µm, TA: 17.5 - 19.25 µm, TS in 10 µm: 12-15

Solitary cells. Frustules oblong with rounded corners, linear valves with broad rounded apices. Raphe slightly biarcuate, distant from ventral margin. External central endings distant and curved; axial area narrow on the dorsal side, central area orbicular. Transapical striae with dash areolae on the dorsal and ventral side.

2. *Amphora* cf. *graeffei* var. *minor* Peragallo Plate.1, d-f

   Ref: Peragallo & Peragallo, 1897

   AA: 28.54 µm, TA: 9.2 µm, TS in 10 µm: 35

Solitary cells. Frustule elliptical or rectangular, ends rounded. Valve with about 2 subdivisions, cymbiform with almost straight ventral edge, extremities not protracted. Raphe on the ventral side with very narrow elevation. Raphe fissure in the centre. Ventral side near the raphe with some scattered dots. Var. *minor* is smaller than the type species and has dense striae. In the species *Amphora graeffei* AA is longer (80 to 130 µm), on the dorsal side central area more or less developed, transapical striae in 10 µm 14 to 15.

3. *Amphora* cf. *inariensis* Krammer, Plate.2, a

   Ref: Krammer, 1980

   AA: 8.4 µm, TA: 4.5 µm, TS in 10 µm:19 (ventral side); TS in 10 µm: 21 (dorsal side)

Solitary cells. Valves semi-elliptical characterized by a typical half-moon shape, dorsal part convex and ventral part slightly concave, with a swelling in the middle part. Raphe positioned towards the ventral margin, generally straight or slightly arched with the ends ending straight on the dorsal margin. Striae are markedly visible and are oblique on the dorsal side.

4. *Amphora* cf. *jostesorum* Witkowski, Lange-Bertalot & Metzeltin Plate.2, b-d

Ref: Witkowski et al., 2000

AA: 26.8 µm, TA: 9.8 µm, TS in 10 µm: 38-40

Solitary cells. Frustules in girdle view linear-elliptic with rounded corners. Valves semi-lanceolate with dorsal margin convex, ventral margin straight in the middle somewhat inflated, with subacute apices. Raphe located around ventral margin, straight, at apices bent towards dorsal side, external central endings distinct, slightly curved. Striae barely distinguishable with very small/pinpoint areolae. Central area (rectangular shape) of the valve is without areolae.

5. *Amphora libyca* Ehrenberg Plate.2, e

Ref: Bérard-Therriault & Cardinal, 1986

AA: 30.5 µm, TA: 5.5 µm, TS in 10 µm:17 (ventral side); TS in 10 µm: 18 (dorsal side)

Solitary cells. Valve more or less broadly elliptical with obtuse ends. Dorsal side convex while ventral is straight or weakly concave. Biarched raphe describe the centre and the ending. Striae segmented on the dorsal side, parallel in the centre and slightly convergent towards the apical ends. On the ventral side stripes short, absent in the centre.

6. *Amphora* cf. *proteus* W.Gregory Plate.2, f

Ref: Gregory, 1857

AA: 47 µm, TA: 9.3 µm, TS in 10 µm: 11

Solitary cells. Valves semi-elliptic with convex dorsal margin, slightly concave on the ventral margin with obtusely rounded apices. Raphe distant from the ventral margin, strongly curved at apex and centre. Axial area narrow and distinct along the dorsal side but on the ventral side somewhat irregular. Dorsal side undulated with transapical striae. Areolae ‘T’ shaped.

7. *Amphora* cf. *copulata* (Kützing) Schoeman & R.E.M.Archibald, Plate.3, a

   Ref: Schoeman & Archibald, 1986

   AA: 13.4 µm, TA: 5.06 µm, TS in 10 µm: 14-15

Solitary cells. Valves semi-elliptical with rounded ends, dorsal margin smoothly arched and ventral margin slightly concave. Raphe straight and positioned toward the ventral margin, central raphe endings slightly curved, and terminal ends dorsally deflected. Ventral fascia distinct and elliptical. Transapical striae parallel, ventral striae interrupted by intercostal rib that is a thickened, hyaline bar often visible on the ventral margin separating valve face and mantle.

8. *Amphora* cf. *helenensis* Giffen, Plate.3, b

   Ref: Giffen, 1973

   AA: 18 µm, TA: 8.3 µm, TS in 10 µm: 20

Solitary cells. Frustule elliptical. Valves lunate with convex dorsal and slightly concave ventral margins. Axial area narrow on both sides. Raphe close to the ventral margin with fissure at central and terminal apices. Transapical striae crossed by a lanceolate blank band across the dorsal striae. Areolae 'dash' like.

9. Araphid sp. 1 Plate.3, c-d

   AA: 12.5 µm, TA: 3.6 µm, TS in 10 µm: 18

Solitary cells. Valves broadly lanceolate, narrowed towards rostrate rounded apices. Sternum narrow, linear. Transapical striae biseriate, in the centre one pair of striae short and leave a hyaline central part. Areolae round in shape, covered with a deposition of silica.

10. *Astartiella* sp. 1- A.Witkowski, Lange-Bertalot & D.Metzeltin Plate.4, a-c

    Ref: Moser et al., 1998; Riaux-Gobin et al., 2013

    AA: 16 µm, TA: 4 µm, TS in 10 µm: 32

Solitary cells. Valves oblong to linear with round apices. Raphe valve flat to slightly concave. Striae parallel and equidistant composed by areolae closed with delicate hymenes. A stigma present on one side of the central area. Central area not expanded, wider towards the stigma. Raphe straight, central raphe endings simple and slightly bent toward the stigma, terminal raphe fissures hooked in the same direction at both ends. Axial area narrow and straight.

11. *Bacillaria paxillifera* (O.F.Müller) T. Marsson, Plate.4, d-f

Basionym: *Vibrio paxillifer* O.F.Müller

Ref: Hustedt, 1930; KRAMMER K & LANGE-BERTALOT H, 2000; Marsson, 1901

AA: 120.6 µm, TA: 4.3 µm, TS in 10 µm: 23, F in 10 µm: 9

Cells forms colony with valve face attached and move by sliding with the neighboring cell. Valves linear to linear-lanceolate with cuneate apices, broadened in the middle. Raphe in the centre, raised in the keel. Fibulae spaced unevenly. Parallel transapical striae with round areolae.

12. *Cyclotella striata* (Kützing) Grunow Plate.5, a-b

Ref: Cleve & Grunow, 1880; Prasad et al., 1990

Basionym: *Coscinodiscus striatus* Kützing

Diameter: 10.5 µm

Solitary cells. Valve circular. Marginal region of the valve surface contains alternating radially oriented linear interstriae and striae. Marginal fultoportulae on every second or third interstriae, arising from the mantle, without a tubular extension. Central area well distinguished and undulated on the external side with seven fultoportulae irregularly arranged on the internally concave portion of the valve. Central fultoportulae with three auxiliary pores.

13. *Nitzschia longissima* (Brébisson) Ralfs Plate.5 c-e

Ref: Pritchard, 1861

Basionym: *Ceratoneis longissima* Brébisson

AA:167.27 µm, TA: 5.9 µm, F: 13

Solitary cells. Valves long, narrow, well silicified with usually straight, abruptly narrowed into very long rostrate ends. Striae weakly visible and irregular not resolvable in LM. Raphe strongly eccentric, fibulae unevenly spaced with a larger interspace in the centre.

14. *Diploneis* sp. 3, Plate.5, f-g

Ref: Cleve, 1894; Hustedt, 1930a; Round et al., 1990; Scott & Thomas, 2005

AA: 6.9-8.6 µm, TA: 3.5-3.09 µm, TS in 5 µm: 17

Solitary cells. Valves elliptical with rounded apices. Straight raphe in the middle. Striae parallel, covered with silica layer. External valve with single line of areolae on each side of raphe which does not open in the internal valve. Distinct raphe canal in the internal valve.

15. *Diploneis* sp. 4. Plate.6, a-c

Ref: Cleve, 1894; Hustedt, 1930a; Round et al., 1990; Scott & Thomas, 2005

AA: 15 µm, TA: 5 µm, TS in 10 µm: 16

Solitary cells. Valves elliptical, constricted in the centre with rounded apices. Straight raphe in the middle, elevated in the centre and at the apices. Areolae open only at the edge of the valve. Distinct raphe canal in the internal valve. Girdle band plain.

16. *Entomoneis alata* (Ehrenberg) Kützing, Pl. 6, d-e.

Basionym: *Navicula alata* Ehrenberg

Ref: Witkowski et al., 2000

AA: 40.88 µm, PA: 4.44 µm, TS in 10 µm: 40

Solitary cells. Frustules lying often in girdle view, bilobate and panduriform with a marked keel constricted in the middle. Girdle composed of numerous ornamented bands. Valves linear to linear-lanceolate with parallel to slightly convex margins, acute, wedge-shaped apices. Valve line barely

wavy. Raphe running on the keel. Transapical striae relatively robust. Interstriae with heavy silica deposition.

17. *Entomoneis* cf. *paludosa* (W.Smith) Reimer Plate.7, a-c

Basionym: *Amphiprora paludosa* W.Smith

Ref: Patrick & Reimer, 1975; Witkowski et al., 2000

AA: 65.18 µm, PA: 13.33 µm, TS in 10 µm: 25

Solitary cells. Frustules in the girdle view strongly constricted in the middle. Valves linear-lanceolate with acutely rounded apices and strongly S-shaped median line. Valve line slightly wavy. Raphe embedded on the keel. Transapical striae delicate with rounded areolae.

18. *Fallacia* cf. *forcipata* (Greville) Stickle & D.G.Mann Plate.7, d-g

Basionym: *Navicula forcipata* Greville

Ref: Round et al., 1990; Witkowski et al., 2000

AA: 23.33 µm, TA: 10 µm, TS in 10 µm: 20

Solitary cells. Valves elliptical with broadly to obtusely rounded apices. Uniseriate striae interrupted by lateral sterna 'lyre' (H shaped) which is depressed (can see in the internal valve). On the external valve striae finely covered with porous conopea. Pores of the conopeum observed at the poles. Internal valve with opened round areolae. Raphe narrow and straight, external central raphe endings expanded and slightly depressed in the valve, while terminal fissure deflected towards the same side. Internal valve with central and terminal raphe endings deflected towards the other side. In this species transapical striae in the middle parallel and at apices slightly radiate.

19. *Fallacia* cf. *tenera* (Hustedt) D. G. Mann Plate.8, a-d

Basionym: *Navicula tenera* Hustedt

Ref:Hofmann et al., 2013; Round et al., 1990; Witkowski et al., 2000

AA: 9.6 µm, TA: 4.5 µm, TS in 5 µm: 14

Solitary cells. Valves elliptic to linear-elliptic with broadly rounded apices. On the external valve striae partially covered in porous conopea, single row of large areolae observed along the valve mantle face. Internal valve areolae open in the round shape with three-four pores in each row on the edges and one or two pores in each row along the raphe. Raphe narrow, straight. External raphe central endings expanded, while terminal fissure deflected in the same direction. Internal central raphe endings deflected towards the same direction while terminal endings are deflected to the other side.

20. *Fallacia* sp. 1. Plate.8, e-g

Ref: Round et al., 1990

AA: 20.66 µm, TA: 10.16 µm

Solitary cells. This species of *Fallacia* resembles with the *Fallacia forcipata* but 'lyre' shape not prominent and distinct conopea present. Conopea is covering the areolate portion of the total valve face, so it is not possible to differentiate between striae and interstriae.

21. *Gyrosigma* cf. *fasciola* (Ehrenberg) J.W.Griffith & Henfrey Plate.9, a-c

Basionym: *Ceratoneis fasciola* Ehrenberg

Ref: Cleve, 1894; Krammer & Lange-Bertalot, 1986; Villac et al., 2016

AA: 86.19 µm, TA: 9.5 µm, TS in 10 µm: 28

Solitary cells. Valve elliptical-lanceolate, with terminal parts narrow and extended on both sides directing opposite to each other, apical ends round. Raphe in the centre. Central end of raphe is deflected on the same direction while terminal end is straight. Transapical striae parallel and perpendicular to each other with small 'dash' like areolae. On the valve margin distinct single straight line of areolae.

22. *Halamphora cuneata* (A cleve) Levkov Plate.10, a-c

Basionym: *Amphora cuneata* Cleve

Ref: Levkov, 2009

AA: 29 µm, TA: 2.8 µm, TS in 10 µm: 18

Solitary cells. Valves narrow, semi lanceolate with convex dorsal margin, constricted in the middle and sub-capitate apices. Raphe straight becoming arcuate at the terminal, central nodule present in the internal valve. Central area forms a transverse hyaline fascia reaching the valve margin. Transapical striae less visible.

23. *Halamphora coffeiformis* (C.Agardh) Mereschkowsky Plate.10, d-f

Basionym: *Frustulia coffeiformis* C.Agardh

Ref: Witkowski et al., 2000

AA: 31.66 µm, TA: 4.5 µm, TS in 10 µm: 18

Solitary cells. Valves semi elliptical with rostrate, slightly capitate apices. Raphe marginal and straight, axial area narrow. Central nodule present. Bi-seriate transapical striae slightly radiate with small round areolae.

24. *Halamphora* cf. *tenerrima* (Aleem & Hustedt) Levkov Plate.11, a-c

Basionym: *Amphora tenerrima* Aleem & Hustedt

Ref: Aleem & Hustedt, 1951; Witkowski et al., 2000

AA: 15 µm, TS: 7.3 µm, TS in 10 µm: 14

Solitary cells. Frustules elliptical to lanceolate with protracted, relatively broad apices. Valves semi-lanceolate to semi-elliptical with slightly capitate apices, dorsal margin convex or arched, ventral margin is straight to slightly concave. Raphe close to ventral margin, straight and have a gradual dorsal bend near the centre of the valve. Dorsal axial area is narrow, while the ventral side is wider. Striae on the dorsal part uninterrupted, slightly radiate, becoming more radiate at the poles. Striae on the ventral part difficult to resolve and radiate near the center, convergent at the poles. Uniseriate striae with large round areolae on the dorsal side and a row of small elongated on the ventral side. Girdle with the numerous striated bands.

25. *Hippodonta* sp. Plate.11, d-f

Ref: Bruder & Medlin, 2008; Witkowski et al., 2000

AA:14.54 µm, TA: 4.8 µm, TS in 10 µm: 18-19

Solitary cells. Valves thick, heavily silicified, lanceolate in valve outline with variously shaped poles. Striae distinct, broad, and uni- or biseriate. Valve end with thickened bands of silica, termed polar bars. Raphe straight and the proximal raphe ends expanded.

26. *Mediolabrus comicus* (H.Takano) Yang Li. Plate.12, a

Basionym: *Minidiscus comicus* H.Takano

Ref: Takano, 1983

Diameter: 3.4 µm

Solitary cells. Valves round with no obvious separated mantle covered with a net of loculate and/or pseudoloculate areolae. Valve margins narrow, with marginal areolae terminating close to the valve edge. Four processes: three fultoportulae and one rimoportula, located around to the valve centre. Position of the rimoportula mostly central with respect to the fultoportulae. Internal view of the valves were not found in our samples.

27. *Minidiscus trioculatus* (F.J.R.Taylor) Hasle Plate.12.b

Basionym: *Coscinodiscus trioculatus* F.J.R.Taylor

Ref: Kaleli, 2022; Li et al., 2020; Percopo et al., 2011

Diameter: 2.615 µm

Solitary cells. Valve face circular, relatively flat with a tangential linear arrangement of loculate areolae with rotae. No obvious mantle. Three fultoportulae, one small, sub-central rimoportula on the valve face.

28. *Lyrella* sp. 1. Plate.12, c-d

Ref: Karayeva, 1978; Round et al., 1990

AA: 47.14 µm, TA: 18.5 µm, TS in 10 µm: 14

Solitary cells. Valve elliptical with rounded apices. Raphe straight, central endings expanded. Terminal raphe endings with fissures curved in the same direction. Transapical striae slightly radiate with very minute round areolae. In the centre of the valve H shaped ’lyre’ where striae interrupted.

29. *Lyrella* cf. *exsul* (A.W.F.Schmidt) D.G.Mann Plate.13, a-c

Basionym: *Navicula exsul* A.W.F.Schmidt

Ref: Siqueiros-Beltrones et al., 2017

AA: 54.3 µm, TA: 6.2 µm, TS in 10 µm: 12

Solitary cells. Valves elliptical, constricted in the centre with rostrate apices. Raphe straight, central endings expanded and relatively approximate. Terminal raphe endings with fissures curved in the same direction. Transapical striae slightly radiate with very minute round areolae. Striae interrupted by prominent valve depression ’lyre’.

30. *Navicula agatae* Witkowski, Lange-Bertalot & Metzeltin Plate.13, d-f

Ref: Witkowski et al., 2000 (as 'agatkae')

AA: 16.6 µm, TA: 4.1 µm, TS in 10 µm: 18

Solitary cells. Valves lanceolate with slightly protracted, sub-capitate apices. Raphe straight with external central endings somewhat expanded, central area distinct, terminal raphe endings hooked. Single line of areolae on the one side of raphe. Transapical striae parallel throughout, at apices slightly convergent, composed of several rows of lineolae.

31. *Navicula* sp. 2. Plate.14, a

Girdle view: 17.83 µm, TS in 10 µm: 13

Solitary cells. Valves linear-lanceolate constricted in the middle. Raphe straight, external central endings approximate, bent above the valve, apical endings hooked in same direction. Transapical striae coarse and parallel. Girdle band plain and open.

32. *Navicula distans* (W.Smith) Brébisson. Plate.14,b-d

Basionym: *Pinnularia distans* W.Smith

Ref: Witkowski et al., 2000

AA: 38 µm, TA: 8.75 µm, TS in 10 µm: 11

Solitary cells. Valves lanceolate with sub-acute apices. Raphe straight, central endings in the internal valve close and uplifted. Valves axial area narrow at apices gradually broadening towards the central area. Transapical striae coarse, parallel but in the centre convergent with less number of areolae. Plain girdle band.

33. *Navicula* sp.1 Plate.15, a-c

AA: 11.6 µm, TA µm: 2.62 TS in 5 µm: 11

Solitary cells. Valves elliptical with rounded apices. Raphe in the centre of the valve. Terminal fissures of the raphe curved, in the middle raphe endings are slightly expanded. 2 to 3 lines of parallel striae. Areolae dash like, in the centre absent. Single line of striae at valve-girdle mantle.

34. *Navicula* sp. 3. Plate.15, d-f

AA: 36 µm, TA: 5.55 µm, TS in 10 µm: 15

Solitary cells. Valves elliptical with acute apices. Raphe in the middle situated on a line of silica deposition, in the centre hooked fissure and slightly turned at terminal. Parallel striae with dash like areolae, absent in valve centre around the raphe central endings.

35. *Navicula* sp. 4. Plate.15, g

AA: 9.2 µm, TA: 2.3 µm, TS in 5µm: 9

Solitary cells. Valves elliptical, very small. Raphe in the middle, fissure at terminal end turned in the same direction, central endings straight. 2 to 3 columns of parallel striae. Dash like areolae, in the centre absent. Single line of striae at valve-girdle mantle and on both side of the raphe canal.

36. *Navicula* sp. 5. Plate.16, a-c

AA: 29.6 µm, TA: 5.3 µm, TS in 10 µm: 20

Solitary cells. Valves elliptical with acute blunt apices. Raphe in the middle, straight. In internal valve raphe distant and slightly elevated in the center. Dense transapical striae with round areolae.

37. Pennate sp. 6. Plate.16, d-e

AA: 6.6 µm, TA: 3.1 µm, TS in 5 µm: 14

Solitary cells. Valves elliptical to oval with round apices, very small in size. Raphe in the middle with terminal fissure curved on the same direction. Centre raphe endings expanded and curved in the opposite direction of the terminal. Striae divergent with round areolae covered in porous silica layer.

38. *Navicula* sp. 6. Plate.16, f-h

AA: 47.2 µm, TA: 5.7 µm, TS in 10 µm: 12

Solitary cells. Valves long, elliptical with acute apices. Raphe in the middle, hooked fissure in the centre and slightly curved at the terminal. Dense parallel striae with dash like areolae, absent in the centre forming an empty rectangular space.

39. *Navicula* sp. 7. Plate.17, a-c

AA in girdle:11.5 µm, TS in 5 µm: 10

Solitary cells. Valves small, elliptical. Raphe in the middle with straight central endings, terminal end expanded. Parallel striae with areolae strong and dash like, in the centre absent, at apices there are some structure similar areolae. Girdle band plain and open.

40. *Navicula* sp. 8 Plate.7, d-f

AA: 30.36 µm, TA: 5.27 µm, TS in 10 µm: 11

Solitary cells. Valves elliptical with acute apices. Raphe in the middle, terminal end pinched with helictoglossa. Dense transapical striae with closed round areolae in the internal valve view. In the centre few areolae missing, at apices in the mantle there are some areolae.

41. *Navicula* sp. 9. Plate.17, g-i

AA: 6.66 µm, TA: 4.66 µm, TS in5 µm: 7-8

Solitary cells. Valves elliptical with acute apices. Raphe in the middle with terminal fissure turned in the same direction. Central raphe ending expanded and distant. Striae divergent with dash like areolae forming a unique pattern. Large interspace in the centre.

42. *Navicula* sp. 10 Plate.18, a

AA: 15.6 µm, TA: 3.3 µm, TS in 10 µm: 18-19

Solitary cells. Valves elliptical with acute apices. Raphe in the middle straight. Central raphe endings slightly expanded. Striae parallel with dash like areolae, Large interspace in the centre.

43. *Navicula* sp. 11 Plate.18, b-c

AA:13.33 µm, TA: side view, TS in 10 µm: 14

Solitary cells. Valves elliptical to oval with round apices. Raphe in the middle. Central raphe endings expanded. Striae with dash like areolae arranged in different directions. At apices single line of areolae at the edge between mantle and girdle.

44. *Nitzschia* sp. 1. Plate.18, d-g

AA: 17.4 µm, TA: 3.2 µm, TS in 10 µm: 41, F: 16

Solitary cells. Valves lanceolate to linear lanceolate with shortly rostrate to obtusely rounded apices. Raphe eccentric, fibulae not equidistantly placed and highly silicified, central nodule absent. Transapical striae poorly developed.

45. *Nitzschia* sp. 6. Plate.19, a-c

AA: 27.5 µm Approx, TA: 1.8 µm, F in 10 µm: 9, TS in 10 µm: 3

Solitary cells. Valves lanceolate to linear lanceolate with shortly rostrate, obtusely rounded apices. Raphe eccentric, fibulae equidistantly placed and highly silicified, central fibulae with a large interspace. Central nodule present. Transapical striae dense with round areolae.

46. *Nitzschia hybrida* Grunow Plate.19, d-f

Ref: Cleve & Grunow, 1880; Hustedt, 1930b; Witkowski et al., 2000

AA: 38.88 µm, TA: 4 µm, TS in 10 µm: 45

Solitary cells. Valves linear with acutely rounded apices, in the middle weakly constricted. Raphe strongly eccentric, elevated in the keel. Dense transapical striae.

47. *Nitzschia* sp. 2. Plate.20, a-c

AA: 36.6 µm, TA: 2.9 µm, F in 10 µm: 7, TS in 10 µm: 42

Solitary cells. Valves lanceolate to linear lanceolate with obtusely rounded apices undulate in the apical axis. Raphe eccentric, central nodule absent apical terminal end curved. Fibulae quite equidistantly placed. Transapical striae dense with very small round areolae that become less frequent on the opposite of the canal raphe.

48. *Nitzschia* sp. 4. Plate.20, d-f

AA: 28 µm, TA: 2.46 µm, TS in 10 µm: 48, F in 10 µm: 11

Solitary cells. Valves linear with acutely rounded apices. Raphe strongly eccentric with hooked terminal fissure. Dense transapical striae. Impression of fibulae heavily silicified, placed nearly equidistantly.

49. *Nitzschia* sp. 5. Plate.21, a-c

AA: 25.6 µm, TS in 10 µm: 50, F in 10 µm: 12

Solitary cells. Valves lanceolate to linear lanceolate with obtusely rounded apices. Raphe eccentric, fibulae highly silicified, central fibulae with a large interspace. Transapical striae dense with round-elliptical areolae arranged parallely. Open girdle bands with two lines of areolae.

50. *Ralfsiella smithii* (Ralfs) P.A.Sims, D.M.Williams & Ashworth. Plate.21, d-g

Basionym: *Cerataulus smithii* Ralfs

Ref: Kaleli, 2022; Sims et al., 2018

AA: 36.52 µm, TA: 45.21 µm

Valve outline circular, a barely raised narrow elevation with a circular ocellus at summit. Valve face almost flat with a narrow slightly convex valve mantle bordering expanded hyaline valve margin. Valve face, mantle and elevations covered in irregular network of false pseudoloculi. Equidistant between the elevations an external opening of rimoportula that are 'spines' in submarginal position. while internal opening is like a slit (labiate process). Girdle bands with vertical rows of poroid areolae, valvocopula and remaining copulae open.

51. *Pleurosigma* sp. 1 W.Smith. Plate.22, a-c

Ref: Round et al., 1990

AA: 58.33 µm, TA: 12 µm, TS in 10 µm: 15-16

Solitary cells. Valve sigmoid. Raphe sigmoid, central, becoming slightly eccentric near the apices. External central raphe fissures with one centered and the other deflected to one side. Hyaline area absent. Striae change orientation at the apex. Areolae arranged in quinqux and undivided.

52. *Pleurosigma elongatum* W.Smith. Plate.22, d-f

Ref: Park et al., 2022

AA: 155.8 µm, TA: 14.16 µm, TS in 10 µm: 25

Solitary cells. Valve moderately sigmoid, narrow lanceolate, gradually tapering to rather acute ends. Raphe with single curvature, almost straight and median in the middle portion, curving gently and

somewhat displaced to its convexity near the ends. Central raphe fissures distinct, extending far into the central area with variation in shape and deflection. Terminal fissures very long and recurving on the mantle. Central area oval.

53. *Pleusrosigma* cf. *latum* Cleve. Plate.23, a-f

Ref: Cleve 1880, 14, pl. III [3]: fig. 68, 42., Sims, P.A. (ed.) 1996.

AA: 74-77.91 µm, TA: 11.6, TS in 10 µm: 28-29

Solitary cells. Valve approximately rhombic with acute ends. Raphe sternum in the middle, slightly curved. Transverse striae distinct or finer. Central area fairly large. Externally terminal and central raphe fissure distinct and hooked. Internally central raphe ending is straight and distant while terminal endings show helictoglossae. Areolae divides into two parts by silica bar.

54. *Psammodictyon panduriforme* var. *continuum* (Grunow) Snoeijis. Plate.24, a-c

Basionym: *Nitzschia panduriformis* var. *continua* Grunow

Ref: (Grunow) Snoeijis 1998: 88, fig. 476 (as 'continua'), Dirican et al., 2022

AA: 11.3 µm, TA: 5.1 µm, TS in 5 µm: 15

Differs from the nominate variety by having slightly panduriforme valves and distinctly smaller size. Striae contains quadrangular to roundish areolae.

55. *Psammodictyon roridum* (Giffen) D.G.Mann. Plate.24, d-f

Basionym: *Nitzschia rorida* Giffen

Ref: Round et al., 1990

AA: 21.13 µm, TA: 6.5 µm, TS in 10 µm: 27

Solitary cells. Valves linear, more or less strongly constricted in the middle with shortly rostrate apices. Raphe strongly eccentric. Fine areolae in quincunx arrangement. Interrupted by a distinct apical fold.

56. *Psammodictyon* sp. 1 D.G.Mann. Plate.25, a-b

AA: 15.76 µm, TA: 4.3 µm, TS in 10 µm: 50

Solitary cells. Valves broadly linear with slightly constricted in middle and shortly rounded apices. Raphe strongly eccentric. Dense striae with small, rounded areolae.

57. *Psammodictyon* sp. 2 D.G.Mann. Plate.25, c-e

AA: 16 µm, TA: 6.5 µm, TS in 10 µm: 32

Solitary cells. Valves linear, slightly constricted in the middle with shortly rostrate apices. Raphe strongly eccentric, central nodule present. Fine areolae in quincunx arrangement. Areolae closed with ornamental silica deposition, Interrupted in the middle of the cell by a distinct short fold.

58. *Psammodictyon* sp. 3 D.G.Mann. Plate.26, a-b

AA: 25.11 µm, TA: 7.7 µm, TS in 10 µm: 23

Solitary cells. Valves panduriform with cuneate, rostrate apices, constricted in the middle. Raphe eccentric in keel. Central nodule is not visible. Striae composed of large decussate, round areolae line. Valve face undulate.

59. *Tryblionella* sp. W.Smith. Plate.26, c

Ref: Round et al., 1990

AA: 33.6 µm; TA: 5.4 µm; TS in 10 µm: 23; F in 10 µm: 11

Solitary cells. Valves linear slightly constricted in the centre with rounded apices. Raphe strongly eccentric. Valves surface undulated. Striae uniseriate, parallel in the valve center slightly radial close to the apices with circular areolae. External central raphe endings close.

60. *Campylodiscus* sp.1 Ehrenberg ex Kützing. Plate.26, d-f

Ref: Hustedt, 1930a; Kützing, 1844

AA: 40 µm; TA: 25.2 µm; TS in 10 µm: 2-3

Solitary cells. Saddle shape valve with ridges. Striae multiseriate interrupted by sterna contains small areolae. Marginal raphe raised on a keel. Simple raphe endings.

61. *Cocconeis* sp.2 Ehrenberg. Plate.27, a

Ref: Hustedt, 1930a; Scott & Thomas, 2005

AA: 9.9 µm, TA: 3.3 µm, TS in 5 µm: 22

Solitary cells. Pseudoraphe-valve elliptical. Uniseriate striae parallel with rectangular areolae getting divergent at apices. Narrow 'pseudoraphe sternum'.

62. *Fogedia* sp. Witkowski, Lange-Bertalot, Metzeltin & Bafana Plate.27, b-d

Ref: Park et al., 2013; Witkowski et al., 1997

AA:26.76 µm, TA: 8.76 µm, TS in 10 µm: 12-13

Solitary cells. Valve naviculoid in shape with sub rostrate ends. Transapical striae uniseriate, composed of apically elongate and slit-like areolae sometime with different orientation. Striae interrupted by hyaline lateral areas slightly depressed on the surface of the valve face. Straight central raphe. External central raphe endings straight and expanded. At terminal raphe endings very short.

63. *Gomphonema*. Sp. Ehrenberg Plate. 28, a-c

Ref: Bruder & Medlin, 2008a

AA: 18.3 µm, TA: 6.2 µm, TS in 10 µm: 18

Solitary cells. Valves lanceolate and slightly heteropolar with obtuse apices. The axial area moderately wide. Raphe in the middle and sinuous, with expanded central endings. Terminal raphe ends on the mantle. Striae parallel or slightly radiate at the valve center with small areolae. Stigma is present.

64. *Licmophora* sp. 1. Plate.28, a-c

Ref: Park et al., 2022; Round et al., 1990

AA: 18.13 µm, TA: 5.4 µm at head pole, 1.2 µm at foot pole, TS in 10 µm: 33

Colonies attached to substratum with a stalk. Cells wedge-shaped in girdle view. Valve surface slightly convex with a pronounced mantle near the round head pole, becoming shorter close to the foot pole. Uniseriate striae, consisting of small areolae with an ornamented velum. Girdle bands ornamented. Apical pore field at foot pole.

65. *Pteroncola* sp. Plate.29, a-b

Ref: Round et al., 1990

AA: 10.6 µm, girdle view, TS in 10 µm: 62

Solitary cells. In girdle view cells oblong, valves linear to elliptical. Externally, small ridges between the row of areolae, while plain internally. Apical pore field at both ends. Two rimoportulae at each apex, positioned transapically. The second copula presents one line of areolae, others splits and overlaps.

66. *Seminavis* sp. Plate.29, c-e

Ref: Round et al., 1990

AA: 34.85 µm, TA: 5.4 µm, TS in 10 µm: 11-12

Solitary cells. Valves semi-lanceolate with a curved dorsal margin and straight ventral margin. Well-developed dorsal mantle. Areolae slit-like. Dorsal striae moderately chambered. Raphe placed toward the ventral margin elevated, terminal end strongly hooked facing to dorsal side. Central end of raphe slightly deflected.

67. *Surirella* sp. Plate.30, a-c

Ref: Round et al., 1990

AA: 57.6 µm, TA: 36 µm (at the widest), TS in 10 µm: 2

Solitary cells. Valves heteropolar strongly silicified. Valve face concave ornamented with siliceous ridges. Striae multiseriate containing small round poroids. Raphe system occupied on the entire wall perimeter.

68. Pennate sp. 15. Plate.30, d-e

AA: 23.53 µm, TA: 6.1 µm, TS in 10 µm: 32

Solitary cells. Valves lanceolate with bluntly rounded apices. Uniseriate striae with simple areolae. External valve with straight raphe separated by narrow axial sternum. Straight and distant central ending of raphe. Cingulum ornamented. Apical pore field at both apices.

69. Pennate sp. 16. Plate.31, a

AA: 23.83 µm, TA: 7.5 µm, TS in 10 µm: 18

Solitary cells. Valves broadly lanceolate, narrowed towards acutely rounded apices. Sternum very narrow, linear. Transapical striae parallel slightly alternating each other.

70. Pennate sp. 4. Plate.31, b

AA: 10.64 µm, TA: 4.32 µm, TS in 5 µm: 9

Solitary cells. Valves elliptical with obtuse apices. Raphe sternum broad, in the centre slightly depressed. Transapical striae mono or bi seriate with small round areolae.

71. Pennate sp. 5. Plate.31, c-d

AA: 11.8 µm, TA: 3.25 µm, TS in 10 µm cell: 28

Solitary cells. Valves lanceolate with slightly rostrate apices. Raphe in the middle, straight, in the centre expanded while at terminal end turned to other side of valve. Biseriate transapical striae only at the edge of valve.

72. Pennate 13. Plate.32, a-c

AA: 12.16 µm, TA: 4.8 µm

Solitary cells. Valves elliptical with rostrate apices. Apical pore field present. Central raphe sinuous, slightly turned in the same direction at the apices, in the centre with simple endings. Transapical striae parallel to apical axis. Areolae embedded in the striae producing thick lines of silica.

73. *Thalassiosira* cf. *minima* Gaarder. Plate.32, d-e

Ref: Gaarder, 1951; Hasle, 1980; Li et al., 2013

Diameter: 8.95 µm

Cells forming a chain. Valves nearly flat. Shallow and indistinct valve mantle. Areolae radially arranged, irregular, and hexagonal in shape. Areolae loculate, with circular external foramina. The external tubes of the marginal fultoportulae are short, located between the valve-face and mantle junction. Near each marginal fultoportula a short, occluded process is located. Two central fultoportulae. Single rimoportula present.

74. *Thalassiosira gravida* Cleve. Plate.33, a-b

Ref: Bérard-Therriault et al., 1999; Cleve, 1896; Sar et al., 2011

Diameter: 31.14 µm

Cells forming a chain. Valves flat and weakly silicified. Fine radial ribs on the valve face, whereas areolae only visible near the valve margin. A cluster of fultoportulae is located in the valve centre. including a single rimoportula with a long external tube at valve margin. Several fultoportulae scattered on the valve face.

75. *Thalassiosira* sp. 1. Plate.33, c-d

Ref: Round et al., 1990

Diameter: 9.08 µm

Cells forming a chain. Valves circular. Shallow indistinct valve mantle. Areolae radially-arranged, irregular and undetermined in shape. On the margin a ring of fultoportulae. Each marginal fultoportula with two auxiliary processes. Labiate process positioned near the centre.

76. *Thalassiosira* sp. 2. Plate.33, e-f

Ref: Round et al., 1990

Diameter: 30.4 µm

Cells forming a chain. Valve face shallow in internal view. Fultoportulae on the margin and scattered on the valve face. Each marginal fultoportula with four or five auxiliary pores. Areolae irregular in shape. Single labiate process at the edge of valve mantle.

77. *Thalassiosira* sp. 3. Plate.34, a-c

Ref: Round et al., 1990

Diameter: 4.4 µm

Cells forming a chain. Valves circular with shallow mantle. Areolae radially arranged, irregular, and hexagonal in shape in the centre and towards edge. Six marginal and one central fultoportulae. Each marginal fultoportula has two or three auxiliary pores, while central fultoportulae has two auxiliary pores. A labiate process at the margin.

78. *Thalassiosira* sp. 4. Plate.34, d-e

Ref: Round et al., 1990

Diameter: 28.57 µm

Cells forming a chain. External valve face circular, flat with round areolae, less in the centre and getting dense at the edge. Areolae loculate. The external tubes of the marginal fultoportulae are very short. Single rimoportula present. We can observe silica grains scattered on the valve.

79. *Thalassiosira* sp. 5 Plate.35, a-b

Ref: Round et al., 1990

Diameter: 15.28 µm

Cells forming a chain. Valve face deep in internal view. Marginal fultoportulae equidistant from each other. Six fultoportulae scattered on the valve face out of which one is almost at centre. Each marginal fultoportula with two auxiliary pores. Fultoportulae at centre has three auxiliary pores. Areolae irregular in shape. Single labiate process at the edge of valve mantle.

80. *Actinocyclus* sp. Plate.35, c-d

Ref: Witkowski et al., 2000

Diameter: 27.75 - 28.8 µm sp. 1

Centric valve in outline with a deep mantle. The valve face is flat. Internal openings of rimoportulae visible. This genus is distinguished by the presence of a pseudonodulus (fan shaped). The pseudonodulus may only be visible on the inside valve. Outside pseudonodulus appear like a hole. One of this is bigger than the others. The round areolae on the valve face are smaller and denser on the edge and bigger and disperse in the centre.

81. Centric sp. 2. Plate.35, e-f

Diameter: 16.6 µm

Valves circular with well-developed mantle. Round areolae forming radiating pattern. Fultoportulae placed equidistantly on the margin and one is in the centre. Inside for each fultoportulae we observe four satellite pores. A labiate process is present.

Detailed characteristics of the following species are provided in 'Chapter 3' with their molecular information and phylogenetic position.

82. *Psammodictyon panduriforme* (W.Gregory) D.G.Mann. Pl. 36, a-c.

Basionym: *Nitzschia panduriformis* W.Gregory

Ref: Round et al., 1990; Witkowski et al., 2000

AA: 30 µm, TA: 9.4 µm, TS in 10 µm: 22, F in 10 :24 µm

Solitary cells. Valves panduriform with apiculate apices in valve view. Keeled raphe. External central raphe endings are not visible, while terminal raphe endings are slightly turned. Striae are uniseriate consisting of quadrangular to roundish loculate areolae with large perforations.

83. *Diploneis weissflogiopsis* Lobban & Pennesi. Pl. 36, d.

Ref: Pennesi et al., 2017

AA: 27.3 µm, TA: 10.9 µm, TS in 10 µm: 10

Solitary cells. Valves panduriform, with rounded apices. Externally, the raphe consists of two straight branches ending in deep central pores and terminal fissures bent towards the same side. Raphe-sternum narrow and depressed central area constrained by two triangular spines and four pores. A pair of modified striae extend from these spines to the valve margin with one loculus in the middle of each. Radiate transapical striae, composed of transapically elongated areolae.

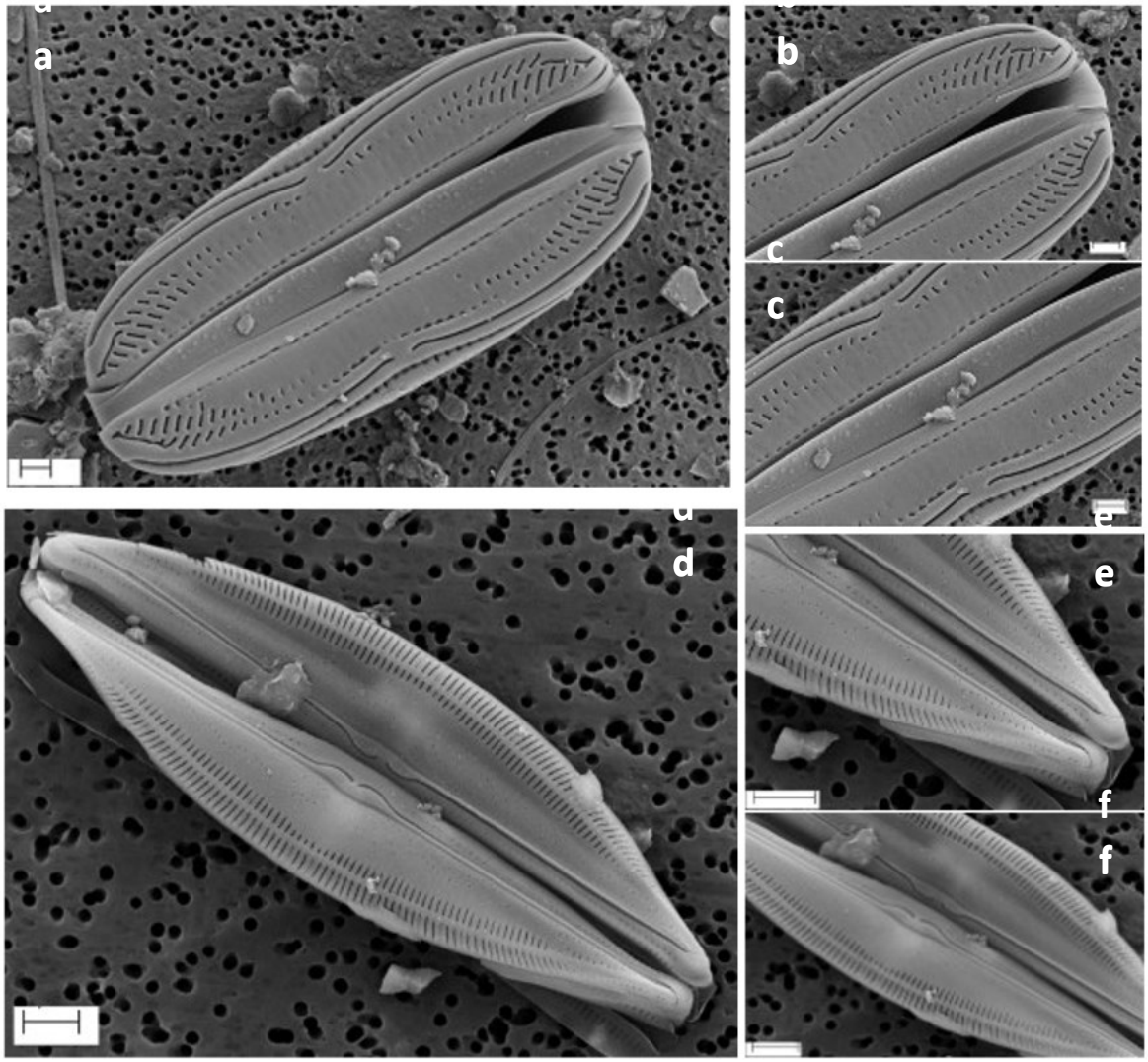

Plate 1: a-c= *Amphora arenicola* SEM, a= External view of the frustule, b=terminal end of the frustule showing straight raphe endings, c=curved central endings of the raphe. d-f= *Amphora* cf. *graeffei* var. *minor* SEM, d= External view of the frustule, e=terminal end of the frustule, f=curved central endings of the raphe. Scale bars: a-f = 2 µm

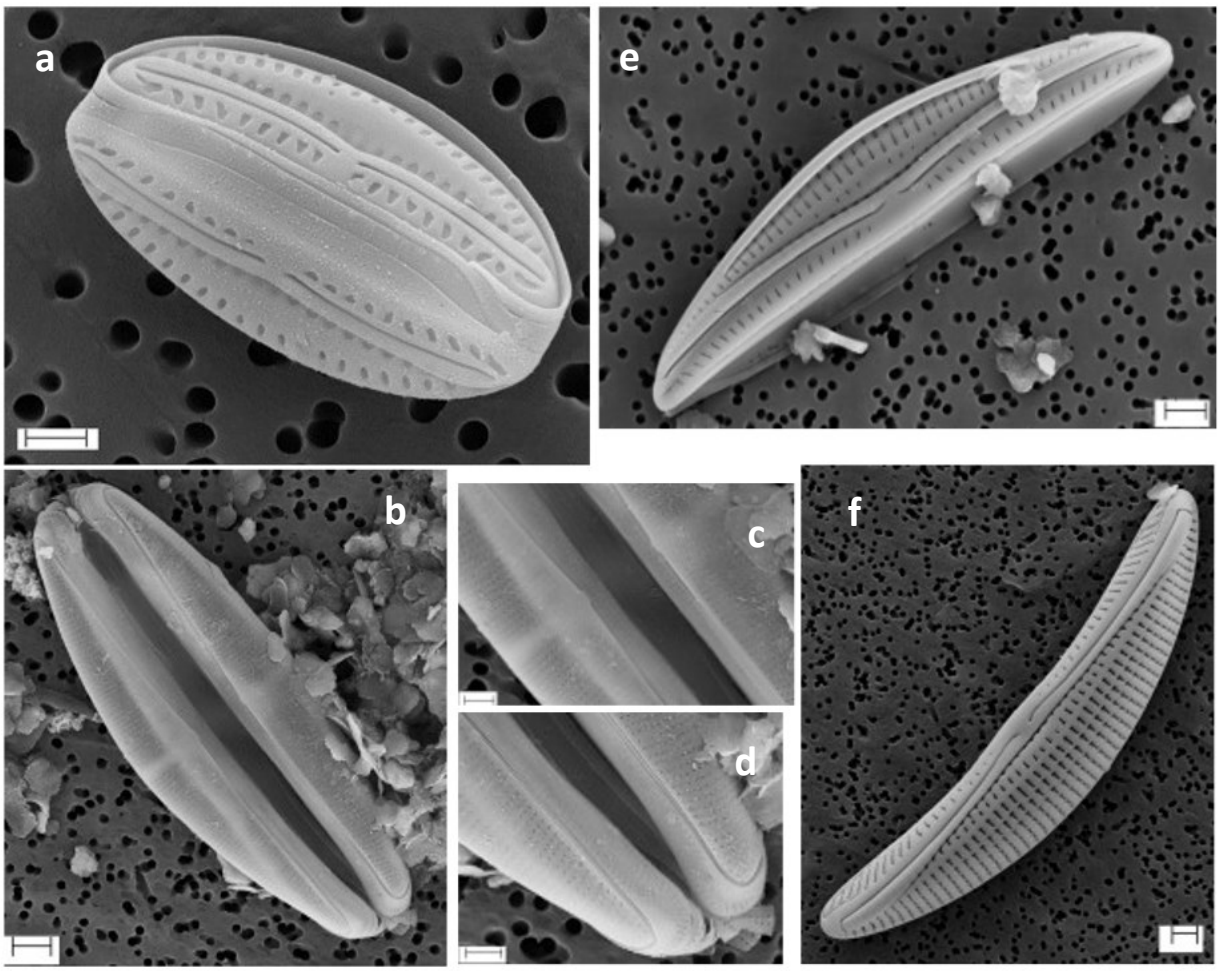

Plate 2: a= *Amphora* cf. *inariensis,* SEM, Ventral view of the cell showing all the structures of raphe and arrangement of the areolae, b-d= *Amphora* cf. *jostesorum,* SEM, b= External view of the frustule, c= central endings of the raphe showing the central nodule, d= terminal end of the frustule showing curved raphe endings, e= *Amphora libyca,* SEM, External valve view showing biarched centre, f= *Amphora* cf. *proteus,* SEM, External valve view showing curved raphe at centre and terminal end. Scale bars: a, c, d= 1 µm; b, e, f= 2 µm.

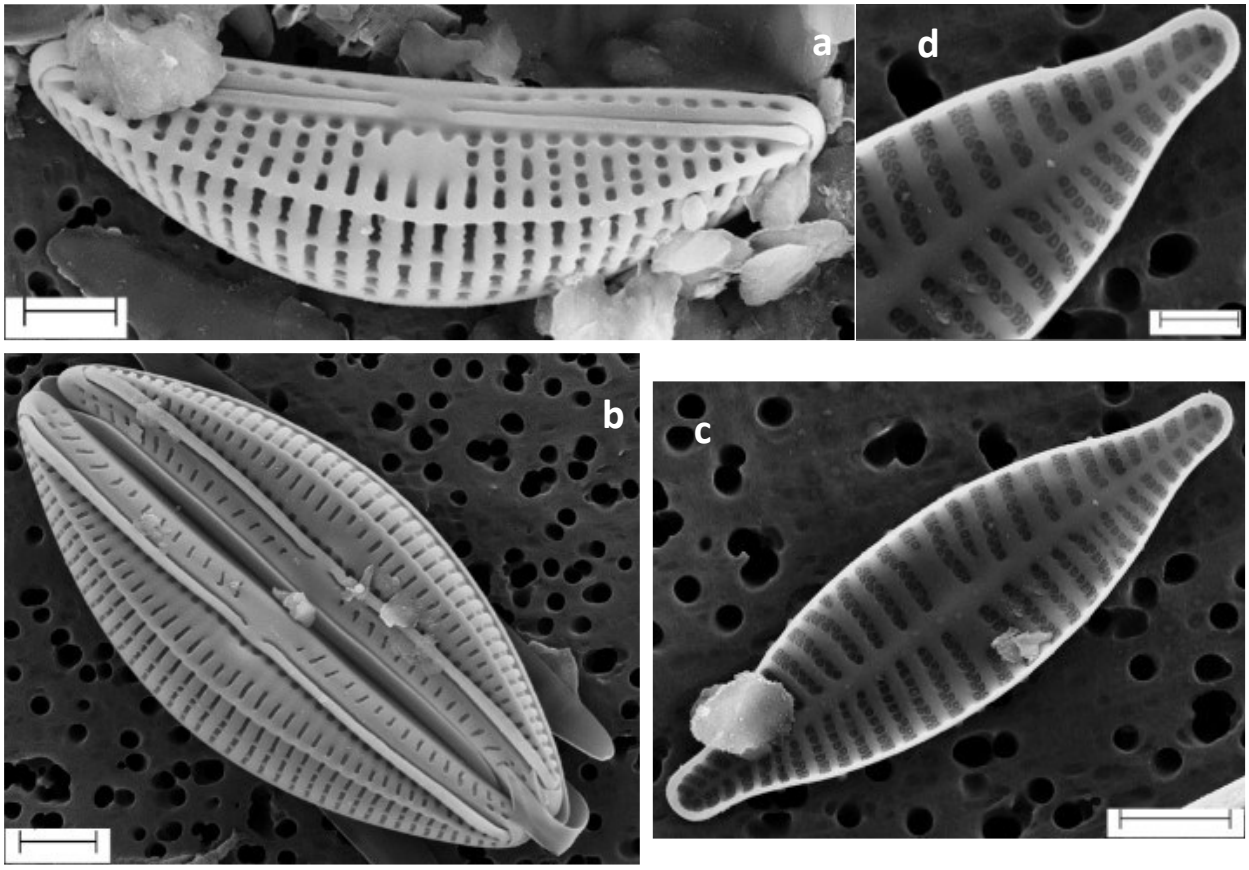

Plate 3: a= *Amphora* cf. *copulata,* SEM, External valve view showing distinct fascia, b= *Amphora* cf. *helenensis,* SEM, External valve view showing raphe with fissure at central and terminal apices with a lanceolate blank band across the dorsal striae, c-d= Araphid species, SEM, c= internal valve view, d=distinct biseriate striae. Scale bars: a, b, c= 2 μm; d= 1 μm

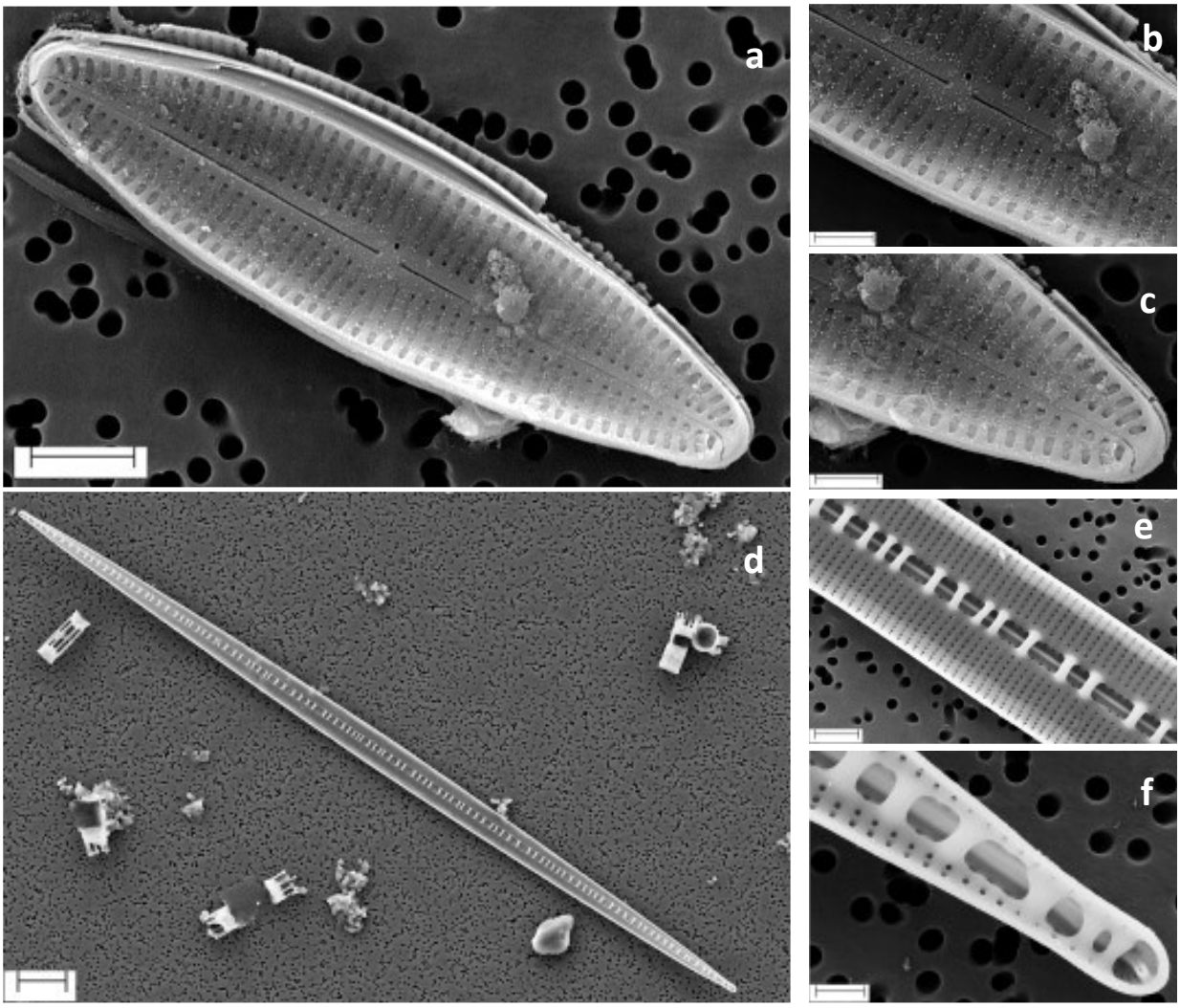

Plate 4: a-c= *Astartiella* sp. 1, SEM, a= External valve view, b= centre showing stigma at one side of raphe, c= terminal part of the valve showing raphe fissure and straie showing delicate hymen; d-f= *Bacillaria paxillifera,* SEM, d= Internal valve showing broadened central part, e= fibulae and central part of the valve with round areolae and raphe in the keel, f= raised raphe ending. Scale bars: a, e= 2 µm; b, c, f=1 µm; d=10 µm.

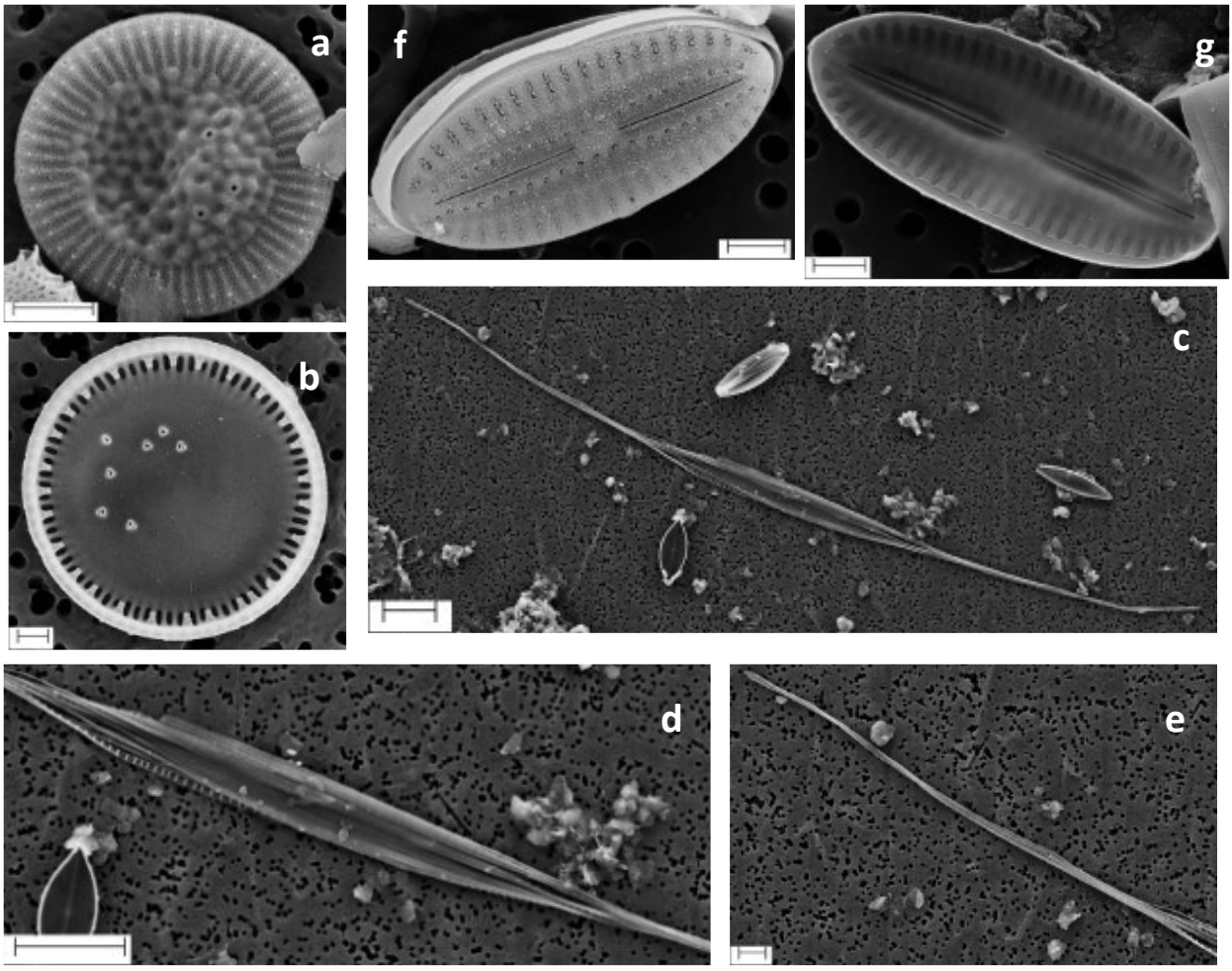

Plate 5: a-b= *Cyclotella striata,* SEM, a=external valve view, b=internal valve view; c-e= *Nitzschia longissima,* SEM, c= external valve view shoing very long rostrate ends, d= central part of the valve showing fibulae, e= terminal end of the valve; f-g= *Diploneis* sp. 3, SEM, f= external valve showing straight raphe endings and row of areolae around raphe, g= Internal valve view showing distinct raphe canal and absence of areolae around the raphe canal. Scale bars: a= 2 µm; b, f, g=1 µm; e=3 µm; c, d=10 µm.

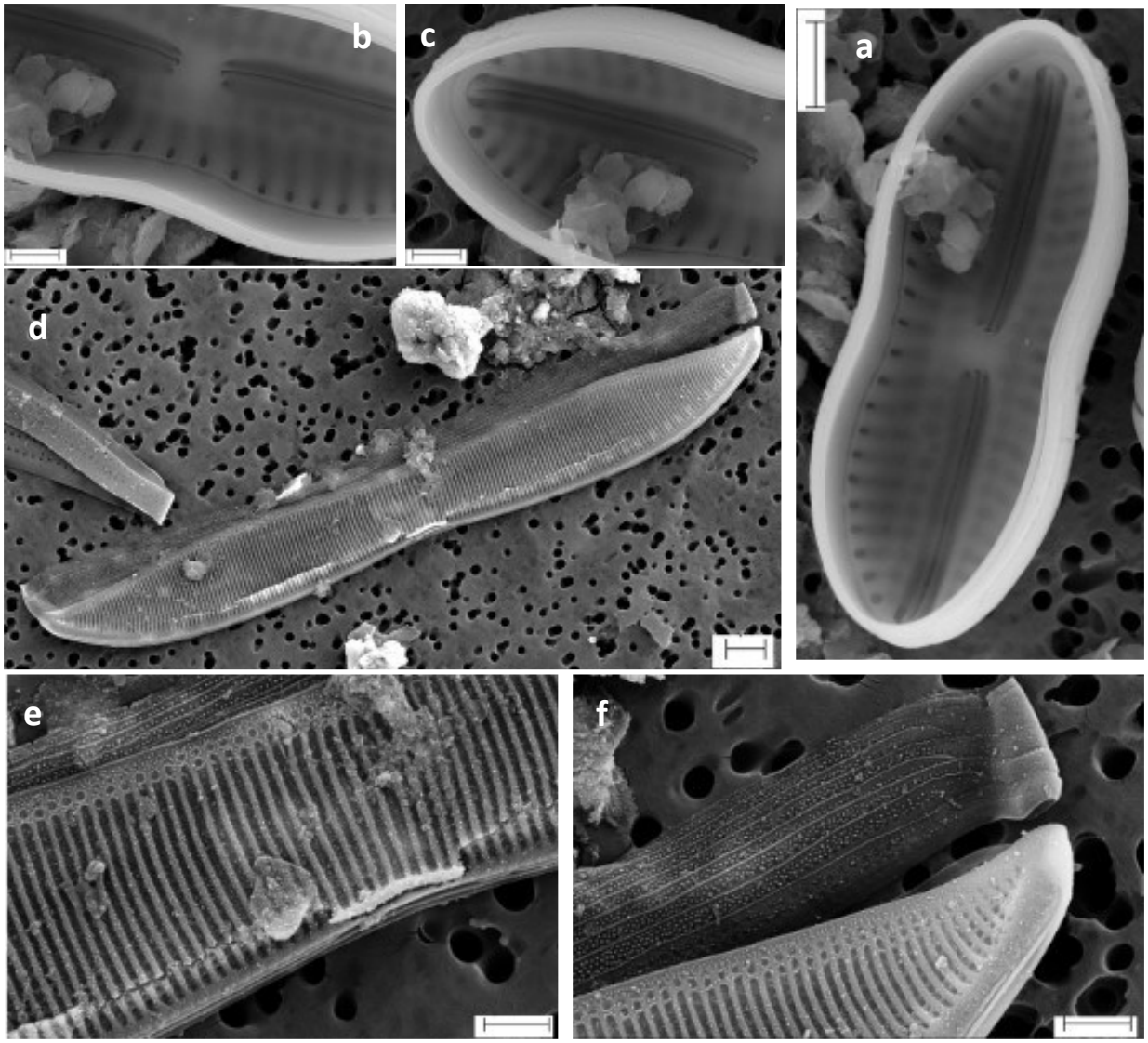

Plate 6: a-c= *Diploneis* sp. 4, SEM, a=Internal valve view showing distinct raphe canal and absence of areolae openings around the canal, b & c = central and terminal valve view showing the elevated raphe ending; d-e= *Entomoneis alata,* SEM, d= Enternal valve view, e= Central part of the valve with thick interstriae, f= terminal end with raphe ending and girdle bands with numerous poroids. Scale bars: a, d=2 µm; b, c, e, f=1 µm.

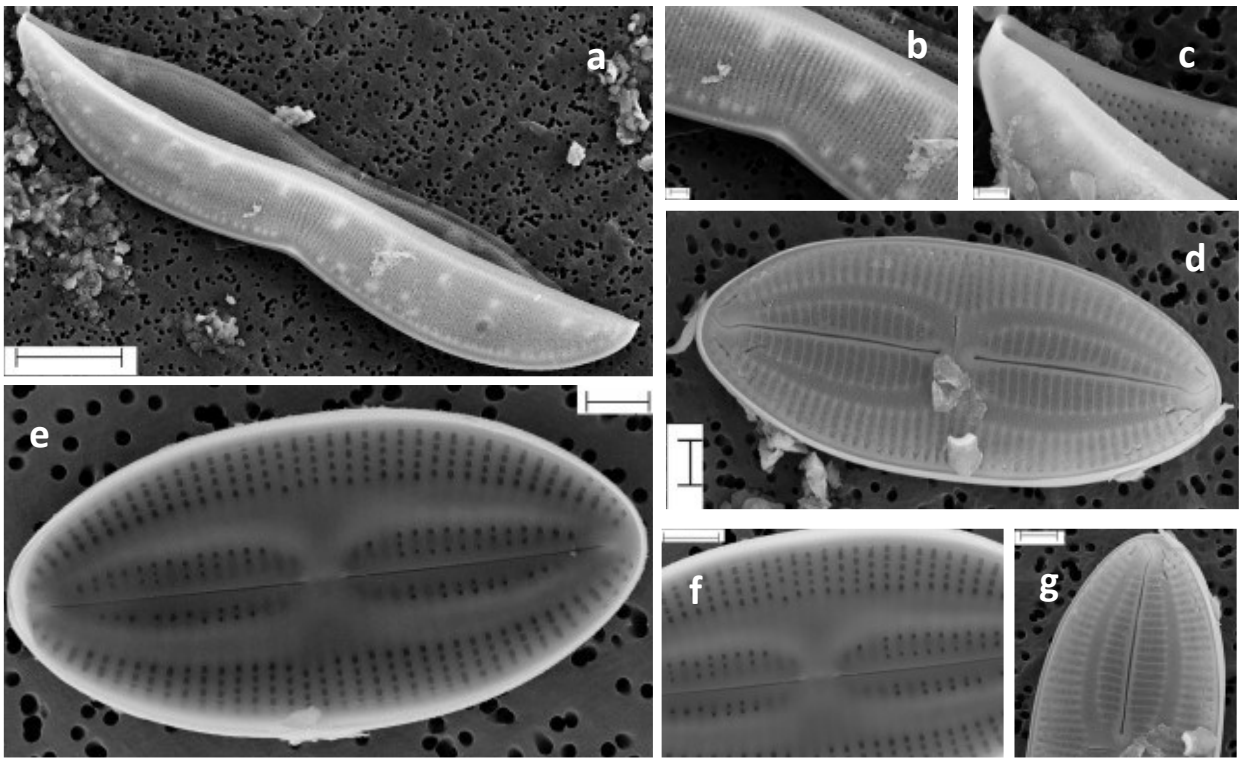

Plate 7: a-c= *Entomoneis* cf. *paludosa,* SEM, a= External valve view, b= strongly constricted in the middle, c= terminal part of the valve showing rounded areolae in the internal view; d-g= *Fallacia* cf. *forcipata,* SEM, d= external valve view showing 'H' shaped lyre, e= internal valve view showing blank 'H' shaped lyre and areolae lines around raphe canal, f= deflected central raphe endings and round areolae, g= distinct 'conopea' at terminal end. Scale bars: a= 10 µm; b, c= 1 µm; d, e, f, g= 2 µm.

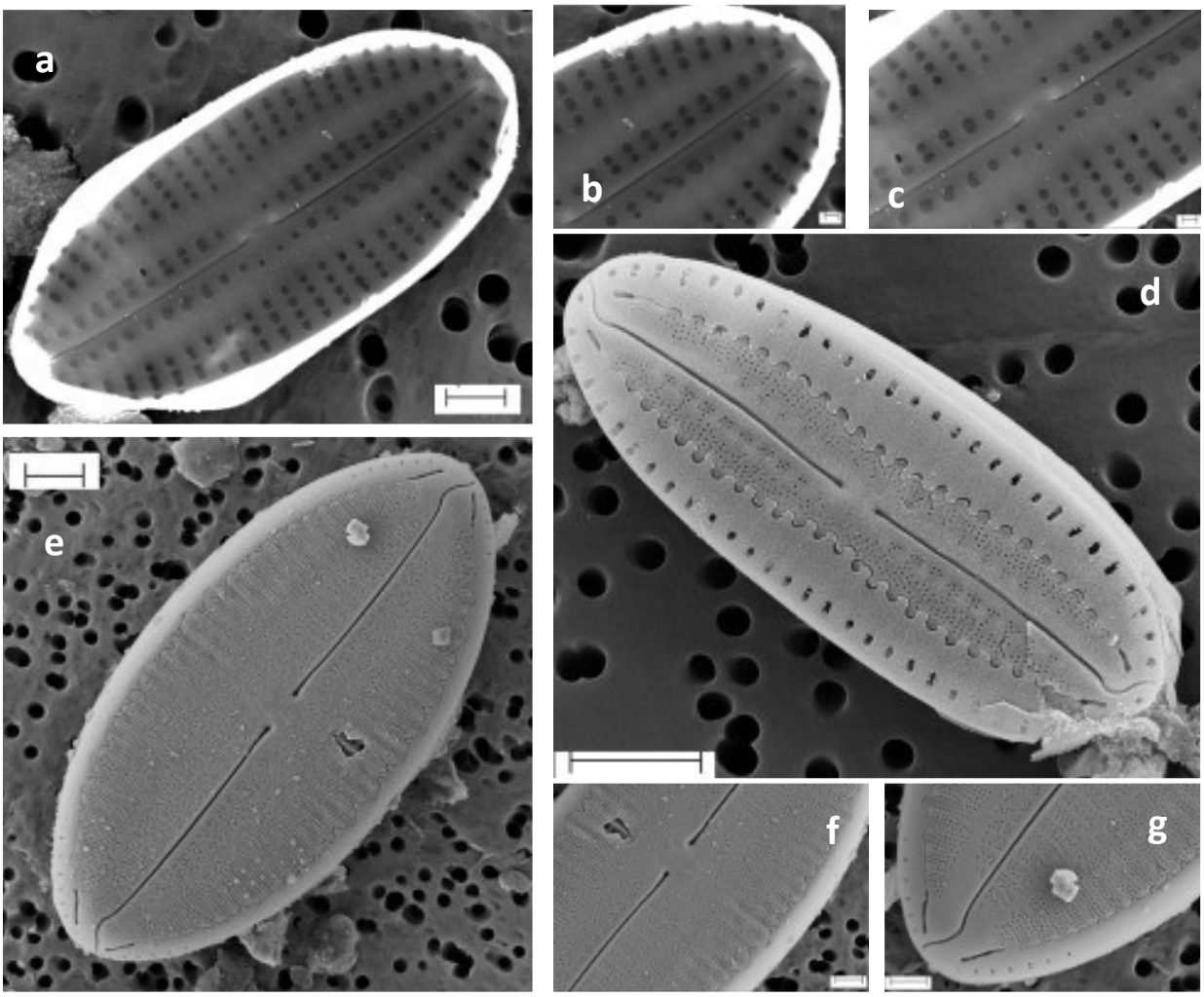

Plate 8: a-d= *Fallacia* cf. *tenera,* SEM, a= internal valve view showing blank 'H' shaped lyre and areolae lines around raphe canal, b= terminal end showing deflected raphe, c= central raphe with deflected endings, d= external valve view with 'conopea' at the terminal ends; e-g= *Fallacia* sp. 1, SEM, e= external valve view with porous silica layering and conopea at the terminal ends, f= central raphe ending which are turning inside, g= terminal ends showing conopea and line of puncta. Scale bars: a, f, g=1 µm; d, e=2 µm; b, c= 200nm.

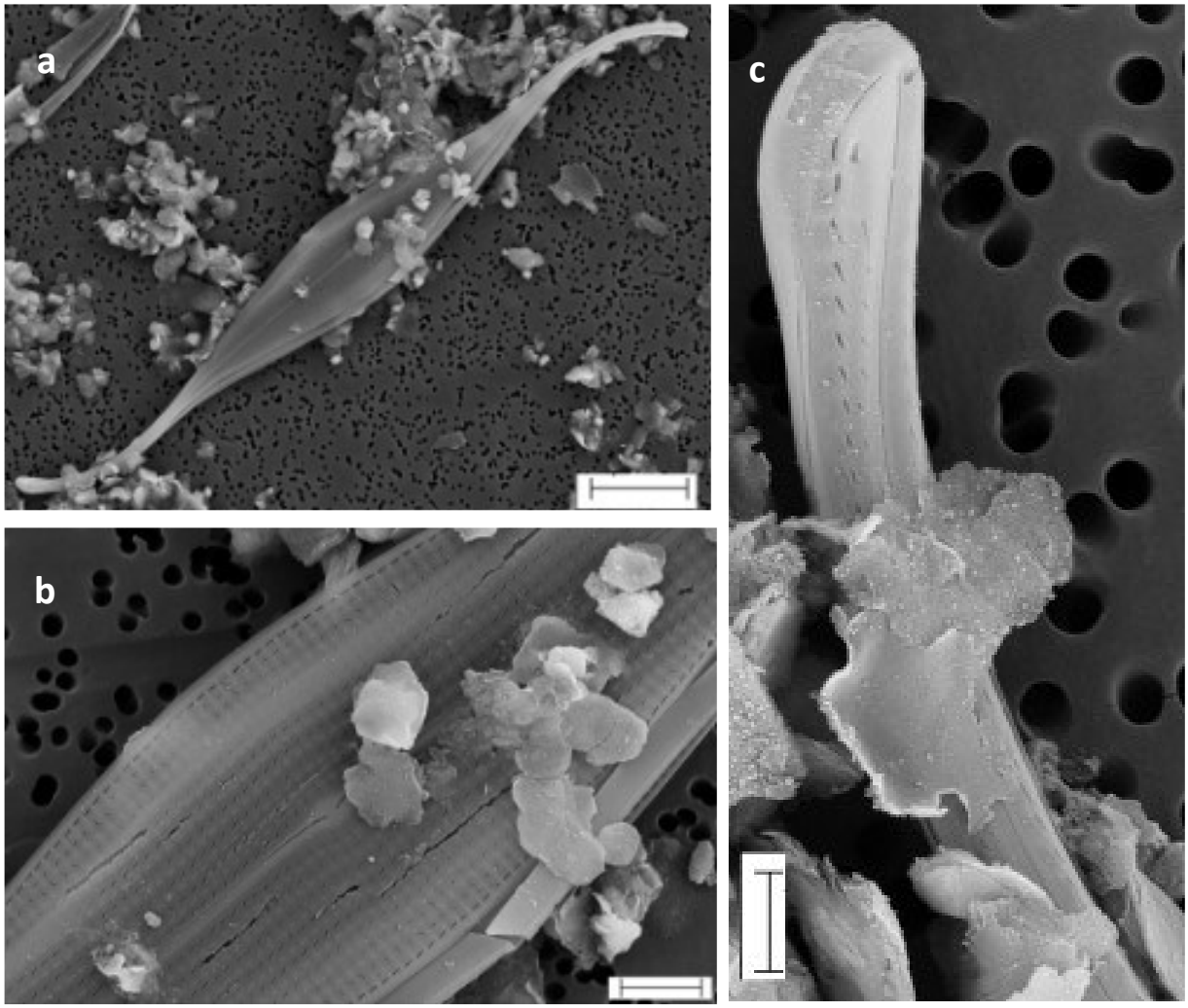

Plate 9: a-c= *Gyrosigma* cf. *fasciola,* SEM, a=valve view showing extended terminal ends in the opposite sides, b= central part of the valve showing parallel-perpendicular arrangement of dash-lile areolae, c= terminal end of the valve showing bended raphe and line of poroids. Scale bars: a=10 µm; b=2 µm; c=1 µm.

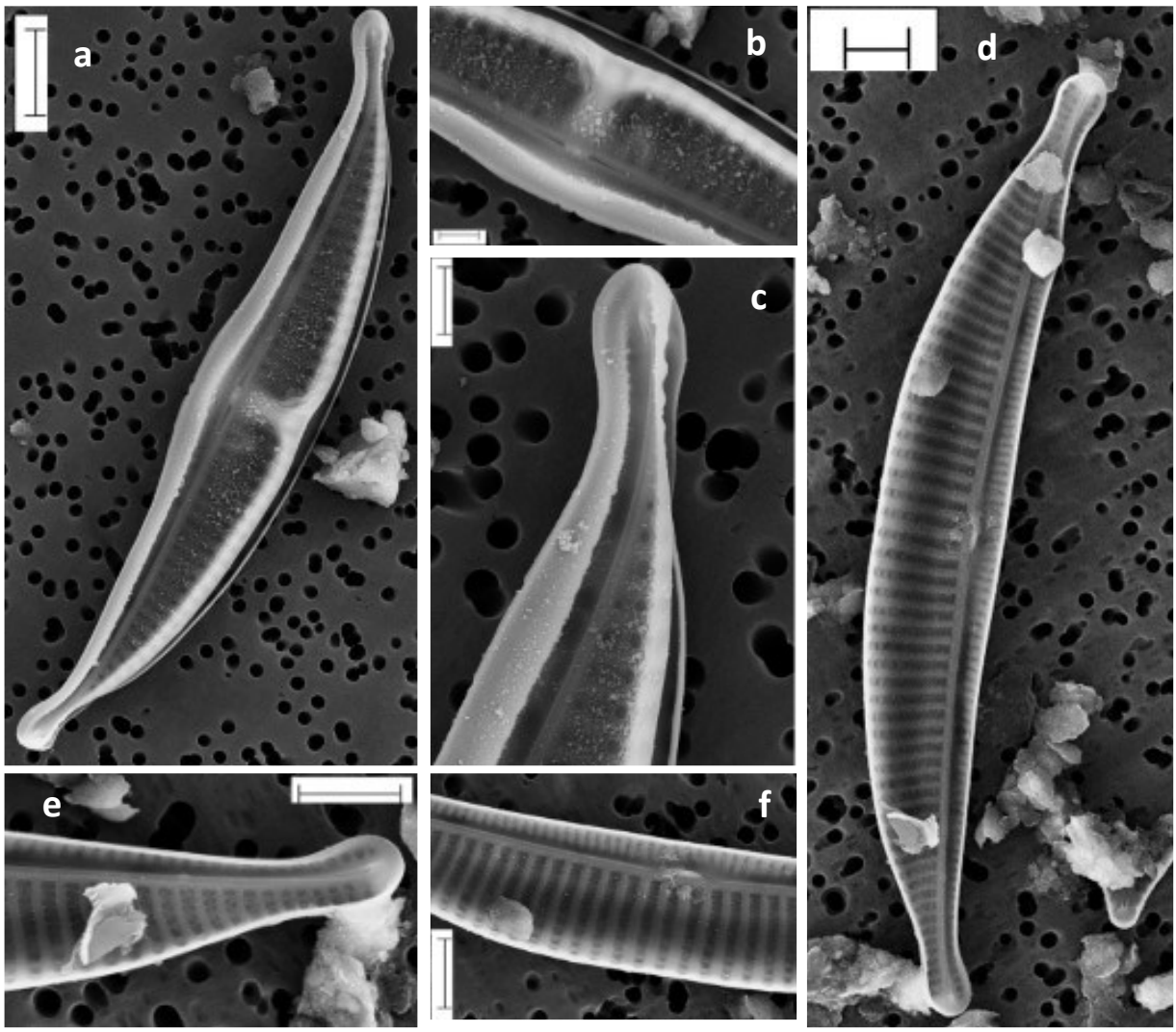

Plate 10: a-c= *Halamphora cuneata,* SEM, a= Internal valve view showing constriction in the middle, b= central part of the valve showing hyaline fascia and central nodule, c= terminal raphe with deflected ending; d-f= *Halamphora coffeiformis,* SEM, d= internal valve view, e= terminal end of the raphe showing deflection, f= central endings of the raphe with central nodule and biarcuate areolae. Scale bars: a=3 µm; b, c= 1 µm; d, e, f= 2 µm.

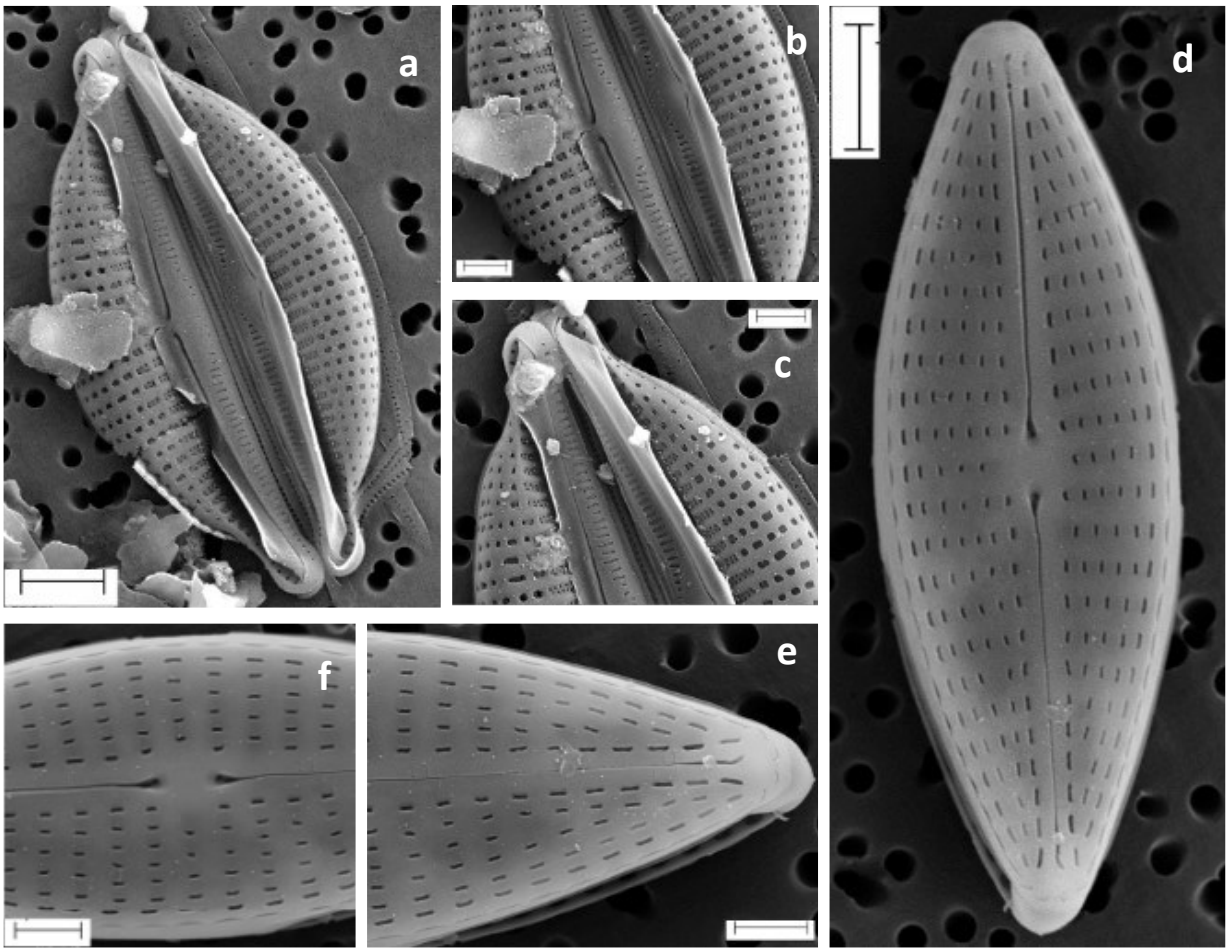

Plate 11: a-c= *Halamphora* cf. *tenerrima,* SEM, a= External valve view showing protracted ends, b= central raphe endings showing curved ends, c= terminal end of the valve; d-f= *Hippodonta* sp., SEM, d= external valve view, e= terminal end of the valve showing slight curve in the raphe and divergent striae, f= expanded central raphe endings. Scale bars: a, d= 2 µm; b, c, e, f= 1 µm.

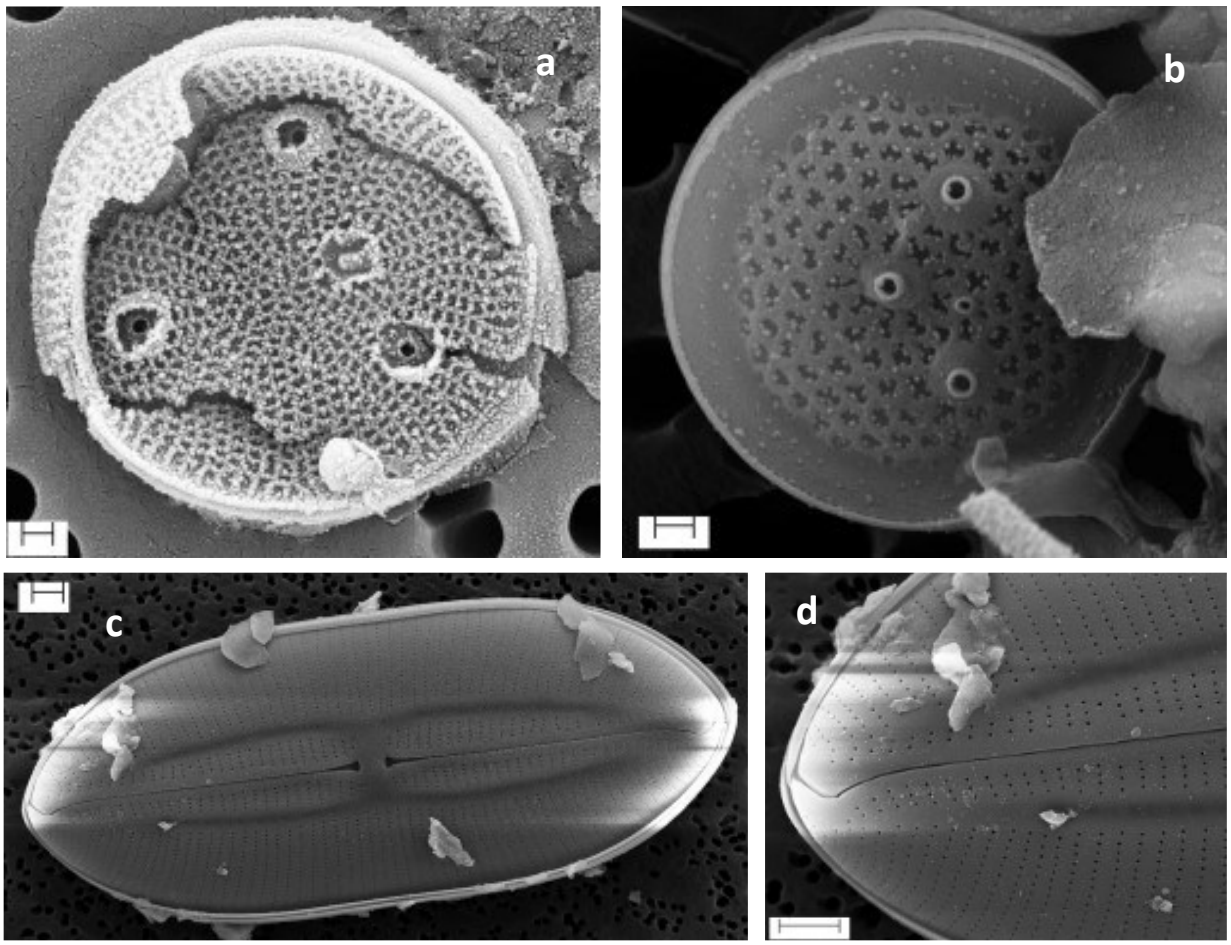

Plate 12: a= *Mediolabrus comicus,* SEM, External valve view showing three fultoportulae and one rimoportula around the centre; b= *Minidiscus trioculatus,* SEM, External valve view with Three fultoportulae and sub-central small rimoportula also round radiate areolae with rotae can be noticed; c-d= *Lyrella* sp. 1, SEM, c= faint 'H' shaped lyre with straight raphe with expanded central endings, d= terminal raphe endings are like fissures and radiating small areolae. Scale bars: a, b=200nm; c, d= 2 µm.

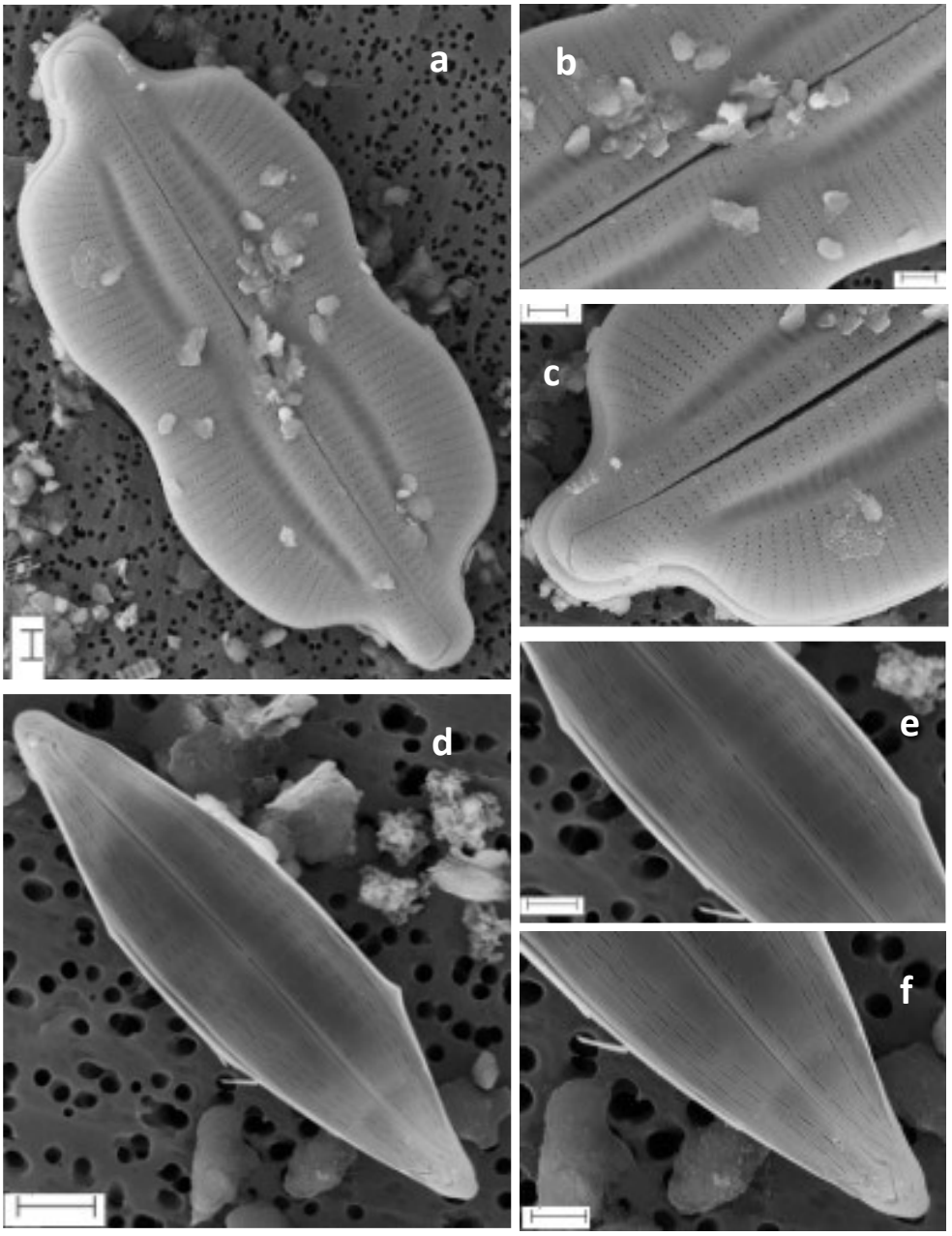

Plate 13: a-c= *Lyrella* cf. *exsul,* SEM, a= external valve view showing distinct 'H' shape lyre and depression where areolae are absent, b= central part showing expanded raphe endings, c= terminal endings showing raphe turning on the another side; d-f= *Navicula agatae,* SEM, d= external valve view showing limited parallel striae with dash like areolae, e= central raphe endings are expanded, f= terminal end of the raphe hooked. Scale bars: a, b, c, d= 2 µm; e, f= 1 µm.

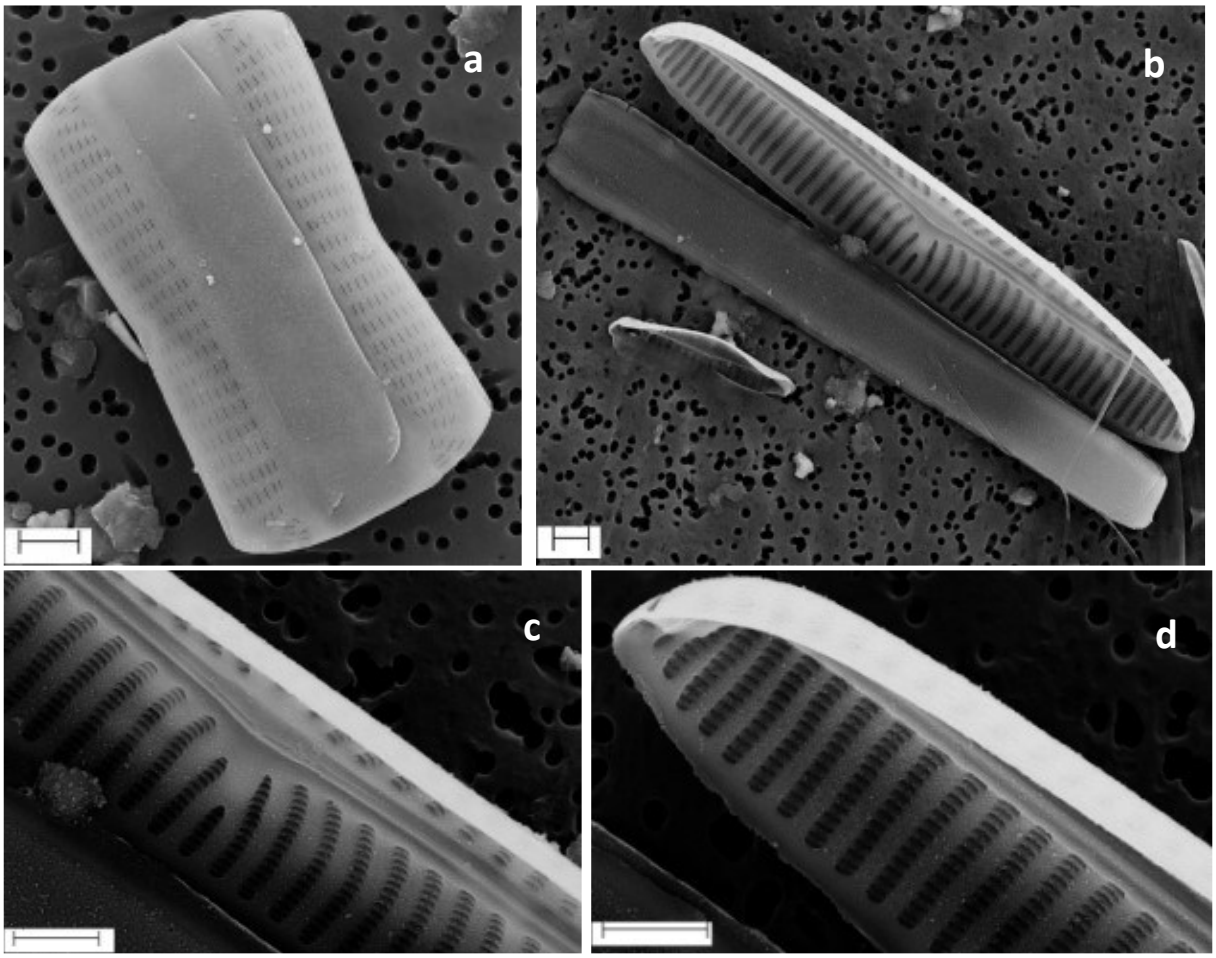

Plate 14: a= *Navicula* sp. 2, SEM, External valve view showing constriction in the middle; b-d= *Navicula distans,* SEM, b= internal and side view of the valve with plain girdle band, c= uplifted central raphe endings and missing striae in the centre, d= terminal end of the raphe. Scale bars: a, b, c, d =2 µm.

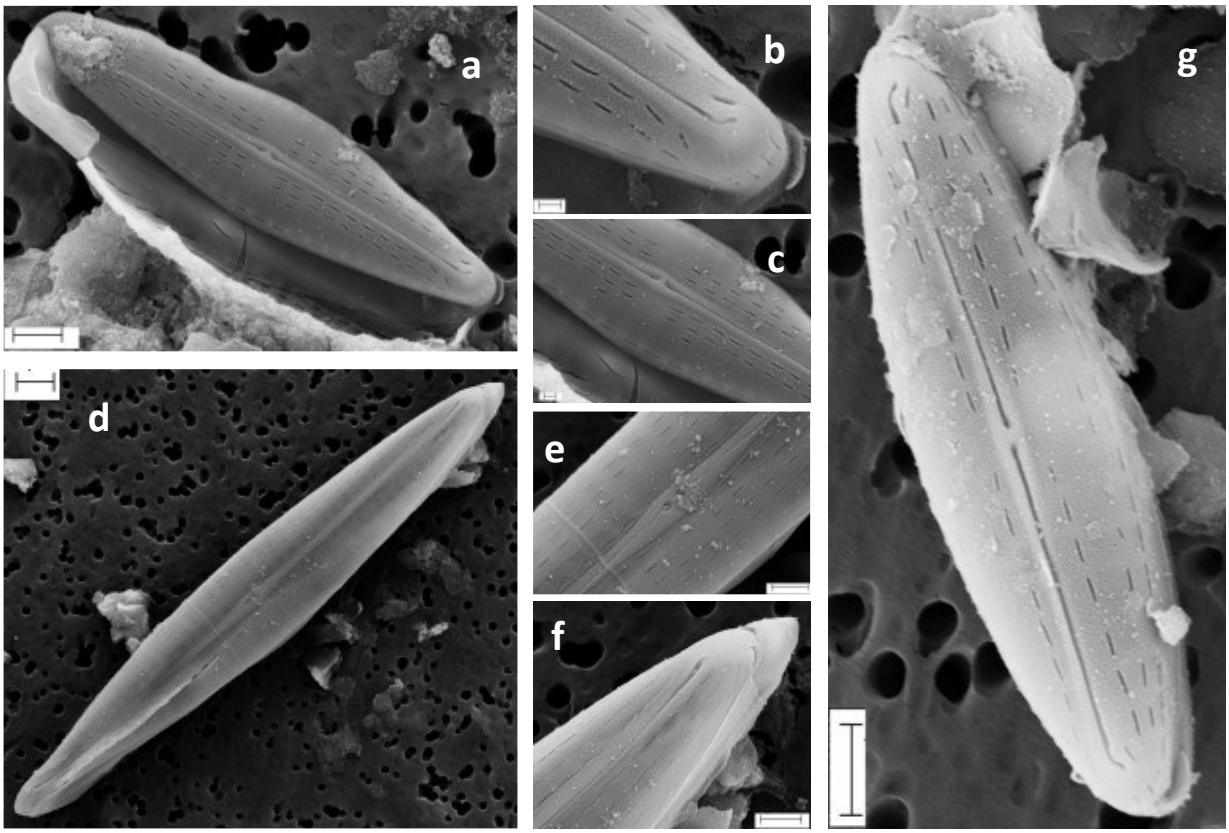

Plate 15: a-c= *Navicula* sp. 1, SEM, a= External valve view showing few lines of parallel striae, b= terminal part of the valve showing slightly curved raphe and apical pore field, c= central raphe ending curved towards same side; d-f= *Navicula* sp. 3, SEM, d= external valve view with dash like areolae, e= central raphe endings strongly hooked and few areolae missing in the central part, f= terminal raphe straight slightly expanded; g= *Navicula* sp. 4, SEM, external valve view showing sparse areolae and structure of raphe. Scale bars: a, e, f, g=1 μm; b, c= 200nm, d=2 μm.

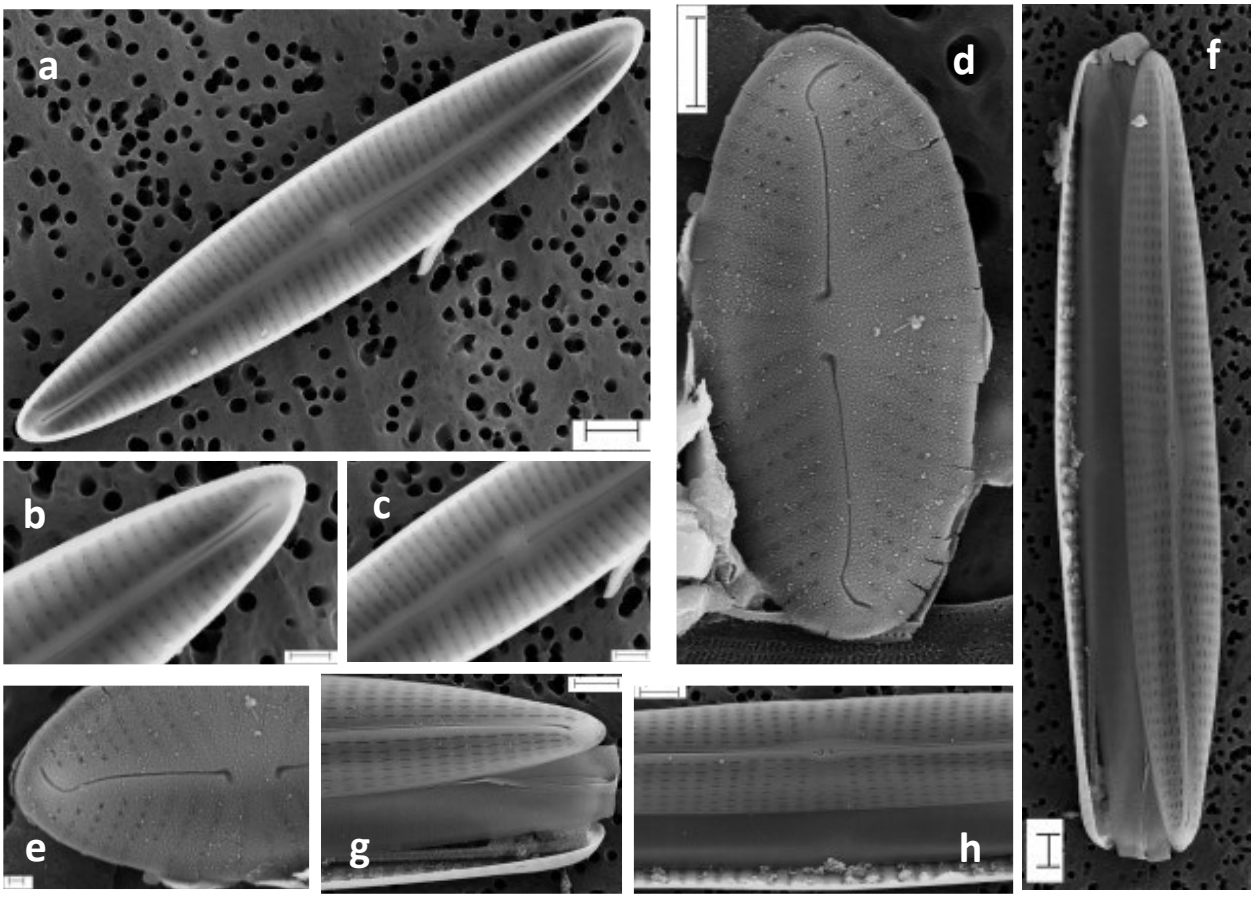

Plate 16: a-c= *Navicula* sp. 5, a=internal valve view showing round areolae and parallel transapical striae, b= terminal end of the raphe with fissure, c= central endings of the raphe distant and slightly elevated; d-e= Pennate sp. 6, SEM, d= external valve view showing radiating striae, e= deflected terminal and central raphe endings; f-h= *Navicula* sp. 6, SEM, f= external valve view showing the missing striae in the centre, g= terminal raphe endings slightly curved, h= hooked central raphe endings. Scale bars: a, d, f, g, h=2 µm; b, c=1 µm; e= 200nm.

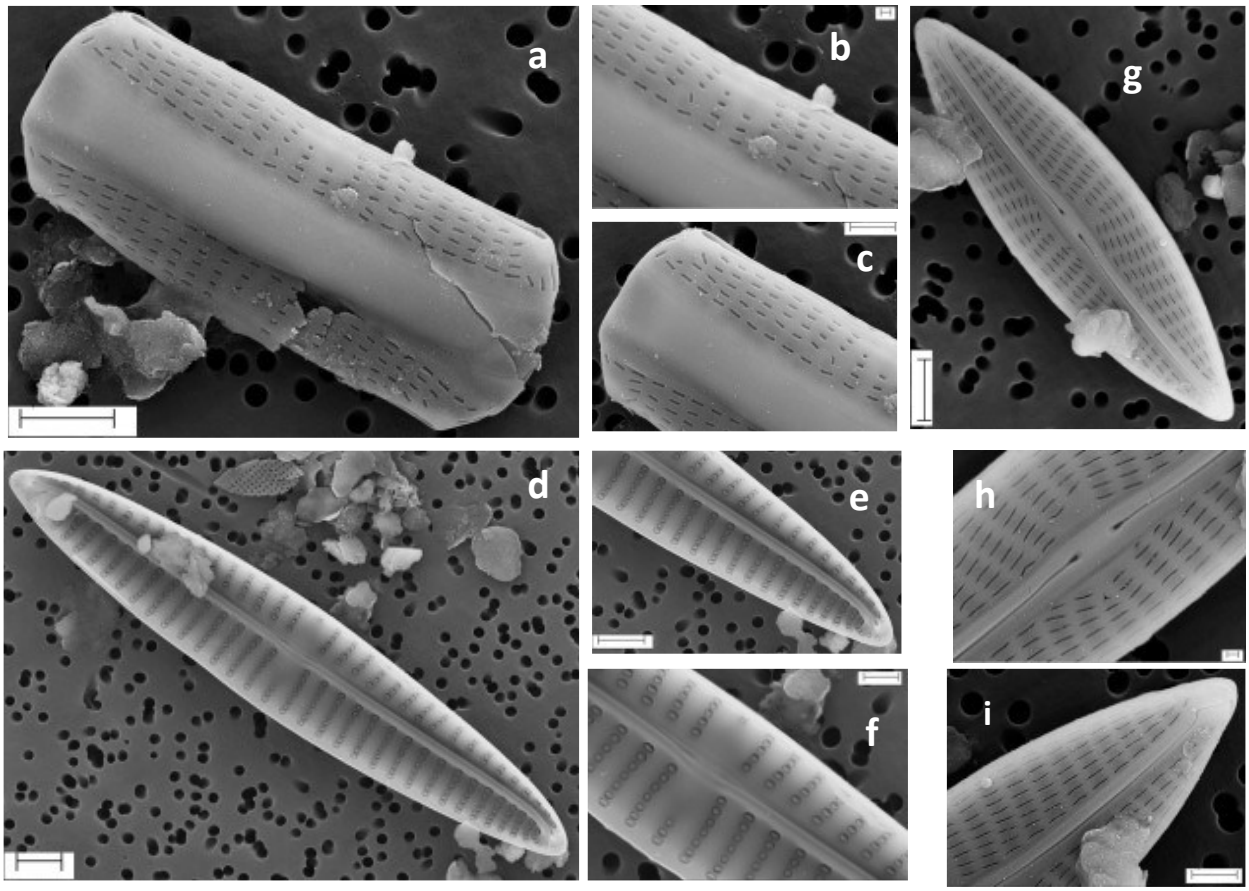

Plate 17: a-c= *Navicula* sp. 7, SEM, a= external side view of the valve, b= central part of the valve slightly depressed, few areolae missing in the centre, c= terminal end showing straight raphe and few areolae like structure; d-f= *Navicula* sp. 8, SEM, d= Internal valve view showing absence of few areolae in the centre, e= elevated terminal end of the raphe, f= raphe in the centre pinched; g-i= *Navicula* sp. 9, SEM, g= external valve view with divergent striae structure, h= expanded and distant central raphe endings, i= terminal part of the valve with turned raphe ending. Scale bars: a, d, e, g=2 µm; c, f, i=1 µm; b, h= 200nm

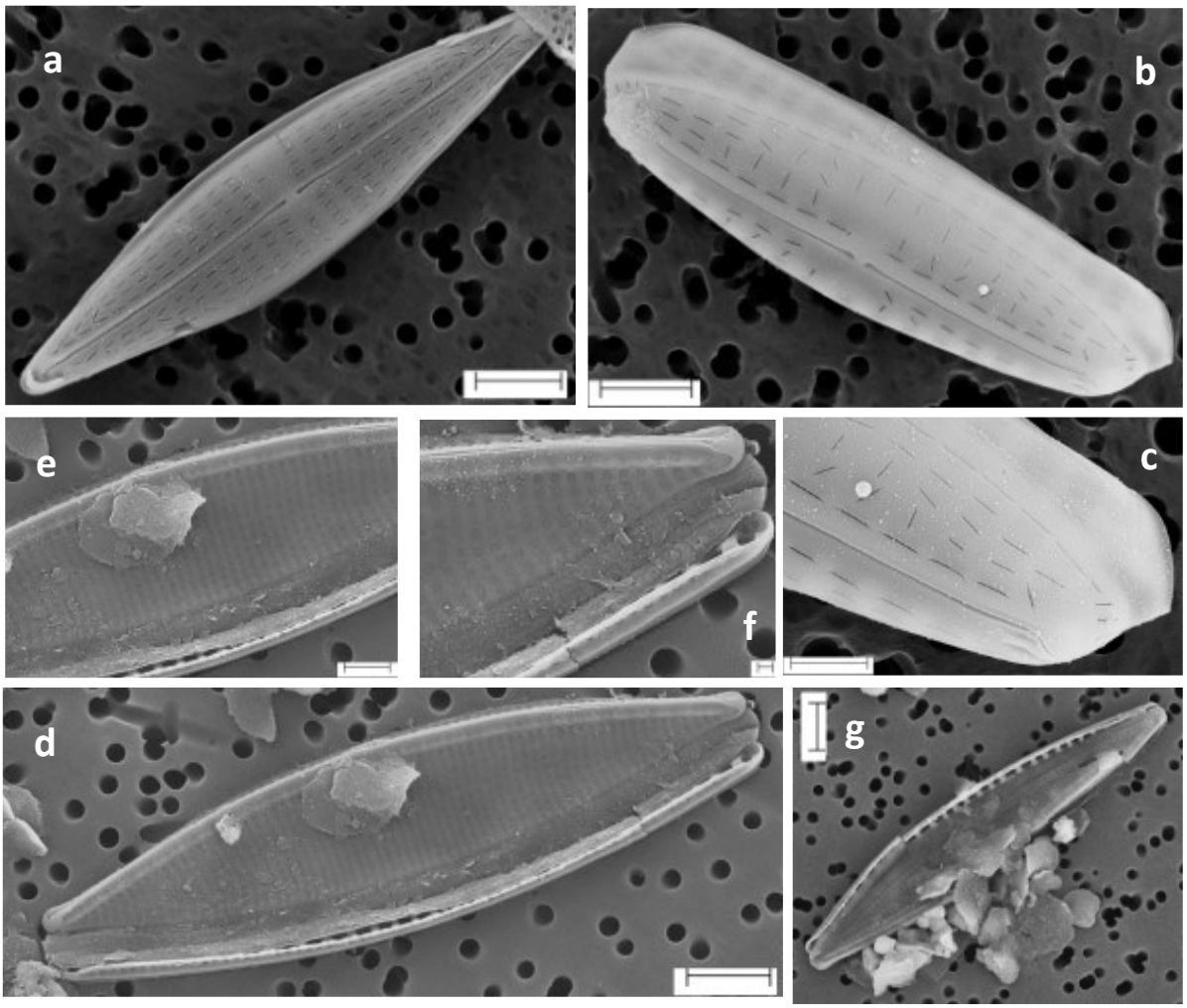

Plate 18: a= *Navicula* sp. 10, SEM, External valve view showing large interspace in the centre and divergent striae; b-c= *Navicula* sp. 11, SEM, b= External valve view showing random arrangement of areolae, c= terminal part of the valve showing turned raphe; d-g= *Nitzschia* sp. 1, SEM, d= external valve view showing poorly developed striae, e= dense striae with eccentric raphe, f= terminal end of the valve showing raphe, g= fibulae structure. Scale bars: a, b, d, g=2 μm; c, e=1 μm; f= 200nm.

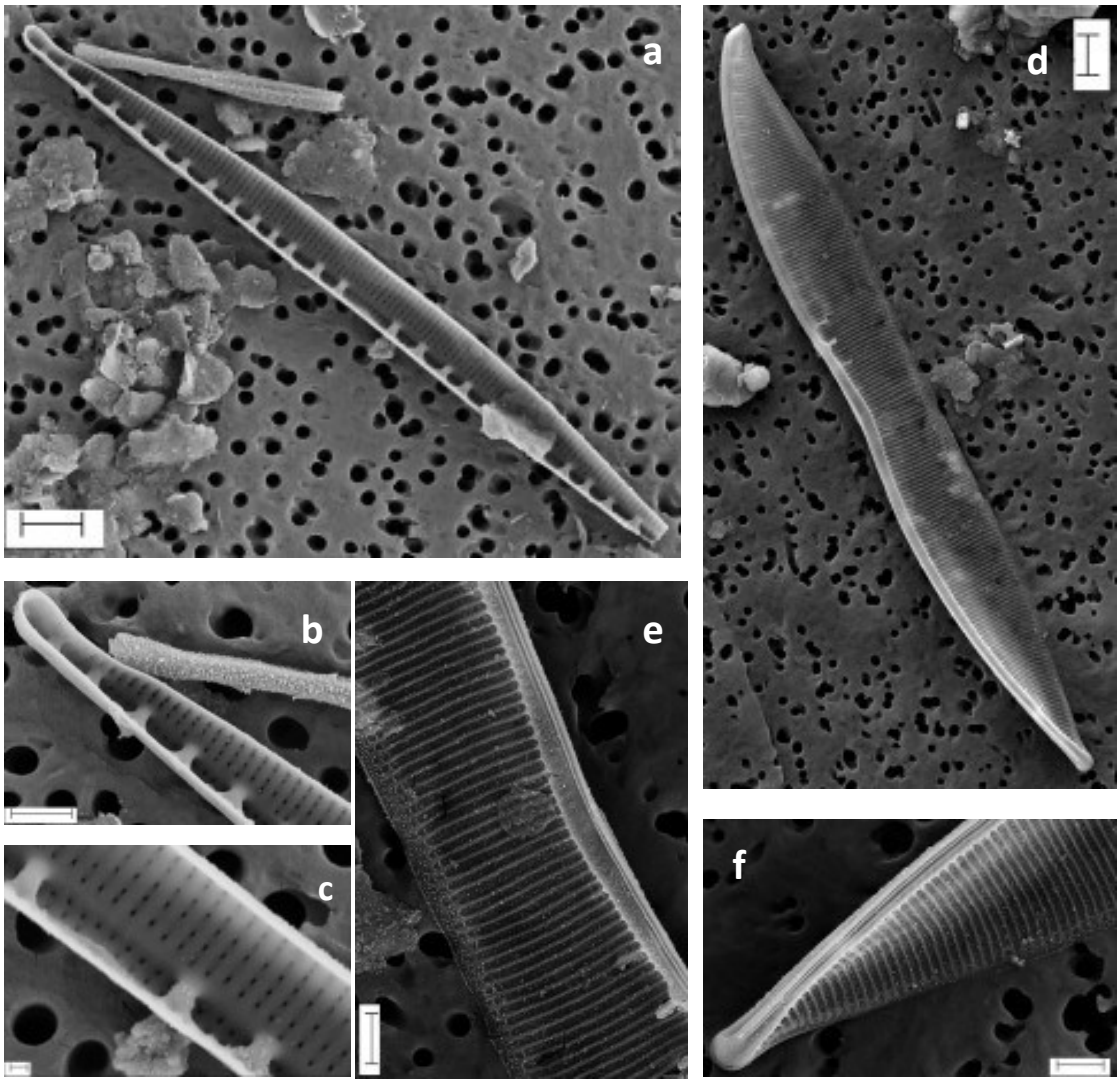

Plate 19: a-c= *Nitzschia* sp. 6, SEM, a= Internal valve view showing central fibulae distant from each other, b= terminal part of the valve, c= central part of the valve showing central nodule; d-f= *Nitzschia hybrida,* SEM, d= external valve view showing slight constriction in the centre with dense transapical striae, e= eccentric raphe raised in the keel, f= terminal part of the valve showing straight raphe ending. Scale bars: a, d=2 μm; b, e, f=1 μm; c= 200nm

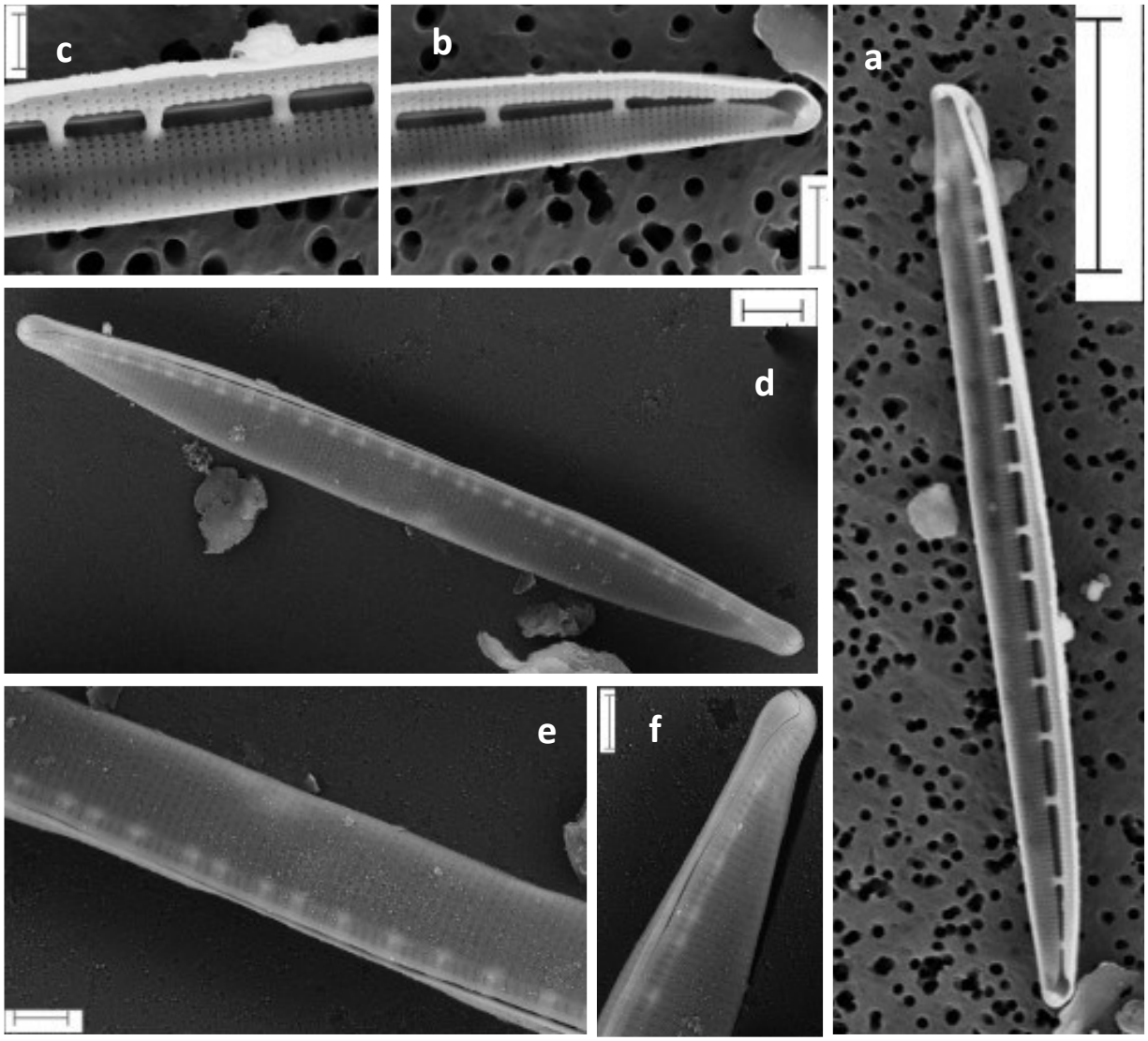

Plate 20: a-c= *Nitzschia* sp. 2, SEM, a= internal valve view showing fibulae placement, b= terminal part of the valve showing curved raphe, c= continuous raphe in the centre; d-f= *Nitzschia* sp. 4, SEM, d= external valve view with dense transapical striae and eccentric raphe, e= valve showing dense impression of the fibulae and continuous raphe, f= terminal fissure of raphe. Scale bars: a= 10 µm; b, d= 2 µm; c, e, f=1 µm.

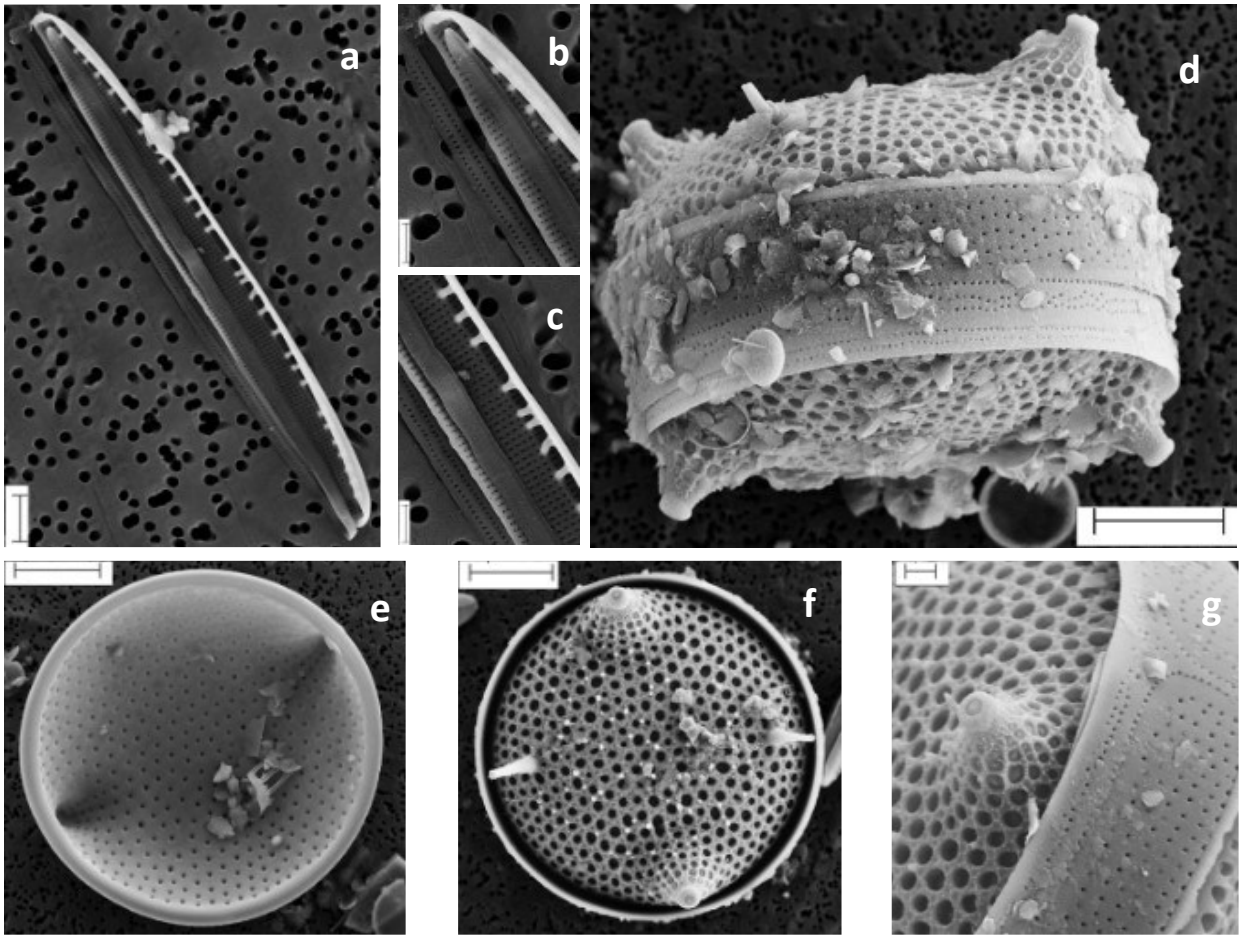

Plate 21: a-c= *Nitzschia* sp. 5, SEM, a= internal valve showing fibulae placements and girdle bands two lines of poroids, b= terminal part of the valve, c= round areolae arranged parallely; d-g= *Ralfsiella smithii* , SEM, d= girdle view of the valve, e= internal valve view showing opening of the ocellus, f= external circular valve view with two ocellus and 'spine' like rimoportulae, g= porous summit of ocellus and girdle bands with poroids. Scale bars: a, g=2 μm; b, c= 1 μm; d, e, f= 10 μm

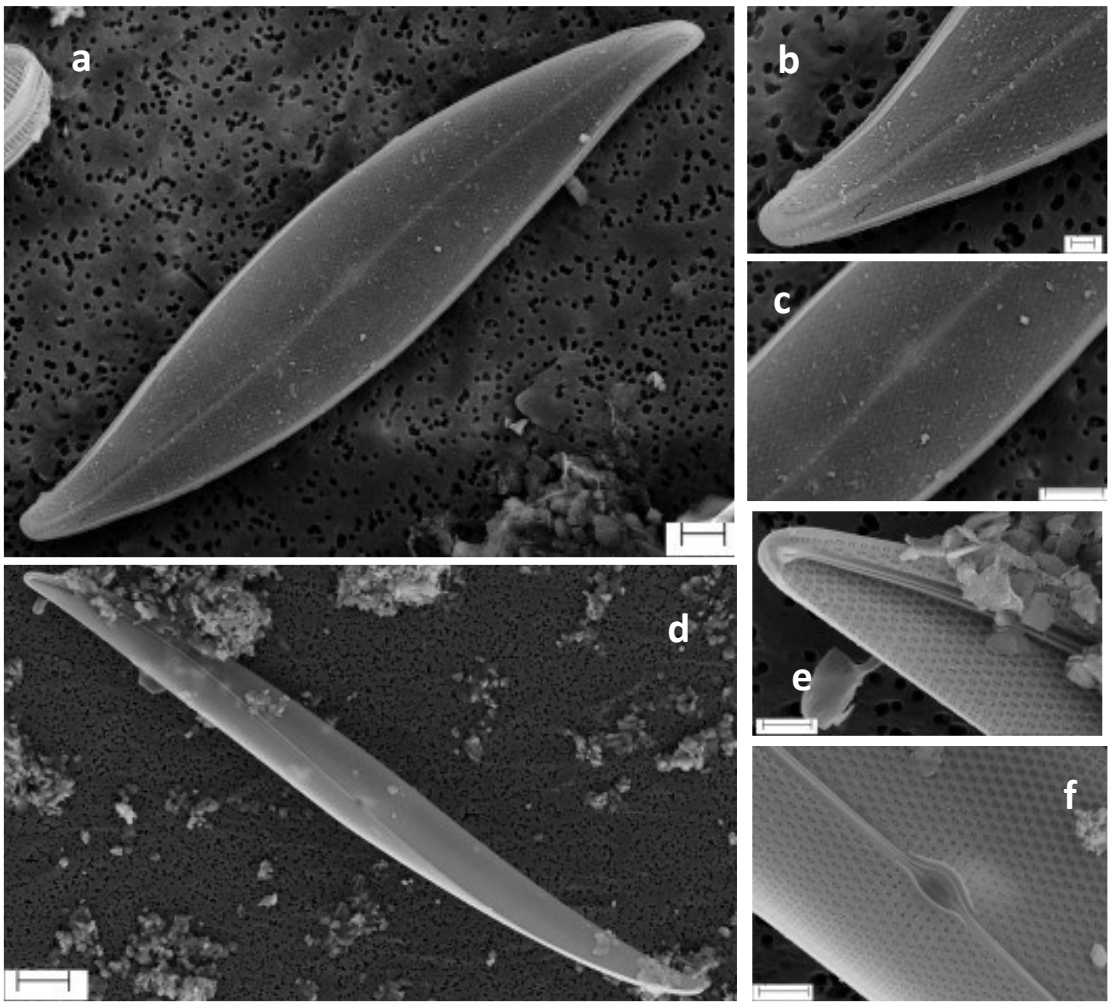

Plate 22: a-c= *Pleurosigma* sp. 1, SEM, a= External valve view showing median raphe and quincunx arrangement of the areolae, b= terminal valve showing change in the areolae orientation, c= External central raphe fissures with one centred and the other deflected to one side; d-f= *Pleurosigma elongatum,* SEM, d= Internal valve view showing raphe in the middle and getting slightly merged at the terminal parts, e= uplifted terminal raphe endings, f= central raphe fissures distinct. Scale bars: a, c= 3 µm; b= 1 µm; d= 10 µm; f, e= 2 µm

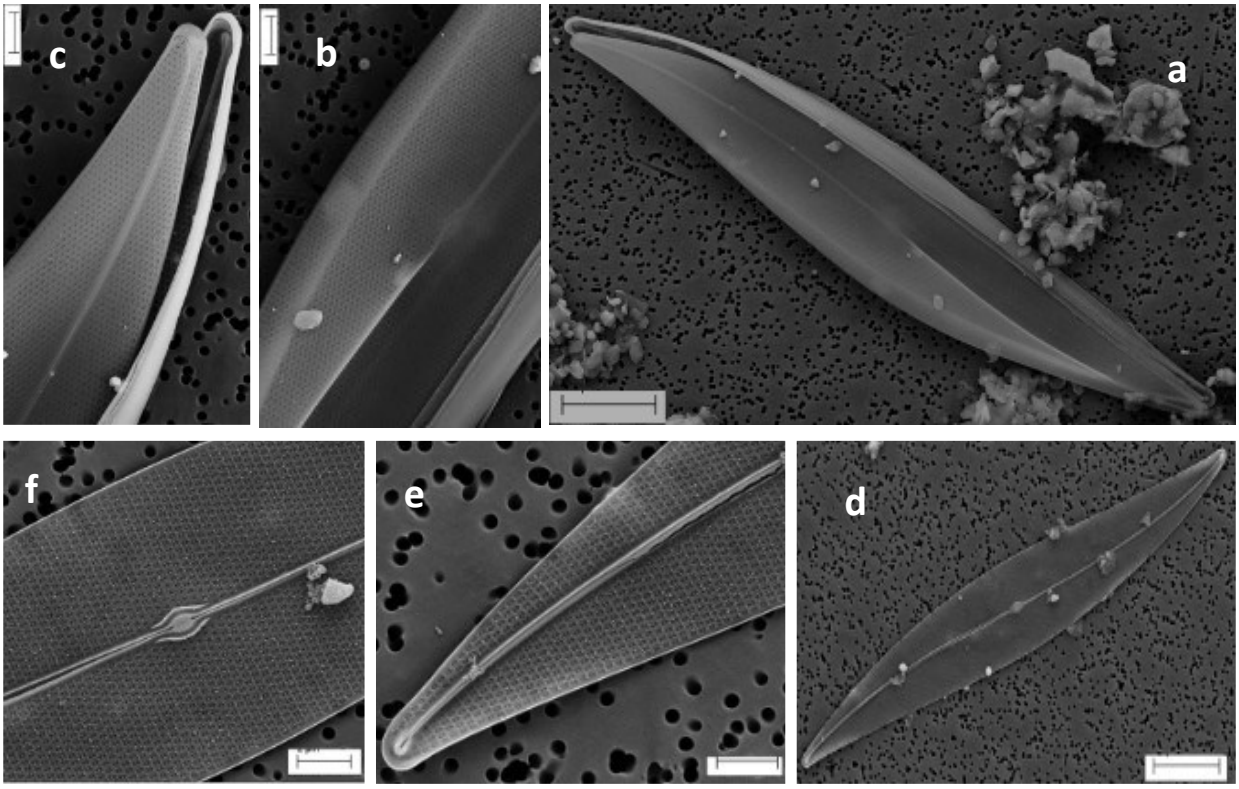

Plate 23: a-f= *Pleurosigma* cf. *latum,* SEM, a= external valve view, b= deflected central raphe endings, c= hooked terminal raphe endings, d= internal valve view, e= terminal fissure of the raphe, f= distinct central raphe endings. Scale bars: a, d =10 µm; c, b, e, f= 2 µm.

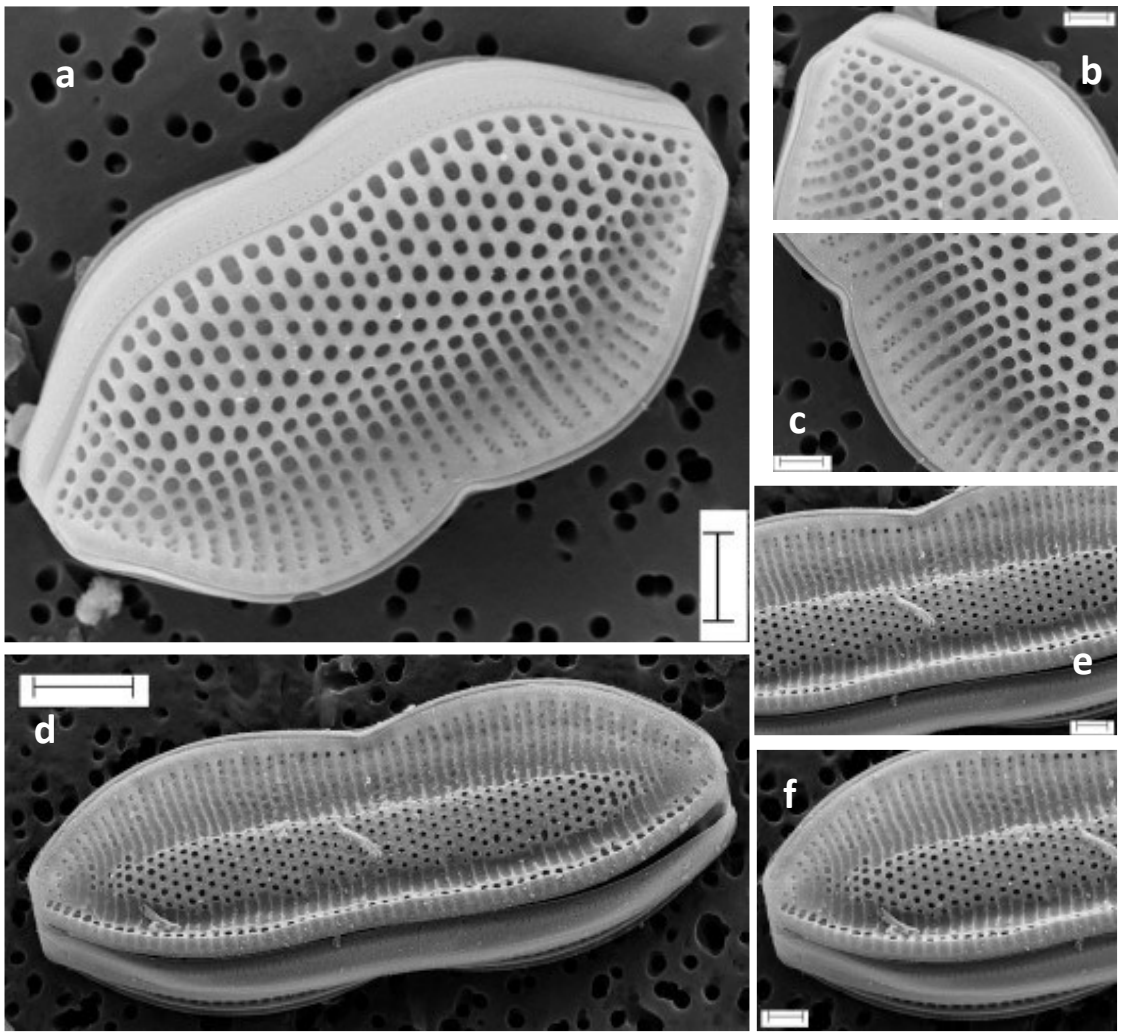

Plate 24: a-c= *Psammodictyon panduriforme* var. *continuum,* SEM, a= external valve view showing round areolae with slight undulation and girdle bands with poroids, b= slightly bended raphe at terminal, c= central nodule is unclear (unvisible); d-f= *Psammodictyon roridum,* SEM, d= external valve face showing high undulation, e= strong eccentric raphe, f= terminal end of raphe straight. Scale bars: a=2 µm; b, c, e, f= 1 µm; d= 3 µm

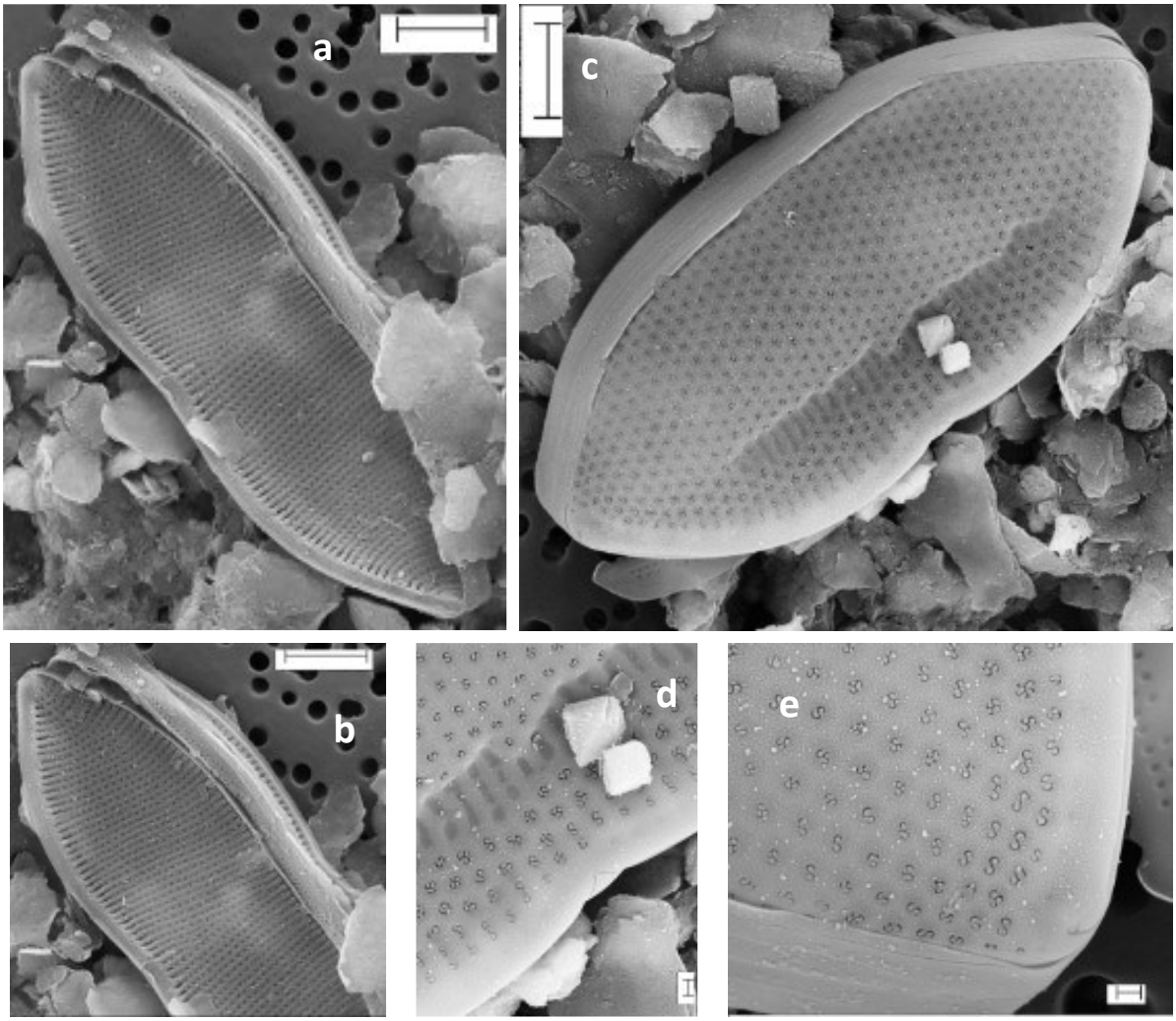

Plate 25: a-b= *Psammodictyon* sp. 1, SEM, a= external valve with slight constriction in the middle and dense transapical striae, b= eccentric raphe and dense round areolae; c-e= *Psammodictyon* sp. 2, SEM, c= external valve with distinct apical fold on the valve face, d= central nodule, e= turned terminal raphe endings. Scale bars: a, b, c= 2 μm; d, e= 200 nm.

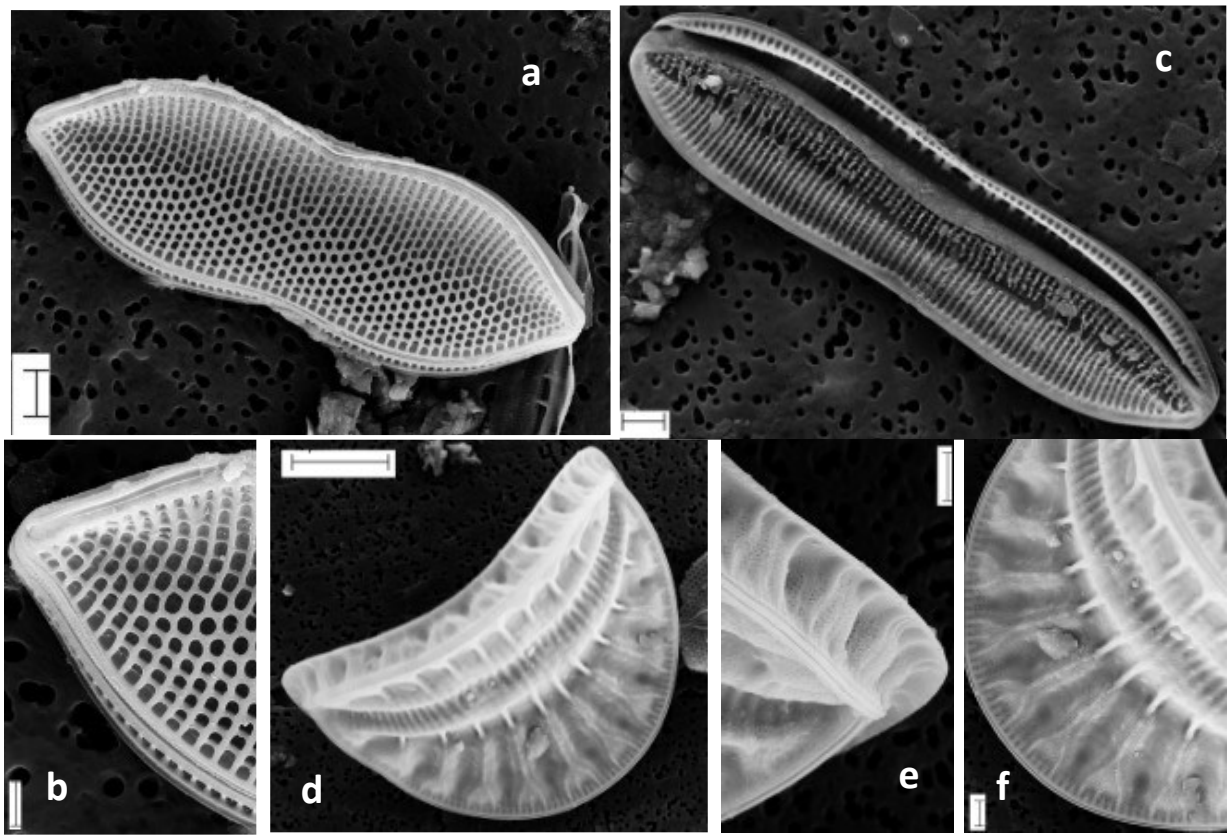

Plate 26: a-b= *Psammodictyon* sp. 3, SEM, a= External valve view with large round areolae, b= eccentric raphe endings, c= *Tryblionella* sp., external valve with fold on the valve face and highly silicified interstriae, d-f= *Campylodiscus* sp.1, SEM, d= saddle shaped valve, e= raphe raised on the keel, f= multiseriate striae interrupted by sterna. Scale bars: a, c, e, f=2 µm; b=1 µm, d=10 µm.

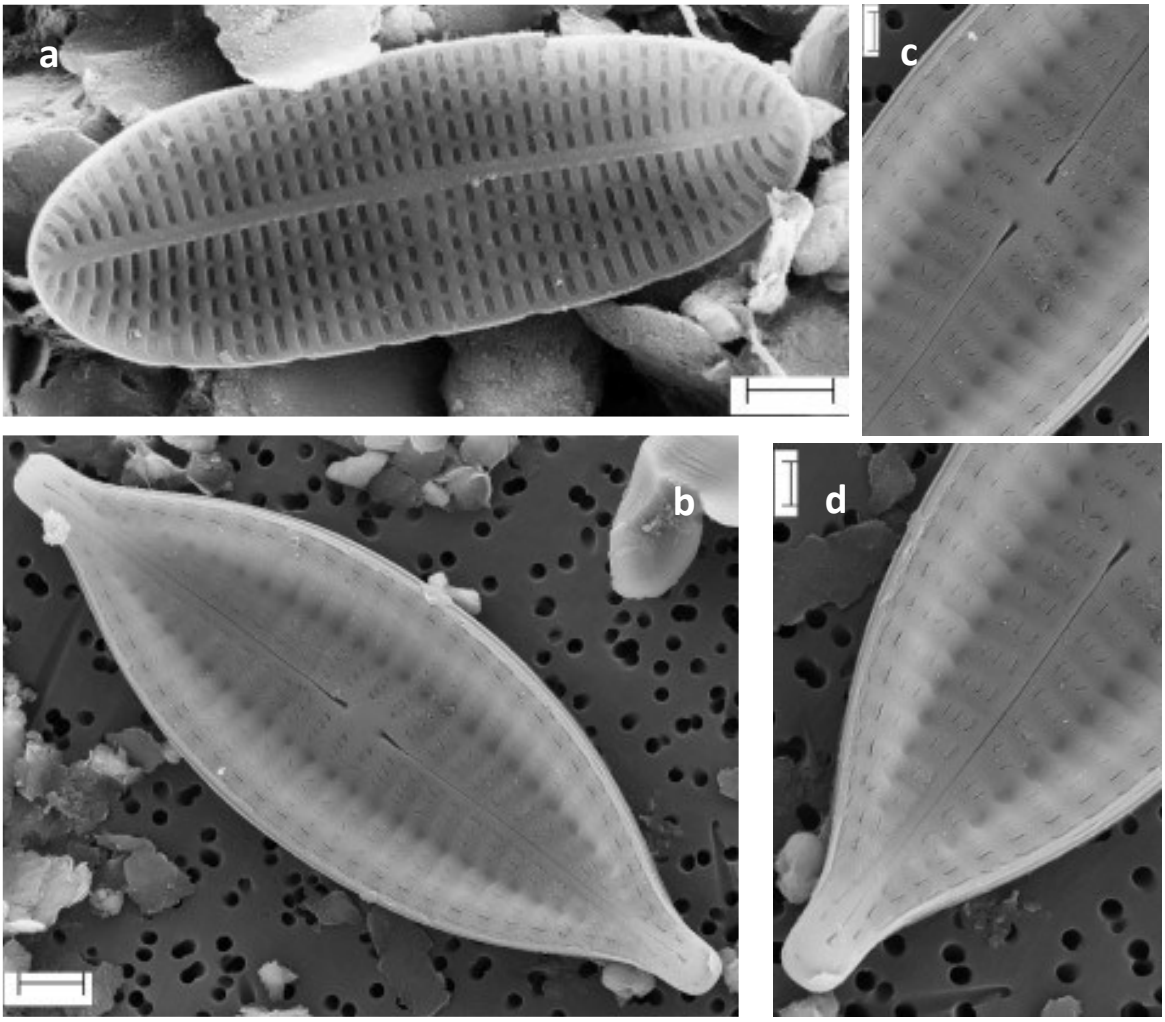

Plate 27: a= *Cocconeis* sp. 2, SEM, Pseudoraphe-valve with rectangular areolae getting divergent at apices, b-d= *Fogedia* sp. SEM, b= valve face showing dash like areolae and depressed area in the centre, c= expanded central raphe endings, d= terminal raphe endings slightly curved. Scale bars: a, c, d=1 µm; b= 2 µm.

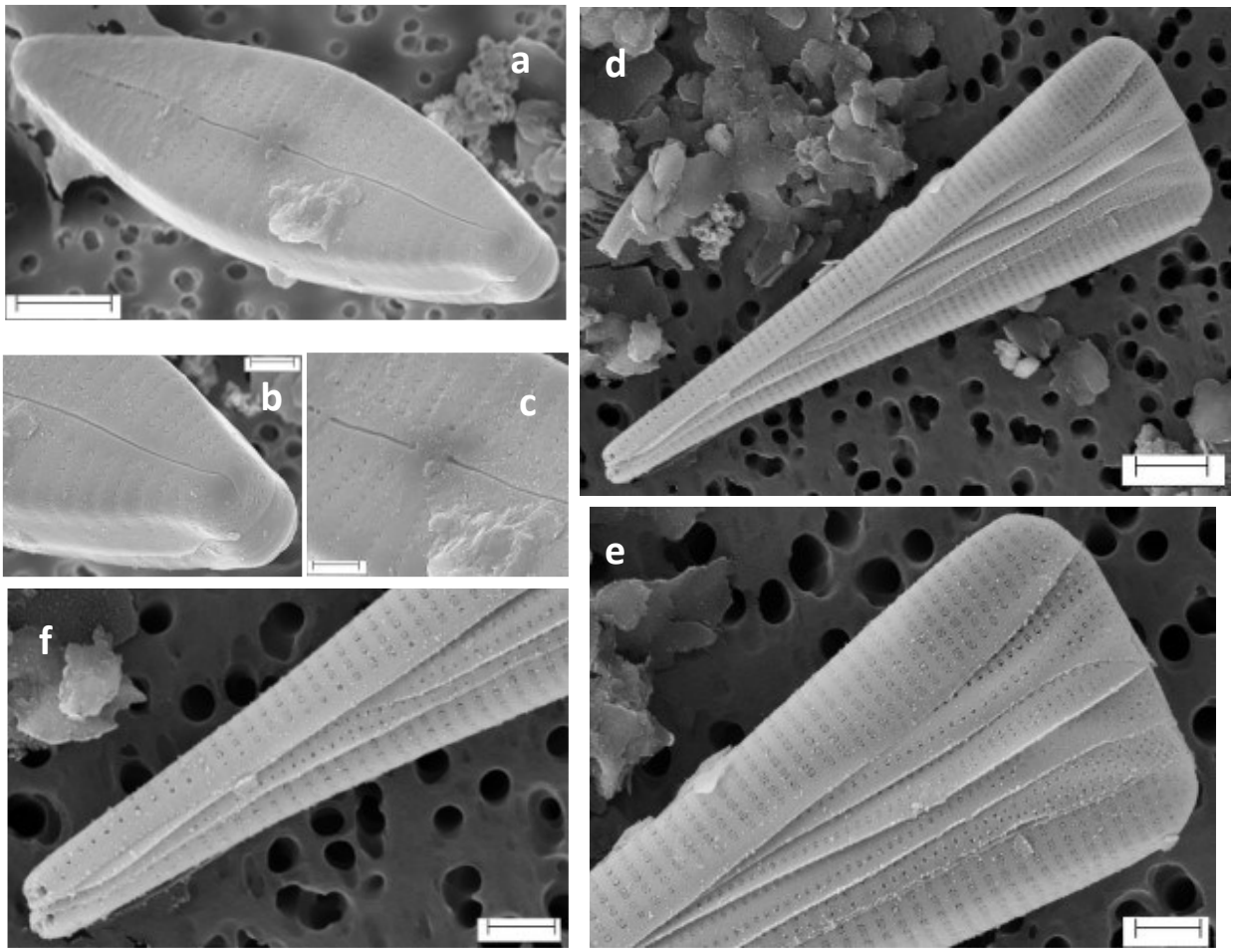

Plate 28: a-c= *Gomphonema* sp. , SEM, a= external valve view, b= terminal end of the valve showing raphe turning on the other side, c= deflected central raphe endings and stigma on one side of the raphe; d-f= *Licmophora* sp. 1, SEM, d= girdle view showing larger head pole getting narrow at foot pole, e= head pole with areolae with silica porous layer and girdle bands with poroids, f= foot pole showing distinct pores. Scale bars: a= 3 µm; b, c, e, f= 1 µm; d=2 µm.

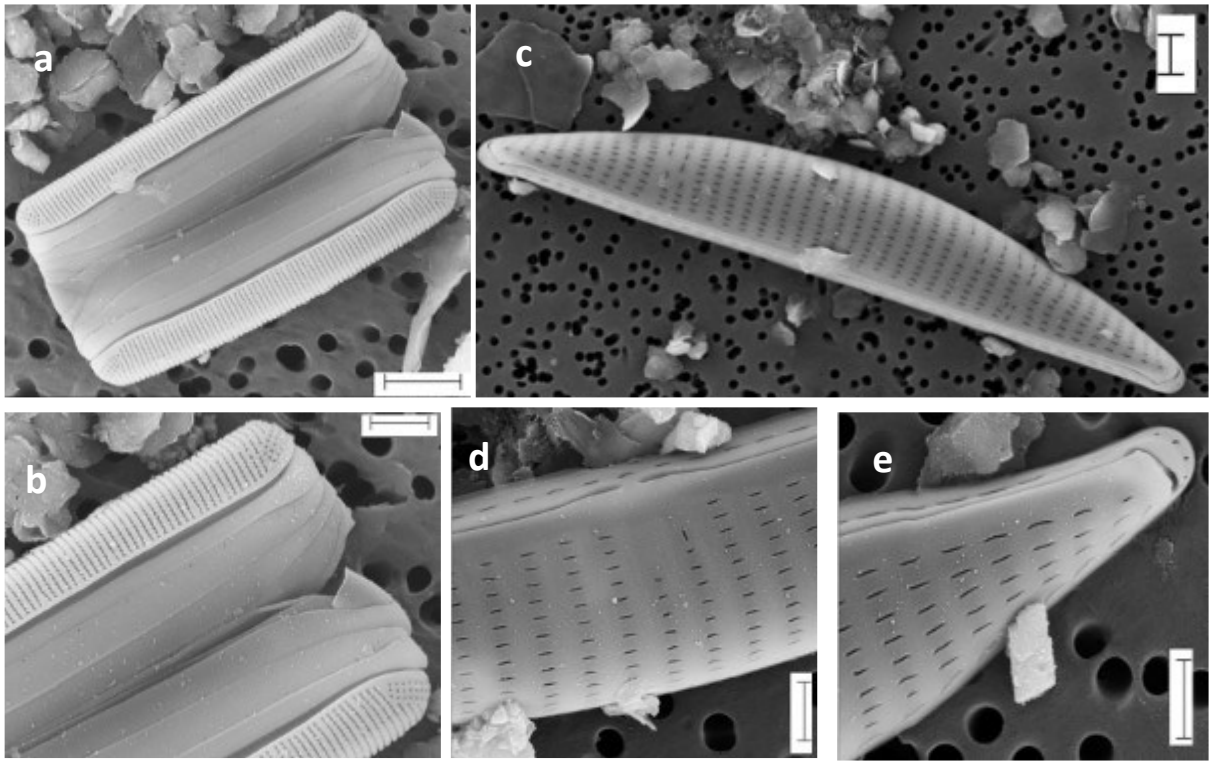

Plate 29: a-b= *Pteroncola* sp., SEM, a= valve in girdle view, b= apical pore field; c-e= *Seminavis* sp., SEM, c= valve view with dash like areolae, d= central endings of the raphe elevated, e= turned terminal raphe endings. Scale bars: a, c=2 µm; b, d, e=1 µm.

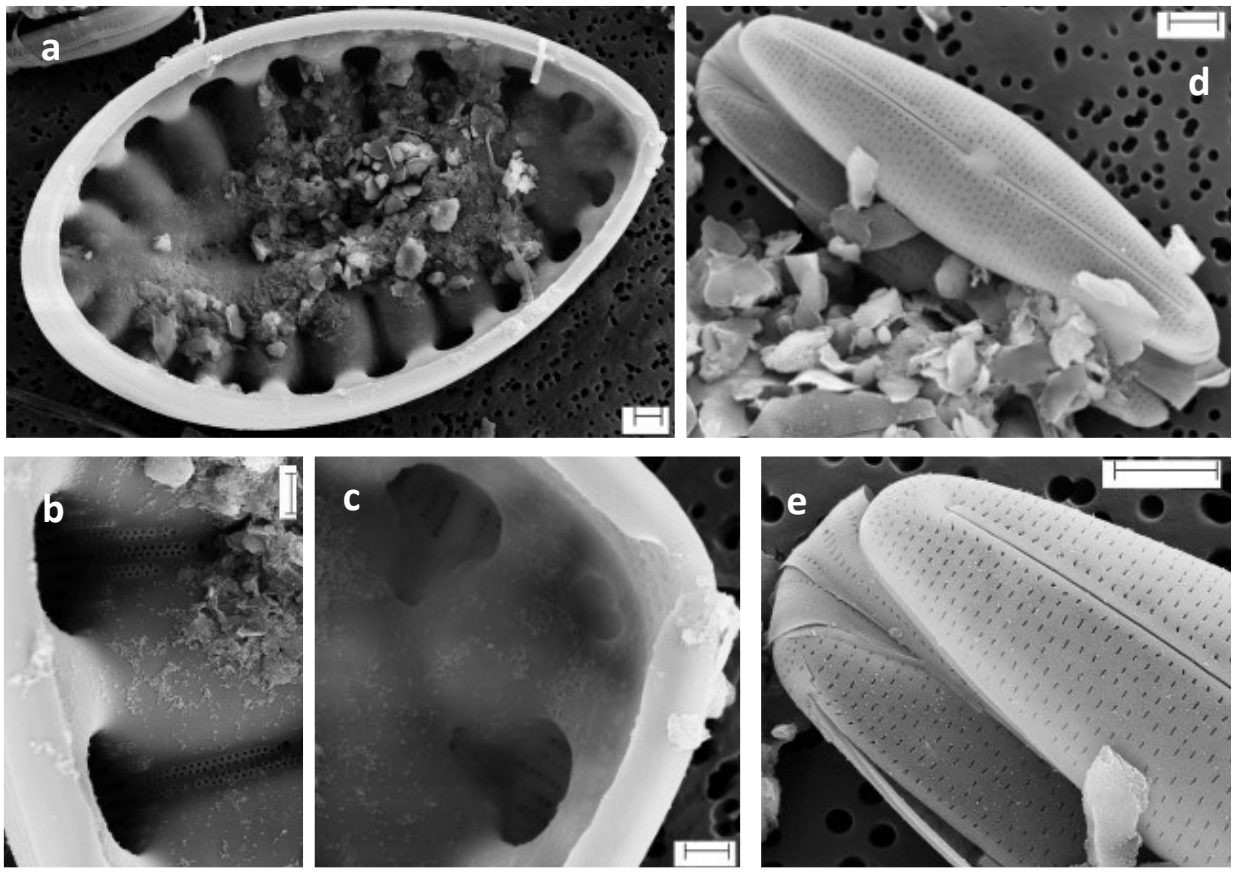

Plate 30: a-c= *Surirella* sp., SEM, a= internal valve view, b= multiseriate striae, c= raphe endings; d-e= Pennate sp. 15, SEM, d= external valve view with raphe in the median and areolae with small dash like areolae and distinct central raphe endings, e= terminal end of the raphe straight and apical pore field, girdle bands with two lines of areolae. Scale bars: a, d, e=2 μm; b, c=1 μm.

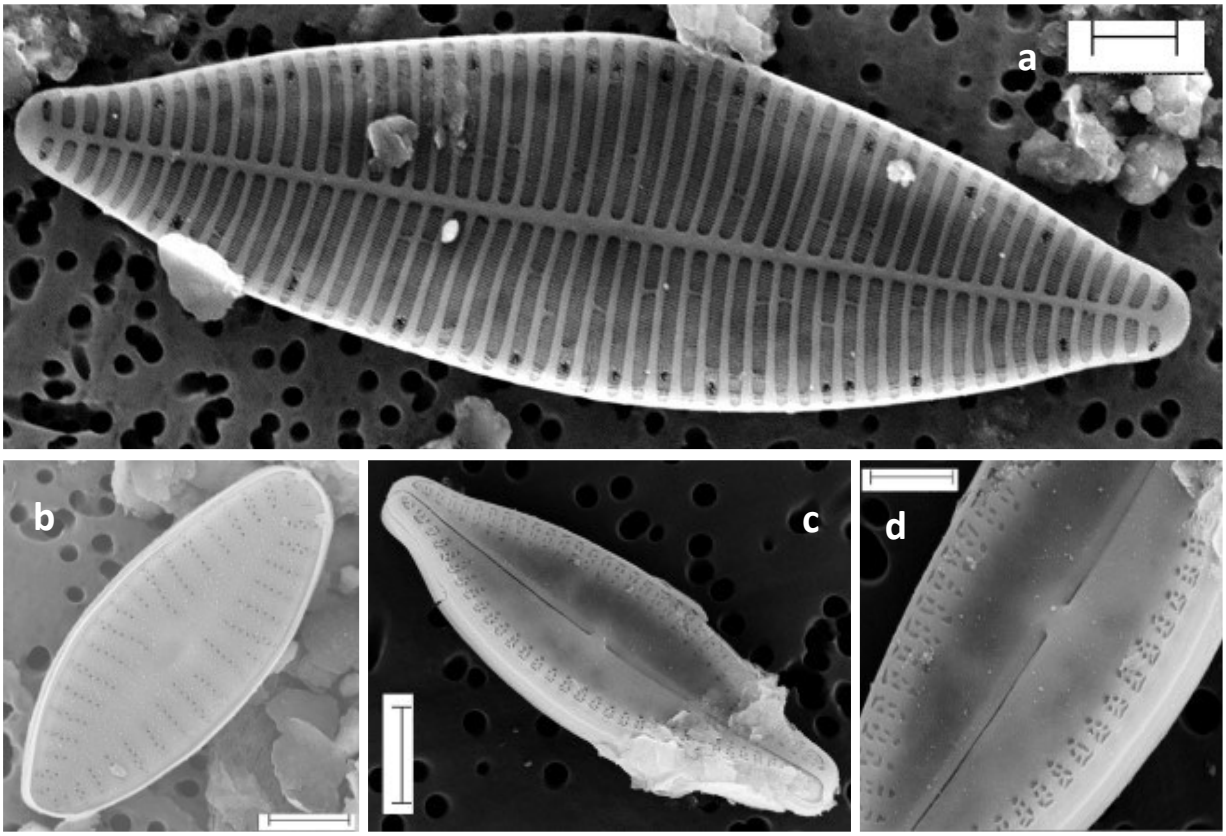

Plate 31: a= Pennate sp. 16, SEM, internal valve view showing narrow sternum and alternating transapical striae; b= Pennate sp. 4, SEM, external valve showing bi and tri- seriate striae and slight depression in the central part; c-d= Pennate sp. 5, SEM, external valve view showing unique pattern of the areolae, terminal of the median raphe is turning to the other side of the valve, d= central endings of the raphe slightly turned on the same side. Scale bars: a, b, c=2 µm; d=1 µm.

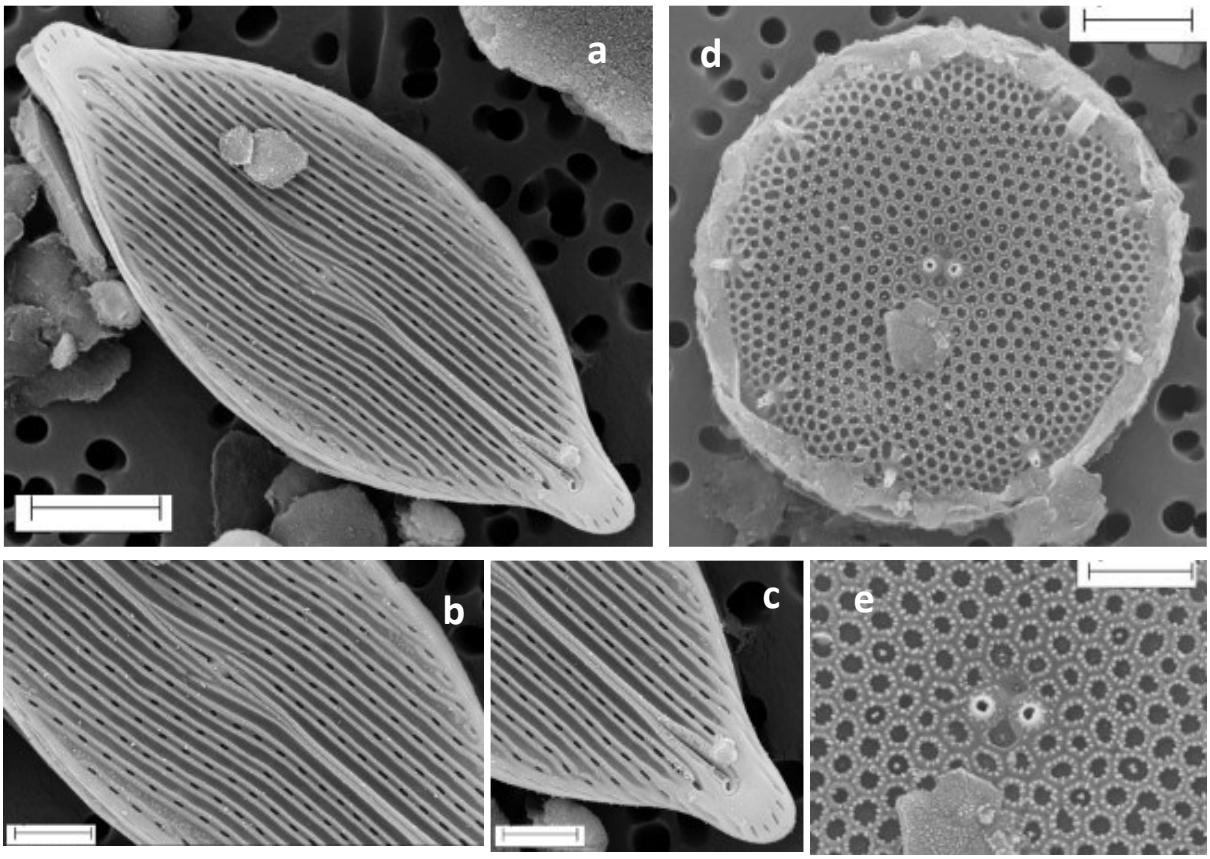

Plate 32: a-c= Pennate sp. 13. SEM, a= external valve view showing unique pattern of parallel striae where interstriae are thickened, b= central part of the valve showing endings of the raphe and round areolae, c= expanded and curved terminal raphe ending with apical pore field. d-e= *Thalassiosira* cf. *minima,* SEM, d= External view showing radiating arrangement of areolae, more less equally distance marginal futoportulae and two central fultoportulae, d= Loculate areolae with external circular foramina. Scale bars: a, d=2 µm; b, c, e=1 µm.

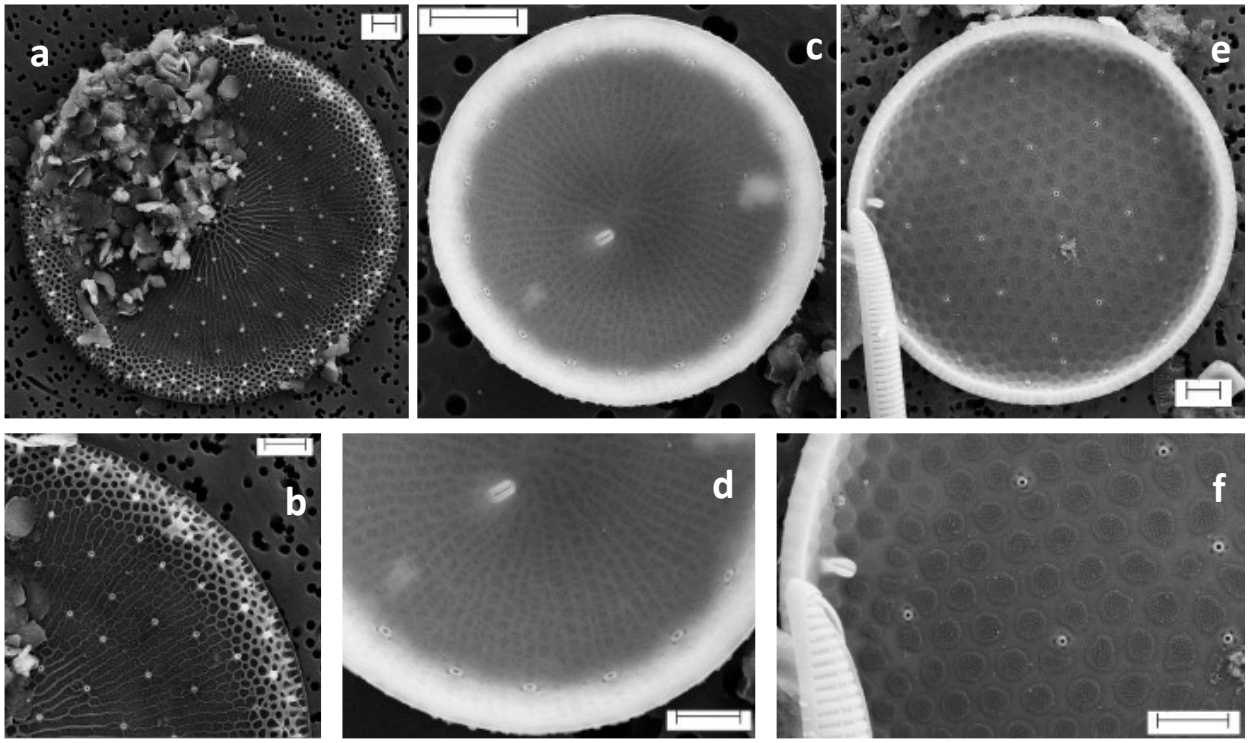

Plate 33: a-b= *Thalassiosira gravida,* SEM, a= External valve view showing radiating arrangement of striae and unique pattern of fultoportulae, b= single rimoportulae position; c-d= *Thalassiosira* sp. 1. SEM, c= Internal valve view equidistantly placed marginal fultoportulae, d= labiate process and auxiliary process of fultoportulae; e-f= *Thalassiosira* sp. 2, e= Internal valve view with scattered fultoportulae and irregular shape of areolae, f= single labiate process at margin and auxiliary process of the fultoportulae. Scale bars: a, c, e, f =2 µm; b, d=1 µm.

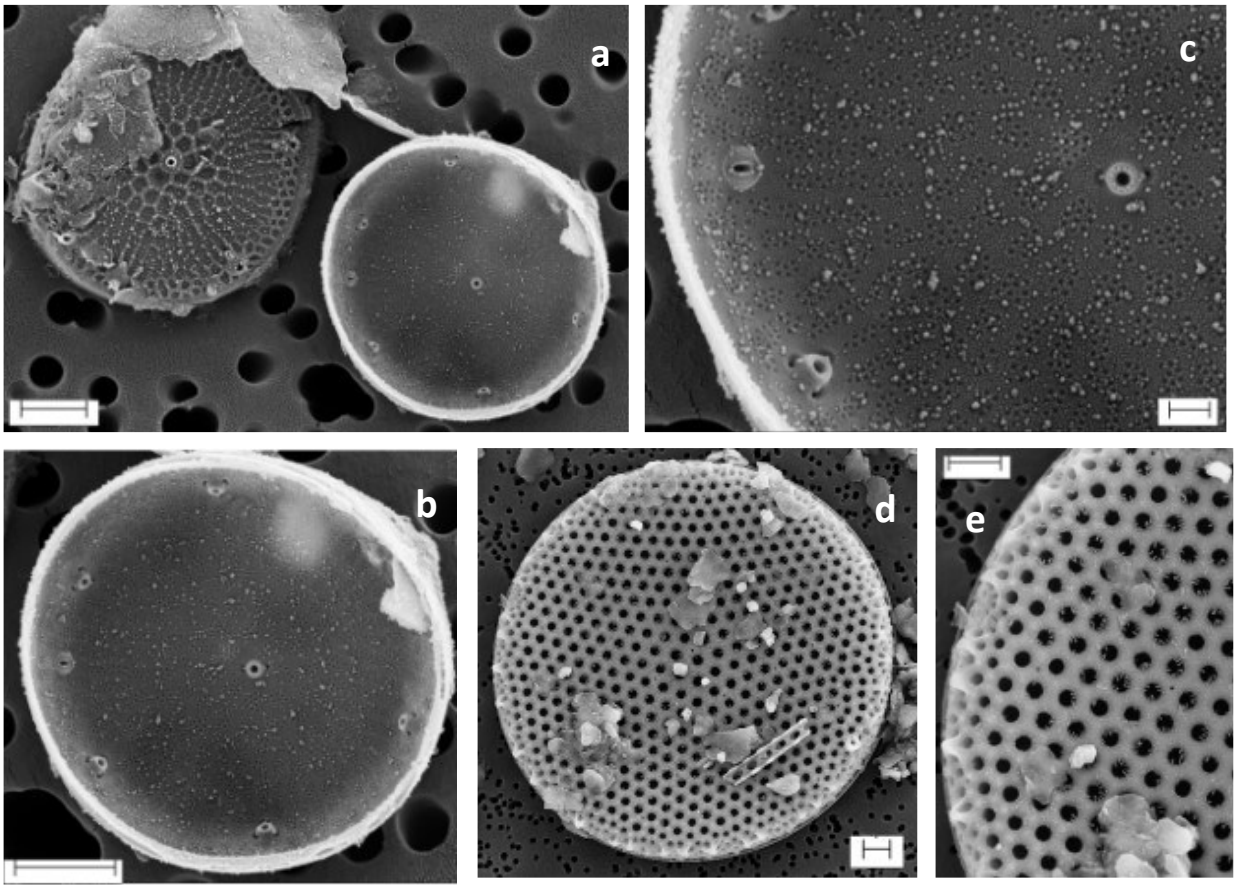

Plate 34: a-c= *Thalassiosira* sp. 3, SEM, a= external and internal valve view, external view showing radially-arranged areolae, irregular, and hexagonal in shape in the centre and towards edge, b= in the internal view six marginal and one central fultoportulae observed, c= each marginal fultoportula with two or three auxiliary pores and central fultoportulae with two auxiliary pores, a single labiate process at the margin; d-e= *Thalassiosiras* sp. 4, SEM, d= external valve view showing round areolae, less in the centre and dense around edge, e= loculate areolae and showing marginal short tubes of fultoportulae. Scale bars: a, b=1 µm; c=200nm; d, e= 2 µm.

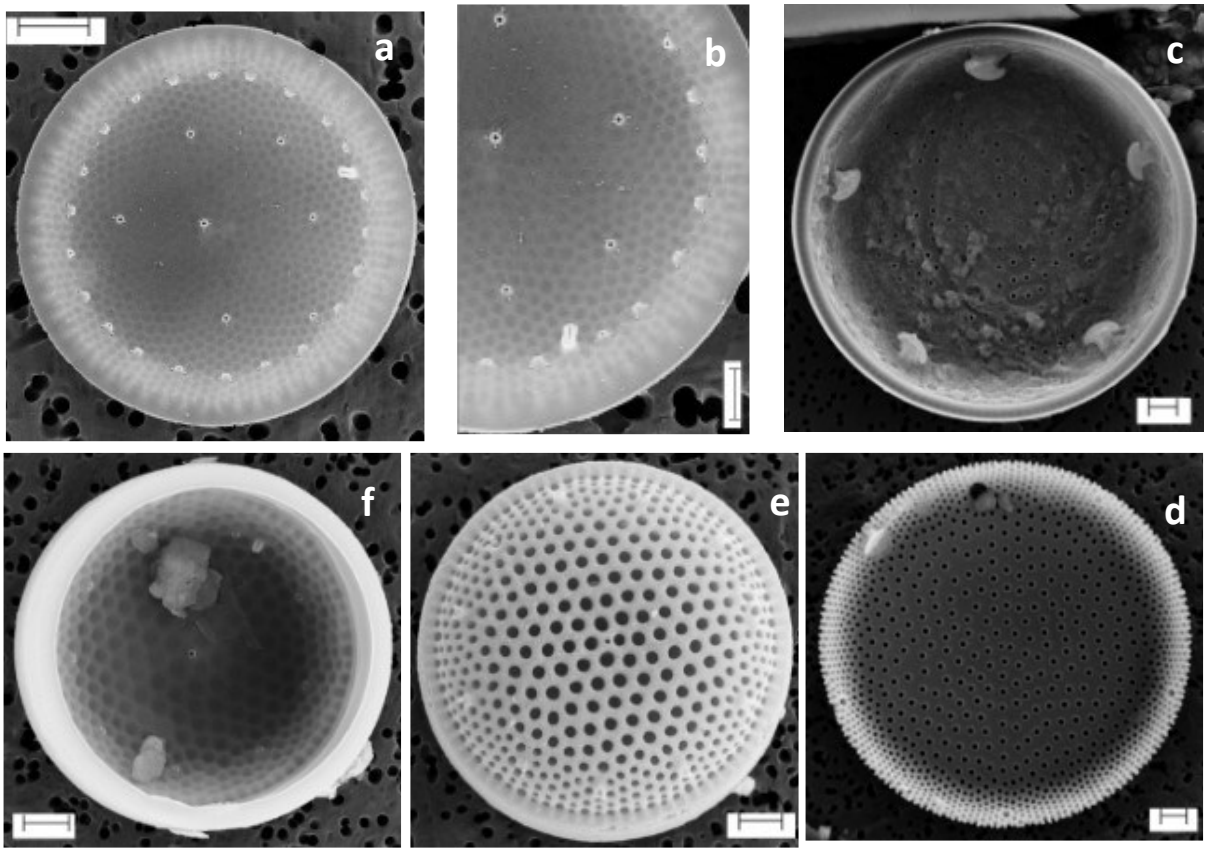

Plate 35: a-b= *Thalassiosira* sp. 5, SEM, a= internal valve view showing equidistantly placed marginal fultoportulae and six fultoportulae scattered in the valve, b= single labiate process and auxiliary pores of fultoportulae; c-d= *Actinocyclus* sp., SEM, c=internal view of the valve showing 5 marginal unique 'pseudonodulus (fan shaped)' and round areolae, d= external valve view with round areolae, less in the centre and dense around margin, pseudonodulus appear like a hole and one is bigger; e-f= Centric sp. 2, SEM, e= external valve view with big round areolae less in the centre and dense around margin, marginal fultoportulae placed equidistantly and one is in the centre. F= Internal valve view with marginal fultoportulae each with four auxiliary pores and a labiate process is present. Scale bars: a, c, d, e, f=2 µm; b=1 µm.

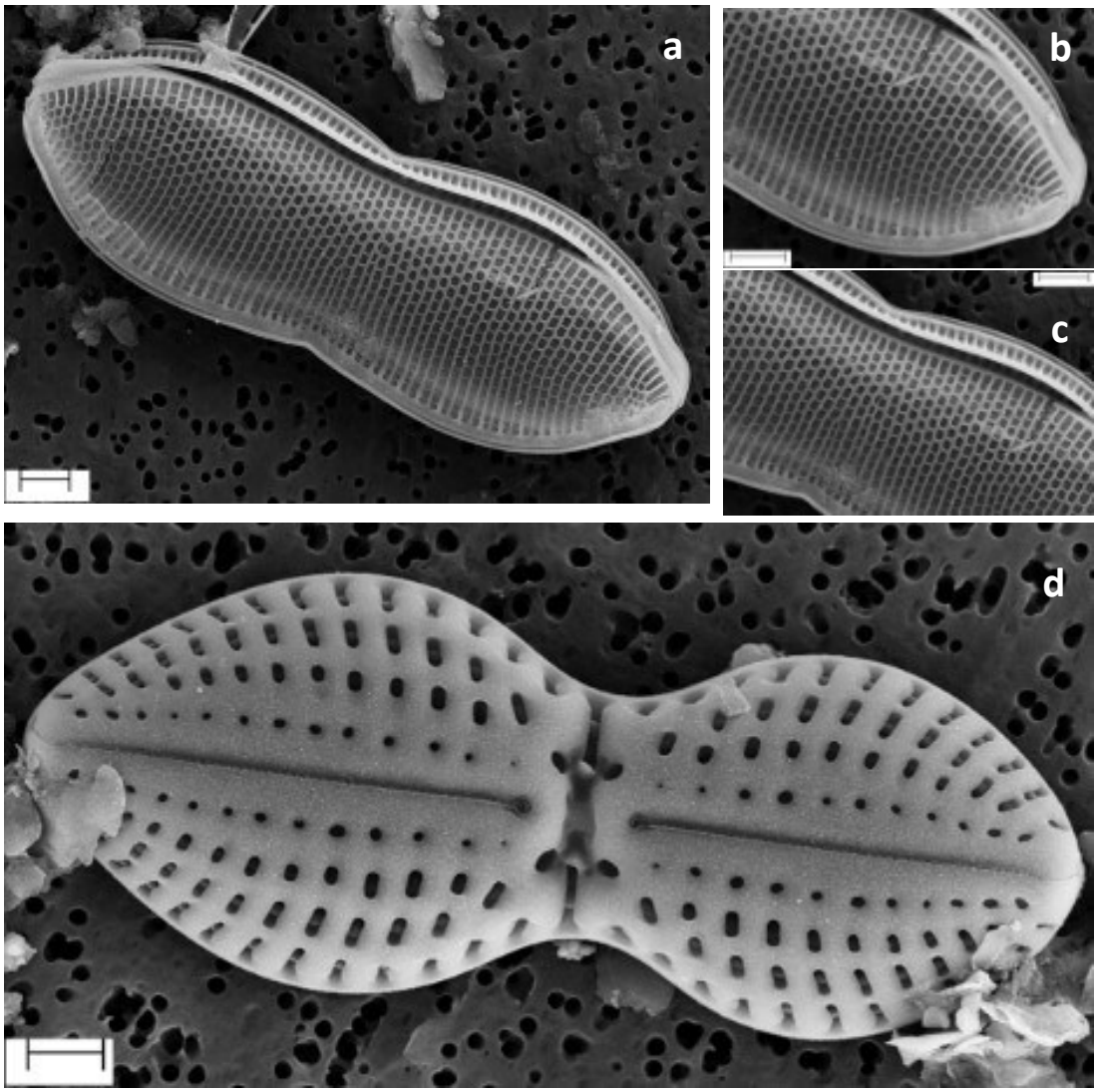

Plate 36: a-c=*Psammodictyon panduriforme,* SEM, a=external valve view with big round areolae, eccentric raphe and fibule, b= turned terminal part of the raphe, c= central part of the raphe is not visible for the better understanding of the central nodule; d=*Diploneis weissflogiopsis,* SEM, external valve view showing median raphe, radiating striae with round areolae and depressed central area constrained by two triangular spines and four pores.

Chapter 5. **General conclusions and future perspectives**

Ecological studies have great benefits if they rely on consistent and correct taxonomy, which can provide accurate diversity and abundance estimates (Kociolek, 2005). Many ecologists have applied a comparative approach to understand the diversity and the spatio/temporal variability of benthic flora between different regions of world. Their published floristics lists provide information on species regional distribution and habitat preference. This study highlighted the seasonality and biodiversity of marine benthic diatoms with focus on their community structure in terms of life forms composition (Chapter 2). In addition, in the current study the comparison between morphological and molecular approaches was applied to identify diatom taxa (Chapter 3). Chapter 4 consists of an exercise that aims to identify diatoms based on their ultrastructure and provide information on taxa that were found in Adriactic sea sample sites (PN and SG).

Chapter 2 provides important results in terms of the quantitative distribution (abundance and biomass), community structure in terms of life forms and taxonomic composition about the marine epipelic diatoms in the subtidal sediments of the Adriatic Sea. The seasonal species composition was also highlighted. Given the ecological importance of MPB, further studies on benthic diatom communities in subtidal areas are required to increase the knowledge about their diversity and variability, and it should be recommended that the study of microphytobenthic communities be inserted in the long-term monitoring programs.

Chapter 3 highlights the importance of the integration of the molecular and morphological approach to identify and characterize diatom species. Moreover, in many cases it confirms the need of a molecular marker more sensitive than the 18S rRNA, as the rbcL, useful for the identification at the species level. This study highlighs the importance of ultrastructural observation to integrate and improve species identification based on molecular information. It also shows the limited data availability of 18S rRNA reference sequences for the pennate benthic diatoms and suggests that more

effort should be taken to construct a reliable reference database containing polyphasic taxonomic data for diatom identification and classification.

Chapter 4 provides the description of the 83 taxa which creates the important literature for the identification of the benthic diatoms. These taxa are observed in the samples collected from the Adriatic Sea sites (PN and SG).

Future Perspectives:

Benthic diatom abundance and diversity show complex patterns, and their diversity is considerably unknown in comparison with planktonic diatoms. Exploration of benthic diatom communities from different environments will help to use them as indicators for long-term environmental changes (climate change, increasing anthropogenic pressures, introduction of invasive alien species). Sequences obtained in this study will contribute to enrich the database of reference sequences for benthic diatoms. Moreover, for both areas (Adriatic and Tyrrhenian Seas) a sound knowledge of plankton communities and environmental context exists (LTER- projects) but knowledge of the microphytobenthos is limited. Despite the ecological importance of benthic diatom community, their identification and classification systems still need to be improved by LTER-projects and more molecular data building.

References

Abarca, N., Jahn, R., Zimmermann, J., & Enke, N. (2014). Does the cosmopolitan diatom *Gomphonema parvulum* (Kützing) Kützing have a biogeography? *PLoS ONE*, *9*(1). https://doi.org/10.1371/journal.pone.0086885.

Accoroni, S., Romagnoli, T., Penna, A., Capellacci, S., Ciminiello, P., Dell'Aversano, C., Tartaglione, L., Abboud–Abi Saab, M., Giussani, V., Asnaghi, V., Chiantore, M., & Totti, C. (2016). *Ostreopsis fattorussoi* sp. nov. (Dinophyceae), a new benthic toxic *Ostreopsis* species from the eastern Mediterranean Sea. *Journal of Phycology*, *52*(6), 1064–1084. https://doi.org/10.1111/jpy.12464.

Admiraal, W., Peletier, H., & Brouwer, T. (1984). The seasonal succession patterns of diatom species on an intertidal mudflat: An experimental analysis. *Oikos, 42*(1), 3040. https://about.jstor.org/terms.

Akcaalan, R., Kaleli, A., & Köker, L. (2022). Distribution of marine benthic diatoms on the coasts of the sea of Marmara and their responses to environmental variables. *Journal of Marine Systems*, *234*, 103780. https://doi.org/10.1016/j.jmarsys.2022.103780.

Aleem, A. A., & Hustedt, F. (1951). Einige neue Diatomeen von der Südküste Englands. *Botaniska Notiser*, *1*, 13–20.

Álvarez-Blanco, I. & B. S. (2014). *Benthic diatoms from Mediterranean coasts. Bibliotheca Diatomologica* (Vol. 60:).

Alverson, A. J., & Theriot, E. C. (2005). Comments on recent progress toward reconstructing the diatom phylogeny. *Journal of Nanoscience and Nanotechnology*, *5*(1), 57–62. https://doi.org/10.1166/jnn.2005.007.

Amato, A., & Montresor, M. (2008). Morphology, phylogeny, and sexual cycle of *Pseudo-nitzschia mannii* sp. nov. (Bacillariophyceae): a pseudo-cryptic species within the *P. pseudodelicatissima* complex. *Phycologia*, *47*(5), 487–497. https://doi.org/10.2216/07-92.1.

Armbrust, E. V. (2009). The life of diatoms in the world's oceans. In *Nature* (Vol. 459, Issue 7244, pp. 185–192). https://doi.org/10.1038/nature08057.

Ashworth, M. P., Nakov, T., & Theriot, E. C. (2013). Revisiting Ross and Sims (1971): Toward a molecular phylogeny of the Biddulphiaceae and Eupodiscaceae (Bacillariophyceae). *Journal of Phycology*, *49*(6), 1207–1222. https://doi.org/10.1111/jpy.12131.

Ashworth, M. P., Ruck, E. C., Lobban, C. S., Romanovicz, D. K., & Theriot, E. C. (2012). A revision of the genus *Cyclophora* and description of *Astrosyne* gen. nov. (Bacillariophyta), two genera with the pyrenoids contained within pseudosepta. *Phycologia*, *51*(6), 684–699. https://doi.org/10.2216/12-004.1.

Aubry, F. B., Cossarini, G., Acri, F., Bastianini, M., Bianchi, F., Camatti, E., de Lazzari, A., Pugnetti, A., Solidoro, C., & Socal, G. (2012). Plankton communities in the northern Adriatic Sea: Patterns and changes over the last 30 years. *Estuarine, Coastal and Shelf Science*, *115*, 125–137. https://doi.org/10.1016/j.ecss.2012.03.011.

Balsamo, M., Albertelli, G., Ceccherelli, V. U., Coccioni, R., Colangelo, M. A., Curini-Galletti, M., Danovaro, R., D'Addabbo, R., de Leonardis, C. D., Fabiano, M., Frontalini, F., Gallo, M., Gambi, C., Guidi, L., Moreno, M., Pusceddu, A., Sandulli, R., Semprucci, F., Todaro, M. A., & Tongiorgi, P. (2010). Meiofauna of the adriatic sea: Present knowledge and future perspectives. *Chemistry and Ecology*, *26*(SUPPL. 1), 45–63. https://doi.org/10.1080/02757541003705492.

Balzano, S., Sarno, D., & Kooistra, W. H. C. F. (2011). Effects of salinity on the growth rate and morphology of ten *Skeletonema* strains. *Journal of Plankton Research*, *33*(6), 937–945. https://doi.org/10.1093/plankt/fbq150.

Barranguet, C., Kromkamp, J., & Peene, J. (1998). Factors controlling primary production and photosynthetic characteristics of intertidal microphytobenthos. *Marine Ecology Progress Series*, *173*, 111–126.

Beltrami, M. E., Blanco, S., Scheidecker, N., Ciutti, F., Cappelletti, C., Mancini, L., Hoffmann, L., & Ector, L. (2010). *Gomphonema vidalii* sp. nov. A new diatom from mediterranean streams. *Diatom Research*, *25*(2), 29–42.

Bennett, A., Bianchi, T. S., & Means, J. C. (2000). The effects of PAH contamination and grazing on the abundance and composition of microphytobenthos in salt marsh sediments (Pass Fourchon, LA, U.S.A.): II: The use of plant pigments as biomarkers. *Estuarine, Coastal and Shelf Science*, *50*(3), 425–439. https://doi.org/10.1006/ecss.1999.0572.

Bérard-Therriault, L., & Cardinal, A. (1986). Les diatomées (Bacillariophyceae) benthiques de substrats durs des eaux marines et saumâtres du Québec. 6. Naviculales: Cymbellaceae et Gomphonemaceae. *Naturaliste Can*, *113*, 405–429.

Bérard-Therriault, L., Poulin, M., & Bossé, L. (1999). Guide d'identification du phytoplancton marin de l'estuaire et du Golfe du Saint-Laurent incluant également certains protozoaires. *Publication Spéciale Canadienne des Sciences Halieutiques et Aquatiques*, *128*, 1–387.

Blackford, J. C. (2002). The influence of microphytobenthos on the Northern Adriatic ecosystem: A modelling study. *Estuarine, Coastal and Shelf Science*, *55*(1), 109–123. https://doi.org/10.1006/ecss.2001.0890.

Blasutto, O., Cibic, T., de Vittor, C., & Umani, S. F. (2005). Microphytobenthic primary production and sedimentary carbohydrates along salinity gradients in the Lagoons of Grado and Marano (Northern Adriatic Sea). *Hydrobiologia*, *550*(1), 47–55. https://doi.org/10.1007/s10750-005-4361-5.

Bruder, K., & Medlin, L. K. (2007). Molecular assessment of phylogenetic relationships in selected species/genera in the naviculoid diatoms (Bacillariophyta). I. The genus *Placoneis*. *Nova Hedwigia*, *85*(3–4), 331–352. https://doi.org/10.1127/0029-5035/2007/0085-0331.

Bruder, K., & Medlin, L. K. (2008a). Morphological and molecular investigations of naviculoid diatoms. II. Selected genera and families. *Diatom Research*, *23*(2), 283–329. https://doi.org/10.1080/0269249X.2008.9705759.

Bruder, K., & Medlin, L. K. (2008b). Morphological and molecular investigations of naviculoid diatoms. III. *Hippodonta* and *Navicula* s.s. *Diatom Research*, *23*(2), 331–347.

Brzezinski, M. A. (1985). The Si:C:N ratio of marine diatoms: Interspecific variability and the effect of some environmental variables. *Journal of Phycology*, *21*, 347–357.

Cahoon, L. (1999). The role of benthic microalgae in neritic ecosystems. The role of benthic microalgae in neritic ecosystems. *Oceanogr. Mar. Biol. Ann. Rev*. 37, 47–86.

Campanelli, A., Grilli, F., Paschini, E., & Marini, M. (2011). The influence of an exceptional Po River flood on the physical and chemical oceanographic properties of the Adriatic Sea. *Dynamics of Atmospheres and Oceans*, *52*(1–2), 284–297. https://doi.org/10.1016/j.dynatmoce.2011.05.004.

Car, A., Hafner, D., Dupčić Radić, I., Kaleli, A., Ljubimir, S., & Solak, C. N. (2021). Comparison of benthic diatom community structures on natural and artificial substrates in marine lake (Adriatic Sea). *Acta Adriatica 62*(1), 21–44.

Car, A., Hafner, D., Ljubimir, S., Radić, I. D., Bobanović-Ćolić, S., & Jasprica, N. (2020). Colonization of bacteria and diatoms on an artificial substrate in a marine lake (eastern Adriatic Sea, NE Mediterranean). *Acta Botanica Croatica*, *79*(2), 212–227. https://doi.org/10.37427/botcro-2020-028.

Car, A., Witkowski, A., Dobosz, S., Burfeind, D. D., Meinesz, A., Jasprica, N., Ruppel, M., Kurzydłowski, K. J., & Płociński, T. (2012). Description of a new marine diatom, *Cocconeis caulerpacola* sp. nov. (Bacillariophyceae), epiphytic on invasive *Caulerpa* species. *European Journal of Phycology*, *47*(4), 433–448. https://doi.org/10.1080/09670262.2012.735255.

Cerino, F., Orsini, L., Sarno, D., Dell'Aversano, C., Tartaglione, L., & Zingone, A. (2005). The alternation of different morphotypes in the seasonal cycle of the toxic diatom *Pseudo-nitzschia galaxiae*. *Harmful Algae*, *4*(1), 33–48. https://doi.org/10.1016/j.hal.2003.10.005.

Cibic, T., Facca, C., (2010). Microphytobenthos. In: Relini, G. (Ed.), Checklist della flora e della fauna dei mari italiani. Parte II. *Biologia Marina Mediterranea, 17* (suppl. 1), 754-800.

Cibic, T., Blasutto, O., Falconi, C., & Fonda Umani, S. (2007). Microphytobenthic biomass, species composition and nutrient availability in sublittoral sediments of the Gulf of Trieste (northern Adriatic Sea). *Estuarine, Coastal and Shelf Science*, *75*(1–2), 50–62. https://doi.org/10.1016/j.ecss.2007.01.020.

Cibic, T., Comici, C., Bussani, A., & del Negro, P. (2012). Benthic diatom response to changing environmental conditions. *Estuarine, Coastal and Shelf Science*, *115*, 158–169. https://doi.org/10.1016/j.ecss.2012.03.033.

Cleve, P. T. (1894). Synopsis of the naviculoid diatoms. *Part I. Kongliga Svenska Vetenskapsakademiens Handlingar Series*, *26*(2), 1–194.

Cleve, P. T. (1895). Synopsis of the naviculoid diatoms. Part II. *Kongliga Svenska Vetenskapsak Akademiens Handlingar*, *27*(3), 1–219.

Cleve, P. T. (1896). Diatoms from Baffin Bay and Davis Strait. *Bihang till Kungliga Svenska Vetenskapsakademiens Handlingar*, *22*(Afd. III), 1–22.

Cleve, P. T., & Grunow, A. (1880). Beiträge zur Kenntniss der arctischen Diatomeen. *Kongliga Svenska Vetenskaps-Akademiens Handlingar*, *17*(2), 1–121.

Cochero, J., Licursi, M., & Gómez, N. (2015). Changes in the epipelic diatom assemblage in nutrient rich streams due to the variations of simultaneous stressors. *Limnologica*, *51*, 15–23. https://doi.org/10.1016/j.limno.2014.10.004.

Çolak Sabanci, F., (2011). Relationship of epilithic diatom communities to environmental variables in Homa lagoon (Izmir, Turkey). *Aquatic Biology, 13,* 233-241.

Cox, E. J. (2011). Morphology, cell wall, cytology, ultrastructure, and morphogenetic studies. Overview and specific observations. In: The Diatom World (J. Seckbach and J.P. Kociolek, Eds.). *Cellular Origin, Life in Extreme Habitats and Astrobiology, Springer, Dordrecht.*, *19*, 21–45.

Cox, E. J. (2012). Ontogeny, homology, and terminology-wall morphogenesis as an aid to character recognition and character state definition for pennate diatom systematics. In *Journal of Phycology* (Vol. 48, Issue 1, pp. 1–31). https://doi.org/10.1111/j.1529-8817.2011.01081.x.

Cox, E. J. (2014). Diatom identification in the face of changing species concepts and evidence of phenotypic plasticity. *Journal of Micropalaeontology*, *33*(2), 111–120. https://doi.org/10.1144/jmpaleo2014-014.

Cox, E. J., & Ross, R. (1981). The striae of pennate diatoms. *In: R. Ross, Ed., Proceedings of the Sixth Symposium on Fossil and Recent Diatoms. O. Koeltz, Koenigstein,* 267–278.

Cozzi, S., & Giani, M. (2011). River water and nutrient discharges in the Northern Adriatic Sea: Current importance and long term changes. *Continental Shelf Research*, *31*(18), 1881–1893. https://doi.org/10.1016/j.csr.2011.08.010.

de Jonge, V. N. (1979). Quantitative separation of benthic diatoms from sediments using density gradient centrifugation in the colloidal silica Ludox-TM. *Marine Biology*, *51*(3), 267–278. https://doi.org/10.1007/BF00386807.

de Stefano, M., Marino, D., & Mazzella, L. (2000). Marine taxa of *Cocconeis* on leaves of *Posidonia oceanica*, including a new species and two new varieties. *European Journal of Phycology*, *35*(3), 225–242. https://doi.org/10.1080/09670260010001735831.

DeNicola, D. M., & McIntire, C. D. (1990). Effects of substrate relief on the distribution of periphyton in laboratory streams, I. Hydrology. *Journal of Phycology*, *26*(4), 624–633. https://doi.org/10.1111/j.0022-3646.1990.00624.x.

Dirican, S., Kaleli, A., Yilmaz, E., Özer, A., & Dayioglu, H. (2022). New records of diatoms (Bacillariales, Rhopalodiales & Surirellales) with ultrastructure details from the Black Sea coast of Turkey. *Aquatic Sciences and Engineering*, *37*(1), 19–28.

D'Ortenzio, F., & Ribera D'Alcalà, M. (2009). On the trophic regimes of the Mediterranean Sea: a satellite analysis. *Biogeosciences, 6*, 139–148. https://doi.org/10.5194/bg-6-139-2009, 2009.

Dufrêne, M., & Legendre, P. (1997). Species assemblages and indicator species: the need for a flexible asymmetrical approach. *Ecological Monographs*, *67*(3), 345–366 https://doi.org/10.1890/0012-9615(1997)067[0345:SAAIST]2.0.CO;2

Evans, K. M., Wortley, A. H., & Mann, D. G. (2007). An assessment of potential diatom "barcode" genes (cox1, rbcl, 18s and its rDNA) and their effectiveness in determining relationships in *Sellaphora* (Bacillariophyta). *Protist*, *158*(3), 349–364. https://doi.org/10.1016/j.protis.2007.04.001.

Evans, K. M., Wortley, A. H., Simpson, G. E., Chepurnov, V. A., & Mann, D. G. (2008). A molecular systematic approach to explore diversity within the *Sellaphora pupula* species complex

(Bacillariophyta). *Journal of Phycology*, *44*(1), 215–231. https://doi.org/10.1111/j.1529-8817.2007.00454.x.

Evrard, V., Huettel, M., Cook, P. L. M., Soetaert, K., Heip, C. H. R., & Middelburg, J. J. (2012). Importance of phytodetritus and microphyto benthos for heterotrophs in a shallow subtidal sandy sediment. *Marine Ecology Progress Series*, *455*, 13–31. https://doi.org/10.3354/meps09676.

Facca, C., & Sfriso, A. (2007). Epipelic diatom spatial and temporal distribution and relationship with the main environmental parameters in coastal waters. *Estuarine, Coastal and Shelf Science*, *75*(1–2), 35–49. https://doi.org/10.1016/j.ecss.2007.03.033.

Facca, C., Sfriso, A., & Socal, G. (2002). Temporal and spatial distribution of diatoms in the surface sediments of the Venice Lagoon. *Botanica Marina*, *45*(2), 170–183. https://doi.org/10.1515/BOT.2002.016.

Franzo, A., Cibic, T., del Negro, P., & de Vittor, C. (2015). Spatial distribution of microphytobenthos, meiofauna and macrofauna in the north-western Adriatic sea: A synoptic study. *Advances in Oceanography and Limnology*, *6*(1–2), 58–75. https://doi.org/10.4081/aiol.2015.5470.

Gaarder, K. R. (1951). Bacillariophyceae from the Michael Sars North Atlantic deep-Sea expedition 1910. Report on the Scientific Results of the "Michael Sars. *North Atlantic Deep-Sea Expedition*, *2*(2), 1–36.

Gaonkar, C. C., Kooistra, W. H. C. F., Lange, C. B., Montresor, M., & Sarno, D. (2017). Two new species in the *Chaetoceros socialis* complex (Bacillariophyta): *C. sporotruncatus* and *C. dichatoensis*, and characterization of its relatives, *C. radicans* and *C. cinctus*. *Journal of Phycology*, *53*(4), 889–907. https://doi.org/10.1111/jpy.12554.

Giffen, M. H. (1973). Diatoms of the marine littoral of Steenberg's Cove in St. Helena Bay, Cape Province, South Africa. *Botanica Marina*, *16*(1), 32–48.

Gregory, W. (1857a). *New forms of Marine Diatomaceae*.

Gregory, W. (1857b). On new forms of marine Diatomaceae found in the Firth of Clyde and in Loch Fyne, illustrated by numerous figures drawn by R.K. *Transactions of the Royal Society of Edinburgh*, *21*, 9–14, 473–542.

Greville, R. K. (1827). Scottish Cryptogamic Flora. *MacLachlan and Stewart, Edinburgh.*, *V*.

Griffith, D. M., Veech, J. A., & Marsh, C. J. (2016). Cooccur: Probabilistic species co-occurrence analysis in R. *Journal of Statistical Software*, *69*(1). https://doi.org/10.18637/jss.v069.c02.

Grilli, F., Accoroni, S., Acri, F., Bernardi Aubry, F., Bergami, C., Cabrini, M., Campanelli, A., Giani, M., Guicciardi, S., Marini, M., Neri, F., Penna, A., Penna, P., Pugnetti, A., Ravaioli, M., Riminucci, F., Ricci, F., Totti, C., Viaroli, P., & Cozzi, S. (2020). Seasonal and interannual trends of oceanographic parameters over 40 years in the Northern Adriatic Sea in relation to nutrient loadings using the EMOD net chemistry data portal. *Water*, *12*(8), 2280. https://doi.org/10.3390/w12082280.

Guillard, R. R. L. (1975). Culture of phytoplankton for feeding marine invertebrates. *In Smith W.L. and Chanley M.H (Eds.) Culture of Marine Invertebrate Animals. Plenum Press, New York, USA.*, 26-60.

Guillard, R. R. L., & Ryther, J. H. (1962). Studies of marine planktonic diatoms. I. *Cyclotella nana* Hustedt and *Detonula confervacea* Cleve. *Can. J. Microbiol.*, *8*, 229–239.

Guiry, M. D., & Guiry, G. M. (2023). *https://www.algaebase.org/*. AlgaeBase. World-Wide Electronic Publication, National University of Ireland, Galway.

Hafner, D., Car, A., Jasprica, N., Kapetanović, T., & Radić, I. D. (2018). Relationship between marine epilithic diatoms and environmental variables in oligotrophic bay, NE Mediterranean. *Mediterranean Marine Science*, *19*(2), 223–239. https://doi.org/10.12681/mms.14151.

Hall, T. A. (1999). BioEdit: a user-friendly biological sequence alignment editor and analysis program for Windows 95/98/ NT. *Nucleic Acid. S.*, *41:*(95–8.).

Hamsher, S. E., & Saunders, G. W. (2014). A floristic survey of marine tube-forming diatoms reveals unexpected diversity and extensive co-habitation among genetic lines of the *Berkeleya rutilans* complex (Bacillariophyceae). *European Journal of Phycology*, *49*(1), 47–59. https://doi.org/10.1080/09670262.2014.885582.

Hasle, G. R. (1980). Examination of *Thalassiosira* type material: *T. minima* and *T. delicatula* (Bacillariophyceae). *Norwegian Journal of Botany*, *27*, 167–173.

Hebert, P. D. N., Cywinska, A., Ball, S. L., & DeWaard, J. R. (2003). Biological identifications through DNA barcodes. *Proceedings of the Royal Society B: Biological Sciences*, *270*(1512), 313–321. https://doi.org/10.1098/rspb.2002.2218.

Hendey, N. I. (1964). An introductory account of the smaller algae of British coastal waters. Part V. Bacillariophyceae (Diatoms). *Ministry of Agriculture, Fisheries and Food, Fisheries Investigations, Series IV, London,* 317.

Hewson, I. (2001). A low-latitude bloom of the surf-zone diatom, *Anaulus australis* (Centrales, Bacillariophyta) on the coast of Southern Queensland (Australia). *Journal of Plankton Research*, *23*(11), 1233–1236. https://doi.org/10.1093/plankt/23.11.1233.

Hillebrand, H., & Sommer, U. (1997). Response of epilithic microphytobenthos of the Western Baltic Sea to in situ experiments with nutrient enrichment. *Marine Ecology Progress Series,* 160, 3546.

Hillebrand, H., & Sommer, U. (1999). The nutrient stoichiometry of benthic microalgal growth: Redfield proportions are optimal. *Limnology and Oceanography*, *44*(2), 440–446. https://doi.org/10.4319/lo.1999.44.2.0440

Hoek, C. van den, Mann, D. G., & Jahns, H. M. (1995). *Algae: An introduction to phycology*. Cambridge University Press, UK.

Hofmann, G., Werum, M., & Lange-Bertalot, H. (2013). Diatomeen im Süßwasser—Benthos von Mitteleuropa. Bestimmungsflora Kieselalgen für die ökologische Praxis. In *Über 700 der häufigsten Arten und ihre Ökologie*. Koeltz Scientific Books. (Vol. 133, pp. 1–908).

Hooker, W. J. (1833). *In, The English Flora, Class XXIV Cryptogamia. Longman, London*. 401–415.

Hudon, C., & Legendre, P. (1987). The ecological implications of growth forms in epibenthic diatoms. *Journal of Phycology*, *23*(3), 434–441. https://doi.org/10.1111/j.1529-8817.1987.tb02529.x.

Hustedt, F. (1930a). Bacillariophyta. *Süsswasserflora von Mitteleuropa*, *10*.

Hustedt, F. (1930b). Bacillariophyta (Diatomeae) Zweite Auflage. *Die Süsswasser-Flora Mitteleuropas*, *10*, 1 –466.

Jahn, R. (2007). Diatoms and DNA barcoding: a pilot study on an environmental sample. 63–68. https://doi.org/10.3372/cediatom.113.

Jahn, R., & Lange-Bertalot, H. (Horst). (2001). *Lange-Bertalot festschrift: studies on diatoms dedicated to Prof. Dr. Dr. h.c. Horst Lange-Bertalot on the occasion of his 65th birthday*. A.R.G. Gantner Verlag.

Janisch, C., R. L. (1863). Ueber Meeres-Diatomaceen von Honduras. *In Beitriige Zur Nliheren Kenntniss Und Verbreitung Der Algen (Rabenhorst, L. Editor), Eduard Kummer, Leipzig.*, *1:*1-16.

Kaczmarska, I., Ehrman, J. M., & Ashworth, M. P. (2022). Sexual reproduction and auxospore development in the diatom *Biddulphia biddulphiana*. *PLoS ONE*, *17*. https://doi.org/10.1371/journal.pone.0272778.

Kaleli, A. (2022). Contributions to the diatom flora of the Aegean Sea and the Mediterranean Sea from the Turkish coasts with remarks on rare taxa. *Mediterranean Marine Science*, *23*(4), 952–967.

Kaleli, M. A., Kociolek, J. P., & Solak, C. N. (2020). Taxonomy and distribution of diatoms on the Turkish Mediterranean Coast, Dalyan (Muğla). *Mediterranean Marine Science*, *21*(1), 201. https://doi.org/10.12681/mms.17293.

Karayeva, N. I. (1978). New genus of the family Naviculaceae West. *Botanicheskii Zhurnal*, *63*(11), 1593–1596.

Karsten, G. (1928). Abteilung Bacillariophyta (Diatomeae). *In: Die Natürlichen Pflanzenfamilien Nebst Ihren Gattungen Und Wichtgeren Arten Inbesodere Den Nutzpflanzen Unter Mirwirkung Zahlreichter Hervorrangender Fachgelehrten Begründet Vom A. Engler Und K. Prantl. Zweite Stark*, *(Engler, A. Eds)* Leipzig: Verlag von Wilhelm Engleman., 105–303.

Kermarrec, L., Ector, L., Bouchez, A., Rimet, F., & Hoffmann, L. (2011). A preliminary phylogenetic analysis of the Cymbellales based on 18S rDNA gene sequencing. *Diatom Research*, *26*(3), 305–315. https://doi.org/10.1080/0269249X.2011.633255

Kermarrec, L., Bouchez, A., Rimet, F., & Humbert, J. F. (2013). First evidence of the existence of semi-cryptic species and of a phylogeographic structure in the *Gomphonema parvulum* (Kützing) Kützing complex (Bacillariophyta). *Protist*, *164*(5), 686–705. https://doi.org/10.1016/j.protis.2013.07.005.

Kimura M. (1980). A simple method for estimating evolutionary rate of base substitutions through comparative studies of nucleotide sequences. *Journal of Molecular Evolution*, *16*, 111-120.

Kollár, J., Pinseel, E., Vanormelingen, P., Poulíčková, A., Souffreau, C., Dvořák, P., & Vyverman, W. (2019). A polyphasic approach to the delimitation of diatom species: a case study for the genus *Pinnularia* (Bacillariophyta). *Journal of Phycology*, *55*(2), 365–379. https://doi.org/10.1111/jpy.12825

Kooistra, W. H. C. F., de Stefano, M., Mann, D. G., Salma, N., & Medlin, L. K. (2003). Phylogenetic position of *Toxarium*, a pennate-like lineage within centric diatoms (Bacillariophyceae). *Journal of Phycology*, *39*(1), 185–197. https://doi.org/10.1046/j.1529-8817.2003.02083.x

Kooistra, W. H. C. F., Gersonde, R., Medlin, L. K., & Mann, D. G. (2007). The origin and evolution of the diatoms: Their adaptation to a planktonic existence. https://doi.org/10.1016/B978-0-12-370518-1.50012-6

Krammer, K. (1980). Morphologic and taxonomic investigations of some freshwater species of the diatom genus *Amphora* Ehr. *Bacillaria*, *3*, 197–225.

Krammer, K., & Lange-Bertalot, H., (1991). Bacillariophyceae: Achnanthaceae, Kritische Ergänzungen zu *Navicula* (Lineolatae) und Gomphonema. Gesamtliteraturverzeichnis. p. 1-437. In: *Süßwasserflora von Mitteleuropa. Ettl, H., Gerloff, J., Heynig, H., Mollenhauer, D. (Eds). Vol. 2/4. Stuttgart: Gustav Fischer Verlag.*

Krammer, K., & Lange-Bertalot, H. (1986). Bacillariophyceae 1 Teil: Naviculaceae In: Süßwasserflora von Mitteleuropa. Begründet von A. Pascher. Herausgegeben von. H. Ettl, J. Gerloff, H. Heynig & D. Mollenhauer. Band 2/1. In S. H. Ettl, J. Gerloff, H. Heynig, & D. Mollenhauer (Eds.), *In: Süßwasserflora von Mitteleuropa. Begründet von A. Pascher. Herausgegeben von. H. Ettl, J. Gerloff, H. Heynig & D. Mollenhauer. Band 2/1. pp. [i]-xvi, [1]- Stuttgart & New York: Gustav Fischer Verlag.* (pp. 876, 206). Gustav Fischer Verlag.

Krammer, K., & Lange-Bertalot, H. (1997). Bacillariophyceae, Teil 1: Naviculaceae. *In: Ettl, H., Gerloff, J., Heyning, H. and Mollenhauer, D., Ed., Süsswasserflora von Mitteleuropa (Begründet von A. Pascher), Spektrum Akademischer Verlag, Nachdr. Heidelberg, 2*, 1-876.

Krammer K, & Lange-Bertalot H. (2000). Bacillariophyceae. 5. In: Ettl H, Gerloff J, Heynig H and Mollenhauer D (eds) Süßwasserflora von Mitteleuropa Band 2. *Spektrum Akademischer Verlag, Heidelberg, Berlin.*

Kulikovskiy, M., Maltsev, Y., Andreeva, S., Glushchenko, A., Gusev, E., Podunay, Y., Ludwig, T. V., Tusset, E., & Kociolek, J. P. (2019). Description of a new diatom genus *Dorofeyukea* gen. nov. with remarks on phylogeny of the family Stauroneidaceae. *Journal of Phycology*, *55*(1), 173–185. https://doi.org/10.1111/jpy.12810

Kumar, S., Stecher, G., Li, M., Knyaz, C., & Tamura, K. (2018). MEGA X: Molecular Evolutionary Genetics Analysis across computing platforms. Molecular Biology and Evolution, 35, 1547-1549.

Kützing, F. T. (1844). Die Kieselschaligen Bacillarien oder Diatomeen. In *Nordhausen: zu finden bei W. Köhne. Vol. [i-vii], [1]-152,* (pp. 1–30).

Lange, K., Liess, A., Piggott, J. J., Townsend, C. R., & Matthaei, C. D. (2011). Light, nutrients and grazing interact to determine stream diatom community composition and functional group structure. *Freshwater Biology*, *56*(2), 264–278. https://doi.org/10.1111/j.1365-2427.2010.02492.x

Levkov, Z. (2009). *Amphora sensu lato. In: Diatoms of Europe: Diatoms of the European Inland Waters and Comparable Habitats* (H. E. Lange-Bertalot, Ed.; Vol. 5). A.R.G. Gantner Verlag K.G.

Li, C. L., Ashworth, M. P., Witkowski, A., Dabek, P., Medlin, L. K., Kooistra, W. H. C. F., Sato, S., Zglobicka, I., Kurzydlowski, K. J., Theriot, E. C., Sabir, J. S. M., Khiyami, M. A., Mutwakil, M. H. Z., Sabir, M. J., Alharbi, N. S., Hajarah, N. H., Qing, S., & Jansen, R. K. (2015). New insights into Plagiogrammaceae (Bacillariophyta) based on multigene phylogenies and morphological characteristics with the description of a new genus and three new species. *PLoS ONE*, *10*(10). https://doi.org/10.1371/journal.pone.0139300

LI, C. L., Witkowski, A., Ashworth, M. P., Dabek, P., Sato, S., Zglobicka, I., Witak, M., Khim, J. S., & Kwon, C.-J. (2018). The morphology and molecular phylogenetics of some marine diatom taxa within the Fragilariaceae, including twenty undescribed species and their relationship to *Nanofrustulum*, *Opephora* and *Pseudostaurosira*. Phytotaxa, 355(1), 1. https://doi.org/10.11646/phytotaxa.355.1.1

Li, Y., Guo, X.-H., & Lundholm, N. (2020). Molecular phylogeny and taxonomy of the genus *Minidiscus* (Bacillariophyceae), with description of *Mediolabrus* gen. nov. *Journal of Phycology*, *56*(6), 1443–1456.

Li, Y., Zhao, Q., & Lü, S. (2013). The genus *Thalassiosira* off the Guangdong coast, South China Sea. *Botanica Marina*, *56*(1), 83–110.

Ligowski, R., Jordan, R. W., & Assmy, P. (2012). Morphological adaptation of a planktonic diatom to growth in Antarctic Sea ice. *Marine Biology*, *159*(4), 817–827. https://doi.org/10.1007/s00227-011-1857-6

Lobban, C. S. (1985). Marine tube-dwelling diatoms of the Pacific coast of North America. I. *Berkeleya*, *Haslea*, *Nitzschia*, and *Navicula* sect. Microstigmaticae. *Canadian Journal of Botany, 63*, 1779–1784.

Lobban, C. S., Schefter, M., Jordan, R. W., Arai, Y., Sasaki, A., Theriot, E. C., Ruck, C., & Pennesi, C. (2012). Coral-reef diatoms (Bacillariophyta) from Guam: new records and preliminary checklist, with emphasis on epiphytic species from farmer-fish territories. *Micronesica, 43*(2), 237479.

Longphuirt, S. N., Leynaert, A., Guarini, J.-M., Chauvaud, L., Claquin, P., Herlory, O., Amice, E., Huonnic, P., & Ragueneau, O. (2006). Discovery of microphytobenthos migration in the subtidal zone. MARINE ECOLOGY PROGRESS SERIES, 328, 143–154.

MacDonald, J. D. (1869). On the structure of the diatomaceous frustule, and its genetic cycle. *J. Nat. Hist.*, *3*(I), 1–8.

MacIntyre, H. L., Geider, R. J., & Miller, D. C. (1996). Microphytobenthos: the ecological role of the secret garden of unvegetated shallow-water marine habitats. I. Distribution abundance and primary production. *Estuaries*, *19*(2A), 186–201.

Mann, A. (1937). Diatoms. Australasian Antarctic Expedition, 1911-1914. *Scientific Reports. Series 1 c. Zoology and Botany, 1*(1), 1-82.

Mann, D.G. (1986a). *Nitzschia* subgenus *Nitzschia* (Notes for a monograph of the Bacillariaceae 2). In M. Ricard (ed.), Proceedings of the 8th International Diatom Symposium, 215-226. O. Koeltz, Koenigstein.

Mann, D. G. (1984). An ontogenetic approach to diatom systematics. In: Mann DG (ed) Proceedings of the 7th Int Diatom Symp. Koeltz, Koenigstein, pp 113–144

Mann, D. G., & Chepurnov, V. A. (2004). What have the Romans ever done for us? The past and future contribution of culture studies to diatom systematics. *Nova Hedwigia*, 237-291.

Mann, D. G. , Sato, S., Trobajo, R., Vanormelingen, P., & Souffreau, C. (2010). DNA barcoding for species identification and discovery in diatoms *Cryptogam., Algol. 31(4):* 557-577

Marchetti, A., & Harrison, P. J. (2007). Coupled changes in the cell morphology and the elemental (C, N, and Si) composition of the pennate diatom *Pseudo-nitzschia* due to iron deficiency. *Limnology and Oceanography*, *52*(5), 2270–2284. https://doi.org/10.4319/lo.2007.52.5.2270

Marsson, T. (1901). Diatomaceen von Neu-Vorpommern, Rügen und Usedom. *Zeitschrift für Angewandte Mikroskopie und Klinische Chemie*, *6*, 253–268.

Medlin, L., Elwood, H. J., Stickel, S., & Sogin, M. L. (1988). The characterization of enzymatically amplified eukaryotic 16S-like rRNA-coding regions. *Gene 71*(2): 491-499. https://doi.org/10.1016/0378-1119(88)90066-2

Medlin, L. K. (2016). Evolution of the diatoms: Major steps in their evolution and a review of the supporting molecular and morphological evidence. *Phycologia*, *55*(1), 79–103. https://doi.org/10.2216/15-105.1

Medlin, L.K. (2008). Molecular clocks and inferring evolutionary milestones and biogeography. In: The microalgae. *Origin and Evolution of Natural Diversity (Ed. by H. Okada, S.F. Mawatari, N. Suzuki & P. Gautam), 21st Century COE for Neo-Science of Natural History, Hokkaido, Japan.*, 31–42.

Méléder, V., Rincé, Y., Barillé, L., Gaudin, P., & Rosa, P. (2007). Spatiotemporal changes in microphytobenthos assemblages in a macrotidal flat (Bourgneuf Bay, France). *Journal of Phycology*, *43*(6), 1177–1190. https://doi.org/10.1111/j.1529-8817.2007.00423.x

Menden-Deuer, S., & Lessard, E. J. (2000). Carbon to volume relationships for dinoflagellates, diatoms, and other protist plankton. *Limnology and Oceanography*, *45*(3), 569–579. https://doi.org/10.4319/lo.2000.45.3.0569

Mereschkowsky, C. (1903). Tipy endokhroma u Diatomovykh [pp. 1-106]. Le types de l'endochrom chez les Diatomées [107-193]. *Scripta Botanica (Botanisheskia Zapiski)*, *21:*(i-ii,), 1-193.

Miller, D. C., R. J. Geider and H. L. MacIntyre. (1996). *Microphytobenthos: The Ecological Role of the "Secret Garden" of Unvegetated, Shallow-Water Marine Habitats. II. Role in Sediment Stability and Shallow-Water Food Webs* Estuaries 19 (2A): 202–212.

Moniz, M. B. J., & Kaczmarska, I. (2009). Barcoding diatoms: Is there a good marker? *Molecular Ecology Resources*, *9* (1), 65–74. https://doi.org/10.1111/j.1755-0998.2009.02633.x

Moniz, M. B. J., & Kaczmarska, I. (2010). Barcoding of Ddiatoms: Nuclear encoded ITS revisited. *Protist*, *161*(1), 7–34. https://doi.org/10.1016/j.protis.2009.07.001

Montuori, P., Lama, P., Aurino, S., Naviglio, D., & Triassi, M. (2013). Metals loads into the Mediterranean Sea: estimate of Sarno River inputs and ecological risk. *Ecotoxicology*, *22*(2), 295–307. https://doi.org/10.1007/s10646-012-1026-9

Moser, G., Lange-Bertalot, H., & Metzeltin, D. (1998). Insel der Endemiten. Geobotanisches Phänomen Neukaledonien. Island of endemics New Caledonia - a geobotanical phenomenon. *Bibliotheca Diatomologica*, *38*, 101, 1 –464.

Mucko, M., Bosak, S., Mann, D. G., Trobajo, R., Wetzel, C. E., Peharec Štefanić, P., Ljubešić, Z. (2020a). A polyphasic approach to the study of the genus *Nitzschia* (Bacillariophyta): three new planktonic species from the Adriatic Sea. *Journal of Phycology, 57*, (1), 143-159 https://doi.org/10.1111/jpy.13085

Müller, O. F. (1773). Vermium terrestrium et fluviatilium sue animalium infusorium helminthecorum et cestaceorum non marinarum succinta historia. *Havniae et Lipsiae.*, *1*(30), 135.

Munda, I. M. (2005). Seasonal fouling by diatoms on artificial substrata at different depths near Piran (Gulf of Trieste, Northern Adriatic) Original scientific paper. *ACTA ADRIATICA,* , *46*(2), 137–157.

Nelson, D., Treguer, P., Brzezinski, M., Leynaert, A., & Queguiner, B. (1995). Production and dissolution of biogenic silica in the ocean: Revised global estimates, comparison with regional data and relationship to biogenic sedimentation. *Global Biogeochemical Cycle*, *9*(3), 359–372.

Neri, F., Romagnoli, T., Accoroni, S., Campanelli, A., Marini, M., Grilli, F., & Totti, C. (2022). Phytoplankton and environmental drivers at a long-term offshore station in the northern Adriatic Sea (1988–2018). *Continental Shelf Research*, *242*. https://doi.org/10.1016/j.csr.2022.104746

Longphuirt, N. S., Clavier, J., Grall, J., Chauvaud, L., le Loc'h, F., le Berre, I., Flye-Sainte-Marie, J., Richard, J., & Leynaert, A. (2007). Primary production and spatial distribution of subtidal microphytobenthos in a temperate coastal system, the Bay of Brest, France. *Estuarine, Coastal and Shelf Science*, *74*(3), 367–380. https://doi.org/10.1016/j.ecss.2007.04.025

Oksanen, Simpson Gavin Leslie, Blanchet F. Guillaume, & Kindt Roeland. (2022). Community ecology package version: Vols. 2.6-2. https://github.com/vegandevs/vegan

Park, J., Khim, J. S., Ryu, J., Koh, C. H., & Witkowski, A. (2013). An emended description of the genus *Fogedia* (Bacillariophyceae) with reports of four species new to science from a Korean sand flat. *Phycologia*, *52*(5), 437–446.

Park, J. S., Lobban, C. S., Lee, K.-W., & Jung, S. W. (2022). Additional floristic study of planktonic and seaweed-associated diatoms in Chuuk, Micronesia. *Journal of the Marine Biological Association of the United Kingdom*, *102*(1–2), (1–35) 27-61.

Patrick, R., & Reimer, C. W. (1975). The diatoms of the United States exclusive of Alaska and Hawaii- Entomoneidaceae, Cymbellaceae, Gomphonemaceae, Epithemiaceae. In *Philadelphia: The Academy of Natural Sciences of Philadelphia.* (Vols. 2, Part 1, p. [i]-ix, [1]-213, 28 pls.).

Pennesi, C., Caputo, A., Lobban, C. S., Poulin, M., & Totti, C. (2017a). Morphological discoveries in the genus *Diploneis* (Bacillariophyceae) from the tropical west Pacific, including the description of new taxa. *Diatom Research*, *32*(2), 195–228. https://doi.org/10.1080/0269249X.2017.1343752

Pennesi, C., & Danovaro, R. (2017). Assessing marine environmental status through microphytobenthos assemblages colonizing the Autonomous Reef Monitoring Structures (ARMS) and their potential in coastal marine restoration. *Marine Pollution Bulletin*, *125*(1–2), 56–65. https://doi.org/10.1016/j.marpolbul.2017.08.001

Pennesi, C., Poulin, M., de Stefano, M., Romagnoli, T., & Totti, C. (2012). Morphological studies of some marine *Mastogloia* (Bacillariophyceae) belonging to section Sulcatae, including the

description of new species. *Journal of Phycology*, *48*(5), 1248–1264. https://doi.org/10.1111/j.1529-8817.2012.01215.x

Peragallo, H. and M. Peragallo. 1897–1908. Diatomées marines de France et des districts maritimes voisins. M. J. Tempère, Grez-sur-Loing. pp. 491; I–XII: 48 pp. 135 pls.

Percopo, I., Siano, R., Cerino, F., Sarno, D., & Zingone, A. (2011). Phytoplankton diversity during the spring bloom in the northwestern Mediterranean Sea. *Botanica Marina*, *54*(3), 243–267.

Pérez-Burillo, J., Valoti, G., Witkowski, A., Prado, P., Mann, D. G., & Trobajo, R. (2022). Assessment of marine benthic diatom communities: insights from a combined morphological–metabarcoding approach in Mediterranean shallow coastal waters. *Marine Pollution Bulletin*, *174*. https://doi.org/10.1016/j.marpolbul.2021.113183

Pfitzer, E. H. H. (1871). Untersuchungen über Bau und Entwicklung der Bacillariaceen (Diatomaceen). *Botanische Abhandlungen Aus Dem Gebiet Der Morphologie Und Physiologie. Herausg. von J. Hanstein, Bonn*, *1(2)*, 189.

Pinckney, J. L. (2018). A mini-review of the contribution of benthic microalgae to the ecology of the continental shelf in the South Atlantic Bight. In *Estuaries and Coasts* (Vol. 41, Issue 7, pp. 2070–2078). Springer New York LLC. https://doi.org/10.1007/s12237-018-0401-z

Poulíčková, A., Veselá, J., Neustupa, J., & Škaloud, P. (2010). Pseudocryptic diversity versus cosmopolitanism in diatoms: A case study on *Navicula cryptocephala* Kütz. (Bacillariophyceae) and morphologically similar taxa. *Protist*, *161*(3), 353–369. https://doi.org/10.1016/j.protis.2009.12.003

Prasad, A. K. S. K., Nienow, J. A., & Livingston, R. J. (1990). The genus *Cyclotella* (Bacillariophyta) in Choctawhatchee Bay, Florida, with special reference to *C. striata and C. choctawhatcheeana Sp. Nov. Phycologia*, *29*, 418–436.

Pringle CM. (1990). Nutrient spatial heterogeneity: effects on community structure, physiognomy and diversity of stream algae. *Ecology*, *71*, 905–920.

Pritchard, A. (1861). A history of infusoria, including the Desmidiaceae and Diatomaceae, British and foreign. Fourth edition enlarged and revised by J. T. Arlidge, W. Archer, J. Ralfs, W. C. Williamson, pp. [1]-xii, [1]-968, 40 pls. London: Whittaker and Co.

Riaux-Gobin, C., Witkowski, A., & Romero, O. E. (2013). An account of *Astartiella* species from tropical areas with a description of *A. societatis* sp. nov. and nomenclatural notes. *Diatom Research*, *28*(4), 419–430. https://doi.org/10.1080/0269249X.2013.827590

Rimet, F., Kermarrec, L., Bouchez, A., Hoffmann, L., Ector, L., & Medlin, L. K. (2011). Molecular phylogeny of the family bacillariaceae based on 18s rDNA sequences: Focus on freshwater *Nitzschia* of the section Lanceolatae. *Diatom Research*, *26*(3), 273–291. https://doi.org/10.1080/0269249X.2011.597988

Rogelja, M., Cibic, T., Pennesi, C., & de Vittor, C. (2016). Microphytobenthic community composition and primary production at gas and thermal vents in the Aeolian Islands (Tyrrhenian Sea, Italy). *Marine Environmental Research*, *118*, 31–44. https://doi.org/10.1016/j.marenvres.2016.04.009

Romagnoli, T., Bavestrello, G., Cucchiari, E. M., de Stefano, M., di Camillo, C. G., Pennesi, C., Puce, S., & Totti, C. (2007). Microalgal communities epibiontic on the marine hydroid *Eudendrium racemosum* in the Ligurian Sea during an annual cycle. *Marine Biology*, *151*(2), 537–552. https://doi.org/10.1007/s00227-006-0487-x

Romagnoli, T., Totti, C., Accoroni, S., de Stefano, M., & Pennesi, C. (2014). SEM analysis of the epibenthic diatoms on *Eudendrium racemosum* (Hydrozoa) from the Mediterranean Sea. *Turkish Journal of Botany*, *38*(3), 566–594. https://doi.org/10.3906/bot-1305-52

Ross, R., Cox, E., Karajeva, N., Mann D G, Paddock, T. B. B., Simonsen, R., & Sims P A. (1979). An amended terminology for the siliceous components of the diatom cell. *Nova Hedwigia Beiheft* , *64*, 513–533.

Ross, R., & Sims, P. A. (1972). The fine structure of the frustule in centric diatoms: A suggested terminology. *British Phycological Journal*, *7*(2), 139–163. https://doi.org/10.1080/00071617200650171

Round, F. E. (1971). Benthic marine diatoms. *Oceanography and Marine Biology. Annual Review, 9*, 83–139.

Round, F. E., Hallsteinsen, H., & Paasche, E. (1999). On a previously controversial "fragilarioid" diatom now placed in a new genus *Nanofrustrulum*. *Diatom Research*, *14*(2), 343-356.

Round, F. E., Crawford, R. M., & Mann, D. G. (1990). The diatoms biology and morphology of the genera. In *Cambridge: Cambridge University Press* (pp. 1–747). Cambridge University Press.

Sabanci, F. C. (2012). Taxonomic Survey of Benthic Diatoms on Natural Substrata from Coastal Lagoon (Aegean Sea, Turkey). *Turkish Journal of Fisheries and Aquatic Sciences*, *12*(4). https://doi.org/10.4194/1303-2712-v12_4_12

Sar, E. A., Sunesen, I., Lavigne, A. S., & Lofeudo, S. (2011). *Thalassiosira rotula*, a heterotypic synonym of *Thalassiosira gravida*: morphological evidence. *Diatom Research*, *26*(1), 109–119.

Sarno, D., Kooistra, W. H. C. F., Balzano, S., Hargraves, P. E., & Zingone, A. (2007). Diversity in the genus *Skeletonema* (Bacillariophyceae): III. Phylogenetic position and morphological variability of *Skeletonema costatum* and *Skeletonema grevillei*, with the description of *Skeletonema ardens* sp. nov. *Journal of Phycology*, *43*(1), 156–170. https://doi.org/10.1111/j.1529-8817.2006.00305.x

Sarno, D., Kooistra, W. H. C. F., Medlin, L. K., Percopo, I., & Zingone, A. (2005). Diversity in the genus *Skeletonema* (Bacillariophyceae). II. An assessment of the taxonomy of *S. costatum*-like species with the description of four new species. *Journal of Phycology*, *41*(1), 151–176. https://doi.org/10.1111/j.1529-8817.2005.04067.x

Sato, S., Kooistra, W. H. C. F., Watanabe, T., Matsumoto, S., & Medlin, L. K. (2008). A new araphid diatom genus *Psammoneis* gen. nov. (Plagiogrammaceae, Bacillariophyta) with three new species based on SSU and LSU rDNA sequence data and morphology. *Phycologia*, *47*(5), 510–528. https://doi.org/10.2216/08-04.1

Sato, S., Watanabe, T., Crawford, R. M., Kooistra, W. H. C. F., & Medlin, L. K. (2008a). Morphology of four plagiogrammacean diatoms; *Dimeregramma minor* var. *nana*, *Neofragilaria nicobarica*, *Plagiogramma atomus* and *Psammogramma vigoensis* gen. et sp. nov., and their phylogenetic

relationship inferred from partial large subunit rDNA. *Phycological Research*, *56*(4), 255–268. https://doi.org/10.1111/j.1440-1835.2008.00507.x

Sato, S., Watanabe, T., Crawford, R. M., Kooistra, W. H. C. F., & Medlin, L. K. (2008b). Morphology of four plagiogrammacean diatoms; *Dimeregramma* minor var. nana*, Neofragilaria nicobarica*, *Plagiogramma atomus* and *Psammogramma vigoensis* gen. et sp. nov., and their phylogenetic relationship inferred from partial large subunit rDNA. *Phycological Research*, *56*(4), 255–268. https://doi.org/10.1111/j.1440-1835.2008.00507.x

Schoeman, F. R., & Archibald, R. E. M. (1986). Observations on *Amphora* species (Bacillariophyceae) in the British Museum (Natural History. *V*. Some species from the subgenus *Amphora. S. Afr. J. Bot*, *52*, 425–437.

Schratzberger, M., & Ingels, J. (2018). Meiofauna matters: The roles of meiofauna in benthic ecosystems. *Journal of Experimental Marine Biology and Ecology*, *502*, 12–25. https://doi.org/10.1016/j.jembe.2017.01.007

Scott, F. J., & Thomas, D. P. (2005). *Diatoms. In: Antarctic marine protists* (F. J. Scott & H. J. E. Marchant, Eds.). Australian Biological Resources Study; Australian Antarctic Division.

Sdrigotti, E., Barbariol, V., & Welker, C. (1999). Diatom assemblages in coastal shallow waters at the water-sediment interface (Gulf ff Trieste, North Adriatic Sea) *Annales Ser. Hist. Nat., 2* (17): 191202.

Simonsen, R. (1962). Untersuchungen zur Systematik und Okologie der Bodendiatomeen der westlichen Ostsee. I. *Nternationale Revue Der Gesamten Hydrobiologie, Systematische Beihefte*.

Sims, P. A., Williams, D. M., & Ashworth, M. (2018). Examination of type specimens for the genera *Odontella* and *Zygoceros* (Bacillariophyceae) with evidence for the new family Odontellaceae and a description of three new genera. *Phytotaxa*, *382*(1), 1–56, 156.

Siqueiros-Beltrones, D. A., Argumedo-Hernández, U., & López-Fuerte, F. O. (2017). New records and combinations of *Lyrella* (Bacillariophyceae: Lyrellales) from a protected coastal lagoon of the northwestern Mexican Pacific. *Revista Mexicana de Biodiversidad*, *88*, 1–20, 105.

Skibbe, O., Zimmermann, J., Kusber, W.-H., Abarca, N., Buczkó, K., & Jahn, R. (2018). *Gomphoneis tegelensis* sp. nov. (Bacillariophyceae): a morphological and molecular investigation based on selected single cells. *Diatom Research*, *33*(2), 251–262. https://doi.org/10.1080/0269249X.2018.1518835

Smith, D. J., & Underwood, G. J. C. (1998). Exopolymer production by intertidal epipelic diatoms. *Limnology and Oceanography*, *43*(7), 1578–1591. https://doi.org/10.4319/lo.1998.43.7.1578

Soininen, J., McDonald, R., & Hillebrand, H. (2007). The distance decay of similarity in ecological communities. *Ecography*, *30*(1), 3–12. https://doi.org/10.1111/j.0906-7590.2007.04817.x

Sospedra, J., Niencheski, L. F. H., Falco, S., Andrade, C. F. F., Attisano, K. K., & Rodilla, M. (2018). Identifying the main sources of silicate in coastal waters of the Southern Gulf of Valencia (Western Mediterranean Sea). *Oceanologia*, *60*(1), 52–64. https://doi.org/10.1016/j.oceano.2017.07.004.

Souffreau, C., Vanormelingen, P., van de Vijver, B., Isheva, T., Verleyen, E., Sabbe, K., & Vyverman, W. (2013). Molecular Evidence for Distinct Antarctic Lineages in the Cosmopolitan Terrestrial Diatoms *Pinnularia borealis* and *Hantzschia amphioxys*. *Protist*, *164*(1), 101–115. https://doi.org/10.1016/j.protis.2012.04.001

Spaulding, S. A., Potapova, M. G., Bishop, I. W., Lee, S. S., Gasperak, T. S., Jovanoska, E., Furey, P. C., & Edlund, M. B. (2021). *Diatoms.org*: supporting taxonomists, connecting communities. *Diatom Research*, *36*(4), 291–304. https://doi.org/10.1080/0269249X.2021.2006790

Stachura-Suchoples, K., Enke, N., Schlie, C., Schaub, I., Karsten, U., & Jahn, R. (2016). Contribution towards a morphological and molecular taxonomic reference library of benthic marine diatoms from two Arctic fjords on Svalbard (Norway). *Polar Biology*, *39*(11), 1933–1956. https://doi.org/10.1007/s00300-015-1683-2

Stancheva, R., Mancheva, A., & Ivanov, P. (2007). Taxonomic composition of the epilithic diatom flora from rivers Vit and Osum, Bulgaria. *Phytologia Balcanica*, *13*(1), 53–64.

Stepanek, J. G. & K. J. P. (2019). Molecular phylogeny of the diatom genera *Amphora* and *Halamphora* (Bacillariophyta) with a focus on morphological and ecological evolution. *Journal of Phycology*, *55*(2), 442-456.

Takano, H. (1983). New and rare diatoms from Japanese marine waters - IX. A new *Rhaphoneis* emitting mucilaginous threads. *Bulletin of the Tokai Regional Fisheries Laboratory*, *109*, 27–39.

Theriot, E. C., Ashworth, M. P., Nakov, T., Ruck, E., & Jansen, R. K. (2015). Dissecting signal and noise in diatom chloroplast protein encoding genes with phylogenetic information profiling. *Molecular Phylogenetics and Evolution*, *89*, 28–36. https://doi.org/10.1016/j.ympev.2015.03.012

Tolomio, C., Moro, I., Moschin, E., & Valandro, A. (1999). Resultats preliminaires sur les diatomées benthiques de substrats meubles dans la lagune de Venise, Italie (Mars 1994–Janvier 1995). *Diatom Research*, *14*(2), 367–379. https://doi.org/10.1080/0269249X.1999.9705478

Tolomio, C., Moschin, E., & Duzzin, B. (2002). Distribution des diatomées benthiques de substrats meubles dans le bassin sud de la lagune de Venise, Italie. *Diatom Research*, *17*(2), 401–414. https://doi.org/10.1080/0269249X.2002.9705557

Torrisi, M., & Dell'Uomo, A. (2006). Biological monitoring of some Apennine rivers (central Italy) using the diatom-based eutrophication / pollution index (epi-d) compared to other European diatom indices. In *Diatom Research* (Vol. 2).

Totti, C. (2003). Influence of the plume of the River Po on the distribution of subtidal microphytobenthos in the northern Adriatic Sea. *Botanica Marina*, *46*, 161–178.

Totti, C., Cucchiari, E., de Stefano, M., Pennesi, C., Romagnoli, T., & Bavestrello, G. (2007). Seasonal variations of epilithic diatoms on different hard substrates, in the northern Adriatic Sea. *Journal of the Marine Biological Association of the United Kingdom*, *87*(3), 649–658. https://doi.org/10.1017/S0025315407054665

Totti, C., Poulin, M., Romagnoli, T., Perrone, C., Pennesi, C., & de Stefano, M. (2009). Epiphytic diatom communities on intertidal seaweeds from Iceland. *Polar Biology*, *32*(11), 1681–1691. https://doi.org/10.1007/s00300-009-0668-4

Totti, C., Romagnoli, T., Accoroni, S., Coluccelli, A., Pellegrini, M., Campanelli, A., Grilli, F., & Marini, M. (2019). Phytoplankton communities in the northwestern Adriatic Sea: Interdecadal variability over a 30-years period (1988–2016) and relationships with meteoclimatic drivers. *Journal of Marine Systems*, *193*, 137–153. https://doi.org/10.1016/j.jmarsys.2019.01.007

Trobajo, R., Clavero, E., Chepurnov, V. A., Sabbe, K., Mann, D. G., Ishihara, S., & Cox, E. J. (2009). Morphological, genetic and mating diversity within the widespread bioindicator *Nitzschia palea* (Bacillariophyceae). *Phycologia*, *48*(6), 443–459. https://doi.org/10.2216/08-69.1

Trobajo, R., Mann, D. G., Clavero, E., Evans, K. M., Vanormelingen, P., & McGregor, R. C. (2010). The use of partial cox1, rbcL and LSU rDNA sequences for phylogenetics and species identification within the *Nitzschia palea* species complex (bacillariophyceae). *European Journal of Phycology*, *45*(4), 413–425. https://doi.org/10.1080/09670262.2010.498586

Trobajo, R., Rovira, L., Mann, D. G., & Cox, E. J. (2011). Effects of salinity on growth and on valve morphology of five estuarine diatoms. *Phycological Research*, *59*(2), 83–90. https://doi.org/10.1111/j.1440-1835.2010.00603.x

Underwood, G. J. C., & Barnett, M. (2006). What determines species composition in microphytobenthic biofilms? *in Functioning of Microphytobenthos In Estuaries, eds J. Kromkamp,* J. F. C. de Brouwer, G. F. Blanchard, R. M. Forster, and V. Créach, (Amsterdam: Royal Netherlands Academy of Arts and Sciences), 121–138.

Underwood, G. J. C., & Paterson, D. M. (2003). *The importance of extracellular carbohydrate productionby marine epipelic diatoms* (pp. 183–240). https://doi.org/10.1016/S0065-2296(05)40005-1

Valentini, A., Pompanon, F., & Taberlet, P. (2009). DNA barcoding for ecologists. *Trends in Ecology and Evolution*, 24(2), 110–117). https://doi.org/10.1016/j.tree.2008.09.011

Van Heurck, H. (1909). *Exped. Antarct. Belg. l*, 128.

Vanormelingen, P., Chepurnov, V. A., Mann, D. G., Cousin, S., & Vyverman, W. (2007). Congruence of morphological, reproductive and ITS rDNA sequence data in some Australasian *Eunotia bilunaris* (Bacillariophyta). *European Journal of Phycology*, *42*(1), 61–79. https://doi.org/10.1080/09670260600942635

Vanormelingen, P., Chepurnov, V. A., Mann, D. G., Sabbe, K., & Vyverman, W. (2008). Genetic Divergence and Reproductive Barriers among Morphologically Heterogeneous Sympatric Clones of *Eunotia bilunaris sensu lato* (Bacillariophyta). *Protist*, *159*(1), 73–90. https://doi.org/10.1016/j.protis.2007.08.004

Veech, J. A. (2013). A probabilistic model for analysing species co-occurrence. *Global Ecology and Biogeography*, *22*(2), 252–260. https://doi.org/10.1111/j.1466-8238.2012.00789.x

Vilhena, J. C. E., Amorim, A., Ribeiro, L., Ferreira, I. M., & Pombo, M. (2021). Assessing the efficiency of low-cost cleaning methods for diatoms from intertidal sediment samples. *Journal of Microbiological Methods*, *187*, 106255. https://doi.org/10.1016/j.mimet.2021.106255

Villac, M. C., Kaczmarska, I., & Ehrman, J. M. (2016). Diatoms from ship ballast sediments (with consideration of a few additional species of special interest. *Diatom Monographs*, *18*, 235, 1 – 557.

Welker, C., Sdrigotti, E., Covelli, S., & Faganeli, J. (2002). Microphytobenthos in the gulf of Trieste (Northern Adriatic Sea): Relationship with labile sedimentary organic matter and nutrients. *Estuarine, Coastal and Shelf Science*, *55*(2), 259–273. https://doi.org/10.1006/ecss.2001.0901

Williams, D. M., & Round, F. E. (1987). Revision of the genus *Fragilaria*. *Diatom Research*, *2*(2), 267–288. https://doi.org/10.1080/0269249X.1987.9705004

Witkowski, A., Lange-Bertalot, H., & Metzeltin, D. (2000). Diatom flora of marine coasts I. *Iconographia Diatomologica*, *7*, 1–925.

Witkowski, A., Li, C., Zgłobicka, I., Yu, S. X., Ashworth, M., Dabek, P., Qin, S., Tang, C., Krzywda, M., Ruppel, M., Theriot, E. C., Jansen, R. K., Car, A., Płocinski, T., Wang, Y. C., Sabir, J. S. M., Daniszewska-Kowalczyk, G., Kierzek, A., & Hajrah, N. H. (2016). Multigene assessment of biodiversity of diatom (Bacillariophyceae) assemblages from the littoral zone of the Bohai and Yellow Seas in Yantai region of northeast China with some remarks on ubiquitous taxa. *Journal of Coastal Research*, *74*, 166–195. https://doi.org/10.2112/SI74-016.1

Witkowski, A., Metzeltin, D. L.-B., H., & Bafana, G. (1997). *Fogedia* gen. nov. *Nova Hedwigia*, *65*, 79–98.

Zgrundo, A., Lemke, P., Pniewski, F., Cox, E. J., & Latala, A. (2013). Morphological and molecular phylogenetic studies on *Fistulifera saprophila*. *Diatom Research*, *28*(4), 431–443. https://doi.org/10.1080/0269249X.2013.833136

Glossary

This glossary has been adapted in part from: (Cox, 2012; Krammer K & Lange-Bertalot H, 2000; Lobban et al., 2012; Round et al., 1990; Spaulding et al., 2021)

- Apex – the distal tip or point of the valve in the biraphid diatoms.
- Apical –cell poles in pennate diatoms.
- Apical pore-fields – group of pores at a pole (e.g. *Gomphonema*) or at both valve-ends (e.g. many araphid genera and *Cymbella* sensu stricto). Those pores not closed by vela produce a secretion which solidifies into fine threads with which the cells are attached to an appropriate substrate.
- Areolae – chamber-forming perforations, rounded to angular in cross-section, in the valve wall. They are closed either on the outside, or inside, by a velum.
- Axial area – in pennate diatoms this is a puncta-free zone on either side of the apical axis.
- Annulus (centric taxa)-An annulus is a hyaline ring in some centric diatoms. The annulus is the silica that is first formed during valve formation during cell division. It may, or may not, be visible or well developed, a feature that varies across genera.
- Annulus (pennate taxa)- the last few distal striae may have areolae that are larger and more elongate, with more densely spaced pores. These modified areolae are termed "annulae". Internally, the annulae of some species possess a cluster of silica outgrowths. The annulae may be distinctive or barely discernible, depending on the species. For example, the annulae of *Geissleria acceptata* are difficult to resolve in LM.
- Biseriate-Biseriate describes the number of rows of areolae in a stria. A biseriate stria has two rows of areolae. In Latin, biseriate means two series.
- Canal raphe – a raphe whose fissure is in a canal-shaped hollow linked to the inner cell through a slit.
- Conopeum (canopy) – a thin sheath of silica attached to the axial area. It covers the areolate portion of the valve. Cover ranges from minor to total.
- Central – the valve middle.
- Central area – hyaline area in the middle of the valve. In some cases this is identical with the central nodule. Frequently there is no visible border between the central and the axial areas, and thus the two form a single hyaline zone.
- Central nodule – a nodular thickening, of varying degree and extent, of the median costae within the central area.
- Convergent / divergent – striae that radiate towards the terminal nodules.

- Copulae – mostly open elements of the cell girdle, set aside form the other girdle elements by their structure.
- Costae – longitudinal thickenings of the valve.
- Cribrum- is a type of velum that is reticulate or that has regularly arranged pores. The plural is cribra. Cribra may be flat or domed. In some genera they may be visible with LM but are usually visible only with electron microscopy. Domed cribra are characteristic of the Thalassiosirales.
- Decussate- refers to a crossing pattern of striae. The striae may cross in three directions with a transapical row and two oblique rows. The genera *Decussata* and *Pleurosigma* have decussate striae.
- Dorsal – in diatoms that are asymmetrical along the apical axis, it is the side whose outer margin is more convex. The other side is the ventral side.
- Fascia – puncta-free transapical bar in the middle of the valve.
- Fibulae– support in the form of a silica strut, bridging the raphe-bearing keel on the inner side of the valve in many species with a canal raphe. The fibulae can end in one or more transapical striae, and be solid, tubular or flattened.
- Fimbriate-radiating ribs of silica (can be noticed in *Melosira*)
- Footpole- is the narrower apex, or pole, of a clavate valve. It often contains an apical porefield. (can be observed in *Licmophora* genus)
- Frustule – the complete silicified cell-wall, consisting of the epi- and hypovalve.
- Fultoportula – hollow processes on the outside of the valve, normally as a marginal ring; tubes with 2-5 closely associated structures (“satellite pores”) that penetrate the valve wall. They can be arranged in marginal ring and/or otherwise arranged on the valve surface. Their organisation and number (including their presence and absence) are held as important taxonomic characters.
- Girdle – collective term for all structural elements between two valves.
- Girdle view- is the appearance of a frustule when the girdle (cincture) and the mantles of attached valves are in view. It is the view of the frustule when the girdle is perpendicular to the observer.
- Girdle-band – general term for all open and closed bands (segments) of the cell-girdle, i.e. valvocopulae, intercalary bands.
- Headpole- is the broader apex, or pole, of a clavate or cuneate valve (can be observed in *Licmophora* genus).

- Helictoglossae- A helictoglossa is the internal, distal termination of the raphe having the shape of a pair of lips or a rolled tongue. The helictoglossa occurs in many raphid diatoms. If present, it can be distinguished in the light microscope in valve view by optical dissection (focusing through many narrow, optical planes). It may also be visible in girdle view as a thickened lip of silica. The plural is helictoglossae. In Greek, helictoglossa means rolled tongue.
- Hyaline-Hyaline refers to any area of a diatom valve that is unornamented, that is, it lacks pores or other structures.
- Hymen- is a very delicate, porous membrane of silica occluding an areola or an alveolus. It is visible only with SEM. The pores of the hymen may be round or elongated and range from 5-10 nm (0.005-0.010 μm) in their shortest diameter. The plural is hymenes. Hymenes are found in many raphid genera such as *Cocconeis* and *Neidiopsis*.
- In some raphid diatoms (e.g., *Navicula*) a hymen forms the only occlusion of an areola, covering the inner aperture. In others such as *Diploneis* a hymen and a cribrum combine to cover an areola. In this genus the hymen lies beneath the outer cribrum.
- Keel- is a thickening of silica that contains the raphe within a canal. The keel elevates the raphe from the surface of the valve, allowing maximal contact of the raphe with surfaces for motility. A number of genera possess a keel, including *Nitzschia*, *Iconella* and *Entomoneis*.
- Longitudinal bands (longitudinal lines or furrows) – structures outside the median costa, running apically, and visible in LM. Morphologically, they are of varying structure (e.g. inner alveoli openings in *Pinnularia*, longitudinal canals in *Neidium*.
- Lineolae-
- Marginal – near the valve edge.
- Median raphe / central raphe – raphe systems that lie in the median costa (Achnanthaceae, Naviculaceae), and that consist of two raphe branches separated by the central nodule. The raphe fissures end directly inside the cell, in contrast to a canal raphe.
- Ocellus- An ocellus is a porefield that has a distinct hyaline rim between its pores and the areolae. Plural is ocelli. Latin for "small eye"
- Parallel striae – striae running at right-angles to the apical axis. Polar – identical with terminal.
- Pores – circular wall perforations without vela.
- Pervalvar axis- is the axis of the valve which is perpendicular to the center of the valve face. In centric diatoms, the center is the meeting point of the radii. In pennate diatoms, the center is the meeting point of the apical and transapical axes.

- Central/ Proximal raphe ends - raphe ends on the central nodule (internally) and near the central portion of the valve (externally)
- Pseudoloculi- large, irregular and incomplete chambers surrounding the pores on the valve face (can be noticed in *Triceratium)*
- pseudoraphe valve- The valve of a monoraphid pennate diatom lacking a raphe is termed the rapheless valve (*Cocconeis*)
- Radial striae – a striae pattern where they point away from the central nodule.
- Raphe – slit-shaped opening in the valve surface, serving as an organelle for movement. All valves with raphes have two symmetrical raphe branches. In the Achnanthaceae and Naviculaceae, the raphe lies within the median costa. Species with a canal raphe however, have the raphe in the angle between the valve surface and the mantle, or raised on a specialised raphe-keel.
- Raphe fissure – raphe fissure is an extension of the end of the raphe. A fissure is a structure that does not penetrate the valve wall and may be external or internal. The arrangement of the outer and inner fissures is often taxonomically very significant. (also mentioned as raphe endings, see also 'Central/ Proximal raphe ends' and 'Terminal raphe ending')
- Rimoportula (labiate process) – a tube penetrating the valve wall. On the outer valve surface is either only one foramen, or an elongated structure looking like a thorn in LM. The process in centric diatoms lies either near the normal marginal spines or is displaced towards the mantle. On the inner side of the valve it takes the form of a lip-like shaped structure.
- Spine- is a pointed, silica extension of the valve, shorter than a seta. Spines and may be solid or hollow, very long or tiny, single or many, and they may arise from different points on the valve in different taxa.
- Sternum – the "pseudoraphe" of araphid diatoms, i.e. a puncta-free apically running stria.
- Stigmata - perforation through valve face whose external opening is rounded (or nearly so) and whose internal opening is slit-like or highly modified.
- Striae - rows of puncta/areolae, usually oriented along transapical axis, separated by unornamented ribs.
- Terminal (polar) – at the valve ends in pennate diatoms.
- Terminal raphe ending - external terminus of raphe at the pole/apex.
- Transapical striae – Lines on the valve surface formed from rows of puncta or other fine perforations running at ninety degrees to the apical axis

- Undulation- describes a feature as having the shape of a wave, with crests and troughs. A valve may be undulate on the margins or on the face.
- Uniseriate- describes the number of rows of areolae in a stria. A uniseriate stria has a single row of areolae. In Latin, uniseriate means one series.
- Valve - siliceous part of the frustule containing most of the morphological features used to describe diatoms (taxonomically, morphologically, etc.). Each valve has two surfaces, the face and the mantle.
- Valve view-is the appearance of a frustule when the entire valve face is in view. It is the view of the frustule when the valve face is perpendicular to the observer.
- Valve mantle – the side walls of the valve. In many cases it has a different structure from the valve face. Sometimes it is unperforated but may have the same structure as the valve surface. The structure of mantle may be separated from the valve face by a hyaline area.
- Valvocopula- A valvocopula is the copula immediately adjacent to a valve. The plural is valvocopulae.
- Velum – a structured or unstructured thin silica membrane stretched across the inside of the foramen, or that closes off the inside of an areola. Cleaning with strong acid usually destroys the fine velum.
- Ventral – in dorsiventral species, the less convex side.
- Vimen- is the silica connection between adjacent virgae, separating the areolae within a stria. The plural is vimines. In Latin vimen means "pliant twig".
- Virga- is the solid silica band between two striae (also mentioned as ‘interstria’).

Supplementary material for 'Chapter 2'

Table S1: Environmental variables at SG and PN stations during the sampling period

Stations	**Senigallia**				**Portonovo**			
Season Parameter	**Spring**	**Summer**	**Autumn**	**Winter**	**Spring**	**Summer**	**Autumn**	**Winter**
Temperature (°C)	15.16	20.60	18.18	8.73	16.51	23.22	18.29	10.5
Salinity	37.81	38.50	35.39	34.61	38.07	37.43	35.57	36.06
pH	8.2	8.2	8.3	8.3	8.2	8.2	8.2	8.2
Chlorophyll (mg/m^3)	0.73	1.64	2.08	3.07	0.84	0.59	2.12	1.17
Turbidity (NTU)	6.71	3.61	3.39	2.59	4.31	1.69	1.56	0.98
NO_2 (µM)	0.05	1.01	1.18	1.14	0.25	0.72	0.78	0.47
NO_3 (µM)	0.68	1.38	5.88	14.59	2.55	4.74	4.91	6.68
NH_4 (µM)	1.39	6.60	0.66	2.32	6.88	7.95	0.02	3.49
DIN (µM)	2.11	8.99	7.72	18.04	9.67	13.41	5.70	10.64
Phosphate (µM)	0.06	0.06	0.31	0.14	0.07	0.1	0.08	0.14
Silicate (µM)	9.19	19.11	17.30	4.90	8.54	7.56	5.64	8.09

Table S2: Floristic list

Actinocyclus sp.	Plocon
Amphora cf. *graeffei* Grunow	Adnate
Amphora arenicola Grunow ex Cleve	Adnate
Amphora cf. *helenensis* Giffen	Adnate
Amphora cf. *inariensis* Krammer	Adnate
Amphora cf. *jostesorum* Witkowski, Lange-Bertalot & Metzeltin	Adnate
Amphora cf. *libyca* Ehrenberg	Adnate
Amphora cf. *proteus* W.Gregory	Adnate
Amphora copulata (Kützing) Schoeman & R.E.M.Archibald	Adnate
Araphid sp. 1	Araphid
Astartiella sp. 1	Adnate
Bacillaria paxillifera (O.F.Müller) T.Marsson	Motile
Caloneis sp.	Motile
Campylodiscus cf. *thuretii* Brébisson	Motile
Campylodiscus sp. 1	Motile
Centric sp. 1	Plocon
Centric sp. 2	Plocon
Centric sp. 3	Plocon
Cocconeis sp. 1	Adnate
Cocconeis sp. 2	Adnate

Coronia decora (Brébisson) Ruck & Guiry	Motile
Coscinodiscus cf. *apiculatus* Ehrenberg	Plocon
Coscinodiscus cf. *divisus* Grunow	Plocon
Coscinodiscus sp. 1	Plocon
Cyclotella striata (Kützing) Grunow	Plocon
Cylindrotheca closterium (Ehrenberg) Reimann & J.C.Lewin	Motile
Diploneis sp. 3	Motile
Diploneis sp. 4	Motile
Diploneis weissflogiopsis Lobban & Pennesi	Motile
Entomoneis alata (Ehrenberg) Kützing	Motile
Entomoneis cf. *paludosa* (W.Smith) Reimer	Motile
Entomoneis cf. *robusta* (McCall) Reimer	Motile
Fallacia cf. *forcipata* (Greville) Stickle & D.G.Mann	Motile
Fallacia cf. *tenera* (Hustedt) D.G.Mann	Motile
Fallacia sp.	Motile
Fogedia sp.	Motile
Gomphonema sp.	Erect
Gyrosigma cf. *balticum* (Ehrenberg) Rabenhorst	Motile
Gyrosigma cf. *fasciola* (Ehrenberg) J.W.Griffith & Henfrey	Motile
Halamphora cf. *tenerrima* (Aleem & Hustedt) Levkov	Adnate
Halamphora coffeiformis (C.Agardh) Mereschkowsky	Adnate
Halamphora cuneata	Adnate
Hippodonta sp.	Motile
Lauderia annulata Cleve	Plocon/planktonic
Licmophora sp. 1	Erect
Lyrella cf. *clavata* (W.Gregory) D.G.Mann	Motile
Lyrella cf. *exsul* (A.W.F.Schmidt) D.G.Mann	Motile
Lyrella sp. 1	Motile
Mediolabrus comicus (H.Takano) Yang Li	Plocon/planktonic
Minidiscus triculatus	Plocon/planktonic
Navicula agatae Witkowski, Lange-Bertalot & Metzeltin	Motile
Navicula distans (W.Smith) Brébisson	Motile
Navicula sp. 2	Motile
Navicula sp. 1	Motile
Navicula sp. 10	Motile
Navicula sp. 10	Motile
Navicula sp. 11	Motile
Navicula sp. 12	Motile
Navicula sp. 3	Motile
Navicula sp. 4	Motile
Navicula sp. 5	Motile
Navicula sp. 6	Motile
Navicula sp. 7	Motile
Navicula sp. 8	Motile

Navicula sp. 9	Motile
Nitzschia cf. *acuta* Cleve	Motile
Nitzschia cf. *prolongata* Hustedt	Motile
Nitzschia cf. *sigma* (Kützing) W.Smith	Motile
Nitzschia hybrida Grunow	Motile
Nitzschia longissima (Brébisson) Ralfs	Motile
Nitzschia sp. 1	Motile
Nitzschia sp. 6	Motile
Nitzschia sp. 2	Motile
Nitzschia sp. 3	Motile
Nitzschia sp. 4	Motile
Nitzschia sp. 5	Motile
Odontella sp. 1	Plocon
Odontella sp. 2	Plocon
Pennate sp. 10	Motile
Pennate sp. 11	Motile
Pennate sp. 12	Motile
Pennate sp. 13	Motile
Pennate sp. 4	Araphid
Pennate sp. 5	Motile
Pennate sp. 6	Motile
Pennate sp. 9	Motile
Pennate sp. 15	Motile
Pennate sp. 16	Araphid
Pennate sp.3	Motile
Pennate sp.7	Motile
Pleurosigma elongatum W.Smith	Motile
Pleurosigma sp. 1	Motile
Pleurosigma cf. *latum* Cleve	Motile
Porosira sp.	Plocon/planktonic
Proskinia sp.	Motile
Psammodictyon panduriforme (W.Gregory) D.G.Mann	Motile
Psammodictyon panduriforme var *continuum* (Grunow) Snoeijis	Motile
Psammodictyon roridum (Giffen 1975) D. G. Mann	Motile
Psammodictyon sp. 1	Motile
Psammodictyon sp. 2	Motile
Psammodictyon sp. 3	Motile
Pteroncola sp.	Erect
Ralfsiella smithii (Ralfs) P.A.Sims, D.M.Williams & Ashworth	Plocon
Rhaponeis sp.	Erect
Seminavis sp.	Motile
Surirella sp.	Motile
Tabularia sp.	Erect
Thalassiosira gravida Cleve	Plocon/planktonic

Thalassiosira cf. *minima* Gaarder	Plocon/planktonic
Thalassiosira sp. 1	Plocon/planktonic
Thalassiosira sp. 2	Plocon/planktonic
Thalassiosira sp. 3	Plocon/planktonic
Thalassiosira sp. 4	Plocon/planktonic
Thalassiosira sp. 5	Plocon/planktonic
Trachyneis cf. *aspera* (Ehrenberg) Cleve	Plocon
Tryblionella cf.*marginulata* (Grunow) D.G.Mann	Motile
Tryblionella sp. 1	Motile

Table S3. Abundance of the species at stations SG and PN in four seasons. Abundance expressed in cells/cm²

Season	**Spring**	**Spring**	**Summer**	**Summer**	**Autumn**	**Autumn**	**Winter**	**Winter**
Station	**SG**	**PN**	**SG**	**PN**	**SG**	**PN**	**SG**	**PN**
Entomoneis alata (Ehrenberg) Kützing 1844	0	0	0	0	0	10	2	0
Amphora proteus W.Gregory 1857	22,552	9,907	2,615	870	2,790	364	783	503
Amphora copulata (Kützing) Schoeman & R.E.M.Archibald 1986	10,534	15,014	2,318	878	1,434	534	158	188
Amphora cf *graeffei* Grunow 1875	0	278	0	0	7	0	0	241
Halamphora coffeiformis (C.Agardh) Mereschkowsky	73	56	1	0	0	329	0	0
Ralfsiella smithii (Ralfs) P.A.Sims, D.M.Williams & Ashworth 2018	0	213	3	107	406	837	67	335
Odontella sp.1	3	39	5	3	0	0	0	0
Odontella sp. 2	8	13	11	58	0	0	0	0
Caloneis sp.	0	0	2	0	3	9	0	1
Campylodiscus cf. *thuretii* Brébisson 1854	3	0	0	0	0	0	0	0
Coronia decora (Brébisson) Ruck & Guiry 2016	0	0	0	0	0	0	0	0
Campylodiscus sp.	5	0	1	0	8	4	2	1

Cocconeis sp.	0	27	6	2	15	3	141	81
Coscinodiscus cf. *apiculatus* Ehrenberg 1844	0	0	0	0	0	0	2	0
Coscinodiscus cf. *divisus* Grunow 1884	0	3	0	0	0	0	0	0
Coscinodiscus sp. 1	0	3	19	0	1	0	2	8
Cyclotella striata (Kützing) Grunow 1880	1,243	1,951	185	0	346	371	371	649
Diploneis weissflogiopsis Lobban & Pennesi 2017	0	93	6	6	17	20	5	23
Diploneis sp. 3	0	1	0	0	0	0	0	0
Diploneis sp. 4	0	0	0	2	0	0	0	0
Lyrella sp.	0	0	0	0	0	4	0	0
Lyrella cf *exsul* (A.W.F.Schmidt) D.G.Mann 1990	0	0	0	0	0	5	0	0
Fallacia cf *forcipata* (Greville) Stickle & D.G.Mann 1990	5,308	737	61	28	264	57	272	223
Entomoneis cf. *robusta* (McCall) Reimer 1975	0	0	0	0	0	0	1	0
Entomoneis cf. *paludosa* (W.Smith) Reimer 1975	0	17	0	0	0	0	2	0
Gyrosigma cf. *balticum* (Ehrenberg) Rabenhorst 1853	0	0	0	0	15	37	23	3
Gyrosigma cf. *fasciola* (Ehrenberg) J.W.Griffith & Henfrey	0	0	0	0	0	7	5	0
Licmophora sp.	0	0	0	0	1	0	0	0
Lyrella cf. *clavata* (W.Gregory) D.G.Mann 1990	0	0	0	0	0	1	0	0
Navicula distans (W.Smith) Brébisson 1854	6,160	6,023	21	38	84	174	10	106
Navicula sp. 2	194	269	0	15	51	23	5	13

Navicula sp. 3	0	0	0	0	0	0	0	0
Nitzschia cf. *acuta* Cleve 1878	103	0	0	0	0	0	0	0
Nitzschia cf. *sigma* (Kützing) W.Smith 1853	25	57	1	0	1	35	6	1
Nitzschia longissima (Brébisson) Ralfs 1861	242	183	0	0	10	6	8	3
Nitzschia cf. *prolongata* Hustedt 1938	0	10	0	0	0	3	0	0
Cylindrotheca closterium (Ehrenberg) Reimann & J.C.Lewin 1964	0	0	0	0	2	0	0	1
Navicula sp. 4	468	5,584	4	0	4	42	8	31
Pennate sp. 10	1	0	0	0	0	0	0	0
Pennate sp. 11	0	23	0	0	0	0	0	0
Pennate sp. 13	0	0	0	0	0	1	0	0
Pennate sp.3	0	525	0	0	0	0	0	0
Navicula sp. 5	3	38	0	0	0	0	0	0
Nitzschia 17	0	556	0	0	0	0	0	0
Fallacia sp. 1	0	0	0	0	0	0	0	0
Pennate 9	1,280	97	0	0	0	0	0	0
Pleurosigma cf *latum* Cleve 1880	168	408	2	19	470	847	762	146
Psammodictyon panduriforme (W.Gregory) D.G.Mann 1990	53	282	8	10	13	5	20	12
Rhaponeis sp.	0	0	1	0	0	0	0	0
Surirella sp.	12	3	22	12	16	64	21	9
Tabularia sp.	9	470	0	0	0	0	0	0
Thalassiosira sp.	3	1	1	1	70	3	4	95
Trachyneis cf. *aspera* (Ehrenberg) Cleve 1894	0	0	0	1	0	0	0	0
Tryblionella cf.*marginulata* (Grunow) D.G.Mann 1990	0	117	0	2	0	16	1	3
Und. centric diatoms <20 µm	0	57	111	192	371	1187	139	1391
Und. centric diatoms >20 µm	17	0	19	40	236	81	63	323

Und. pennate diatoms <20 µm	20,846	36,196	1,706	2,003	8,284	10,101	6,908	7,344
Und. pennate diatoms >20 µm	197	427	96	353	11,429	527	683	1,020

Table S4: Biomass of the species at stations SG and PN in four seasons. Biomass expressed in µg C/cm².

Season	**Spring**	**Spring**	**Summer**	**Summer**	**Autumn**	**Autumn**	**Winter**	**Winter**
Station	**SG**	**PN**	**SG**	**PN**	**SG**	**PN**	**SG**	**PN**
Entomoneis alata (Ehrenberg) Kützing 1844	0	0	0	0	0	0	0	0
Amphora proteus W.Gregory 1857	1.82	0.88	0.20	0.06	0.17	0.07	0.09	0.06
Amphora copulata (Kützing) Schoeman & R.E.M.Archibald 1986	0.51	0.70	0.09	0.03	0.05	0.03	0.01	0.02
Amphora cf *graeffei* Grunow 1875	0	0.04	0	0	0	0	0	0.02
Halamphora coffeiformis (C.Agardh) Mereschkowsky	0.01	0.01	0	0	0	0.06	0	0
Ralfsiella smithii (Ralfs) P.A.Sims, D.M.Williams & Ashworth 2018	0	0.45	0.01	0.20	1.25	1.84	0.18	0.96
Odontella sp.1	0	0.12	0.01	0.01	0	0	0	0
Odontella sp. 2	0.01	0.02	0.03	0.14	0	0	0	0
Caloneis sp.	0	0	0	0	0	0.01	0	0
Campylodiscus cf. *thuretii* Brébisson 1854	0	0	0	0	0	0	0	0
Coronia decora (Brébisson) Ruck & Guiry 2016	0	0	0	0	0	0	0	0
Campylodiscus sp.	0.01	0	0	0	0.01	0.01	0	0
Cocconeis sp.	0	0	0	0	0	0	0.03	0.02
Coscinodiscus cf. *apiculatus* Ehrenberg 1844	0	0	0	0	0	0	0.01	0
Coscinodiscus cf. *divisus* Grunow 1884	0	0.03	0	0	0	0	0	0

Coscinodiscus sp. 1	0	0.01	0.09	0	0.04	0	0.04	0.03
Cyclotella striata (Kützing) Grunow 1880	0.03	0.04	0.01	0	0.02	0.02	0.02	0.02
Diploneis weissflogiopsis Lobban & Pennesi 2017	0	0.03	0	0	0	0	0	0
Diploneis sp. 3	0	0	0	0	0	0	0	0
Diploneis sp. 4	0	0	0	0	0	0	0	0
Lyrella sp.	0	0	0	0	0	0	0	0
Lyrella cf *exsul* (A.W.F.Schmidt) D.G.Mann 1990	0	0	0	0	0	0	0	0
Fallacia cf *forcipata* (Greville) Stickle & D.G.Mann 1990	0.65	0.13	0.01	0.01	0.04	0.02	0.04	0.03
Entomoneis cf. *robusta* (McCall) Reimer 1975	0	0	0	0	0	0	0	0
Entomoneis cf. *paludosa* (W.Smith) Reimer 1975	0	0.01	0	0	0	0	0	0
Gyrosigma cf. *balticum* (Ehrenberg) Rabenhorst 1853	0	0	0	0	0.01	0.07	0.02	0.01
Gyrosigma cf. *fasciola* (Ehrenberg) J.W.Griffith & Henfrey	0	0	0	0	0	0	0	0
Licmophora sp.	0	0	0	0	0	0	0	0
Lyrella cf. *clavata* (W.Gregory) D.G.Mann 1990	0	0	0	0	0	0	0	0
Navicula distans (W.Smith) Brébisson 1854	0.34	0.35	0	0	0	0.02	0	0.01
Navicula sp. 2	0.02	0.03	0	0	0.01	0	0	0
Navicula sp. 3	0	0	0	0	0	0	0	0
Nitzschia cf. *acuta* Cleve 1878	0.01	0	0	0	0	0	0	0
Nitzschia cf. *sigma* (Kützing) W.Smith 1853	0	0.01	0	0	0	0.01	0	0
Nitzschia longissima	0.02	0.01	0	0	0	0	0	0

(Brébisson) Ralfs 1861								
Nitzschia cf. *prolongata* Hustedt 1938	0	0	0	0	0	0	0	0
Cylindrotheca closterium (Ehrenberg) Reimann & J.C.Lewin 1964	0	0	0	0	0	0	0	0
Navicula sp. 4	0.02	0.13	0	0	0	0.01	0	0.01
Pennate sp. 10	0	0	0	0	0	0	0	0
Pennate sp. 11	0	0	0	0	0	0	0	0
Pennate sp. 13	0	0	0	0	0	0	0	0
Pennate sp.3	0	0.04	0	0	0	0	0	0
Navicula sp. 5	0	0.01	0	0	0	0	0	0
Nitzschia 17	0	0	0	0	0	0	0	0
Fallacia sp. 1	0	0	0	0	0	0	0	0
Pennate 9	0.02	0.01	0	0	0	0	0	0
Pleurosigma cf *latum* Cleve 1880	0.02	0.08	0	0	0.03	0.13	0.11	0.03
Psammodictyon panduriforme (W.Gregory) D.G.Mann 1990	0.01	0.02	0	0	0	0	0	0
Rhaponeis sp.	0	0	0	0	0	0	0	0
Surirella sp.	0.01	0	0.03	0.01	0.02	0.05	0.02	0.01
Tabularia sp.	0	0.08	0	0	0	0	0	0
Thalassiosira sp.	0	0	0	0	0.07	0	0	0.04
Trachyneis cf. *aspera* (Ehrenberg) Cleve 1894	0	0	0	0	0	0	0	0
Tryblionella cf.*marginulata* (Grunow) D.G.Mann 1990	0	0.01	0	0	0	0	0	0
Und. centric diatoms <20 µm	0	0.01	0.01	0.01	0.10	0.12	0.01	0.15
Und. centric diatoms >20 µm	0.01	0	0.03	0.04	0.13	0.05	0.05	0.12
Und. pennate diatoms <20 µm	0.15	0.17	0.02	0.03	0.10	0.15	0.12	0.07
Und. pennate diatoms >20 µm	0.02	0.01	0	0.02	0.19	0.02	0.02	0.03

Supplementary material for 'Chapter 3'

Light Microscopy observations of the isolated strains

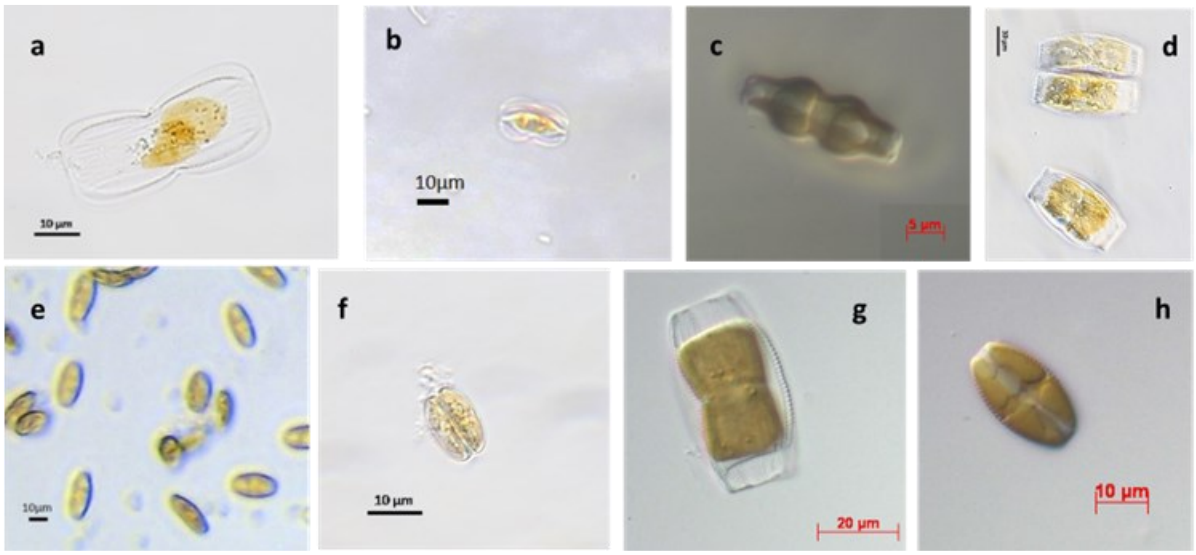

Plate 1: a= PN4Am, *Amphiprora* sp., b= PN4C, *Amphiprora* sp., c= BD10, *Amphora* sp., d= NM14, *Amphora* sp., e= PN4B, *Amphora* sp., f= SG31, *Amphora* sp., g= SRA, *Amphora* sp., h= SRD, *Amphora* sp.

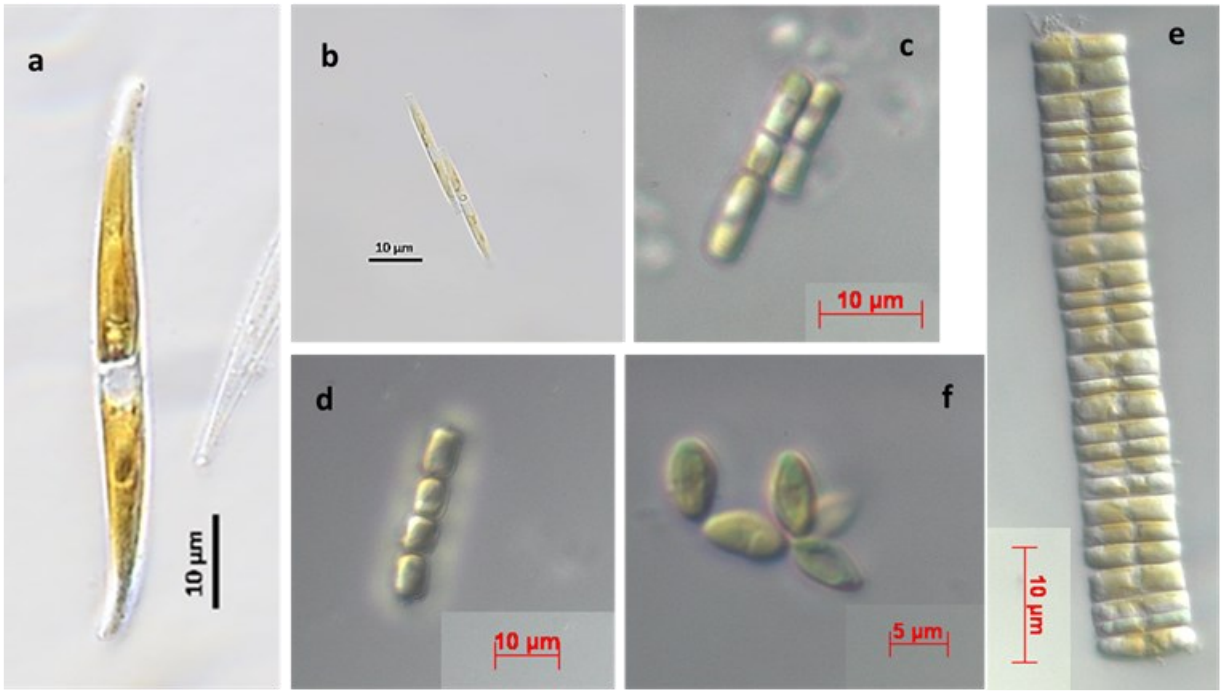

Plate 2: a= NM12, *Bacillaria* sp., b= PN4BA, *Bacillaria* sp., c= BD2, *Dimeregramma* sp. Or *Plagiogramma* sp., d= BD11, *Dimeregramma* sp. Or *Plagiogramma* sp., e= BD4, *Dimeregramma* sp. Or *Plagiogramma* sp., f= BD15, *Dimeregramma* sp., *Plagiogramma* sp. Or *Psammogramma.*

Plate 3: a= PN4DP, *Diploneis* sp., b= NB29, *Gyrosigma* Or *Pleurosigma* sp., c= NM17, *Halamphora* Or *Amphora* sp., d= BD9, *Nanofrustulum* sp., e= LR13, *Nanofrustulum* sp., f= LR26, *Nanofrustulum* sp.

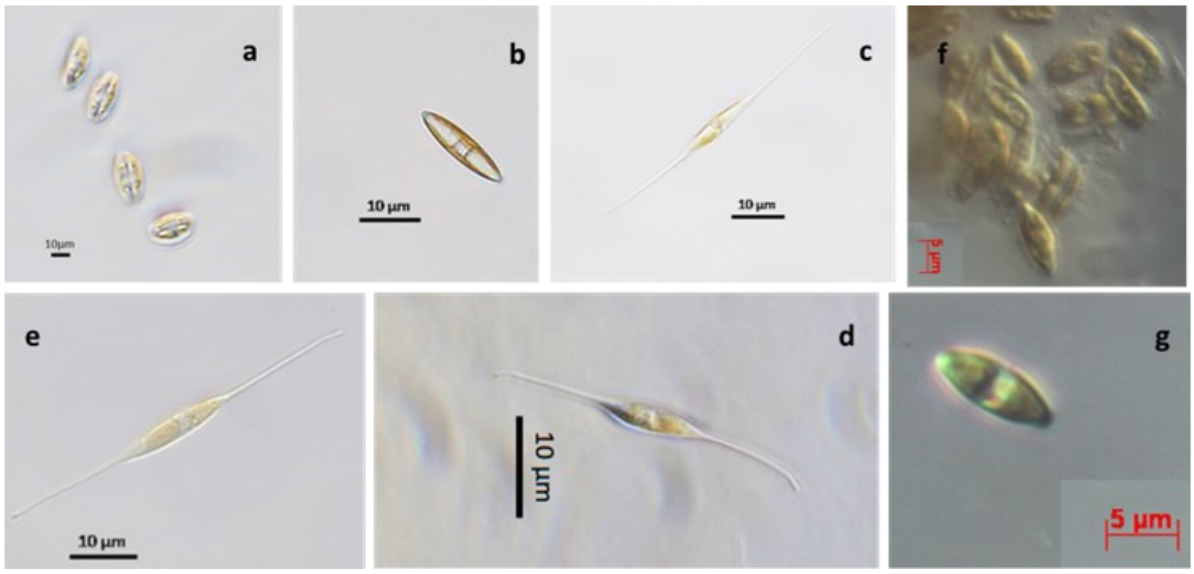

Plate 4: a= NM11, *Navicula* sp., b= PN4A, *Navicula* sp., c= PN4F, *Nitzschia longissima*., d= SG35, *Nitzschia longissima*., e= SG4C, *Nitzschia longissima*., f= BD3, *Nitzschia* sp., g= BD6, *Nitzschia* sp.

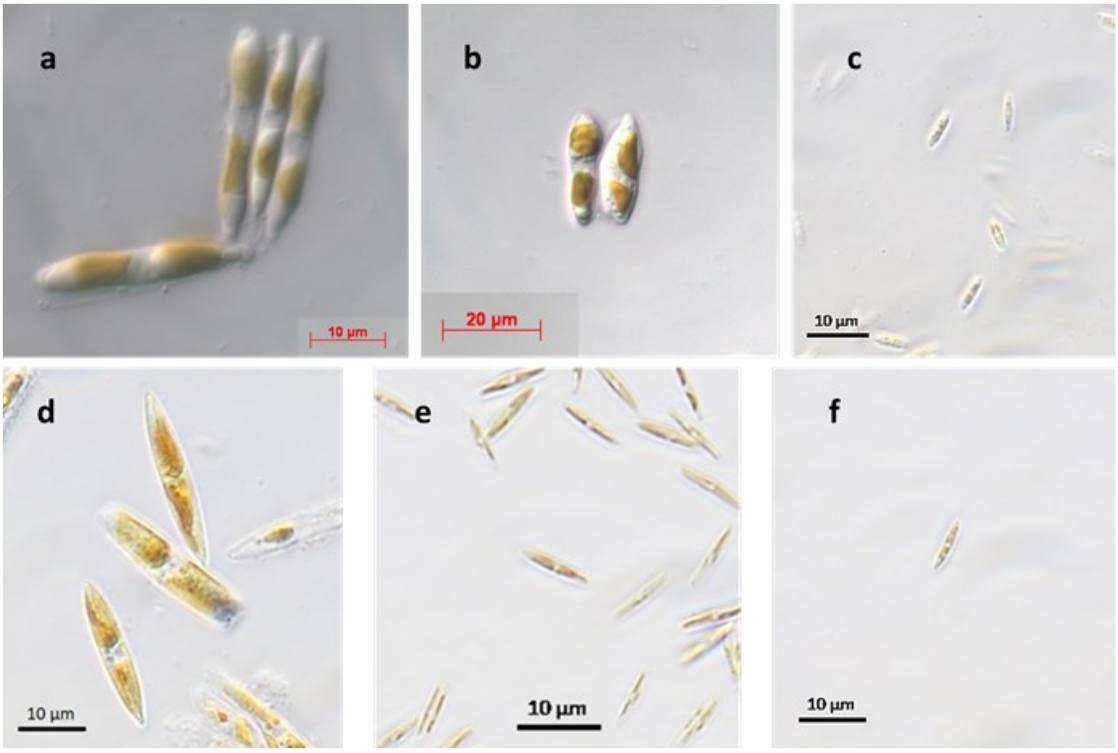

Plate 5: a= LR40, *Nitzschia* sp., b= LR43, *Nitzschia* sp., c= NaMC3, *Nitzschia* sp., d= NB21, *Nitzschia* sp., e= NB22, *Nitzschia* sp., f= NB23, *Nitzschia* sp.

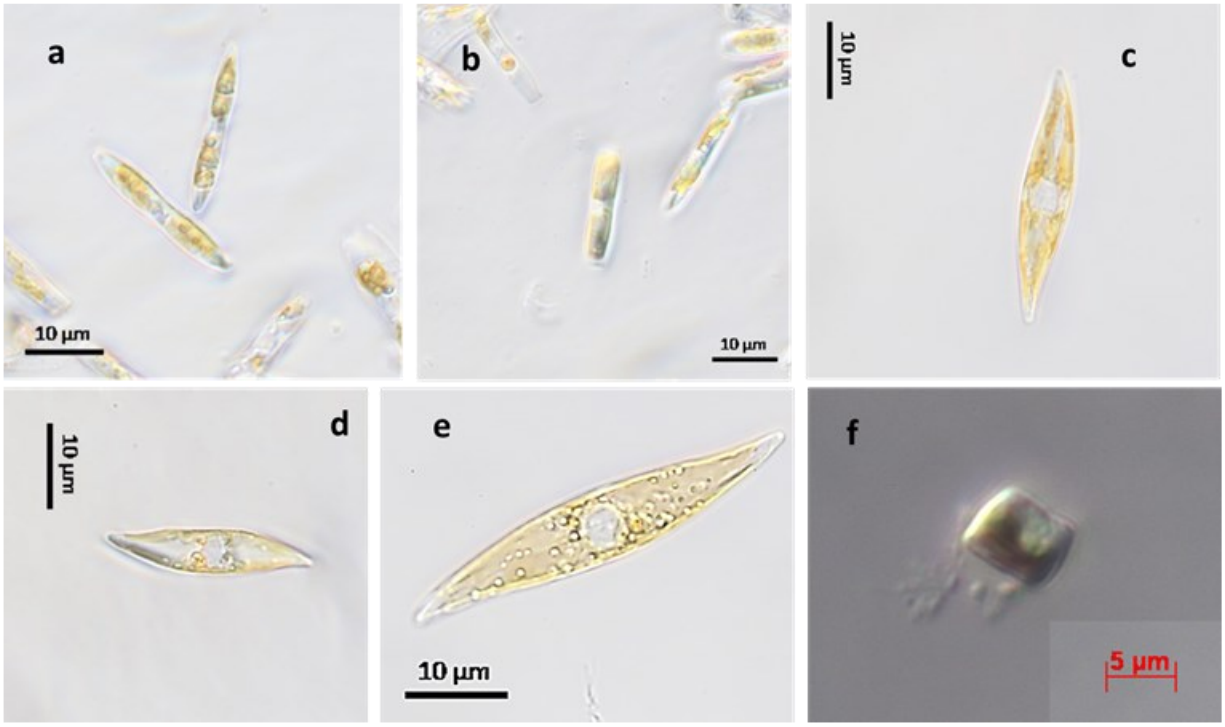

Plate 6: a= PN11, *Nitzschia* sp., b= PN21, *Nitzschia* sp., c= PN4G, *Pleurosigma* sp., d= SG11, *Pleurosigma* sp., e= SG4A, *Pleurosigma* sp., f= BD1, *Psammodictyon* sp.

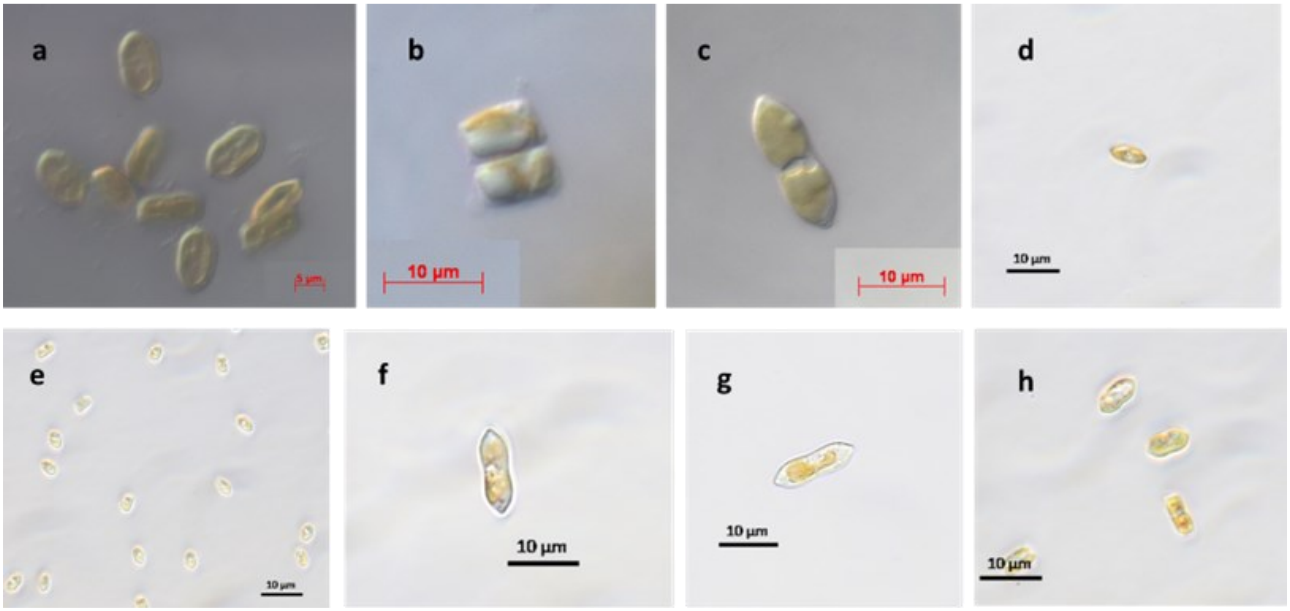

Plate 7: a= BD8, *Psammodictyon* sp., b= BD12, *Psammodictyon* sp., c= BD13, *Psammodictyon* sp., d= NaMC2, *Psammodictyon* sp., e= NB11, *Psammodictyon* sp., f= PN12, *Psammodictyon* sp., g= PN4E, *Psammodictyon* sp., h= SG12, *Psammodictyon* sp.

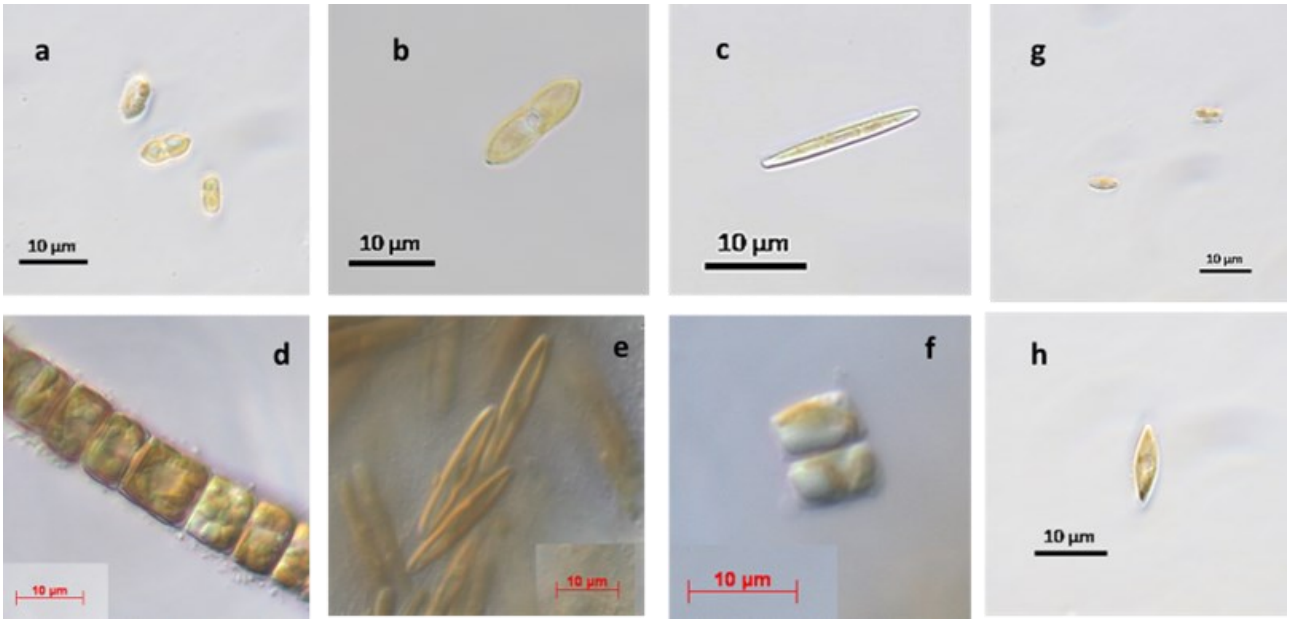

Plate 8: a= SG22, *Psammodictyon* sp., b= SG4E, *Psammodictyon* sp., c= SG4D, *Tabularia* sp., d= BD5, Undetermined sp., e= BD16, Undetermined sp., f= LR34, Undetermined sp., g= PN23, Undetermined sp., h= PN31, Undetermined sp.

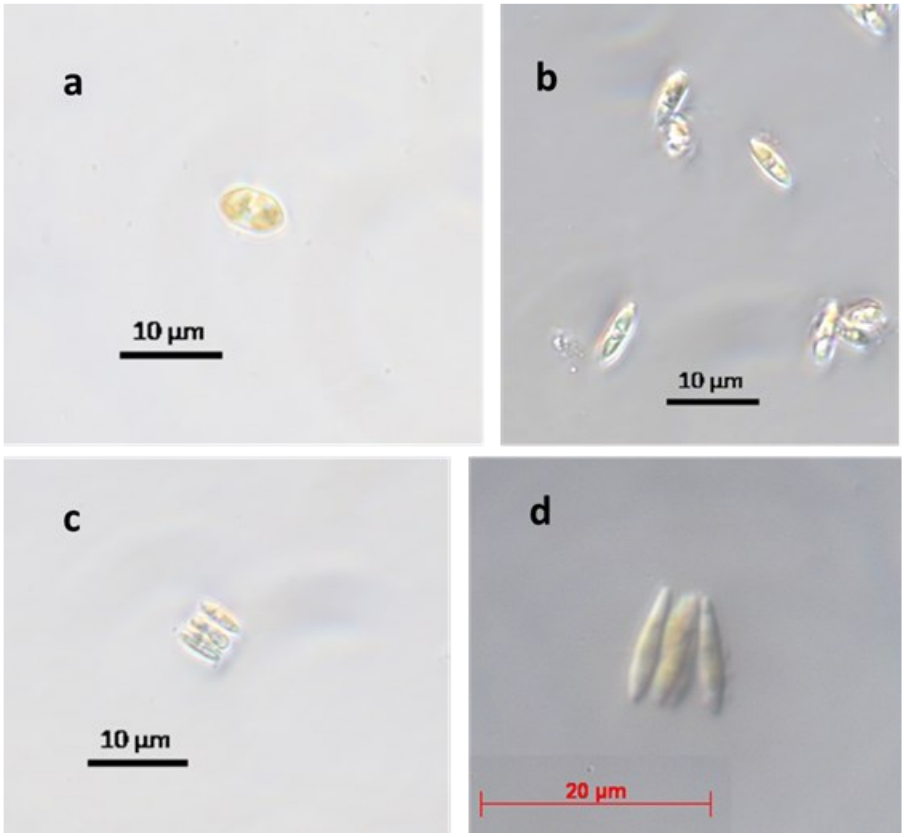

Plate 9: a= SG23, Undetermined sp., b= SG27, Undetermined sp., c= SG34, Undetermined sp., d= BD7, Undetermined sp.